PETROLOGY OF SYENITES FROM CENTRE III

OF THE COLDWELL ALKALINE COMPLEX, NORTHWEST ONTARIO

by

JŪRATĖ LUKOŠIUS-SANDERS©

A THESIS SUBMITTED IN PARTIAL FULFILLMENT OF

THE REQUIREMENTS FOR THE DEGREE OF

MASTER OF SCIENCE

LAKEHEAD UNIVERSITY, THUNDER BAY, ONTARIO

MARCH, 1988

ProQuest Number: 10611776

All rights reserved

INFORMATION TO ALL USERS
The quality of this reproduction is dependent upon the quality of the copy submitted.

In the unlikely event that the author did not send a complete manuscript
and there are missing pages, these will be noted. Also, if material had to be removed,
a note will indicate the deletion.

ProQuest 10611776

Published by ProQuest LLC (2017). Copyright of the Dissertation is held by the Author.

All rights reserved.
This work is protected against unauthorized copying under Title 17, United States Code
Microform Edition © ProQuest LLC.

ProQuest LLC.
789 East Eisenhower Parkway
P.O. Box 1346
Ann Arbor, MI 48106 - 1346

Permission has been granted to the National Library of Canada to microfilm this thesis and to lend or sell copies of the film.

The author (copyright owner) has reserved other publication rights, and neither the thesis nor extensive extracts from it may be printed or otherwise reproduced without his/her written permission.

L'autorisation a été accordée à la Bibliothèque nationale du Canada de microfilmer cette thèse et de prêter ou de vendre des exemplaires du film.

L'auteur (titulaire du droit d'auteur) se réserve les autres droits de publication; ni la thèse ni de longs extraits de celle-ci ne doivent être imprimés ou autrement reproduits sans son autorisation écrite.

ISBN 0-315-44794-X

ABSTRACT

The Coldwell Alkaline Complex, situated on the north shore of Lake Superior, is of Neohelikian age. It is intruded into Archean supracrustal rocks of the Superior Province, near Marathon, Ontario. The complex has a diameter of 25 km and consists of three major magmatic centres. Each centre represents the focus of a cauldron subsidence event. From earliest to latest they are: Centre I-saturated alkaline rocks with peralkaline oversaturated residua; Centre II-miaskitic undersaturated alkaline rocks; and Centre III-alkaline rocks with oversaturated residua. This thesis documents the rocks of Centre III.

Centre III magmatism of the Coldwell Alkaline Complex is represented by alkali feldspar syenites and alkali feldspar quartz syenites. In order of intrusion from earliest to youngest these are (1) synneuritic magnesio-hornblende syenite, (2) perthitic ferro-edenite syenite, (3) contaminated ferro-edenite syenite and (4) quartz syenite. Amphiboles are the major mafic phase in all syenite types. Their evolutionary compositional trend ranges from magnesian hastingsite in the magnesio-hornblende syenite to riebeckite in the quartz syenite. Pyroxenes are Ti-Al rich in the earliest syenites, but evolve to Na-Fe rich members in the youngest. The contaminated syenites result from the assimilation of xenoliths of oligoclase basalts which are interpreted to represent contemporaneous lavas. Varying degrees of contamination lead to an apparent plethora of syenite types.

The Centre III syenites are miaskitic and metaluminous with normative quartz content increasing from the earliest to the latest varieties. All of the syenites are enriched in U, Th, REE, and Zr, reflecting the presence of zircon, chevkinite, REE-carbonates, Nb-rutile and aeschylite. Centre III syenites have petrological affinities with A-type granites and are interpreted to have been formed by partial melting of lower crustal material.

ACKNOWLEDGEMENTS

I thank Dr. R. Mitchell who has been a great thesis advisor. His wisdom and patience were valuable in my efforts. He also performed some microprobe analyses and made many useful recommendations. While on sabbatical Dr. G. Platt provided useful guidance. Both are sincerely thanked.

The technicians at Lakehead University are thanked for many hours spent preparing and analyzing specimens: R. Bennett, D. Crothers, A. Hammond, A. MacKenzie, E. Jensen, and K. Pringnitz. S. Spivak skillfully drafted the first two figures of this thesis. M. Artist-Downey is thanked for many hours of computer work and assistance. W. Bons did a wonderful job typing this thesis and was invaluable as a liaison between Dr. Mitchell and myself. A very special thanks to both. Graduate students whose terms have coincided with mine are thanked for their friendship and stimulating discussion.

P. Strassburger of the Ministry of Northern Development and Mines (Terrace Bay) is thanked for granting permission to stay in Neys Provincial Park. Also, M. Kennedy (M.N.D.M., Thunder Bay) helped to organize a trip to Pic Island and A. Dixon (Marathon) provided excellent transportation.

B. McKay at Dalhousie University kindly assisted with the use of the microprobe facility.

My family is thanked for their unending support and encouragement.

TABLE OF CONTENTS

INTRODUCTION

1.1 Location and Access

Situated on the north shore of Lake Superior, the Coldwell Alkaline Complex lies approximately 250 kilometres east of Thunder Bay. A location map indicating the major tectonic features of the region is presented in Figure 1. A summary of the geology (Fig. 2) of the intrusion has been compiled by Mitchell and Platt (1982a). The Coldwell Alkaline Complex is circular in shape with a diameter of approximately 25 kilometres. The eastern contact of the complex is approximately 2 km east of the town of Marathon. The western margin lies nearly 3 km west of the Little Pic River. Exposure over much of the complex is poor. Principal access is provided by the Trans-Canada Highway 17, Canadian Pacific Railway, two hydrolines, together with numerous wave-cut shoreline exposures, forestry roads, and radiotower and microwave access roads.

1.2 Geologic Setting

The Coldwell Alkaline Complex is the largest of its kind in North America, and is unusual in that oversaturated, saturated and undersaturated rocks coexist. The complex is of Neohelikian age, and is intruded into an east-west trending Archean greenstone belt, which is part of the Superior Province of the Canadian Shield. The greenstone belt contains mafic and felsic volcanics, and greywackes, all metamorphosed to greenschist and amphibolite grade. Two episodes of folding and the intrusion of Archean felsic plutons have affected this belt (Walker, 1967).

On a regional scale, the Coldwell Alkaline Complex is within the Trans-Superior Tectonic Zone (Klasner et al. 1982), which bisects the

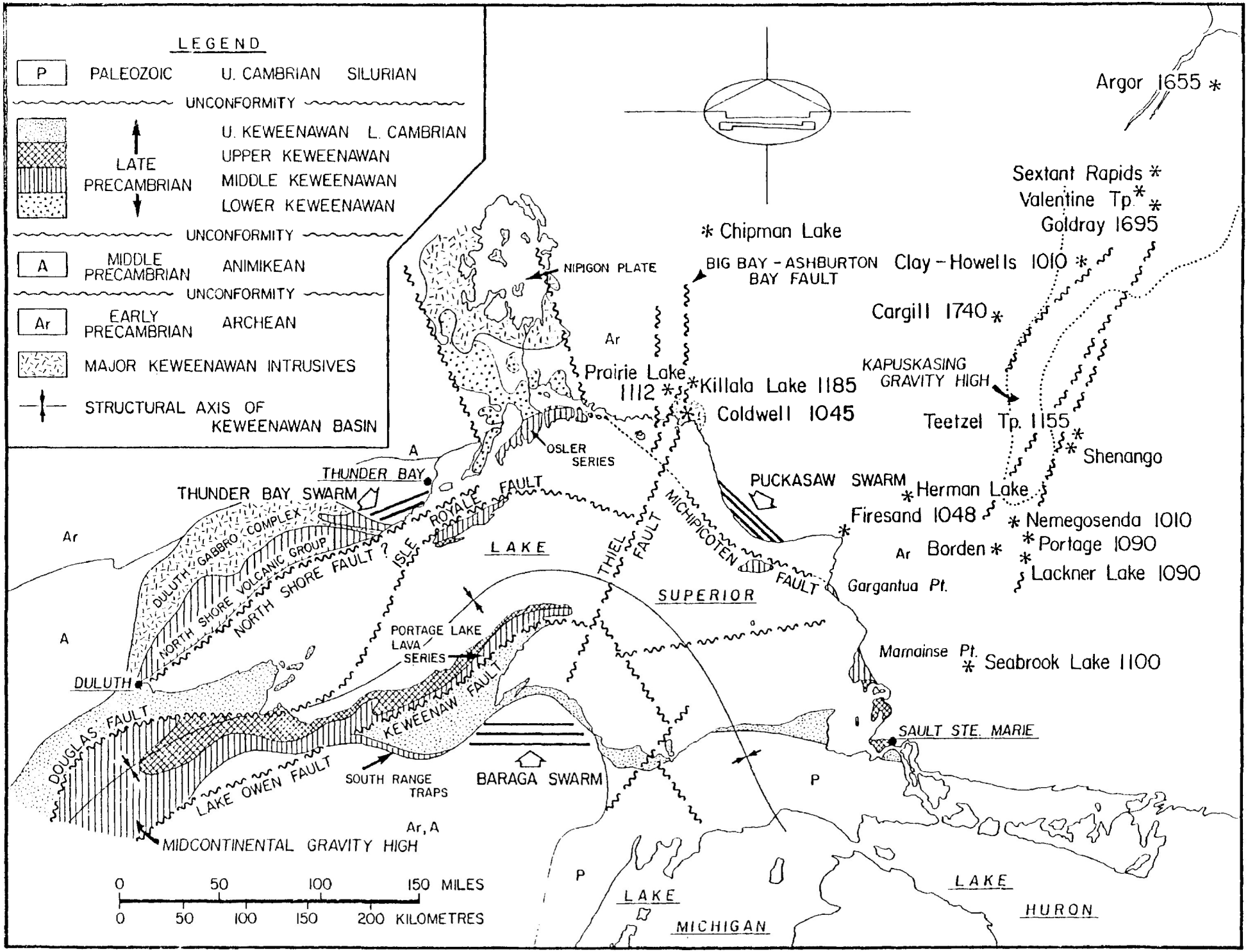

Figure 1 - Tectonic setting of the Lake Superior Basin.
Drafted by S.Spivak.

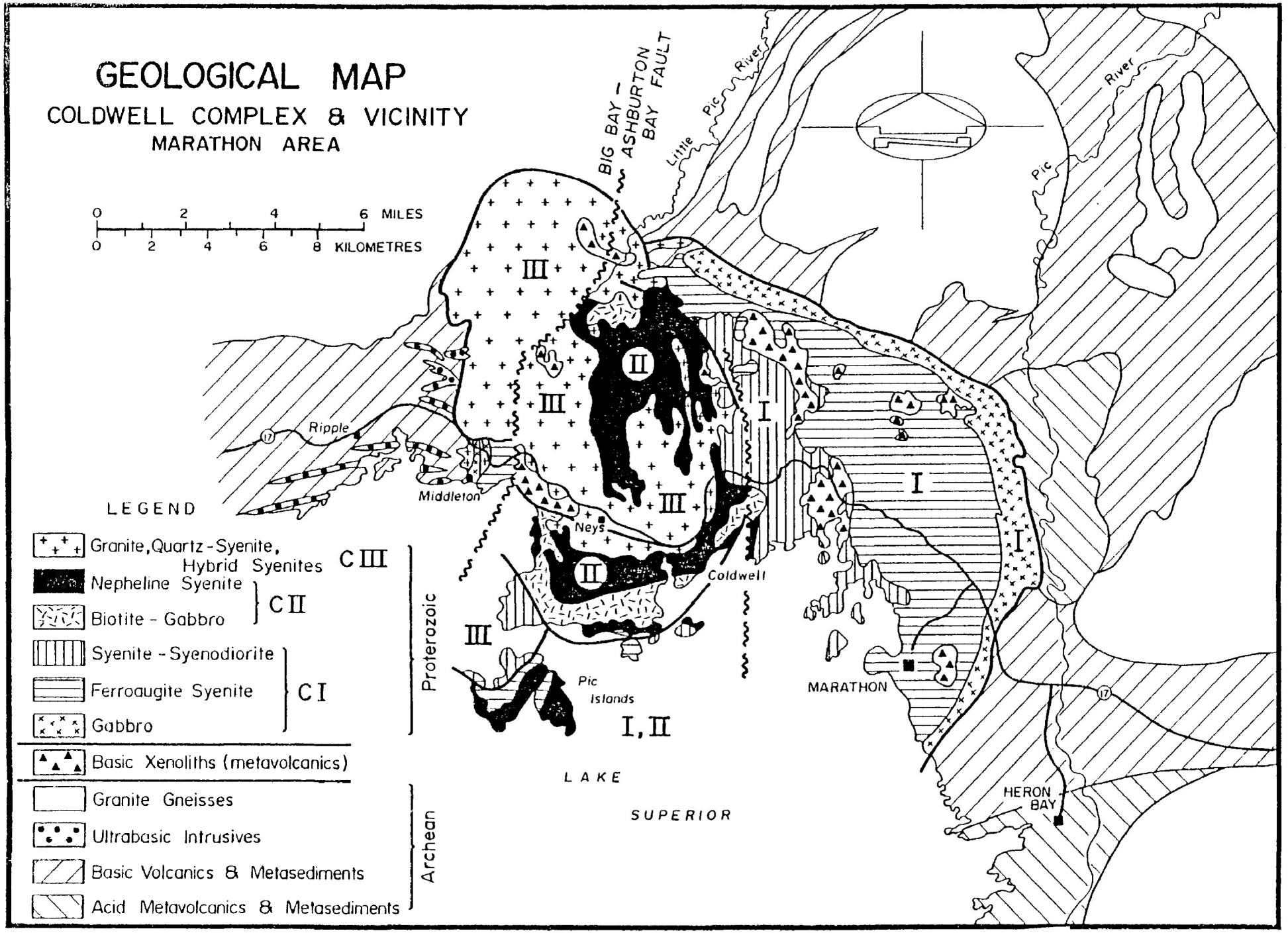

Figure 2 - Geological map of the Coldwell Alkaline Complex.
Drafted by S Spivak.

Midcontinent Rift System. This zone is greater than 1000 km in length, trending from central Wisconsin northward to Hudson Bay. The zone is characterized by the presence of faulting, alkalic intrusive rocks and diatremes. In the vicinity of the study area this tectonic zone has been termed the Big Bay-Ashburton Bay Fault Zone (Sage, 1978a,b) and is approximately 30 km wide. A second fault, trending northeast through the region is the Thiel Fault, which is coincident with a major lineament and a zone of extreme crustal thickening. Klasner et al., (1982) suggests that faults controlled the emplacement of at least four diatremes, several alkalic-carbonatite complexes and intrusions, during the period 1185 Ma to 300 Ma.

The age of the Coldwell Alkaline Complex has been determined by K-Ar, U-Pb and whole rock Rb-Sr methods. Chaudhuri et al. (1971) reported an age of 1052±15 Ma, obtained from whole rock and mineral samples by Rb/Sr methods. Currie (1976) sampled biotite from a gabbro and a syenite and determined K-Ar ages of 1005 and 1015 Ma, respectively. Further Rb/Sr geochronology on Coldwell rocks was reported on by Bell et al. (1979) and Blenkinsop and Bell (1980). They determined an age of 1070±15 Ma for the complex, utilizing a five-point whole rock isochron. Research by Platt and Mitchell (1982) has concluded that the age of the complex is 1044.5± 6.2 Ma, based on a seventeen-point whole rock isochron. The late Neohelikian age indicates that the Coldwell Complex was emplaced after the major period of Keweenawan igneous activity in the Lake Superior basin. Recent U-Pb geochronological investigations by Heaman and Machado (1987) indicate that the Coldwell rocks were emplaced 1108±1 Ma ago. Preliminary research by Heaman and Machado (1987) indicates that quartz syenites from the western portion of the complex have a zircon U/Pb age which is about ten million years younger than those in the central and

eastern zones.

1.3 Historical Overview of Centre III Syenites

The earliest published report, dealing with the suite of rocks which has subsequently become known as Centre III, is by Kerr (1910). Between Port Coldwell and Middleton, Kerr referred to frequent gradations between a red hornblende syenite and a dark augite syenite. This description may correspond to Centre III syenites, but because exact locations were not given, it cannot be confirmed. Kerr also reported on the occurrence of dark greenish grey quartz syenites, in this region, containing abundant microperthite and quartz, along with hornblende, augite and iron oxide. Quartz syenite from the northwest part of Pic Island and Guse Point is red and pink to brown and grey. The porphyritic feldspars are set in a fine- to medium-grained groundmass. These feldspars are microperthitic, with a variable proportion of albite to orthoclase. Kerr reported that the other minerals observed are quartz, hornblende, biotite, magnetite, leucoxene, pyrite, hematite, fluorite, apatite and calcite. A brief mention is made of an eruptive breccia, east of the Little Pic River, along the railway, in which angular blocks of a basic rock are brecciated by acid eruptives. Kerr stated that the quartz syenites are younger than the red hornblende syenites, but erroneously placed the nepheline syenites as the youngest rocks of the complex.

After a long hiatus, Walker (1967) published a report and map on the Jackfish-Middleton area. He dealt with the western margin of the complex, as well as the country rocks. From the western part of the Coldwell complex he described a red, medium-grained to coarse-grained syenite with abundant perthite and noted that some portions contain five percent myrmekitic and graphic quartz. This syenite also contains dark brown

hornblende and reddish-brown biotite. On the highway north of Middleton, he described the occurrence of porphyritic syenite, intruding the previously mentioned red syenite.

In the same year, 1967, Puskas investigated the geology of the Port Coldwell area. He suggested that the Little Pic River granite has intruded the northwestern portion of the complex. He noted the presence of inclusions or xenoliths in this granite, as well as hybridized phases. Evidence was presented for a thermal aureole, overprinting the regional metamorphism, affecting the volcanic and sedimentary country rocks around the complex.

Card et al. (1972) discussed the tectonics of the Lake Superior Basin, which they suggested may be a major rift. Cross-cutting the main structure is a NNE-trending fault south of Coldwell, exhibiting lateral offset (Figure 1). Card et al., (1972) suggest a link between the Coldwell Complex and the formation of the Lake Superior Basin, related volcanism and other mafic intrusions.

In the I.G.C. field trip guidebook (Baer et al., 1972) brief mention is made of quartz syenites from the Little Pic River area. At the Neys Lookout, the guide describes a breccia of fine-grained, hornfelsed, metavolcanic rock in a red, quartz- and amphibole-bearing syenite. It is suggested that the volcanic rocks represent a portion of a roof pendant.

Billings (1974) prepared a government report on the Quaternary geology of the Neys Provincial Park area. From Guse Point he described saturated syenodiorite and nordmarkites, and an aphanitic to fine-grained nordmarkite. On Pic Island, South Bay's eastern shore exposes red syenites.

In "The Alkaline Rocks of Canada", Currie (1976) generalized the structure and lithologies of the Coldwell Complex. He mentioned the

presence of a significant roof remnant in the centre of the complex, consisting of syenites and quartz syenites.

In his major report of 1980, Currie devoted a small segment to quartz-saturated and over-saturated syenites. He suggested that desilication of country rocks raised the melting temperatures of syenites, above those of the original granitic compositions. Thus the quartz-bearing syenites would appear intrusive into, and younger than, metasomatized syenitic rocks. He alluded to the complexities arising in the relationships between quartz-rich syenites.

Sage (1978a,b) discussed regional structures of the Lake Superior Basin. Trending northward from the basin, Sage termed the 30 km-wide fault the Big Bay-Ashburton Bay fault zone. A northeast-trending fault, coincident with a major lineament which bisects Lake Superior, is termed the Thiel Fault. These two faults have been incorporated in the tectonic and geologic maps of Figures 1 and 2.

Jago (1980) studied a portion of the Western Contact Zone of the complex, as an undergraduate research topic. He mapped the zone and conducted petrographic and mineralogical studies of the syenites and quartz syenites of this area. He determined that a red to purple, porphyritic quartz syenite is the earliest phase of the over-saturated magmatism. This syenite hosts variously digested xenoliths of metasomatized volcanic rocks, which contaminated the host syenite. This rock is in turn intruded by three varieties of a medium- to coarse-grained, yellow to red quartz syenite. Dilation and block stoping of the xenolith-bearing syenite resulted in a chaotic mixture of quartz syenites and volcanic blocks. "Lit-par-lit" injections into the country rock and intrusive breccias with the Archean rocks were mapped by Jago.

1.4 General Geology

Mitchell and Platt (1978a) have divided the complex into three intrusive magmatic episodes. Each may be identified by a characteristic differentiation trend. From earliest to latest they are: Centre I-saturated alkaline rocks with peralkaline oversaturated residua; Centre II-miaskitic undersaturated alkaline rocks; and Centre III-alkaline rocks with oversaturated residua.

Centre I is the oldest unit of the complex, and consists of border gabbro, intruded by a ferro-augite syenite. The gabbro occurs in a ring-shaped body forming the eastern and northern margin of the intrusion. The ferro-augite syenite differentiates to peralkaline, iron-rich, quartz-bearing residua. Fayalite, aenigmatite, ferro-richterite and ferro-edenite are characteristic minerals of the ferro-augite syenites (Mitchell and Platt, 1978).

The biotite-bearing gabbro of the Coldwell Peninsula represents the earliest phase of Centre II activity. It consists of biotite, olivine, plagioclase, nepheline and amphibole, and has incorporated xenoliths of mafic volcanic rocks. These gabbros are intruded and metasomatized by Centre II nepheline syenites. They are exposed on Pic Island, the Coldwell Peninsula and Red Sucker Cove area, and east of the Killala Lake road. These leucratic to melanocratic nepheline syenites contain olivine, pyroxene, biotite, natrolite, titanomagnetite, apatite, zeolite, fluorite, zircon, sphene, and sodalite (Mitchell and Platt, 1982b).

Centre III magmatism is characterized by silica saturated and silica over-saturated alkali feldspar syenites. For the sake of brevity they are hereafter referred to as syenites and quartz syenites. Rocks of this intrusive episode are exposed in three main areas: Pic Island/Guse Point; north of the Coldwell Peninsula between the Killala Lake road and the

Little Pic River; and in the Western Contact Zone, at the west margin of the complex. The syenites and quartz syenites are characterized by the presence of sodic amphiboles, fluorite, zircons and braid perthites. Xenoliths of country rock hornfels, Archean volcanics, coeval oligoclase basalts and genetically related syenites are commonly observed. Earlier syenites are veined and brecciated by later syenites, indicating that several episodes of intrusion have occurred (Mitchell and Platt, 1982a).

The dike rocks cutting the complex and the surrounding country rocks include: mafic ocellar lamprophyres; quartz-bearing mafic lamprophyres; sannaite-type lamprophyres;monchiquitic lamprophyres; feldspar glomeroporphyry and alkali basalt dikes; and analcime tinguaites. All of these dikes cut rocks of the Centre I and Centre II episodes, but not those of Centre III. Some felsic dikes, perhaps related to the Centre III magmatism, have been observed cutting Centre III syenites (Mitchell and Platt, 1982a).

The structure of the complex is as yet poorly known. Recent investigations by Currie (1980), of the Geological Survey of Canada, and Mitchell and Platt (1978, 1982a,b) propose that several episodes of magmatism were involved in the formation of the complex. They postulate that the magmas were emplaced by cauldron subsidence, as evidenced by the occurrence of concentric marginal intrusions and down-faulted, partially assimilated remnants of the capping lavas. Mitchell and Platt (1982a) suggest that each magmatic centre was the focus of a particular cauldron subsidence event and that the activity migrated in a westerly direction. In Figure 2, approximate margins for each centre are outlined. Post-intrusive block faulting has complicated the original structures considerably. The central portions of the complex are rich in xenoliths, possibly representing a higher structural level than the eastern or

western xenolith-poor portions. Mitchell and Platt consider this central portion to be a down-faulted block, bordered by the Little Pic River Fault (Big Bay-Ashburton Fault) and the Redsucker Cove Fault Zone (Thiel Fault). Major lineaments are emphasized by the rugged topography of this region. The major lineament trends are: northwest and north, with fewer east and northeast orientations.

A gravity study by Mitchell et al. (1983) reveals that the complex is associated with a positive gravity anomaly. This indicates that a significant volume of dense material occurs below the current levels of exposure, of principally felsic rocks. A gravity profile, used to model the infrastructure of the complex, shows that the felsic rocks form a three to five kilometre thick layer over a differentiated basic intrusion. This is interpreted to consist of a 4 km thick layer of gabbro underlain by peridotite and/or pyroxenite (also approx. 4 km thick).

The focus of this thesis is the characterization of the Centre III syenites and quartz syenites. To this end, geology, petrography and mineral chemistry have been used to distinguish between the various types of syenite. Mineral composition trends for Centre III rocks are compared to those of Centre I and II. Major and minor element whole rock chemistry helps to characterize further the full spectrum of Centre III syenites.

GENERAL GEOLOGY OF THE CENTRE III SYENITES

2.1 Scope of Study

The purpose of this study is to classify and describe the silica-saturated and silica-oversaturated syenites of Centre III. In the field, geological relationships were investigated in detail, and approximately 250 specimens were collected. The mineralogy and textures of many of these specimens were determined petrographically. Based upon thin-section observations, the lithological types were determined, and approximately 85 representative, unaltered specimens were utilized in a microprobe study of mineral chemistry. Selected whole rock analyses were performed to characterize further the lithologies.

2.2 Method of Field Investigation

Rugged topography and mature thick forests preclude traverses away from the highway, roads, railway, powerlines and shorelines. Outcrops are scarce away from these features, and if present, are small, weathered and flat, making sampling and general observations difficult. Systematic geological mapping is impossible, instead relatively linear traverses were carried out, along the best exposures. Rock cuts along the highway, roads and railway provided fresh, unweathered exposures. These man-made features, as well as the Lake Superior shoreline, trend approximately east-west; for this reason most geological traverses were similarly oriented. In many areas, the study of lithological relationships was aided by the existence of very long roadcuts and outcrops, continuous or nearly so, commonly for hundreds of metres. The lack of exposures extending north and south from these good outcrops made it difficult to ascertain the size and morphology of individual syenite intrusions.

Contacts between the main Centre III syenite types may be sharp, unexposed or, as is commonly the case, gradational. Several pulses of magma from the same episode may be injected into a relatively restricted area, giving rise to complex intercalations of intrusions. Minor mineralogical and textural changes in each successive batch of magma give rise to an apparent plethora of syenites. Slight variations in alteration also add to this complexity. Most of the distinguishing mineralogical and textural characteristics are not macroscopically visible. Two specimens that appear to be identical in the field, may turn out to be vastly different syenites. The converse is also true, two macroscopically dissimilar specimens can belong to the same syenite type. For all these reasons, the Centre III syenites cannot be mapped in the field. Thus petrographic study and mineral chemistry are necessary for lithological determination.

2.3 Lithologies

Four syenite types can be recognized as belonging to Centre III magmatism. Based on petrographic study, mineralogical and textural considerations were used in the definition of the four syenite types. All four types are alkali feldspar syenites, with varying proportions of quartz. In order to convey the main differences between these types, descriptive mineralogical names are adopted. They are magnesio-hornblende syenite, ferro-edenite syenite, contaminated ferro-edenite syenite and quartz syenite. The following lithologic descriptions are based on field observations of macroscopic features. Photographs of polished handspecimens are presented in Plate 1. Figures 3 to 8 are sample location maps. Figures 9 to 12 are geological sketch maps that serve to illustrate the complex intrusional relationships between the syenites.

Plate 1 - Polished rock slabs of four Centre III syenite types. Slab on top left measures approx. 3 cm wide.

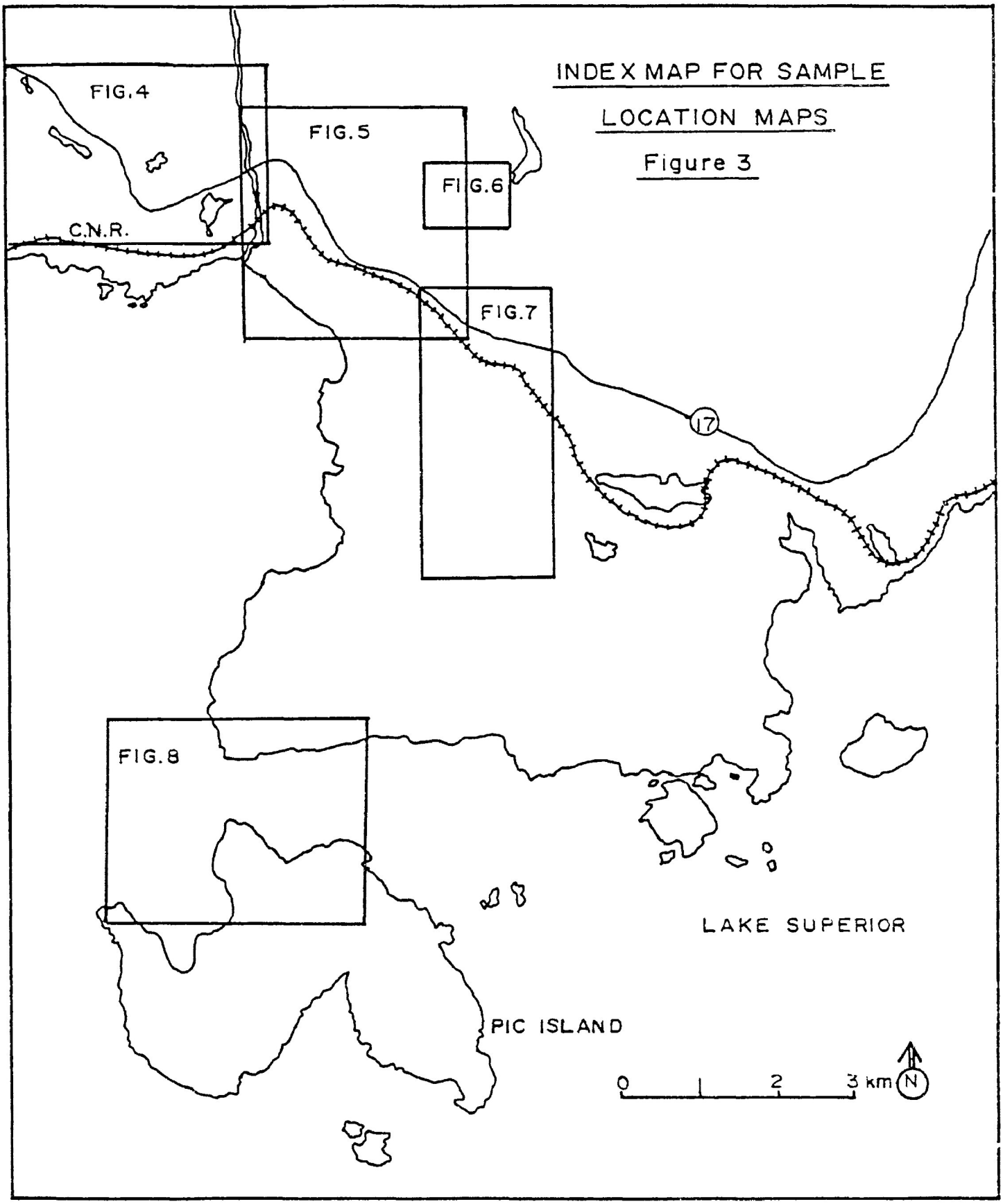
INDEX MAP FOR SAMPLE
LOCATION MAPS
Figure 3
FIG.4
FIG.5
FIG.6
FIG.7
FIG.8
C.N.R.
17
LAKE SUPERIOR
PIC ISLAND
0
2
3 km
N

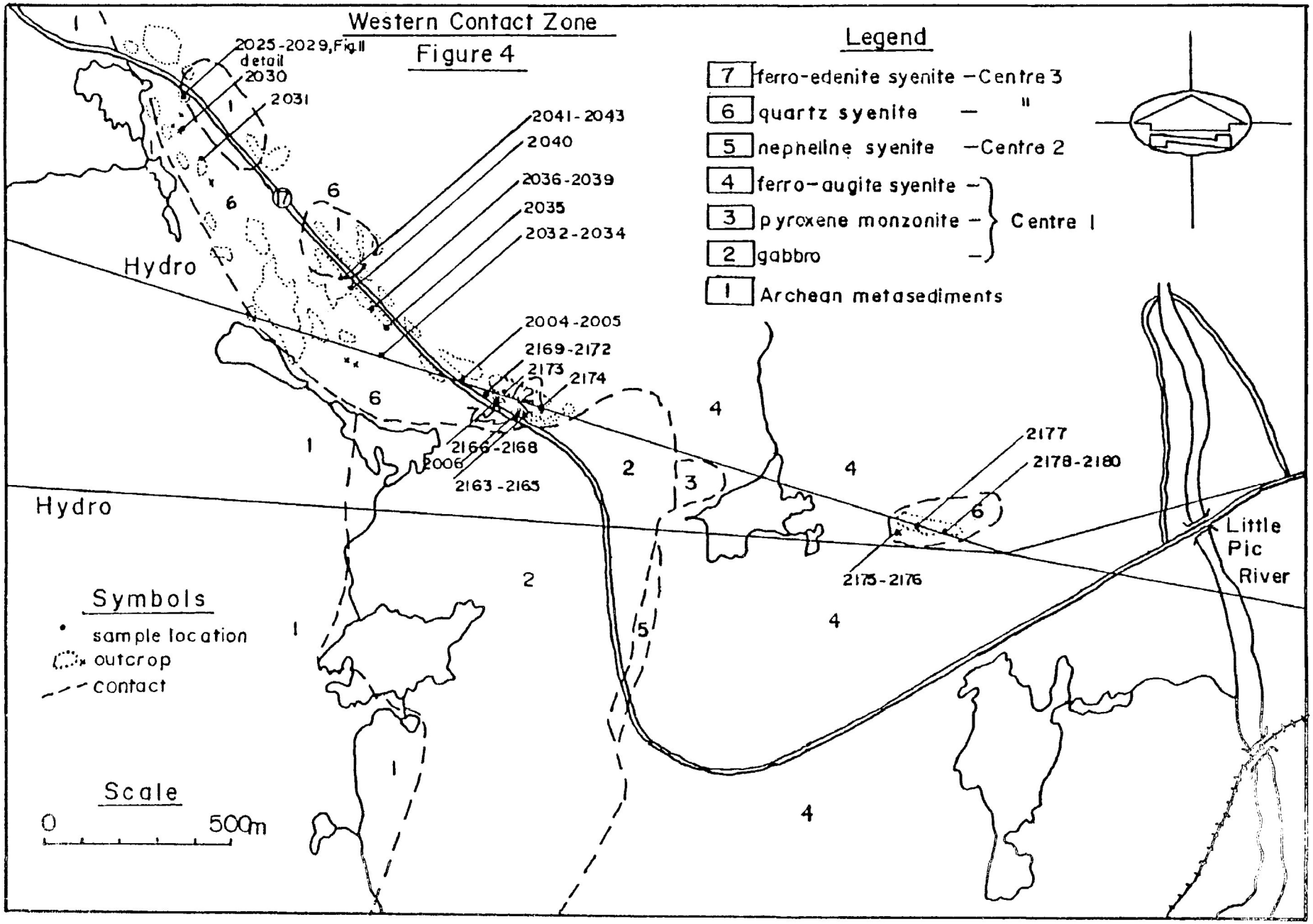
Western Contact Zone
Figure 4
Legend
7 ferro-edenite syenite – Centre 3
6 quartz syenite – "
5 nepheline syenite – Centre 2
4 ferro-augite syenite –
3 pyroxene monzonite – Centre 1
2 gabbro –
1 Archean metasediments
2025-2029, Fig II detail
2030
2031
2041-2043
2040
2036-2039
2035
2032-2034
2004-2005
2169-2172
2173
2174
2166-2168
2006
2163-2165
2177
2178-2180
2175-2176
Hydro
Hydro
Little Pic River
Symbols
sample location
outcrop
contact
Scale
0
500m

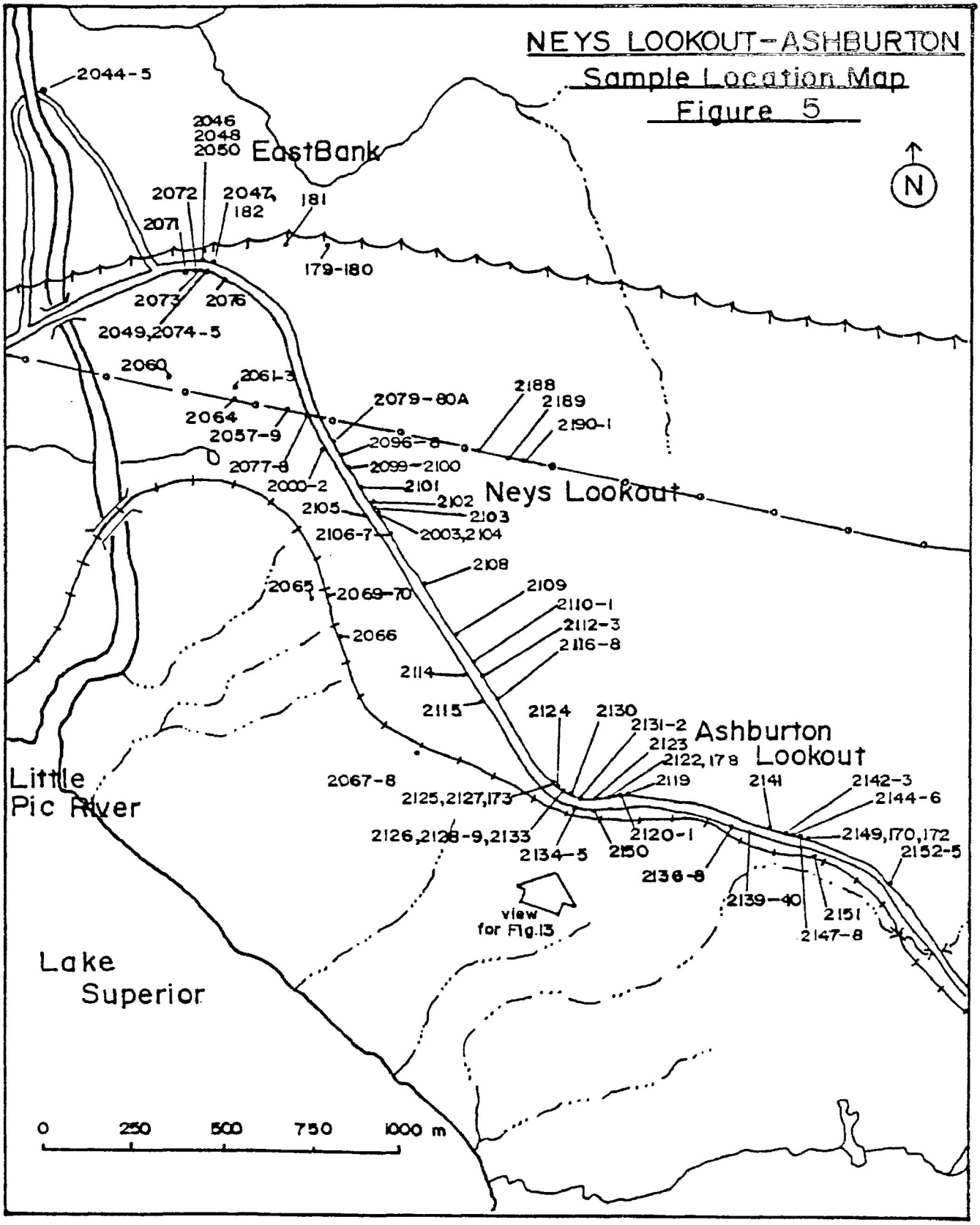
NEYS LOOKOUT-ASHBURTON
Sample Location Map
Figure 5
N
2044-5
2046
2048
2050
EastBank
2072
2047
182
181
2071
179-180
2073
2076
2049,2074-5
2060
2061-3
2064
2057-9
2079-80A
2188
2189
2190-1
2096-8
2077-8
2099-2100
2000-2
2101
2102
Neys Lookout
2105
2103
2106-7
2003,2104
2108
2065
2069-70
2109
2110-1
2112-3
2116-8
2066
2114
2115
2124
2130
2131-2
2123
Ashburton
Lookout
2122,178
2119
2141
2142-3
2144-6
Little
Pic River
2067-8
2125,2127,173
2126,2128-9,2133
2134-5
2150
2120-1
2149,170,172
2152-5
2136-8
2139-40
2151
2147-8
view
for Fig.13
Lake
Superior
0
250
500
750
1000 m

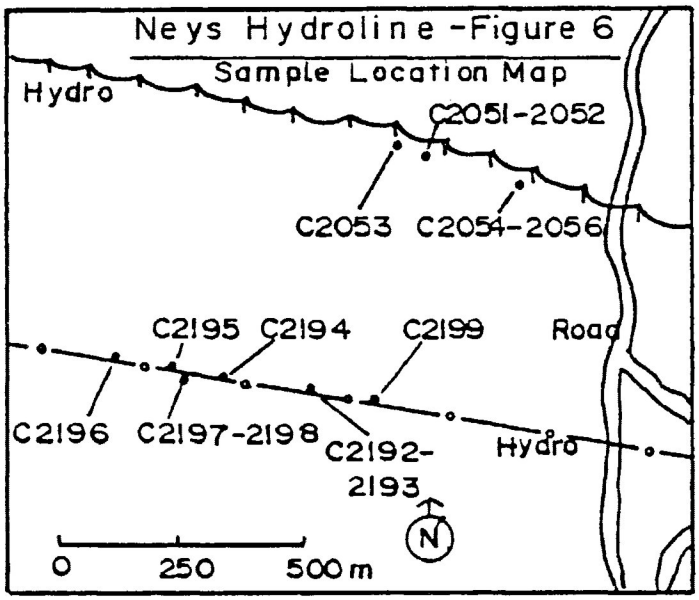
Neys Hydroline -Figure 6
Sample Location Map
Hydro
C2051-2052
C2053
C2054-2056
C2195
C2194
C2199
Road
C2196
C2197-2198
C2192-
2193
Hydro
N
0
250
500 m

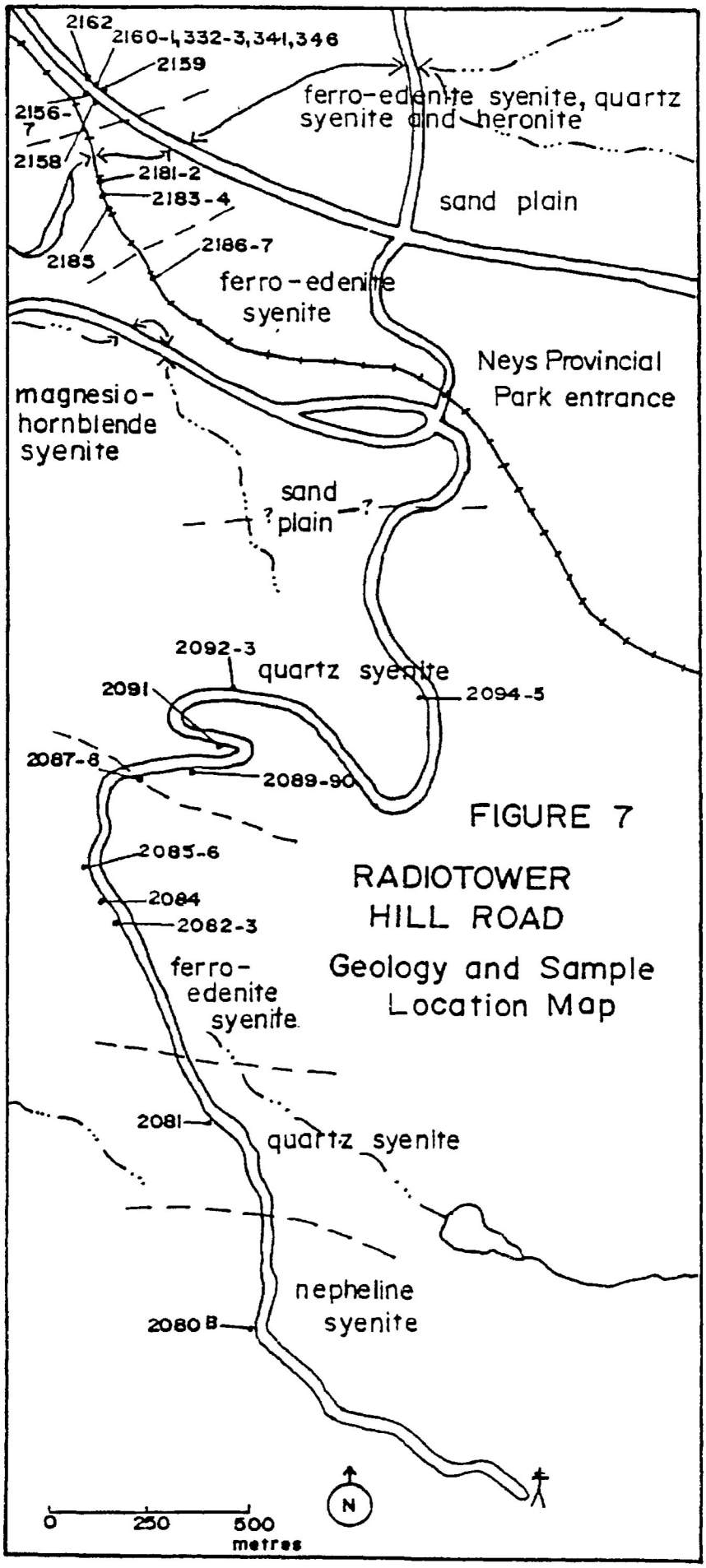

FIGURE 7

RADIOTOWER HILL ROAD

Geology and Sample Location Map

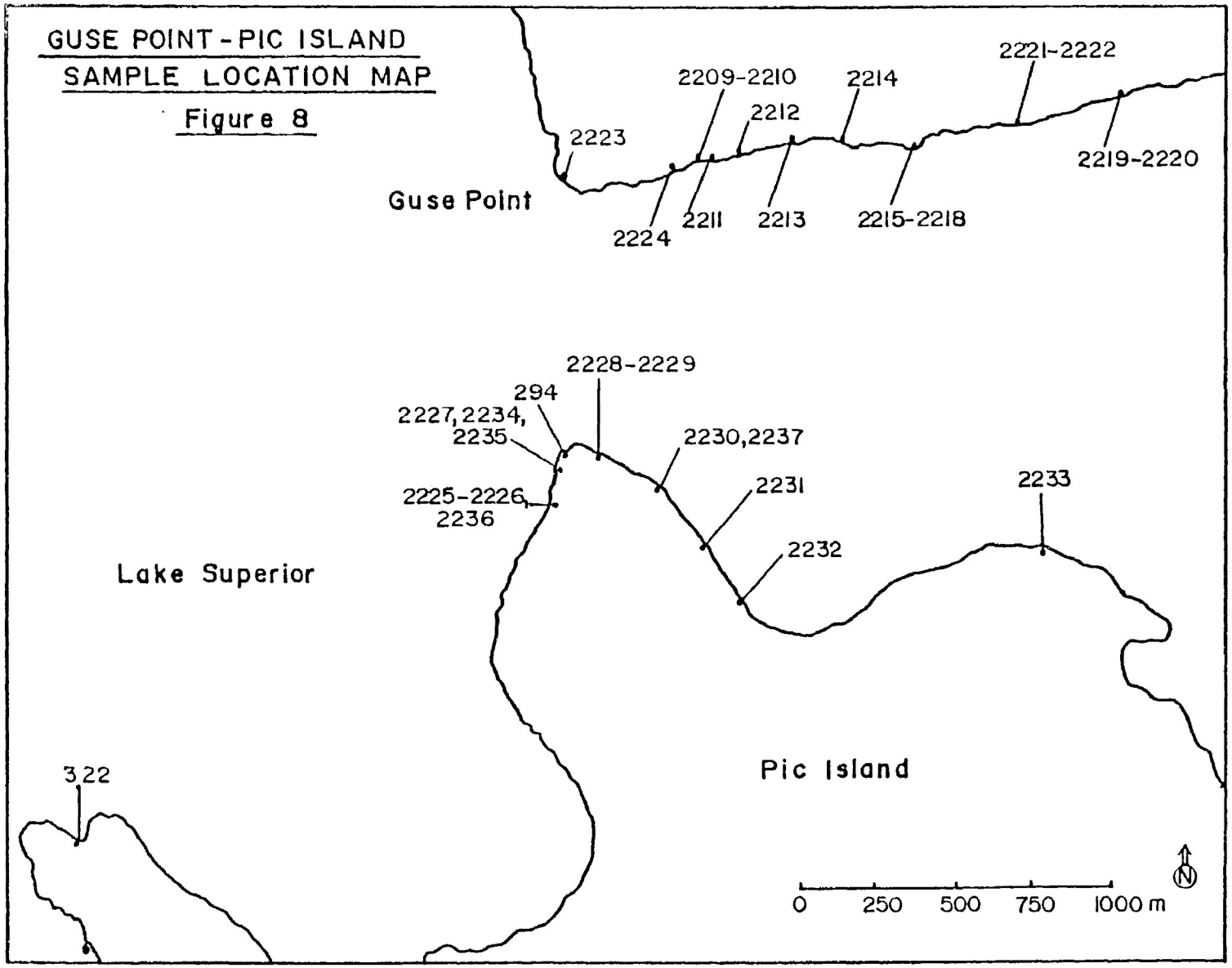
GUSE POINT - PIC ISLAND
SAMPLE LOCATION MAP
Figure 8
2221-2222
2209-2210
2214
2212
2223
2219-2220
Guse Point
2224
2211
2213
2215-2218
2228-2229
294
2227, 2234,
2235
2230, 2237
2231
2225-2226,
2236
2233
2232
Lake Superior
3,22
Pic Island
0
250
500
750
1000 m
N

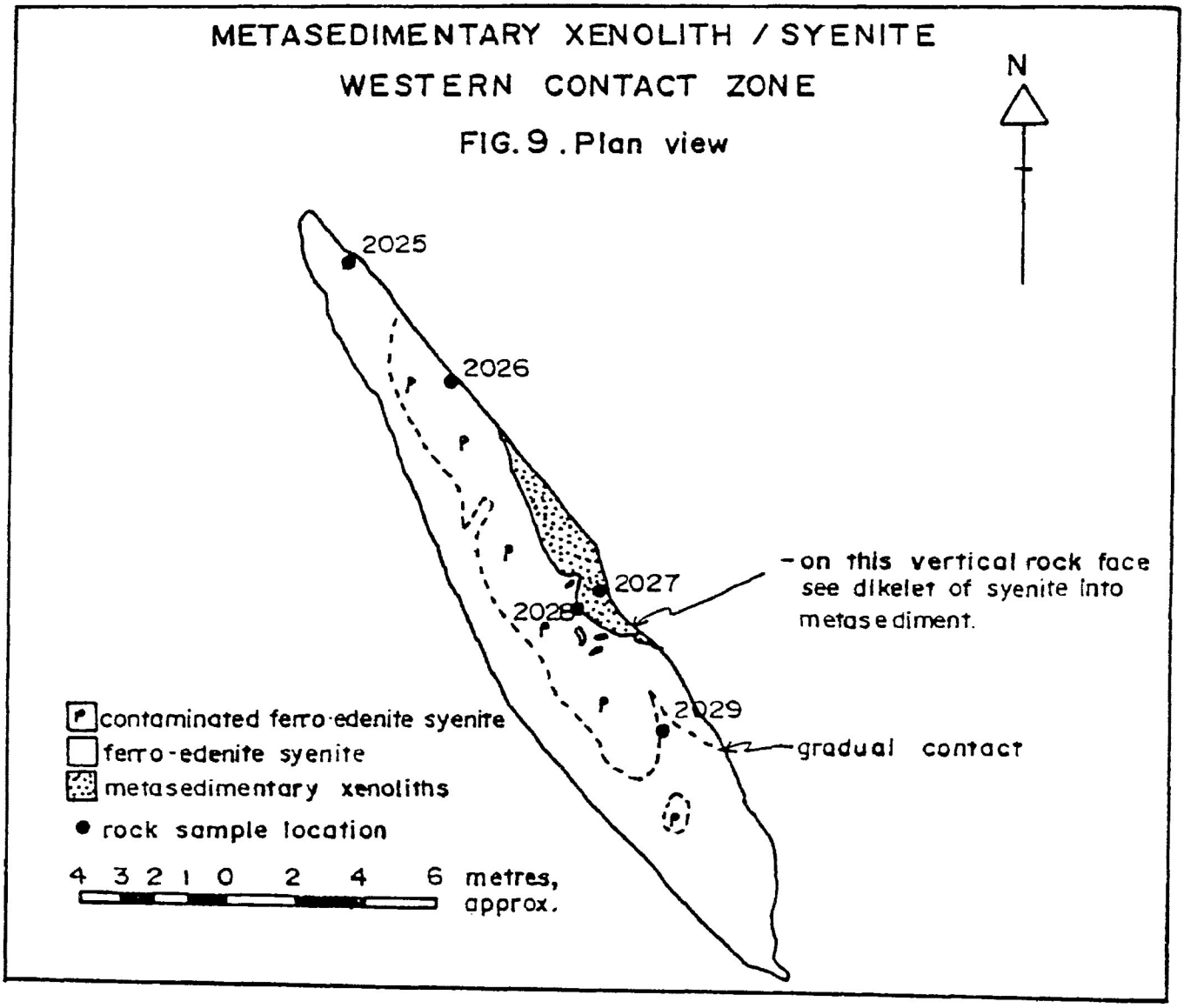
METASEDIMENTARY XENOLITH / SYENITE
WESTERN CONTACT ZONE
FIG. 9. Plan view
N
2025
2026
2027
2028
2029
on this vertical rock face see dikelet of syenite into metasediment.
gradual contact
contaminated ferro-edenite syenite
ferro-edenite syenite
metasedimentary xenoliths
rock sample location
4 3 2 1 0 2 4 6 metres, approx.

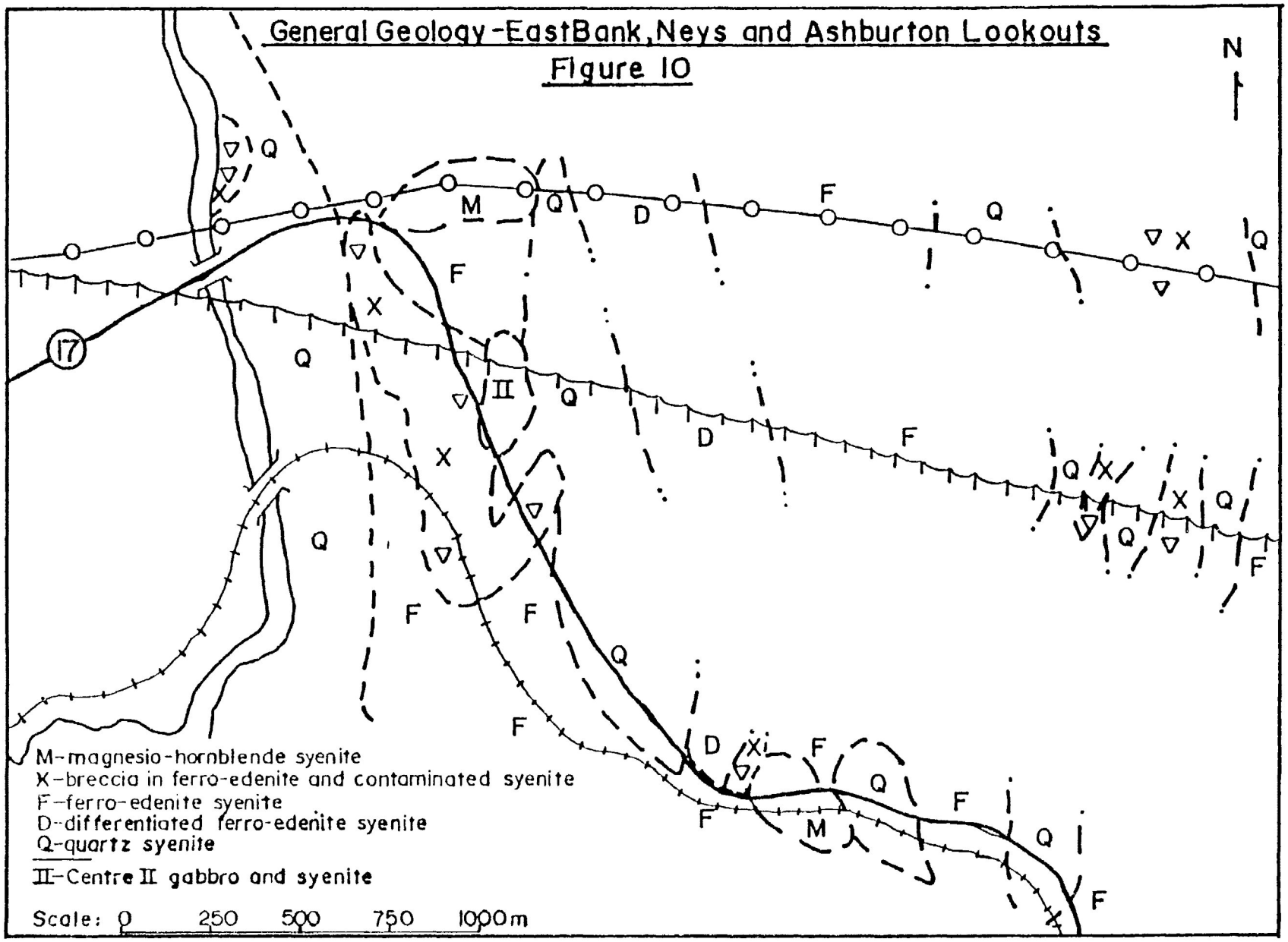
General Geology - EastBank, Neys and Ashburton Lookouts
Figure 10
N
17
M - magnesio-hornblende syenite
X - breccia in ferro-edenite and contaminated syenite
F - ferro-edenite syenite
D - differentiated ferro-edenite syenite
Q - quartz syenite
II - Centre II gabbro and syenite
Scale: 0 250 500 750 1000m

GEOLOGICAL SKETCH
ASHBURTON LOOKOUT ROADCUT

Fig.11. Cross-section looking north

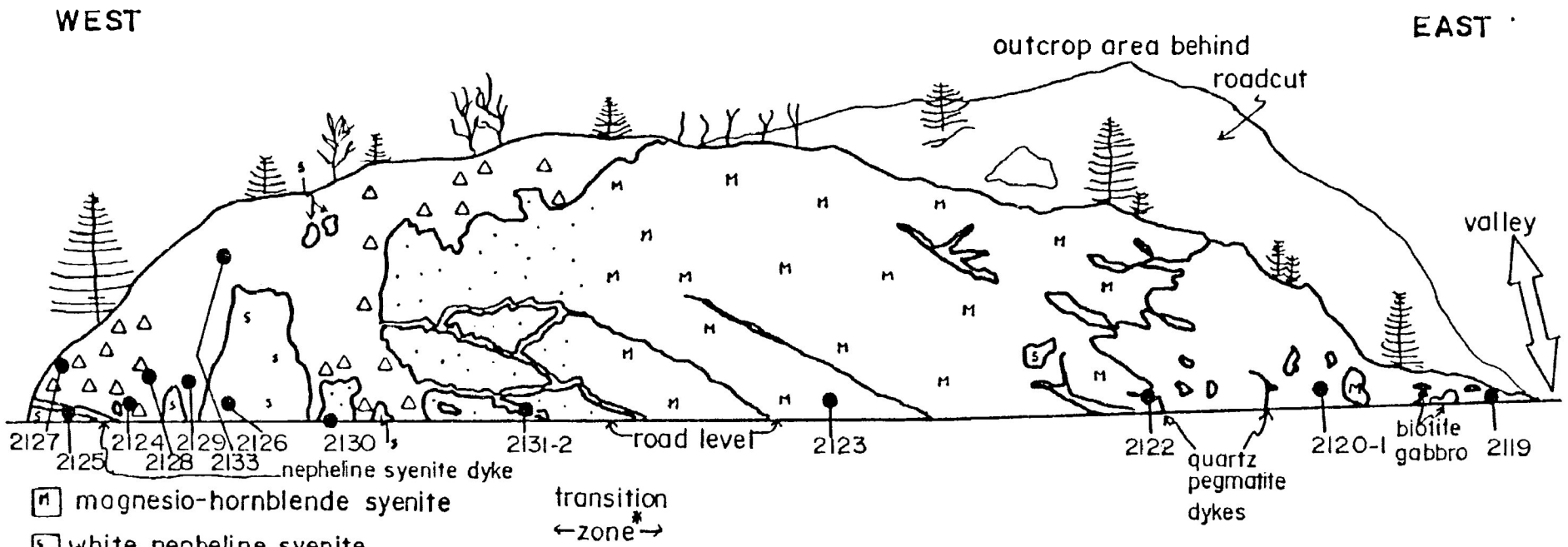

*Somewhat obscured due to weathering on broad joint surfaces. Road slopes slightly downward, to the east.

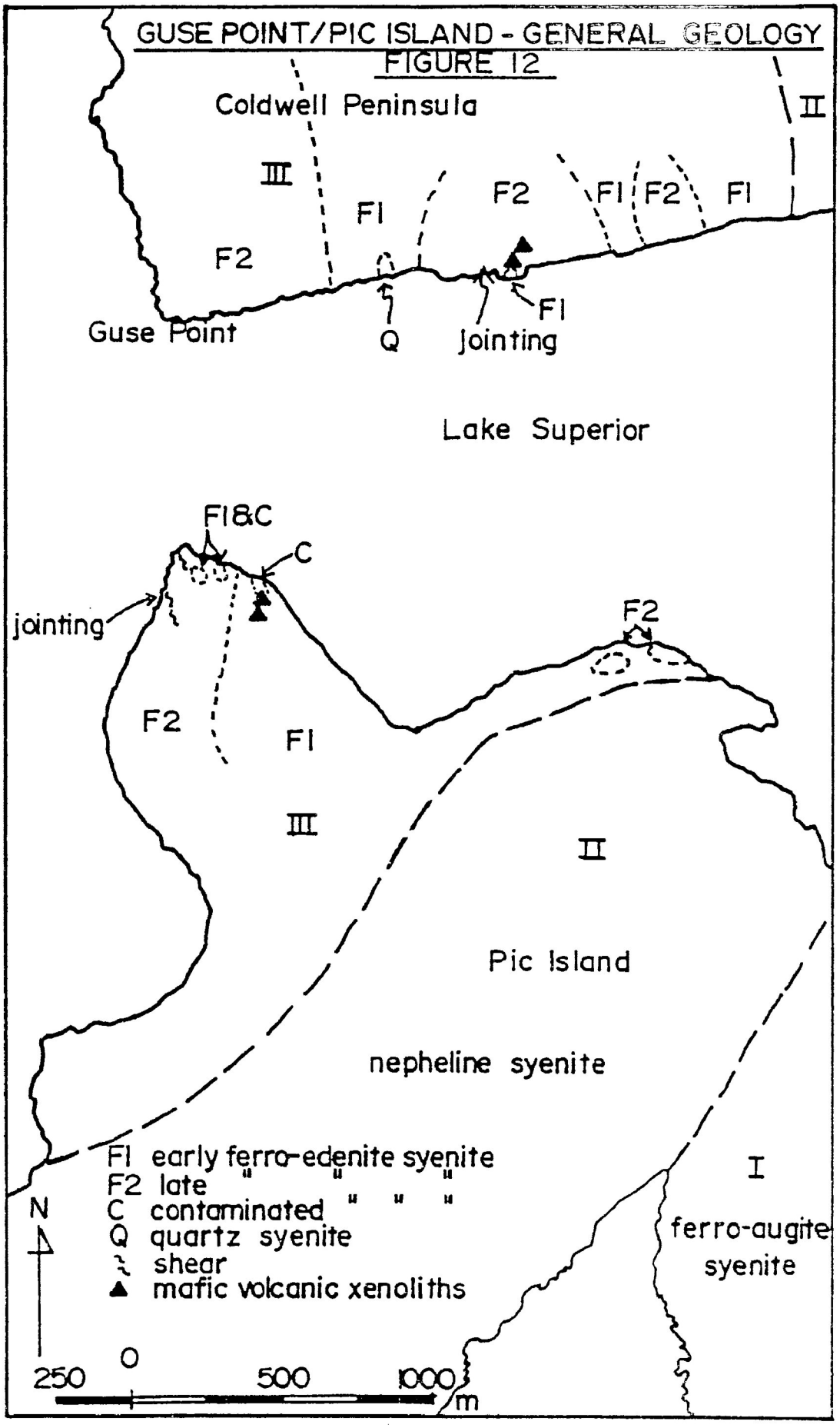
GUSE POINT/PIC ISLAND - GENERAL GEOLOGY
FIGURE 12
Coldwell Peninsula
III
II
F1
F2
F1
F2
F1
F2
F1
Guse Point
Q
Jointing
F1
Lake Superior
F1&C
C
jointing
F2
F2
F1
III
II
Pic Island
nepheline syenite
I
ferro-augite syenite
F1 early ferro-edenite syenite
F2 late " " "
C contaminated " " "
Q quartz syenite
shear
mafic volcanic xenoliths
N
250
0
500
1000
m

Description of Figures 9-12 is given in section 2-4. Additional descriptions of each syenite, based on petrographic study, are given in Chapter 3.

2.3.1 Magnesio-hornblende syenite

The magnesio-hornblende syenites have a limited distribution and form small bodies of undefined size and shape. Three main exposures include: powerline outcrops near the east bank of the Little Pic River (Figure 10); the large road-cut at Ashburton Lookout (Figures 10 and 11); and railway cuts in the vicinity of the Neys Provincial Park entrance (Figure 7). Contacts with other syenites are rarely observed. At Ashburton Lookout the magnesio-hornblende syenite grades into hypabyssal mafic-intermediate rocks towards the west. To the east, the magnesio-hornblende syenite exhibits a sharp contact against ferro-edenite syenite. The presence of magnesio-hornblende syenite xenoliths in the ferro-edenite syenite indicates that the former predates the latter. Dikes of ferro-edenite syenite also intrude the magnesio-hornblende syenite.

A distinctive feature of the magnesio-hornblende syenite is a synneusis texture involving the mafic minerals. The majority of the mafic minerals, with an average abundance of 45%, crystallized in massive or radiating clusters, resembling flowers. This imparts a spotted appearance to the rock. The syenite is pink or red with black or dark green aggregates of mafic minerals. From a distance, the fresh surface is pinkish-grey, dark greenish-grey or dark grey. The rock is fine- to medium-grained, with an allotriomorphic texture. Variably hematized anhedral alkali feldspar is the dominent felsic mineral, constituting 35-80% of the rock. Tabular alkali feldspar phenocrysts may be rarely observed, set in a groundmass of subhedral feldspars. Quartz is generally

not visible. In the mafic clusters black biotite and black or green amphibole can be distinguished. The magnesio-hornblende syenite is generally moderately magnetic. Minor alteration of mafic minerals and feldspar is rarely observed.

2.3.2 Ferro-edenite syenite series

Ferro-edenite syenites are widespread and represent products of a differentiating, evolving, silica-oversaturated magma. Some ferro-edenite syenites contain alkaline basalt xenoliths or country rock enclaves (section 2.3.2.iii). Away from the breccia zones, highly evolved quartz-rich ferro-edenite syenites form significant intrusive bodies (section 2.3.2.ii). As described in the following section, most ferro-edenite syenites contain few or no xenoliths.

2.3.2.i. Ferro-edenite syenite

The ferro-edenite syenite ranges from light pink to orangy-pink to red, when the alkali feldspar is variably hematized, and is white, yellow or buff when the feldspars are unaltered. Typically, the syenite is fine- to medium-grained with medium-grained alkali feldspar phenocrysts. Most phenocrysts are euhedral, tabular and average 5 mm in length. Coarse-grained alkali feldspar phenocrysts are infrequent. The ubiquitous perthitic texture of all feldspars is visible on a microscopic scale, in all but the coarsest phenocrysts (Chapter 3). Rarely a trachytic texture involving both groundmass and feldspar phenocrysts is observed. Mantled alkali feldspar grains are common and are evident from a concentric pattern of varying degrees of hematization. Perthitic exsolution textures also vary from the core of a phenocryst, to the outer rim, but this is generally not macroscopically discernable. The alkali feldspar of the

groundmass commonly displays an allotriomorphic texture. Petrographic study, however, indicates that with increasing differentiation idiomorphic feldspars become dominant (Chapter 3). Altogether 80% to 95% of the ferro-edenite syenite consists of alkali feldspar.

A few percent of fine-grained mafic minerals are always present and amphibole is ubiquitous. Biotite is rarely identified in hand specimens. The mafic minerals crystallized as intergranular grains or small mixed aggregates. One or two percent quartz may be observed macroscopically, as clear, colourless or grey, intergranular grains. Calcite was detected, by means of an acid text, in a small proportion of the ferro-edenite syenite specimens. Traces of molybdenite are found in a few exposures, where it is disseminated in the groundmass, or occurs with biotite along fractures. The ferro-edenite syenite is typically non-magnetic.

2.3.2.ii. Differentiated and pegmatitic ferro-edenite syenite

The more highly evolved varieties of ferro-edenite syenite form substantial intrusions away from the breccia zones, or occur as small intrusions or dikes through the xenolith-bearing syenite. The evolved syenites are free of enclaves and generally differ in having greater contents of quartz. These syenites are predominantly medium-grained and porphyritic, with minor coarse-grained equivalents. The rock is commonly pink or red, although unhematized varieties are white or buff. Randomly oriented perthitic phenocrysts of alkali feldspar may or may not be mantled by perthitic alkali feldspar. The phenocrysts are tabular and range in habit from subhedral to euhedral. Visible interstitial quartz varies from close to nil to approximately 10%. With increasing quartz content, the alkali feldspar crystals approach an idiomorphic texture. Graphic intergrowths of perthite and quartz may be visible on a

macroscopic scale, particularly in the vicinity of Ashburton Lookout. The accessory mafic constituents are usually fine-grained to very fine-grained. Biotite and amphibole concentrations average about 5% and these minerals form very small intergranular clusters.

Where this syenite forms small intrusions and dikes the contacts are very sharp and straight, and infrequently a fine-grained chill margin is observed. Numerous allotriomorphic trachyte dikes are encountered, cross-cutting all other lithologies. Some dikes are zoned, with a narrow biotite border, an intermediate zone of sub-radiating alkali feldspar blades, and a core zone of quartz rods, perpendicular to the dike margins.

Pods of pegmatitic ferro-edenite syenite are widespread in Centre III intrusions, but form relatively small segregations. Pegmatites occur as dikes and apophyses in the fine-grained ferro-edenite syenite. At the pegmatite contact, there is a gradual change in grain-size, ranging up to coarse-grained or very coarse-grained. The pegmatite is usually bright red, consisting primarily of massive alkali feldspar. Quartz is commonly visible, either interstitial to the feldspar, or within miarolitic cavities. These cavities may also contain vitreous, red amethyst. Amphibole may also be present in trace amounts. The pegmatites are non-magnetic.

2.3.2.iii. Xenolith-bearing ferro-edenite syenite

Adjacent to the breccia zones, ferro-edenite syenites containing rare mafic volcanic xenoliths occur. Exposures may be found in the Western Contact Zone (Figure 4), and the Neys Lookout/Ashburton Lookout areas (Figures 5 and 10). In fact this syenite type is transitional in texture and mineralogy between the ferro-edenite syenite described in subsection

2.3.3.i.), and the contaminated variety, described in section 2.3.3.

The xenoliths are commonly mafic volcanic fragments (see sections 2.3.3., 2.4.1. and 2.4.2.) and as such are rich in amphibole and biotite. When incorporated into a molten syenite magma, these xenoliths are variably assimilated. The result may be relatively vague zones bearing an elevated concentration of amphibole and biotite. The mafic fraction may constitute up to 30% of the syenite. Other than this increase in abundance of mafic minerals, changes in the aspect of the syenite are rare. A few specimens exhibit a sub-parallel alignment of both groundmass and phenocryst alkali feldspar, following the outline of the xenoliths.

2.3.3 Contaminated ferro-edenite syenite

The contaminated ferro-edenite syenite occurs only in breccia zones (Sections 2.4.1 and 2.4.2), where it is relatively abundant. Assimilation of mafic metavolcanic xenoliths results in contamination of the ferro-edenite syenite (section 2.3.2). Apart from textural features, this contaminated syenite closely resembles the ferro-edenite syenite. Generally the rock is purple, with variants being: reddish-purple, purpleish-grey, dark greyish-blue, purpleish-pink and grey. Commonly there are gradual colour changes on the outcrop scale, e.g. purple to purpleish-grey to grey. This type of ferro-edenite syenite is typically porphyritic with a fine-grained groundmass and medium-grained phenocrysts. The alkali feldspar phenocrysts are tabular, subhedral and may appear rounded. Various stages of hematization are implied by the colour range from light pink to bright red. The alkali feldspar phenocrysts average 4.5 mm long and constitute up to 45% of the volume of the rock. There is no preferred orientation of phenocrysts, and they are homogenously distributed throughout the groundmass. As in the ferro-

edenite syenite, mantled alkali feldspar phenocrysts are macroscopically visible. The groundmass contains alkali feldspar and biotite in an allotriomorphic texture. Plagioclase and amphibole may also be detected in hand specimens.

The characteristic feature of this contaminated ferro-edenite syenite, apart from its colour, is the presence of biotite ovoids. These ovoids are conspicious and constitute several percent of the volume of the syenite. The ovoids are oval or elliptical and have axes averaging 2 by 3 mm. In a few larger ovoids, the cores contain a massive aggregate of epidote. On weathered surfaces, these ovoids are distinguishable as pits. They are also found within volcanic xenoliths (Section 3.5), and may even straddle xenolith-syenite contacts. This contaminated ferro-edenite syenite is always non-magnetic, and calcite is generally not detected in hand specimens.

The contaminated ferro-edenite syenite surrounds mafic volcanic xenoliths, forming a reaction zone. This purple, contaminated syenite may grade transitionally into red ferro-edenite syenite or a sharp contact may be present. Where both syenite types coexist, the purple contaminated syenite is intruded by or brecciated by the red ferro-edenite syenite. (further discussions sections 2.4.1 and 2.4.2).

2.3.4 Quartz syenite

Quartz syenites are prevalent in the Neys Lookout/Ashburton Lookout area (Figure 5 and 10). The quartz syenite is olive green, black, yellow or buff where fresh, and distinctly red where hematization is advanced. In many outcrops, a gradual colour change (e.g. buff-pink to bright red) may be observed between unaltered and hematized varieties of this quartz syenite. These syenites are typically allotriomorphic, coarse-grained and

not obviously porphyritic. The predominant phase (>75%) is tabular to lath-shaped, olive green or brown alkali feldspar. Where rare alkali feldspar phenocrysts are visible they may measure up to 1 by 2 cm and rarely exhibit a lineated, cumulate texture. In many of the euhedral to subhedral alkali feldspar grains, Carlsbad twins are clearly visible. Many of the feldspars exhibit schillerization.

In the quartz syenite mafic minerals form interstitial clusters and discrete grains, constituting from 8% to 25% (10% on average) of the volume of the rock. Amphibole, biotite and pyroxene can be identified macroscopically, where coarse-grained, euhedral grains are present. Fine-grained, black amphibole prisms are observed in a few exposures. Quartz is colourless, smokey grey or brown. Commonly it is not visible in hand specimen due to the very dark colour of the syenite, but where observed, averages 1% to 2%. Usually this quartz syenite is non-magnetic, although in some instances may be moderately magnetic. Alteration is restricted to hematization of alkali feldspar.

Xenoliths are extremely rare in the quartz syenite, and consist of syenites and gabbros derived from Centre I and Centre II magmatism. These xenoliths are not visibly assimilated by the quartz syenite.

2.4 Main field study areas

Five main study areas were delineated, in which Centre III rocks predominate (Figure 3). These are informally named: Western Contact Zone (Figure 4); Neys Lookout/Ashburton Lookout (Figure 5); Neys Hydroline (Figure 6); Radiotower Hill Road (Figure 7); and Guse Point/Pic Island (Figure 8).

2.4.1 Western Contact Zone

Jago (1980) investigated the geology of the Western Contact Zone. His field mapping revealed that Centre I, II and III lithologies are represented in the area (Figure 4). This study re-examined and sampled only the Centre III rocks and any xenoliths contained therein. A brief examination of Archean country rocks northwest of this study area, was also carried out.

Three of the four Centre III syenite types are exposed in the Western Contact Zone. Ferro-edenite syenite is the dominant lithology and contaminated ferro-edenite syenite is common in xenolith-rich portions of the intrusion. In all cases, contamination-free intrusions of ferro-edenite syenite post-date the xenolith-bearing contaminated syenite. Dikes of the former invade the latter, and breccia fragments of the contaminated syenite are found in the contamination free syenite. Two small, isolated outcrops of quartz syenite were mapped in the eastern portion of this zone. The quartz syenite was previously unrecognized in the Western Contact Zone.

Jago defined three syenite types from the Western Contact Zone: porphyritic quartz-syenite; contaminated porphyritic-porphyroblastic quartz-syenite; and quartz-syenite. Jago's porphyritic quartz-syenite is the ferro-edenite syenite of this study. The contaminated porphyritic-porphyroblastic quartz-syenite is the contaminated ferro-edenite syenite. Jago divided his quartz-syenite into three types, based largely on textural differences. Some of the distinguishing features, such as strained quartz and exsolved plagioclase, formed due to minor structural deformation. Other textural considerations are indicative of progressive stages of an evolving, differentiating quartz syenite magma. Mineralogically Jago's quartz-syenites are similar to his porphyritic

quartz-syenite, and for the purposes of this study, both types belong to the ferro-edenite syenite variety.

Three types of dikes cut the ferro-edenite syenite along dilational zones. Most average 1 to 3 cm in width and have a crude correspondence to joint patterns (Jago, 1980). The preferred joint orientations are: 90-110°, 10-40° and 130-150°. One type are dikes of red syenite and red trachyte that appear to be coeval, because cross-cutting relationships are not observed. The major constituents are perthitic alkali feldspar and quartz, plagioclase is a minor phase, and trace amounts of biotite, amphibole, zircon, fluorite, sphene and tourmaline may be present (Jago, 1980). These syenitic dikes rarely contain biotite ovoids and/or biotite enrichment along the walls of the dike. Coarse-grained, sub-radiating fans of alkali feldspar and quartz are oriented perpendicular to dike walls, in some instances, grading into a more massive, quartz-rich core zone. The mixed feldspar and quartz zone may exhibit a graphic intergrowth texture. Syenite dikes also intrude metasedimentary xenoliths (Figure 11) and trachyte dikes reportedly invade the country rock supracrustal sequence (Puskas, 1967).

Granite and rhyolite dikes constitute a second type of dike in the Western Contact Zone. Some granite dikes have been observed cross-cutting trachyte dikes. The rhyolite dikes occupy tension gashes that are 3 to 4 cm wide, and vary in structural orientation (Jago, 1980). Porphyritic rhyolite dikes contain alkali feldspar phenocrysts up to 7 mm long, that are also glomeroporphyritic, euhedral and exhibit good braid perthite exsolution textures. Quartz phenocrysts measuring 2 to 3 mm long are also present (Jago, 1980). In the groundmass, recrystallized alkali feldspar, quartz and plagioclase predominate.

Composite or zoned dikes form a third group in the Western Contact

Zone. Jago (1980) describes composite dikes with a quartz-syenite border and rhyolitic core of irregular width. Repeated dilation and infilling by different fluids formed these dikes. In another instance, the core zone exhibits vuggy, coarse-grained quartz crystals, in discontinous pinch-and-swell structures. Quartz syenite or rhyolite fills the vugs between quartz grains.

At the western edge of the Western Contact Zone, Centre III rocks have intruded Archean supracrustal sequences, minor ultrabasic intrusions and granite gneisses. The greenstone belt contains mafic and felsic volcanics, and greywackes and shales, all metamorphosed to greenschist and amphibolite grade. Two episodes of folding and the intrusion of Archean felsic plutons have affected this belt. The intrusion of the Coldwell Alkaline Complex has led to the development of a thermal metamorphic aureole, for a distance of approximately 1.6 km from the contact (Walker, 1967).

The Archean mafic volcanics are very fine-grained, dark green, foliated units. Chlorite, biotite and saussuritized plagioclase grains are evident. Fine chloritic wisps define the foliation. No volcanic textures or structures are preserved. Within the thermal aureole, amphibole replaces chlorite and actinolite. As the syenite contact is approached, the amphibole gives way to biotite, and eventually, right at the contact, a pyroxene hornfels is observed (Walker 1967, Aubut, 1977). The hornfelsed rocks are basic in composition and consist of fine-grained andesine and orthopyroxene. The rocks are dark brown to black, with a sugary, granoblastic texture. Some specimens exhibit good layering which may represent primary bedding in sedimentary rocks. Petrographic study reveals that exsolution lamellae of clinopyroxene occur in the orthopyroxene. Accessory phases include opaques, commonly magnetite, and

biotite (Aubut, 1977).

Felsic volcanic country rocks are very fine-grained, green and massive. Conchoidal fractures are prevalent, particularly as the contact with the complex is approached. A weak fabric is defined by elongated quartz pods rimmed with epidotized material, or stringers and elongated blebs of pyrite.

Archean greywackes in this contact zone are well-indurated, siliceous and dark blueish-grey. A banded fabric is rarely observed, due to the presence of silica-rich versus biotite-rich zones. No sedimentary structures are discernable. In massive, black shales elongated blebs of pyrite may locally define foliation. As the contact with the complex is approached, the sediments are marked by the introduction of a reddish-brown biotite. Red garnet is infrequently observed, and the incipient development of sillimanite has been noted (Walker, 1967). It is important to note that the effects of thermal metamorphism have been obscurred locally, due to a later hydrothermal event, involving carbonate, chlorite and sericite (Walker 1967).

The main geological contact between the Archean supracrustal rocks and the Proterozoic alkaline complex is situated in a valley occupied by ponds and unconsolidated Quaternary deposits. Metasedimentary rocks outcrop immediately to the west of the complex, in the study area, and metasedimentary xenoliths are common in these marginal Centre III syenites, suggesting that metasedimentary rocks represent the local host rock. To the south and east, Centre III syenites are in contact with the Western Border Gabbro. Large gabbro xenoliths are localized along a brecciated contact. The presence of a distinct curvi-linear lineament along this contact suggests that the contact is a reactivated fault (Jago 1980). Jago concluded that block faulting occurred along this contact,

after the cessation of Centre III magmatism.

Exotic and cognate inclusions are common in the Centre III syenites of the Western Contact Zone. Exotic metasedimentary xenoliths are by far the most abundant, and are found up to 300 m away from the main Archean/ Proterozoic contact. McGill (1980) observed that large metasedimentary rafts measure up to 30 m long. In the Western Contact Zone specifically, Jago's mapping and that of this study indicates that some roof pendants measure up to 300 m long (Figure 4). Jago (1980) mapped large blocks that are structurally concordant with the country rock metasediments. The contact between metasedimentary xenoliths and Centre III syenites is typically sharp, but may be obscurred by weathering. Narrow dikes of syenite and trachyte intrude the xenoliths in a random fashion. One observed portion of a metasedimentary xenolith measured approximately 6 m long, (Figure 9) and has a relatively straight contact. Smaller, angular to subrounded fragments of metasediment are brecciated by, and suspended within contaminated ferro-edenite syenite. The contaminated zone around the xenolith is of varying width and degree of assimilation.

The metasedimentary rock of the xenoliths closely resembles the country rock sediments just outside of the complex. The sediment is a dark blue to grey, silt-size, turbiditic rock. Many xenoliths appear to be massive-bedded and no foliation is evident. These specimens break unevenly, with no preferred planes apparent. Jago has observed sedimentary xenoliths which exhibit graded, regular to cross-layered bedding. During the course of this study, sediments with poorly developed layering were observed. Macroscopically, individual minerals are not identifiable, but the rock is siliceous. Petrographic examination (Jago, 1980, and section 3, this study) reveals that quartz is the dominant constituent, with an abundance from 45-85%. Biotite typically constitutes

the remainder, of the volume of the rock and may form blasts.

Metavolcanic xenoliths are present in the Centre III syenites of the Western Contact Zone, but are much less abundant than the metasedimentary type. The mafic volcanic rocks resemble the Archean country rocks, just outside the complex. They are fine-grained, massive and very dark green. In the vicinity of Middleton, just south of the study area, the volcanics are hornfelsed and contain phenocrysts and clots of biotite. In the volcanic xenoliths, these ovoids of biotite are preserved.

Towards the east, away from the complex margin, the abundance of mafic volcanic xenoliths increases, but never becomes significant. The xenoliths are black to very dark green, very fine-grained and are subrounded. They measure not more than a few centimetres along their longest axis. Petrographic study reveals that there are plagioclase phenocrysts and alkali feldspar porphyroblasts, in some volcanic specimens. Biotite and chlorite form an allotriomorphic texture, and constitute the predominant phases of the rock. Other constituents of the mafic volcanic xenoliths include: amphibole, quartz, carbonate, hematite, clinopyroxene, fluorite, apatite and zircon (Section 3.5).

The easternmost roadcuts in Centre III syenites, in the Western Contact Zone, also contain cognate inclusions. Biotite gabbro, ferro-augite syenite, syenodiorite and nepheline syenite blocks have a relatively minor abundance in this area. The biotite gabbro fragments are sub-rounded to subangular and are hosted predominantly by ferro-edenite syenite. The biotite gabbro is typically coarse-grained with an allotriomorphic texture. In a few gabbro inclusions a crude layering of biotite-rich versus amphibole-rich bands is observed. Plagioclase, exhibiting incipient alteration to saussurite and sericite, is evident. Some strongly magnetic biotite gabbro blocks occur in an olive green

quartz syenite, along with red and green, coarse-grained ferro-augite syenite fragments. The latter may display gradational contacts over 1 or 2 cm, with the quartz syenite. In other instances though, the ferro-augite syenite blocks have sharp boundaries. The inclusions termed syenodiorite are mafic-rich alkali feldspar syenite, resembling the magnesio-hornblende syenite. These fragments are hosted in ferro-edenite syenite. Only a few of these fragments have been observed, and therefore a conclusive decision regarding their origin is not possible. Centre II nepheline syenite inclusions were observed by Jago (1980). In these blocks, glomeroporphyritic alkali feldspar phenocrysts predominate. Much of the alkali feldspar is a replacement of plagioclase grains. Dark green, anhedral aegirine and zircon are the main accessory phases.

2.4.2 Neys Lookout/Ashburton Lookout/Neys Hydroline Area

The Neys Lookout/Ashburton Lookout/Neys Hydroline area is a relatively large, well-exposed region of Centre III syenites (Figure 10). Outcrops along the highway, powerlines and railway are almost continuous. A segment adjacent to the Little Pic River is informally referred to as the East Bank area. All four Centre III syenite types are well-exposed and the general petrogenetic sequence can be determined from these exposures. Roadcuts displaying breccia zones occur throughout the area. (Plate 2). In the vicinity of the Neys Lookout, in particular, complex multiple igneous breccia are observed. Centre I and II gabbros and syenites form large blocks in the ferro-edenite syenite and quartz syenite, proving that Centre III syenites are younger than Centre I and II lithologies. Oligoclase basalt xenoliths have been brecciated by ferro-edenite syenite with the resulting production of contaminated ferro-edenite syenite. Mitchell and Platt (1978, 1982a) suggest that the

Plate 2 - Breccia of oligoclase basalt in contaminated ferro-edenite syenite. Neys Lookout area (location C2049 of Figure 5).

oligoclase basalt represents a coeval alkaline volcanic rock, that originally capped the complex. Two lamprophyre types are observed in this study area: sannaite-type lamprophyres intruding large Centre I and II blocks; and quartz-bearing camptonites, (Mitchell and Platt, 1982a), within the same large blocks, and as discrete xenoliths.

The petrogenetic sequence of the four Centre III syenite types can be determined from exposures in this area. The sequence is, from earliest to latest: magnesio-hornblende syenite, contaminated ferro-edenite syenite, ferro-edenite syenite and quartz syenite. At Ashburton Lookout the central portion of the roadcut consists of magnesio-hornblende syenite. Blocks of the latter are also found in the ferro-edenite syenite. At several localities in this area the purple contaminated ferro-edenite syenite is brecciated by red ferro-edenite syenite. Successive intruded batches of ferro-edenite syenite are progressively less contaminated. At Neys Lookout the quartz syenite is seen to be younger than the ferro-edenite syenite, as dikes of the former intrude the latter.

The Big Bay-Ashburton Bay Fault coincides with the Little Pic River. Mitchell and Platt (1978, 1982a) consider the region between this fault and the Redsucker Fault Zone, (approximately 9 km to the east), to be a down-faulted crustal block. The abundance of caprock breccia, throughout this region, also suggests that these rocks were once at a higher structural level. In the Ashburton Lookout roadcut (Figure 11) jointing is prominent, with the three major joint orientations being: 021/18^{o}, 056/87^{o} and 141/vertical to steeply-dipping in either direction. Ferro-edenite syenite dikes are localized along the 021/18^{o} joint set, with minor splaying dikes coming off of this plane.

Contact relationships are variable throughout this study area. A sharp contact between Centre III syenite types, without chill margins, is

common. This is the case with the East Bank roadcuts, where ferro-edenite syenite is in contact with quartz syenite, but there are no indications of which syenite was intruded first. A sharp contact is observed between successive batches of ferro-edenite syenite in several exposures. Conversely, gradational contacts are also frequently observed (Plate 3). The contaminated ferro-edenite syenite grades into less contaminated zones and eventually contamination-free portions. The relationship between ferro-edenite syenite and quartz syenite can also be gradational, as observed in the Neys Lookout area. A dike may be present in the place of a distinct contact between various syenite types. Just east of Ashburton Lookout, ferro-edenite syenite is separated from quartz syenite by a dike of red, quartz-rich alkali feldspar syenite. The dike is only 3 to 4 cm wide and is strongly weathered and friable. One sheared contact is also observed just east of Ashburton Lookout. Here, the contact between ferro-edenite syenite and quartz syenite is marked by a 10 cm-wide shear zone. Towards the east and northeast, in this study area, less of the contacts are exposed.

A highly evolved variety of the ferro-edenite syenite forms substantial outcrops throughout the middle of this study area (Figure 10). This ferro-edenite syenite is red, coarse-grained to medium-grained and consists primarily of perthitic alkali feldspar and quartz in a graphic texture (Section 2.3.2.ii.). Traces of fine-grained biotite may be observed.

Dikes similar to those found in the Western Contact Zone are intruded into all rocks of this study area. They are predominantly varieties of ferro-edenite syenite, quartz syenite, trachyte and granite. Natrolite-bearing nepheline syenite dikes also crosscut Centre III rocks throughout this area, and are not especially rare. Quartz-rich camptonites and

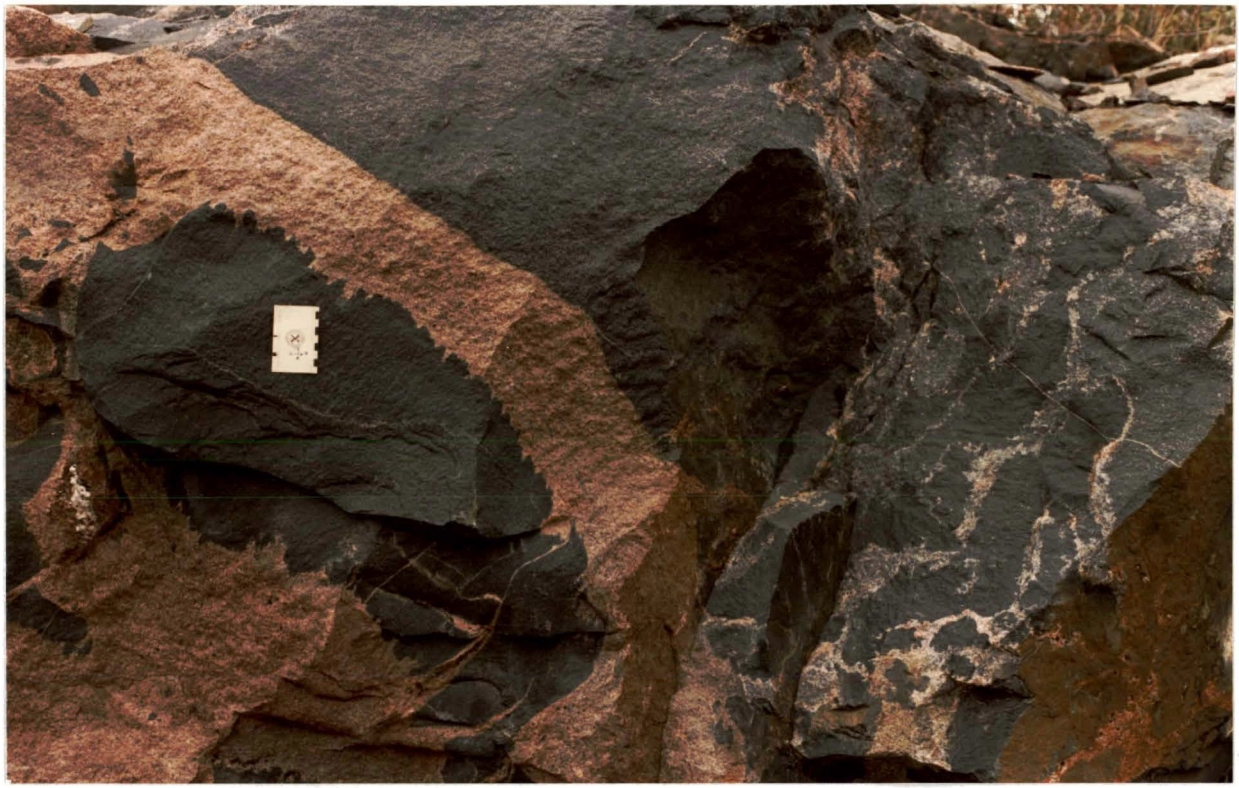

Plate 3 - Detail of xenolith margin types, from same locality as Plate 2.

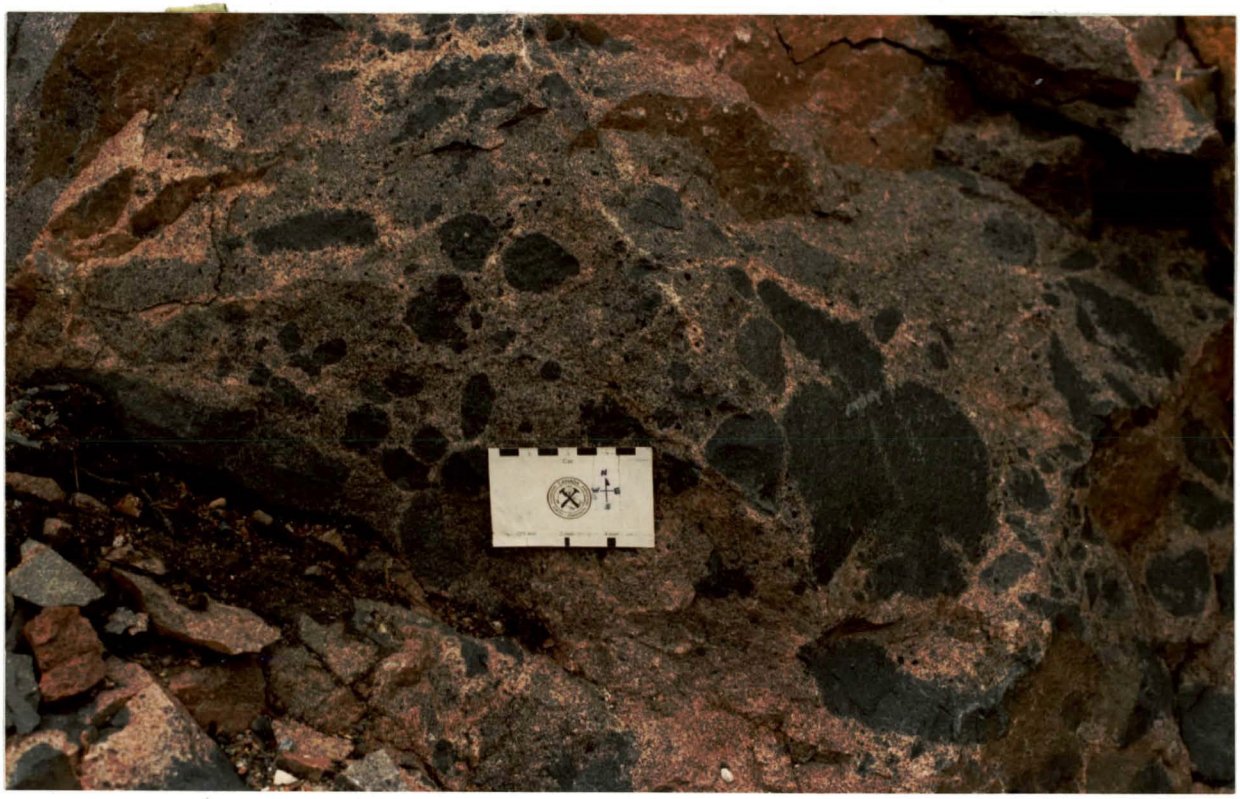

Plate 4 - Typical breccia in contaminated ferro-edenite syenite, displaying various stages of assimilation.

ocellar lamprophyres are observed in Centre III syenites, but are rare. It has not been conclusively determined whether they are dikes or brecciated blocks, because the outcrops are small, and generally only two dimensions are observable.

Enclaves of all types can be found in this study area. Enclave swarms may consist entirely of cogenetic autoliths, or they may be comprised of mixed external xenoliths and comagmatic rock types. The dominant occurrence is a breccia of oligoclase basalt in the contaminated ferro-edenite syenite. Other xenoliths in the contaminated- and contamination-free ferro-edenite syenites are much less abundant, and include: country rock metavolcanics, country rock metasediments, layered and massive ferro-augite syenite, biotite gabbro, nepheline syenite and ocellar lamprophyres. Enclaves are rare in the magnesio-hornblende syenite and quartz syenite. Granite xenoliths are observed in a sannaite-type lamprophyre at Neys Lookout. This granite does not resemble any of the units from within the Coldwell Complex.

As noted above, the oligoclase basalt xenoliths represent coeval alkaline volcanic rocks, that at one time may have capped the complex. These basalt xenoliths are angular to rounded and exhibit a wide range of sizes, commonly within a single outcrop, suggesting that there has been some movement of blocks after brecciation (Plates 2 and 4). In general, as assimilation proceeds, xenoliths become rounded. Various stages of assimilation may be chaotically mixed in a single outcrop. (Plate 4). The xenolith margins are sharp or diffuse, depending on the degree of assimilation. The margins may be straight, undulose, lobated or serrated (Plate 3). Once again, various styles may be juxtaposed, contributing to the general chaotic appearance of the breccia zones. It has not been determined whether the convoluted margins represent incomplete

crystallization of the basalt at the time of brecciation, or if they are a product of the assimilation style. The oligoclase basalt is dark grey, very fine-grained and contains approximately 5 to 20% biotite ovoids. These ovoids are of metasomatic origin (p. 3-14) and are developed during the re-crystallization of the volcanic xenoliths. Xenoliths with relict igneous textures contain few ovoids, whereas in the highly altered xenoliths they are relatively abundant. These ovoids may have cores of epidote. They may straddle the xenolith/syenite contact and also occur throughout the contaminated ferro-edenite syenite host. Anhedral to subhedral microphenocrysts of plagioclase may or may not be macroscopically visible, constituting up to 20% of the basalt. They are typically medium-
grained and may be moderately saussuritized. Petrographic study reveals that biotite and plagioclase comprise the bulk of the rock, with the accessory minerals being: amphibole, epidote, pyroxene, apatite, fluorite, opaque minerals, sericite and hematite.

Other mafic metavolcanic xenoliths are aphyric and chloritic, resembling the country rocks (section 2.4.1) to a great extent. These xenoliths are dark green to black, fine-grained and commonly contain biotite ovoids. The xenoliths are subrounded and occur as isolated blocks, rather than swarms. These xenoliths are not abundant, but are found in all portions of this study area.

In the Neys Hydroline area the quartz syenite exposures contain a few metasedimentary enclaves which resemble those in the Western Contact Zone. This rock is very fine-grained, dark grey and massive. One enclave contains approximately 20% fine-grained, buff, prismatic plagioclase porphyroblasts.

Rarely enclaves of massive and layered ferro-augite syenite are

observed in ferro-edenite syenite. Examples are observed west of Neys Lookout on the powerline and in the roadcuts at Neys Lookout. These ferro-augite syenite xenoliths texturally and mineralogically resemble the Centre I rocks exposed just west of the Little Pic River. Along the powerline near the lookout, a rectangular xenolith of layered ferro-augite syenite measures 58 by 75 cm. The contacts are straight and distinct, and the block is situated in an oligoclase basalt breccia zone.

Biotite gabbro and nepheline syenite inclusions are more common than ferro-augite syenite blocks, but are still quite rare. Ferro-edenite syenite and quartz syenites host both xenoliths at Neys and Ashburton Lookouts. A large xenolith of Centre II rock is located at the turnoff to the Neys Lookout parking lot. Along the highway the exposure is about 50 m wide and appears to extend north to the southernmost of two powerlines (Figure 10). The bulk of the xenolith consists of biotite gabbro that is intruded by dikes of nepheline syenite and pegmatitic natrolite syenite. Amazonite occurs throughout these dikes. Petrographic study (Mitchell and Platt, 1982b) reveals that the biotite gabbro exhibits pervasive development of corona structures. Both biotite gabbro and nepheline syenite are truncated by quartz syenites and ferro-edenite syenites. On the western side of the mega-xenolith, subangular to subrounded blocks of fine- to medium-grained biotite gabbro are hosted in red ferro-edenite syenite. These smaller xenoliths average 15 by 20 cm in length and width and occur in a dense swarm for a distance of a few metres from the large enclave. The gabbro-syenite contacts are macroscopically sharp or are transitional over a very small distance. The smaller gabbro xenoliths contain fine-grained, red, alkali feldspar grains, which are not apparent in the core of the main xenolith. In the syenite host, thin black reaction rims surround the mafic minerals. On the east side of the large

biotite gabbro xenolith the host is quartz syenite, which contains relatively few gabbro xenoliths. One larger block measures 30 by 97 cm and has a sharp, though slightly undulose contact with the quartz syenite. The gabbro is black to dark green with green epidote spherules in a black biotite matrix. The buff to yellow quartz syenite exhibits a zone of contamination approximately 1 cm wide around the xenoliths, in which the syenite is greenish-grey.

At Ashburton Lookout (Figure 11) white nepheline syenite xenoliths are hosted in the magnesio-hornblende syenite and in the ferro-edenite syenite. The largest xenolith there measures at least 10 by 20 m. The nepheline syenite of the xenoliths is white to buff, and coarse-grained. Similar nepheline syenite xenoliths are sporadically hosted in all Centre III syenites throughout the study area. No obvious contamination effects are noted.

In a few instances mafic xenoliths resembling oligoclase basalt also contain vugs filled with white to colourless calcite. These xenoliths may in fact be portions of ocellar lamprophyre dikes. Examples of these lamprophyre-type xenoliths occur in the roadcuts of the East Bank area. Elsewhere, lamprophyre dikes may be observed within larger xenoliths of Centre II rocks.

2.4.3 Radiotower Hill Road Area

This region was investigated because of the good access provided by a long, switchback road. Along it there are numerous small roadcuts, that expose nepheline syenites towards the south and Centre III syenites to the north. Sample locations and the generalized geological contacts are presented in Figure 7.

The nepheline syenite is white to light grey, medium-grained and

typically allotriomorphic-granular. Black amphiboles constitute approximately 30% of the volume of this rock. The amphiboles are acicular and randomly oriented. Nepheline and alkali feldspar make up the remainder of the syenite and are generally unaltered. Coarse-grained dikes of natrolite nepheline syenite intrude the white nepheline syenite. The dikes are pink due to abundant, scattered natrolite patches. Mitchell and Platt (1982b) state that the natrolite is both a late-stage primary phase and a replacement of feldspar and nepheline. The distinctive pink to red colouration of the natrolite is due to an association with hematite.

A single exposure of buff, medium-grained quartz syenite is located just north of the nepheline syenite. Black pyroxene is distinct in this rock, constituting a few percent of the volume. This quartz syenite is non-magnetic.

Further to the north is an intrusion of ferro-edenite syenite. It is typically red, medium- to coarse-grained, and allotriomorphic-granular. These syenites are almost always moderately magnetic and may contain accessory pyroxene and pyrite. Short sections of quartz syenite alternate with this ferro-edenite syenite, along the road. Where the contacts are exposed, they are sharp, but give no indication of relative age.

North of the main body of ferro-edenite syenite more quartz syenites are exposed. They are olive green to buff, non-magnetic and porphyritic. Tabular alkali feldspar phenocrysts are interspersed in a groundmass of alkali feldspar, very fine-grained to coarse-grained biotite and amphibole, and trace molybdenite. The mafic minerals commonly form clusters, scattered homogeneously throughout the syenite. Quartz is not macroscopically visible in these quartz syenites.

Along the railway tracks, north of a sandplain, magnesio-hornblende

syenite is intruded by ferro-edenite syenite. The magnesio-hornblende syenite is very fine-grained in the western most railway cut (location 2181, Figure 7) and gradually coarsens to medium-grained at the ferro-edenite syenite contact. The western cuts may represent a chill margin. Dikes of pink ferro-edenite syenite intrude the magnesio-hornblende syenite and increase in abundance to the east. These dikes are generally less than 15 cm wide, but in places blossom out into small intrusions, less than a metre wide, which contain brecciated fragments of magnesio-hornblende syenite. The main contact between the magnesio-hornblende syenite and ferro-edenite syenite is obscurred, although an abundance of pink syenite dikes are observed in the vicinity. Nevertheless, there is enough evidence to state that the magnesio-hornblende syenite predates the ferro-edenite syenite in this area.

On the highway at the northwest corner of this study area are a few strongly oxidized, weathered outcrops of ferro-edenite syenite and quartz syenite. Of particular interest is an analcite tinguaite dike (Laderoute, personal communication), at location 2159 (Figure 7). It resembles a very fine-grained, deeply weathered and strongly oxidized trachyte. It is purple-red and a foliation is defined by darker, more hematized wisps and bands. This foliation bends about 180^{o} on a single outcrop.

Xenoliths are generally not found, except as already mentioned, within ferro-edenite syenite dikes that cross-cut magnesio-hornblende syenite.

2.4.4 Guse Point/Pic Island Area

The Guse Point/Pic Island area is depicted in Figures 8 and 12. This focus of Centre III magmatism is geographically separated from the previously described study areas by more than 6 km. The contact between

Centre III and Centre II rocks in the area is not exposed.

All of the Centre III rocks in this area are ferro-edenite syenite, except for two very small exposures. At Guse Point, at locality 2213, there are outcrops of quartz syenite. Fresh surfaces are buff-coloured and the rock is medium-grained, with rare coarse-grained, tabular alkali feldspar phenocrysts, and about 15% by volume mafic minerals, in small aggregates. Quartz is not visible in hand specimen. The relationship of this small intrusion to the other syenites in the area is unknown, because contacts are not exposed.

On Pic Island, through an outcrop of ferro-edenite syenite (location 2230), there is a linear breccia zone containing contaminated ferro-edenite syenite and mafic metavolcanic fragments. This zone is 30 to 60 cm wide with sharp, distinct contacts. The material inside the zone is very similar to the oligoclase basalt breccia zones of Neys Lookout. There is no evidence to indicate the sequence of events and intrusions in this exposure.

The predominant lithology exposed in this study area is ferro-edenite syenite, which has a varied appearance, due primarily to deformation and recrystallization textures. The latter will be described in section 3. The structures encountered include: shear zones, hematization "fronts", comagmatic breccia zones and jointing. Well-developed jointing is observed at the northwest point of Pic Island, and at one locality on the south shore of the Coldwell Peninsula. Jointing measurements on Pic Island are: 270/76^{o}, 13/subvertical and 155/4^{o}. On the peninsula, joints are oriented: 024/vertical, 106/vertical to steeply dipping in either direction, and 90/15^{o}. In both cases the jointing is restricted to a small area, and is not found elsewhere. In the comagmatic breccia zones, blocks of ferro-edenite syenite are included in a more highly evolved

ferro-edenite syenite. Two sets of syenite dikes cross-cut these breccia zones. Figure 12 illustrates a few areas where this relationship is observed. The hematization fronts are linear, sometimes bifurcating zones through the ferro-edenite syenite. These fronts are noted along both shorelines and are not obviously related to faults or joints, but are crudely perpendicular to the shoreline, in most cases. These hematized zones are from 20 to 45 cm wide. The syenite on either side of a zone appears similar texturally and mineralogically. In the zone, the ferro-edenite syenite is intensely hematized, in the form of rivulets or braids of massive hematite. Fissile shear zones are prominent at the northwest point of Pic Island. Most trend approximately north-northwest. A couple of these shears appear to follow joint planes. The shear foliation planes are curvilinear, imparting a crumbly friable nature to the syenite. Within the shears the rock is also intensely hematized and mafic minerals are altered, to varying degrees.

As indicated on the general geology sketch (Figure 12) the distinction between early and late ferro-edenite syenite is easily made. Although several progressive types are observed, where contacts are exposed they are sharp and geological relationships can be determined based on dike and breccia evidence. The early ferro-edenite syenite is coarse-grained to medium-grained, with an allotriomorphic granular texture. Mafic minerals are commonly altered and comprise less than 10% of the volume of the rock. With further differentiation and evolution of the magma, the resulting syenites are most distinctly porphyritic, with medium-grained alkali feldspar laths and tablets in a fine-grained feldspar-rich groundmass. The proportion of visible interstitial quartz gradually increases, and the texture is more idiomorphic and eventually graphic. Petrographic study indicates that with structural deformation,

the syenite at any stage of differentiation underwent recrystallization. The textural and mineralogical changes are most obvious on a microscopic scale. Grain margins, particularly for alkali feldspar grains, become more sutured, first lobate and then serrated. Perthitic feldspar phenocrysts are mantled by feldspars of different composition and varied exsolution textures. Secondary albite grains appear at sutured phenocryst margins and within the groundmass. The feldspars may exhibit strained extinction. Interstitial quartz becomes progressively more strained, showing undulose extinction and may recrystallize into anhedral clusters. The biotite and amphibole may be recrystallized, displaying a poikilitic texture. The mafic minerals can also form clusters of anhedral grains. Macroscopically these features are not evident and further observations regarding recrystallization will be presented in the following chapter.

PETROGRAPHY OF THE CENTRE III SYENITES

3.1 Magnesio-hornblende syenite

The magnesio-hornblende syenite is rich in mafic minerals that form a synneusis texture. The overall texture varies between hypidiomorphic granular to porphyritic with a hypidiomorphic groundmass. Both extremes in texture are equally abundant. Of the essential constituents, alkali feldspar and amphibole are the only major phases. Plagioclase and quartz are essential minor phases. The accessory minerals include: amphibole, biotite, pyroxene, olivine, apatite, zircon, sphene, fluorite, pyrite, ilmenite, magnetite and unidentified radioactive phases. Alteration products include: calcite, sericite, saussurite, hematite, chlorite and iddingsite/bowlingsite. Representative modes are presented in Table 1. Alteration and replacement textures affecting the mafic minerals and feldspars are common. Minor recrystallization of feldspars is also observed.

The dominant texture, which is also evident macroscopically, is a synneusis texture involving mafic minerals, and to a lesser extent opaque minerals, fluorite, apatite, sphene and a trace amount of olivine (Plates 5 and 6). These clusters are distributed uniformly throughout the rock, with the dominant feldspars occurring interstitially to the clusters. Within the mafic clusters the minerals are typically subhedral and randomly oriented. These clusters are approximately round and average 3 mm in diameter. The mafic minerals, whether they are in the clusters or in the groundmass, have the same grain size, therefore the texture cannot be referred to as glomeroporphyritic. Mafic minerals and opaque phases are much less abundant in the regions where feldspars dominate. Alteration of all phases is prevalent away from the clusters. Between the

TABLE 1
Magnesio-hornblende syenite - Modes

mineral / abundance in :	C181	C180	C2150
alkali feldspar	84	80	47
amphibole	8.5	15	40
opaques	6	tr	0.5
biotite	0.5	3	5
pyroxene	tr	tr	0.5
quartz	tr	1	2
apatite	tr	tr	2
sericite/saussurite	-	-	1.5
plagioclase	tr	tr	-
zircon	tr	tr	-
sphene	tr	-	tr
fluorite	-	tr	-
iddingsite/bowlingite	-	tr	-
hematite	-	-	tr
chlorite	-	tr	tr
calcite	tr	-	tr

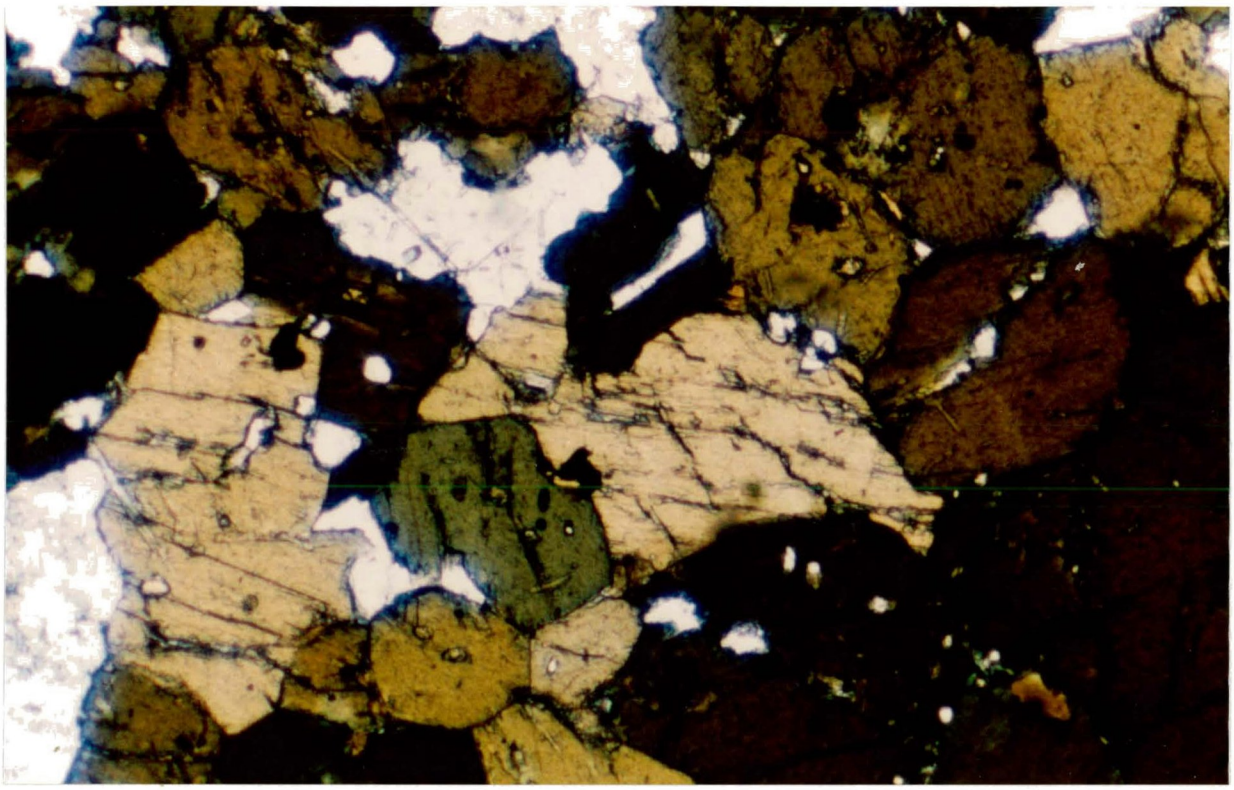

Plate 5 - Photomicrograph of mafic synneusis structure in magnesio-hornblende syenite.Plane polarized light.Width of photo is 2 mm.

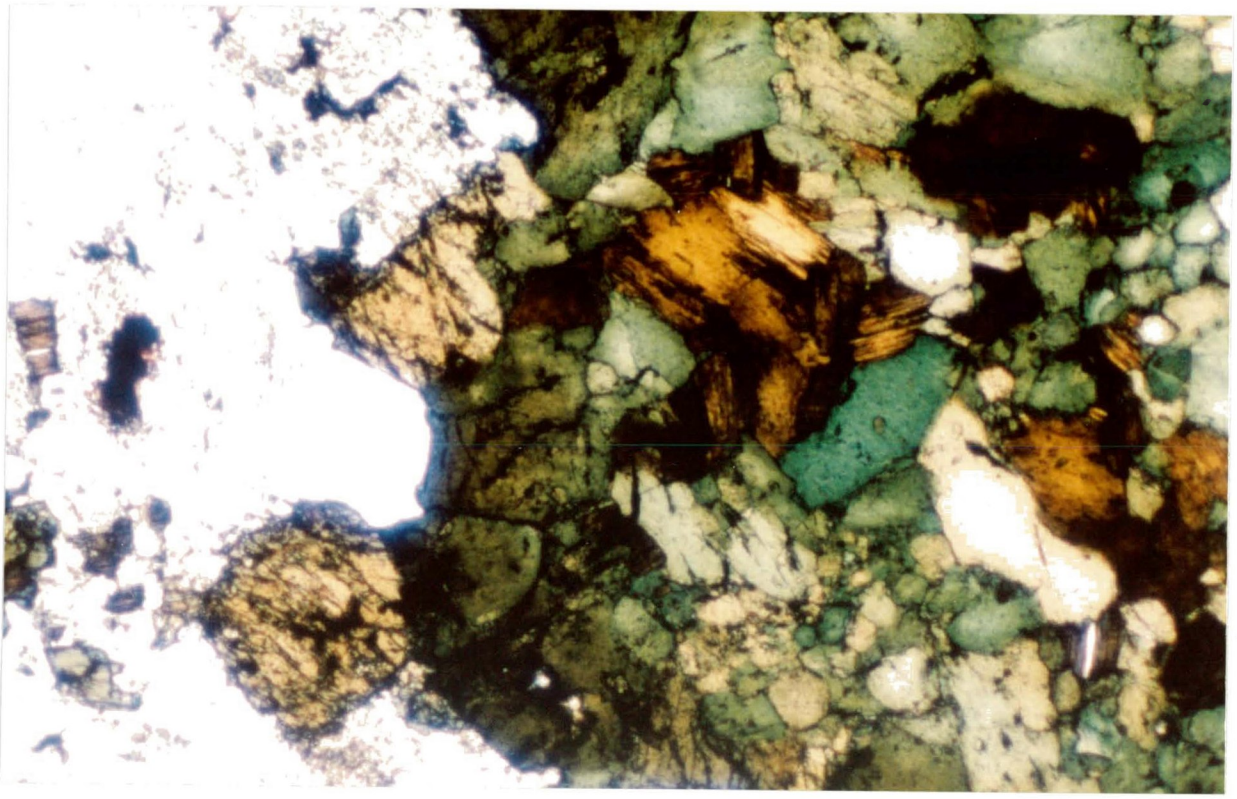

Plate 6 - Photomicrograph of mafic synneusis structure in magnesio-hornblende syenite.Plane polarized light.Width of photo is 2 mm.

clusters the syenite may, or may not, exhibit a porphyritic texture. Phenocrysts consist of perthitic alkali feldspar tablets. These euhedral to subhedral phenocrysts are set in a feldspar-rich groundmass that is hypidiomorphic to allotriomorphic in texture.

Based upon microtextures, the crystallization sequence for magnesio-hornblende syenite appears to be: apatite and magnetite, sphene, pyroxene, early amphibole, biotite, minor alkali feldspar, late amphibole, major alkali feldspar (with apatite and magnetite still crystallizing), and finally interstitial plagioclase and quartz. The alkali feldspar is moderately sericitized, saussuritized and hematized. Pyroxenes are replaced by chlorite or iddingsite/bowlingsite. Amphiboles are replaced by biotite, and this, in turn, by chlorite.

Alkali feldspar constitutes the major phase in all magnesio-hornblende syenites. Perthitic exsolution textures are widespread, but because of their patchy, altered nature, it is difficult to determine which phase is the exsolved one. Determination of feldspar composition by microprobe analysis is rendered difficult because of the strong sericitization and saussuritization of perthitic grains. Mantled perthites display different exsolution textures, degrees of alteration and twinning types from core to rim. In a typical example, a highly sericitized, hematized and saussuritized patch perthite core is surrounded by a single unaltered, untwinned, unexsolved mantle phase. Where several mantles occur, the alteration is present in alternate successive mantles, as well the core. In a few instances hematite may form rims around feldspar grains or may replace irregular portions of perthitic phenocrysts. The cores of perthitic grains typically display Carlsbad twins. Subhedral perthites are characteristic of the hypidiomorphic syenites, but may also display euhedral crystal faces

where adjacent to interstitial quartz. In the porphyritic varieties of this syenite the phenocrysts are patch perthitic alkali feldspar, similar to the mantled grains described above. In these porphyritic syenites the groundmass feldspars form subhedral, randomly oriented laths. Plagioclase is common, in small quantities in the groundmass. It exhibits albite and pericline twinning and is subhedral to anhedral. Continuous concentric zoning may be present and the cores of grains may be sericitized. Although most plagioclase is primary in origin, a small proportion has formed due to recrystallization, particularly along sutured contacts between alkali feldspar grains.

Where quartz is present, it occurs as an interstitial phase and commonly contains abundant fluid inclusions. Undulose extinction may be present, but is rare.

Amphibole is the major mafic constituent of magnesio-hornblende syenite, and two distinct types are commonly observed. The early amphibole typically forms poikilitic anhedral grains with inclusions of biotite, opaque phases, apatite, unidentified radioactive minerals (displaying pleochroic haloes) and traces of alkali feldspar. This is the amphibole of the synneusis texture, and it is usually medium olive green, or rarely, brown. The later amphiboles are light green to blueish and are also generally poikilitic. These amphiboles occur in the groundmass. Some of these grains display a concentric zoning of composition, evident from changes in birefringence and pleochroism.

Biotite is ubiquitous in the magnesio-hornblende syenite. It forms reaction rims around magnetite grains and commonly replaces amphiboles. A minor proportion of the biotite occurs interstitial to the feldspar. The pleochroism of the biotite is straw yellow-beige-brown. Biotite also replaces pyroxene, particularly along cleavage planes and margins. Some

poikilitic biotite is observed, with inclusions of apatite, pyroxene and opaque phases. Intergrowths of biotite and calcite replace amphiboles. Chlorite may be observed replacing biotite.

Pyroxene, when it occurs is in trace amounts, and is in the mafic clusters, as well as the groundmass. The pyroxene may be colourless, very pale green or medium green. Some pyroxene grains exhibit margins that are zoned with respect to birefringence. In many instances the pyroxene is replaced by chlorite and biotite, along grain boundaries and within grains. Iddingsite/bowlingite is rarely observed, altering from pyroxene and olivine. In one specimen a trace amount of olivine was found.

Discrete inclusions of anhedral magnetite, ilmenite or pyrite grains occur within alkali feldspar, biotite and amphibole. Apatite is ubiquitous and is the only commonly euhedral mineral. A single acicular apatite crystal may be included within alkali feldspar, at one end of the crystal, and within amphibole at the other end of the apatite crystal. Granular intergrowths of apatite and an opaque phase may occur in amphibole. Zircon and sphene are rarely observed, and occur as inclusions within amphibole, or interstitial to the mafic phases. Fluorite is a constituent of a few mafic clusters, and also is observed with quartz in feldspar interstices. Some fluorite grains display fluid inclusions. Calcite is almost always present in trace amounts. It may occur as a late stage interstitial phase, but is more commonly a replacement mineral. Similarly, chlorite is predominantly a replacement product, although plumose aggregates of chlorite are found in quartz. The presence of metamict haloes around some unidentified phases suggests that they are radioactive minerals.

3.2 Ferro-edenite syenite series

The mineralogy and textures observed are diverse, depending on whether the rock is: ferro-edenite syenite (2.3.2.i.), differentiated and pegmatitic ferro-edenite syenite (2.3.2.ii.) or xenolith-bearing ferro-edenite syenite (2.3.2.iii).

3.2.1 Ferro-edenite syenite

The essential phases in the ferro-edenite syenite are alkali feldspar (major) and quartz (minor to major). The accessory minerals include: amphibole, biotite, pyroxene, magnetite, ilmenite, pyrite, molybdenite, apatite, zircon, fluorite and sphene. Secondary minerals that may be present are: plagioclase, calcite, iddingsite/bowlingite, chlorite, serpentine, hematite, saussurite and sericite. Several unidentified phases occur in trace amounts and some of these are surrounded by pleochroic haloes, suggesting that they are radioactive. In Table 2 typical modes are given for the constituents of the ferro-edenite syenite. Representative photomicrographs are presented in Plates 7 and 8.

The microscopic and macroscopic texture of the ferro-edenite syenite varies with the degree of differentiation. The least evolved ferro-edenite syenites are massive, coarse-grained to medium-grained, with the predominant phase, alkali feldspar, forming a consertal, allotriomorphic texture. The mafic mineral content is relatively high, attaining a volume of about 15%. In the majority of the least evolved ferro-edenite syenites the mafic minerals, opaque phases and accessory minerals are evenly distributed throughout the rock. A synneusis texture may be observed, although it is rare. These clusters may contain amphibole, biotite, opaque phases and apatite.

With progressive differentiation the mafic content decreases, the

TABLE 2
Ferro-edenite syenite - Modes

mineral / abundance in :	C294	C322	C2224
alkali feldspar	68	78	68
amphibole	10	0.5	2
opaques	7	1.5	tr
biotite	8	4	5
pyroxene	-	tr	-
quartz	4	15	25
apatite and microlites	1	tr	-
sericite/saussurite	-	-	tr
plagioclase	tr	-	-
zircon	tr	tr	-
fluorite	tr	tr	tr
iddingsite/bowlingite	tr	tr	-
hematite	1	-	-
chlorite	tr	tr	-
calcite	tr	-	tr
unidentified phases	-	-	tr

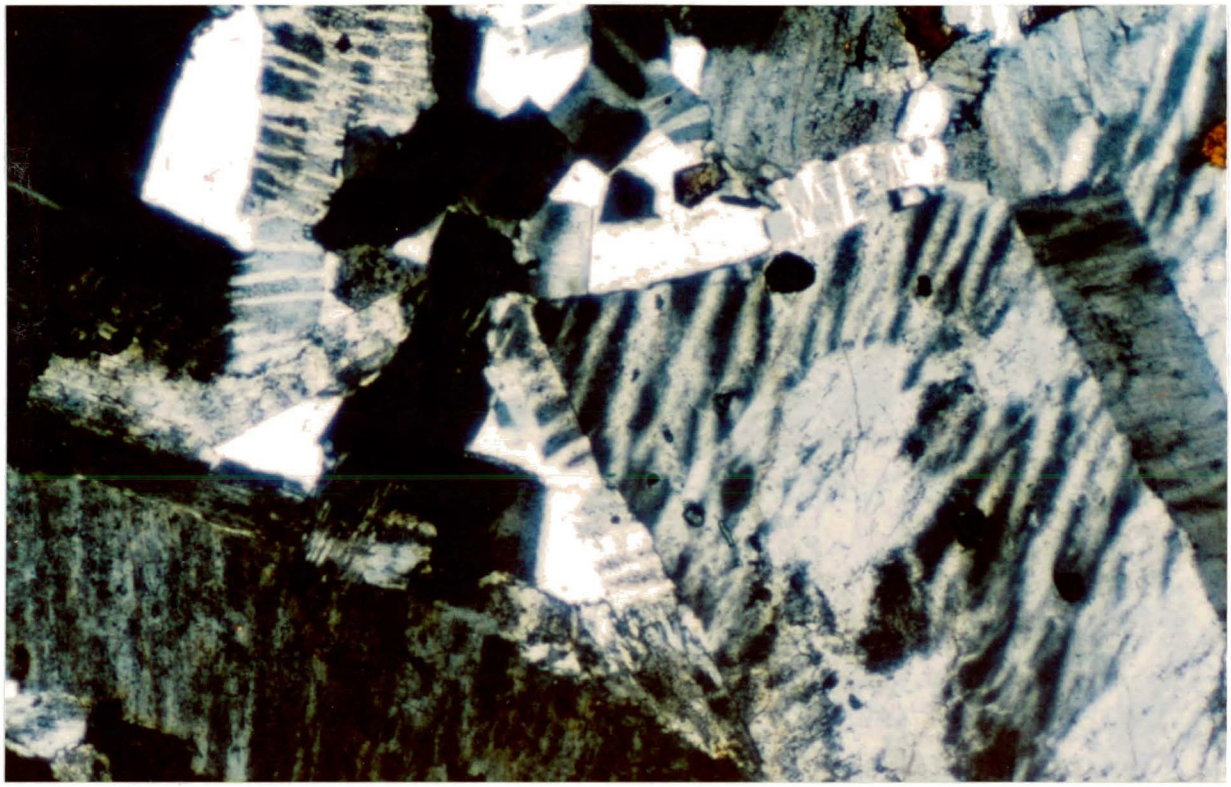

Plate 7 - Photomicrograph of perthitic texture in porphyritic ferro-edenite syenite. Cross polarized light.Width of photo is 2 mm.

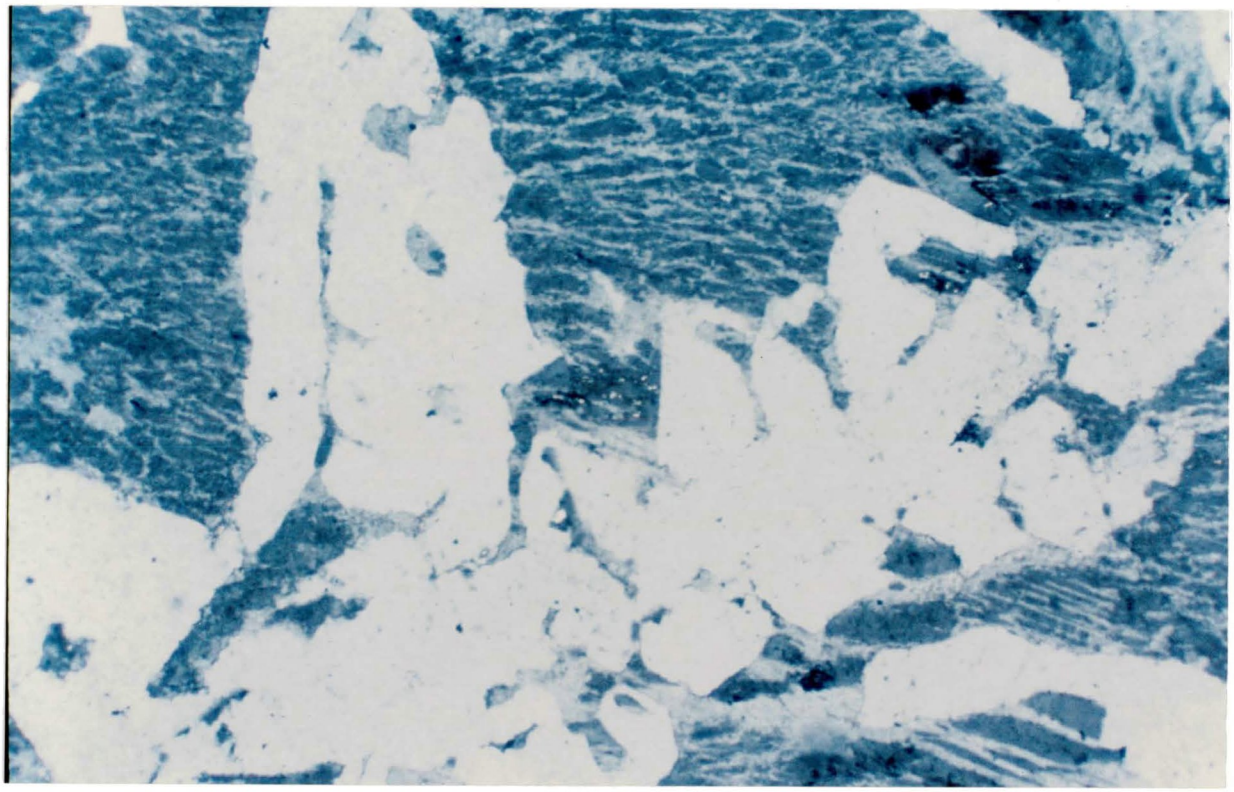

Plate 8 - Photomicrograph of dendritic texture in ferro-edenite syenite. Cross polarized light.Width of photo is 2 mm.

quartz abundance increases and the overall texture becomes porphyritic. Initially, the perthitic alkali feldspar is subhedral and bladed. The alkali feldspar grain size distribution is seriate in the less evolved syenites and grain margins remain conserted.

Further differentiation results in a ferro-edenite syenite in which the porphyritic texture becomes increasingly evident. Porphyritic ferro-edenite syenites are the most abundant rocks in all of the Centre III areas traversed. In these rocks, medium-grained anhedral to subhedral alkali feldspar phenocrysts are set in a hypidiomorphic groundmass, consisting largely of alkali feldspar prisms and laths. All alkali feldspar grains display a perthitic exsolution texture, and microprobe analyses indicate that for grains in which the host versus exsolved status can be determined, the majority are antiperthites. (chemistry in section 7, plate 7). The phenocrysts and other phases are homogeneously distributed and exhibit a decussate texture. In the porphyritic ferro-edenite syenite, the amount of interstitial quartz is volumetrically greater, as is the abundance of fluorite and other accessory phases, than in the massive ferro-edenite syenite.

The typical crystallization sequence for ferro-edenite syenite is: opaque minerals and apatite, alkali feldspar, pyroxene, amphibole, biotite, sphene, fluorite, zircon and quartz. Alteration is insignificant in most ferro-edenite syenite specimens. Weak pervasive hematization and saussuritization of feldspar is rarely found. Replacement textures are not characteristic of this rock type. Recrystallization of this syenite is observed in areas affected by deformation and is recognized by the presence of sutured feldspar boundaries and secondary plagioclase grains at alkali feldspar grain boundaries.

In the antiperthitic alkali feldspar phenocrysts and groundmass

grains, the exsolved potassic phase forms strings and veins, as defined by Cerny et al. (1984). Patchy areas of exsolution are also relatively common. In a small proportion of alkali feldspar grains the lamellae are blebby or flame-like. Commonly, the entire phenocryst is twinned, with Carlsbad twins being the most abundant, followed by Baveno and Manebach twins. The host phase may display albite- or pericline-twinning, particularly in the patch perthites. Groundmass alkali feldspars are generally not twinned. Many of the alkali feldspar phenocrysts are mantled, with a core that is not perthitic on a microscopic scale, surrounded by a mesoperthitic mantle. In the case of multiple mantles about a single core, the core and each successive mantle is perthitic. The saussuritization and hematization may be preferentially distributed in the same manner. Sericitic alteration of alkali feldspar is rare. These alteration minerals occur as an almost submicroscopic clouding or dusting of the alkali feldspar. The phenocrysts are subhedral to euhedral, tabular and almost always randomly oriented. Groundmass alkali feldspars are anhedral to subhedral, and vary in texture from allotriomorphic massive to prismatic. Boundaries between feldspars are commonly slightly convoluted, whereas contacts between feldspars and the interstitial quartz are always straight. The alkali feldspar phenocrysts may enclose smaller perthitic grains, opaque phases, apatite and amphibole. The amphibole inclusions may occur as very fine-grained crystals within a single mantle. Inclusions of alkali feldspar in amphibole are also found.

Quartz is ubiquitous in the ferro-edenite syenite in varying amounts. With differentiation, the ferro-edenite syenite becomes progressively more quartz-rich. The quartz generally crystallized last and occupies interstitial areas. Strained extinction, fracturing and recrystallization

textures are not common. Recrystallization results in a mosaic of strain-free anhedral quartz grains. The primary quartz is generally free of mineral inclusions, but contains abundant fluid inclusions.

Amphibole occurs in all ferro-edenite syenites. A variety of pleochroic colours are exhibited, ranging from: tan to brown, light to medium green, olive green to medium green, and only slightly pleochroic blue grains. In the least evolved ferro-edenite syenites, in which the fluorite content is low, brown amphiboles are present. Green amphiboles are most commonly observed and occur in the widespread porphyritic ferro-edenite syenites. A trace of blue amphibole may be found in this rock as a late-crystallizing phase, adjacent to quartz. In the highly differentiated ferro-edenite syenites, that are mafic-poor and quartz-rich, blue amphiboles are commonly found.

Typically the amphiboles are interstitial to the groundmass feldspars and occur singly or in clusters of a few grains. The crystal habit is anhedral to subhedral. Alteration to hematite or chlorite is rare, except in the recrystallized ferro-edenite syenites of the Guse Point/Pic Island area. In these rocks, the amphiboles and biotites are ragged in appearance, and biotite may replace amphibole.

Biotite typically forms subhedral laths and anhedral grains in the interstices of the groundmass. The biotite is pleochroic from straw yellow to dark brown, although in some ferro-edenite syenites it is orange, green or red. The biotite may occur as a replacement of amphibole, particularly along the edges of grains. Biotite may form reaction rims around magnetite grains. In the least-differentiated ferro-edenite syenites orange-brown biotite is partially replaced by a mosaic of quartz, in the form of spindles parallel to cleavage traces.

Pyroxene is relatively rare in the ferro-edenite syenite. The

observed colours include: light green, medium green and zoned grains with a light green core grading into a light olive green margin. The pyroxene grains are typically equant, though anhedral, and are associated with the mafic minerals in groundmass interstices. Replacement of pyroxene by amphibole and biotite is common. In a few specimens bright orange iddingsite/bowlingite replaces the pyroxene almost entirely, but such alteration is much less prevalent than in the quartz syenites. An opaque mineral may be included in the iddingsite/bowlingite. In two specimens serpentine replaces pyroxene along fractures.

Opaque phases occur as discrete, very fine-grained blebs in alkali feldspar and in very small clusters with apatite. Opaque minerals also form anhedral grains associated with amphibole grains. Magnetite and ilmenite are the main primary opaque phases, although traces of pyrite and molybdenite have been found. Relatively few specimens appear to contain both magnetite and ilmenite, where they may occur as two discrete phases or may be intergrown.

Hematite, as an alteration product of feldspars and mafic grains is widespread, although the degree of alteration is very limited. Alkali feldspars display a homogeneous distribution of very fine-grained hematite specks. Hematite and magnetite also occur as rims around, and irregular blebs within altered amphiboles. Pyrite and molybdenite occur in trace amounts associated with the late-stage fluorite and quartz.

Apatite is present in a majority of ferro-edenite syenite specimens. Euhedral to subhedral prismatic and basal sections are commonly included in alkali feldspar phenocrysts. The apatite is associated with opaque phases and mafic minerals in small clusters. Acicular apatite grains may be of such great relative length, that portions of a single grain can be included in several other phases. Apatite also forms microlites, which

are scattered throughout the groundmass.

Most ferro-edenite syenites contain euhedral zircon, usually associated with late-stage fluorite and quartz. Some zircons display concentric zoning, evident from progressive changes in birefingence.

Fluorite is a relatively common accessory phase. It is usually colourless, but in coarse-grained syenites it is purple. It occurs interstitial to the groundmass feldspars and displays an anhedral crystal habit.

Sphene is found in a few specimens, in trace amounts. This differs markedly from the contaminated ferro-edenite syenite where sphene is the predominant accessory phase. It occurs as euhedral to subhedral grains, adjacent to the fluorite and interstitial quartz.

Plagioclase is apparent only in ferro-edenites which have been recrystallized as a result of deformation. A late influx of water, possibly of meteoric origin, travelling through shear zones, could produce very localized fusion and the crystallization of albite. Thus, although two discrete feldspars are present, it is not a subsolvus assemblage. Albite occurs as anhedral grains in a recrystallized groundmass or it may replace alkali feldspar. In the latter case anhedral albite blebs form along sutured perthite margins. Albite- and pericline-twinning is always evident. Alteration is generally absent, although in a few specimens trace amounts of sericite form patches near the core of albite grains, or along the edges.

Calcite may occur in trace amounts as an alteration mineral. It may be found replacing perthitic alkali feldspars, along their boundaries, but more commonly occurs in the groundmass, as an interstitial phase with quartz. The latter habit is observed in the recrystallized syenites, and the source of the calcite may be the alteration of amphibole or alkali

feldspars, or it may have been introduced by fluids moving through the shear zones.

Chlorite is rare and where present occurs in trace amounts. It replaces amphibole and occasionally forms plumose fans entirely included within quartz. Chlorite may also form anhedral, ragged masses.

3.2.2 Differentiated and pegmatitic ferro-edenite syenite

There are discrete intrusions and transitional zones within the ferro-edenite syenite of highly differentiated and pegmatitic ferro-edenite syenite. Highly differentiated syenites are exposed in the vicinity of Ashburton Lookout (C2135, 2191) and consist largely of coarse-grained mesoperthitic alkali feldspar and quartz in a graphic intergrowth. Other constituents include amphibole, biotite, fluorite, opaque minerals and zircons. The coarse-grained to very coarse-grained perthites display braid or vein exsolution lamellae, Carlsbad twins and are not mantled. Their habit may be tabular, bladed, sheaf-like or dendritic. An example of the dendritic texture is depicted in Plate 8. The quartz content is generally greater than 30% by volume and is strain-free and free of mineral inclusions. The mafic mineral content of these highly differentiated syenites ranges from a couple of percent by volume to nil. Green and blue amphibole and brown biotite may be found in tiny aggregates, interstitial to the feldspar, together with zircon, fluorite, and opaque minerals. The fluorite is purple in some specimens.

Pegmatitic ferro-edenite syenite is widely distributed throughout areas of ferro-edenite syenite, and typical examples include: C2002, C2177, C2189. Mineralogically, these pegmatitic syenites are similar to those differentiated syenites described above. They however lack graphic intergrowths and may contain up to 10% mafic minerals. Alteration and

recrystallization textures were not observed in these two varieties of ferro-edenite syenite.

3.2.3 Xenolith-bearing ferro-edenite syenite

The xenolith-bearing ferro-edenite syenite is petrographically similar to the ferro-edenite syenite. The major mineralogical difference is the dominance of biotite over amphibole in the xenolith-bearing variety. The ubiquitous phases are alkali feldspar, opaque minerals and biotite. Amphibole, quartz, plagioclase, apatite, sphene, zircon, calcite, fluorite, pyroxene, sericite and hematite may be present in small quantities. The macroscopic texture is porphyritic, with medium-grained perthitic alkali feldspar phenocrysts, set in a groundmass of subhedral, perthitic alkali feldspar and anhedral biotite. Minor sericitization and hematization typically affects the feldspars in these syenites, and secondary plagioclase is encountered in deformed syenites. (Guse Pt., Neys Lookout).

The alkali feldspar exhibits the same textures as in the porphyritic ferro-edenite syenite. Vein and braid exsolution lamellae prevail, and in mantled phenocrysts these perthitic textures alternate with homogeneous, non-perthitic phases. Sericitic alteration is present in about half of the syenites examined. It occurs as very fine-grained specks throughout the alkali feldspars, or may form sub-radiating fans. Commonly, the outside margins of the alkali feldspar phenocrysts are most affected by the minor alteration.

3.3 Contaminated ferro-edenite syenite

This syenite differs from the xenolith-bearing ferro-edenite syenite in a few important ways. As the name implies, these rocks are a

contaminated variety of the ferro-edenite syenite, where the xenolith-bearing ferro-edenite syenite is a transitional stage. Macroscopically, the contaminated ferro-edenite syenite is coloured purple and contains abundant metasomatic biotite ovoids and xenoliths of sedimentary and volcanic rocks. Microscopically, the contaminated ferro-edenite syenite contains significant biotite, sphene, and of course the characteristic biotite ovoids. Also the relatively strong hematization and sericitization of alkali feldspar grains serve to distinguish this variety of syenite from the xenolith-bearing ferro-edenite syenite.

The essential minerals of the contaminated ferro-edenite syenite are alkali feldspar (major) and quartz (major to minor). The accessory minerals include: biotite, amphibole, pyroxene, magnetite, ilmenite, sphene, zircon and apatite. The secondary constituents are: plagioclase, sericite, calcite and hematite. Representative modes are presented in Table 3. Plates 9 and 10 show the biotite ovoid texture.

A porphyritic texture, with perthitic alkali feldspar phenocrysts set in an allotriomorphic groundmass of alkali feldspar and quartz is found in the majority of specimens. A seriate texture occurs in a few examples of this rock type. The alkali feldspar phenocrysts are subhedral, and tabular. In the groundmass, the anhedral alkali feldspar and plagioclase display consertal boundaries. Myrmekitic intergrowths are developed in the margins of plagioclase, adjacent to alkali feldspar grains. Quartz is interstitial to all other phases. Oval to spherical clusters of biotite, up to about 3 mm long, are homogeneously distributed in the groundmass. Many ovoids consist only of biotite, others however, contain amphibole, apatite and opaque minerals. The constituent phases of the ovoids are typically subhedral, homogeneously distributed and randomly oriented. Plate 10 displays a photomicrograph in which a biotite ovoid has been

TABLE 3
Contaminated ferro-edenite syenite - Modes

mineral / abundance in :	C2001	C2026	C2029
alkali feldspar	68	55	59
amphibole	20	15	18
opaques	tr	3	tr
biotite	10	10	7
pyroxene	tr	-	tr
quartz	tr	-	3
apatite and microlites	tr	2	7
sericite/saussurite	-	4	3
plagioclase	-	10	tr
zircon	tr	tr	tr
fluorite	tr	-	tr
hematite	-	-	tr
calcite	tr	-	-
sphene	2	tr	2
unidentified phases	tr	tr	-

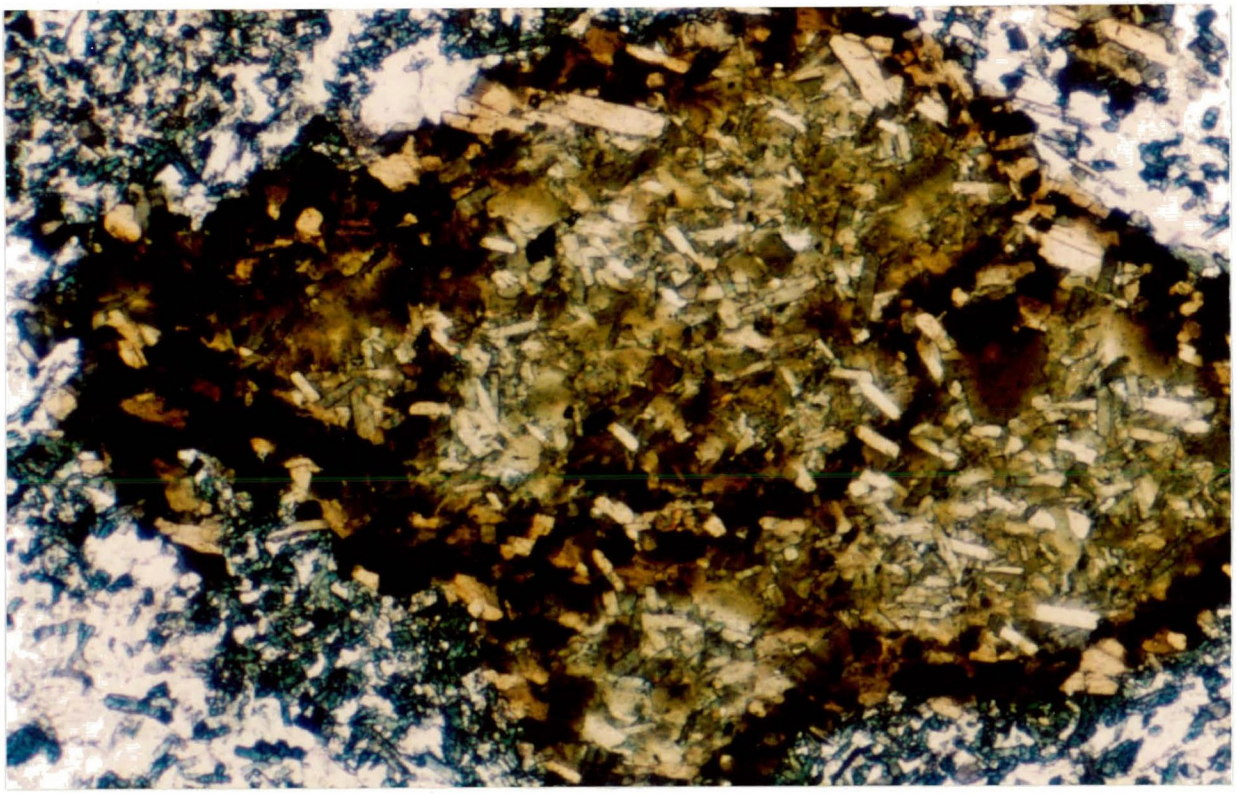

Plate 9 - Photomicrograph of a cluster of biotite ovoids in xenolith within contaminated ferro-edenite syenite. Width of photo is 2 mm.Plane polarized light.

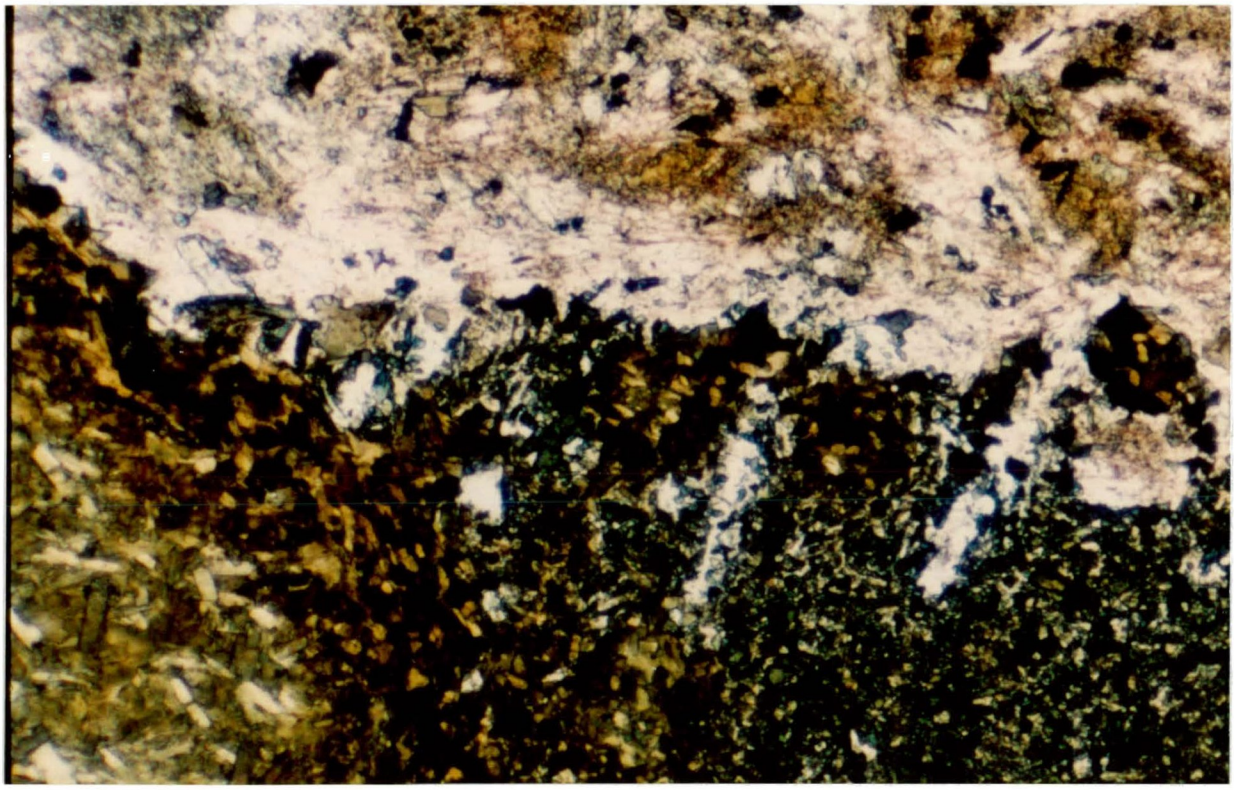

Plate 10 - Photomicrograph of a biotite ovoid physically breaking away from xenolith margin in contaminated ferro-edenite syenite. Width of photo is 2 mm.Plane polarized light.

detached from the edge of a xenolith. The majority of ovoids though, appear to have formed in situ, by metasomatic processes. The ovoids may straddle xenolith/syenite contacts and in some cases incorporate altered alkali feldspar grains, from the groundmass of the syenite.

Xenoliths are encountered in petrographic study and xenolith margins may be highlighted by a higher concentration of biotite and occasionally amphibole and pyroxene. Within the syenite, plagioclase laths within millimetres of the xenolith contact may be oriented subparallel to this contact.

Perthitic alkali feldspar is the predominant phase in the contaminated ferro-edenite syenite. Vein exsolution lamellae are most common, followed by a significant proportion of patch perthites. Carlsbad-twinning is common in alkali feldspar phenocrysts. Mantled alkali feldspar grains are also frequently observed. The exsolution textures and degree of alteration may vary from core to rim in these mantled grains. The alternation of these features is observed where more than one mantle is visible.

Inclusions found within alkali feldspar include: biotite, apatite, opaque minerals, pyroxene and amphibole. The amphibole inclusions may be preferentially distributed through the outer mantle, although this texture is rare. In a few alkali feldspar phenocrysts the host phase appears to be microcline, as indicated by the presence of cross-hatched twinning. As with other syenite types, the microprobe was utilized to determine whether the host phase is typically sodic or potassic. In these contaminated ferro-edenite syenites, the strong hematization and sericitization precluded analysis, and thus, the distinction could not be made. In a few altered feldspars, opaque cubes and equant grains may be found. Some of these grains may be hematite, although typically it is

much more fine-grained.

Quartz is present in the majority of contaminated ferro-edenite syenites. Being the last primary phase to crystallize, it occupies the interstices in the groundmass. A mosaic texture is observed where quartz has crystallized in larger interstices. In one specimen of contaminated ferro-edenite syenite, glomeroporphyritic alkali feldspar is surrounded by hypidiomorphic quartz.

Biotite is commonly the predominant mafic mineral, occurring in the groundmass as discrete subhedral grains. The biotite is typically brown, although it may be straw yellow or light brown.

Amphiboles are subhedral to euhedral and are typically coloured brown, brownish-green, or light to medium green. In one specimen of syenite, the amphiboles vary in colour from olive green to blue green. In one thin section (C2067) the amphibole is porphyritic. Another thin section of contaminated ferro-edenite syenite, from another exposure, contains amphiboles with concentrically zoned pleochroism and birefringence.

Pyroxene is found as cores to amphibole grains, in which amphibole (±calcite) replaces pyroxene. Less commonly it occurs as anhedral to subhedral grains, which are: colourless, light green or medium green and may be concentrically zoned.

The opaque minerals, magnetite and ilmenite occur as discrete inclusions in alkali feldspar and in the mafic ovoids. Subhedral sphene is present in the trace amounts in almost every specimen of contaminated ferro-edenite syenite. Zircon is not observed as commonly as in the contamination-free ferro-edenite syenites. Apatite prisms occur as inclusions in perthitic phenocrysts, as microlites throughout the groundmass, and rarely, within the ovoids.

Secondary albite is found in the groundmass of all contaminated ferro-edenite syenites. The albite commonly displays albite-twinning, and rarely, pericline-twinning. The textures displayed by the albite are similar to those exhibited by albite in the contamination-free ferro-edenite syenite. Anhedral plagioclase occurs in a consertal texture with alkali feldspar and quartz in the groundmass. In recrystallized syenites albite occurs as euhedral to subhedral laths in the groundmass, or anhedral blebs of albite at granulated alkali feldspar phenocryst edges.

3.4 Quartz syenite

The essential constituents of the quartz syenite are alkali feldspar (major) and quartz (minor to major). The accessory phases are found in minor quantities and may include: pyroxene, amphibole, biotite, opaque minerals, apatite, zircon, fluorite, chevkinite, synchisite-bastnesite, olivine, niobian rutile, parrisite, aeschylite and several other as yet unidentified minor phases. The secondary minerals, generally found in trace amounts, include: iddingsite/bowlingite, plagioclase, chlorite, sericite, hematite and calcite. Typical modes for the constituents of quartz syenite are presented in Table 4. The texture of the quartz syenite is hypidiomorphic-granular. It is generally not porphyritic. In two exposures in the East Bank area, a strong lineation fabric is evident, defined essentially by a parallel alignment of alkali feldspar prisms. To a lesser extent, the mafic minerals of these syenite exposures are aligned parallel to this same lineation. Generally, the alkali feldspar and mafic minerals are coarse-grained to medium-grained, and subhedral to anhedral. Several of the accessory phases are euhedral to subhedral, and are typically very fine-grained. Typically all minerals are homogeneously distributed throughout the quartz syenite. In a few

TABLE 4
Quartz syenite - Modes

mineral / abundance in :	C182	C367	C369
alkali feldspar	87	81	85
amphibole	10	10	13
opaques	tr	2	0.5
biotite	tr	0.5	tr
pyroxene	-	tr	tr
quartz	2	4	tr
apatite and microlites	tr	tr	tr
zircon	tr	0.5	tr
iddingsite/bowlingite	tr	tr	tr
chlorite	-	-	tr
REE-phases	tr	tr	tr
fluorite	tr	1	tr

specimens, particularly the rare porphyritic quartz syenites, the mafic minerals form small clusters. The replacement of pyroxene and possibly olivine by iddingsite/bowlingite is widespread and characteristic of these quartz syenites. Other replacement textures and alterations are rare. Pyroxene may also be replaced by amphibole, which is in turn replaced by biotite. Chloritic alteration of biotite is observed, but is rare. Sericitization and hematization of alkali feldspar is also very minor. Typical quartz syenite minerals and textures are depicted in Plates 11 and 12.

The sequence of crystallization is: olivine, pyroxene, apatite and opaques, alkali feldspar, more pyroxene, amphibole, biotite, fluorite, zircon and chevkinite and unidentified phases, and finally quartz.

The predominant phase of the quartz syenite is alkali feldspar. Typically coarse-grained and subhedral, all alkali feldspar grains within a single specimen are of approximately the same size. Porphyritic specimens are rare, but where observed, contain coarse-grained, euhedral tablets of braid perthitic alkali feldspar in a groundmass of coarse-grained to medium-grained subhedral braid perthitic alkali feldspar. In both the porphyritic and hypidiomorphic-granular quartz syenites, the predominant alkali feldspar exsolution texture is vein- or braid-type. Wispy, flame-like and patchy exsolution lamellae are found, but are much less common. The microprobe analyses reveal that, for alkali feldspars in which the host versus exsolved relationship is clear, most grains are in fact anti-perthites (Section 7). Carlsbad twins are common, whereas Baveno and Manebach twins are rare. In one specimen the phenocrysts display Carlsbad twinning, while the groundmass feldspars have Baveno twins. Mantling of alkali feldspar by alkali feldspar is observed, but is not as common as in the three other syenite types. Generally, the core of

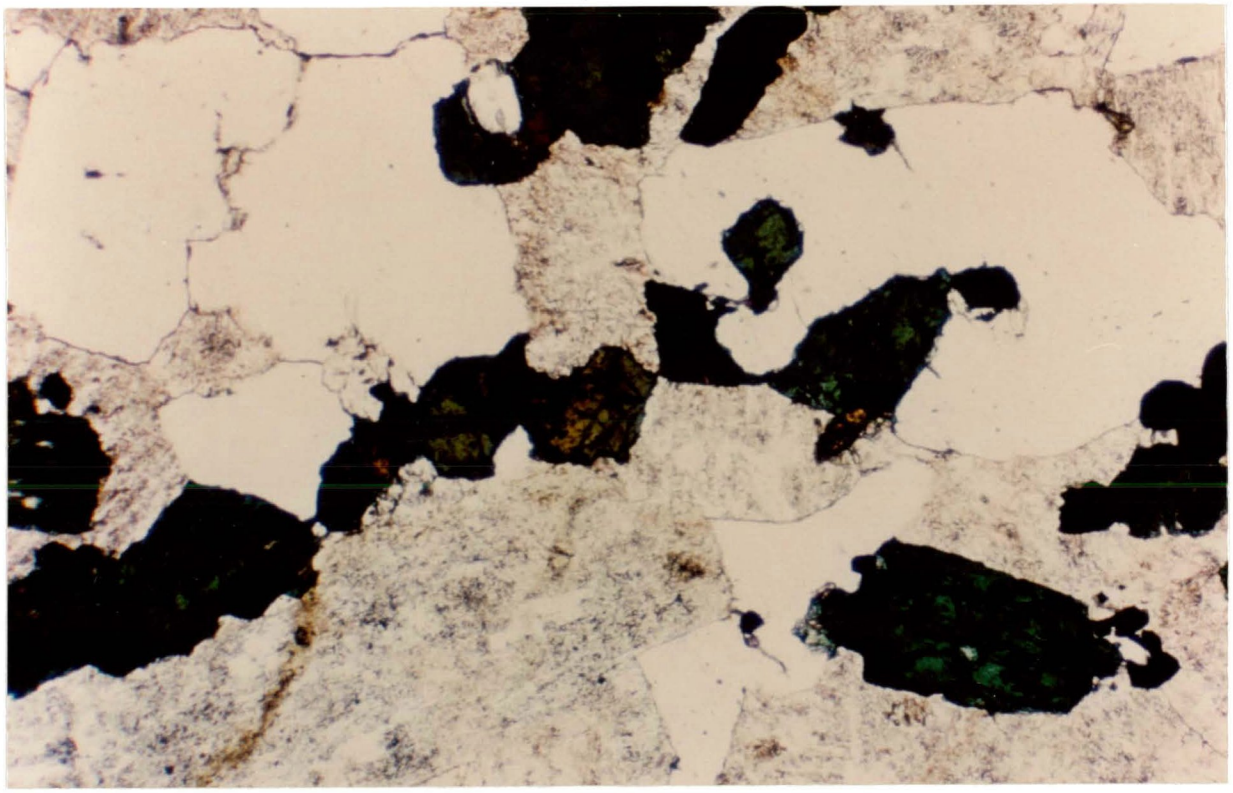

Plate 11 - Photomicrograph of the typical mineralogy and texture of quartz syenite. Width of photo is 2 mm.Plane polarized light.

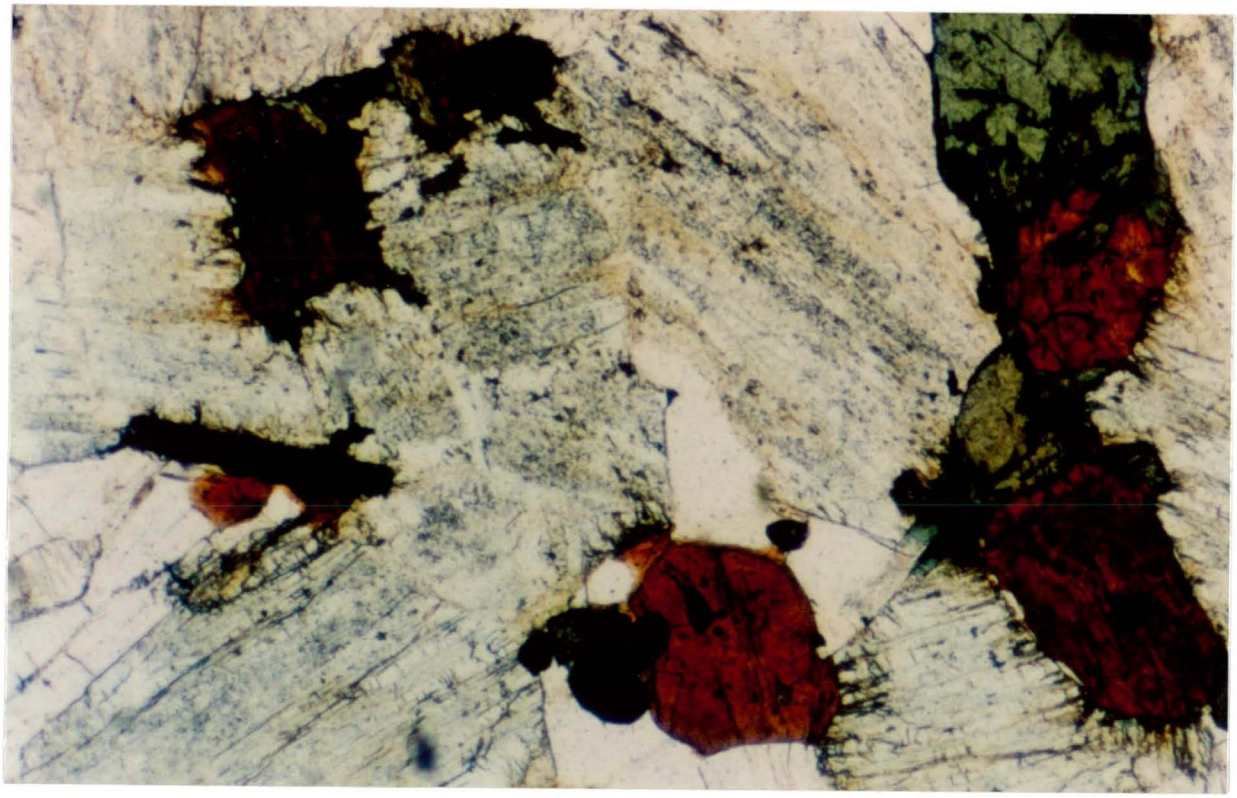

Plate 12 - Photomicrograph of the typical mineralogy and texture of quartz syenite. Width of photo is 2 mm.Plane polarized light.

the grain is homogeneous and non-perthitic and the mantle is perthitic. Intergranular margins between alkali feldspar grains are usually straight and sharp, although in a few specimens incipient suturing of margins is found. Minute inclusions of fluorite, opaque minerals, apatite, pyroxene and amphibole may be found in a small proportion of the alkali feldspar grains. The pyroxene inclusions are commonly zoned and are euhedral to subhedral. In one specimen, mafic inclusions are prominent in only one half of the Carlsbad-twinned alkali feldspars. In another specimen, mafic inclusions are aligned parallel to the twin plane, near the centres of alkali feldspar grains. Hematization and sericitization of alkali feldspar in quartz syenites is extremely rare, and where present, occurs along very small fractures and cleavage traces. A few ragged sericite plates are observed at alkali feldspar grain margins. Microcline is the host phase of some patchy perthites, as evident from the cross-hatched twinning.

Interstitial quartz is always present and is strain-free. It contains abundant fluid inclusions. Primary and secondary inclusions are evident. Some examples show pseudo-Brownian motion of the vapour phase. Mineral inclusions are typically opaque phases and zircon.

Pyroxene is the characteristic mafic phase of the quartz syenites. The pyroxene displays a variety of pleochroism: bright green, light green, medium olive-green to dark green, medium green to light green. In a majority of the quartz syenite thin sections studied, there are two distinct pyroxene habits. Pyroxenes that crystallized prior to the alkali feldspar occur as equant grains partly or totally included within the alkali feldspar. The bright green pyroxene that crystallized after the majority of the alkali feldspar is relatively coarser than the early pyroxene, forms subhedral inclusions in quartz and commonly displays

replacement by amphibole. In either generation of pyroxenes, the grain margins may be zoned. Inclusions of opaque phases in the pyroxene are common.

Both the early- and late-crystallizing pyroxenes are replaced partly or completely by iddingsite/bowlingite. The iddingsite/bowlingite alteration product is bright orange and non-pleochroic. In a few specimens of quartz syenite, this alteration product is more of a gold or honey-yellow colour. The relief of the iddingsite/bowlingite is medium positive and the birefringence varies from upper first order to upper second order. Under crossed-polars the iddingsite/bowlingite appears to form a very fine-grained felted aggregate. This alteration replaces the pyroxene from the core outwards and in completely altered grains, maintains the original outline of the pyroxene. Inclusions of opaque minerals and zircon may be found in the altered portions of pyroxene grains. Very minor hematitic alteration of pyroxene along cleavage traces is noted.

Amphibole is always present in the quartz syenite and displays a wide variety in pleochroic colours: medium olive green to dark green, medium olive green to medium green, blue green, blue, brown, light brown to dark olive green, light green to medium green, light brown to dark green, yellowish green to grass green, olive-gold to brown, and dark brown to dark olive green. The blue amphiboles are restricted to the late-stage interstitial quartz-rich regions. A minor amount of blue-green amphibole replaces green varieties of amphibole. Most of the amphibole that replaces and mantles pyroxene is olive green. Alteration of amphibole is rare, but where present, the amphibole is replaced by biotite, opaque phases and rarely, by chlorite. The majority of the primary amphibole crystallized after the alkali feldspar and therefore the amphibole forms

subhedral laths to anhedral interstitial grains. Very minor clustering of amphibole, pyroxene, opaque minerals and zircons may be observed. Inclusions of alkali feldspar and apatite are also contained in the amphibole.

The biotite of the quartz syenite also displays a variety of pleochroic colours. Much of the primary biotite is brown, although these pleochroic colours have also been noted: green, orange, green to orange, honey-yellow to dark orange, straw yellow to brown, orange to dark brown and scarlet red to brown. The primary biotite is typically interstitial to amphiboles and alkali feldspars, forming anhedral laths and irregular aggregates. Subsolidus overgrowths of biotite around opaque phases are found, particularly when the opaque mineral is included in amphibole. Biotite also replaces amphibole, along ragged edges or cleavages. Sericite replaces biotite along margins in two quartz syenite specimens. In one specimen rod-like opaque minerals are included in the biotite, along cleavage traces.

Most of the opaque minerals are equant, i.e. circular, oval or rounded rectangles. Anhedral, interstitial opaque grains are rarely found. The most common opaque minerals in the quartz syenite are magnetite, ilmenite and pyrite. Typically these minerals form inclusions in mafic minerals. Some magnetite grains in amphibole are rimmed by biotite. A small proportion of the opaque minerals are observed as a replacement of pyroxene and amphibole. One late-stage opaque phase is prismatic, with monoclinic crystal terminations and occurs in quartz-filled interstices. This mineral is commonly a very dark brown colour in transmitted plane-polarized light.

Euhedral apatite prisms are included within pyroxene, amphibole and may also be partly included in both amphibole and alkali feldspar. A less

significant fraction of the apatite forms inclusions in the late-stage interstitial quartz.

The zircon in the quartz syenite typically forms discrete, euhedral, rectangular and rhombic crystals, set in the interstitial quartz. This zircon is colourless to very pale yellow, and commonly displays concentric zoning. The cores of many zircons are highly metamict and dark brown or black. The zircon may occur in clusters with opaque phases, chevkinite and other unidentified radioactive phases. Less commonly, zircon is included within pyroxene.

Fluorite is one of the last phases to crystallize and is found in or adjacent to the quartz. The fluorite is colourless to very pale purple, forming subhedral to anhedral equant grains. Fluid inclusions are plentiful in much of the fluorite. Opaque minerals are partly or completely included in the fluorite. Fluorite can also be found in the rare clusters of mafic minerals, opaque minerals and iddingsite/ bowlingite. Biotite is characteristically associated with fluorite in these quartz syenites. In two specimens, fluorite inclusions are found in alkali feldspar grains.

Trace amounts of chevkinite, synchisite-bastnesite, olivine, niobian rutile, parrisite, and aeschylite have been identified by Dr. R.H. Mitchell from specimens C2153, C2138 and C367.

Secondary plagioclase laths are observed in two quartz syenite specimens, adjacent to the contact with biotite gabbro xenoliths. More than a few millimetres away from this contact, plagioclase is not observed. These plagioclase laths display albite-twinning and some are bent. A trace amount of calcite is observed, altering from this plagioclase. Calcite is also an alteration product of the amphibole, but this is very rare. In one specimen, calcite rims an opaque grain that is

TABLE 5

Estimated Modes for Metavolcanic Xenoliths

	Alk-feld.	Qtz.	Plag.	Amph.***	Bio.	Fl.	Sph.	Zr.	Ap.	Op.	% Phenos.*
C880	82/7**	2-3	1/2	5/1	1	1	1	1	1	1	10
C889	8/10	2-3	7/65	6/1	1-2	1	1	1	1	1	76
C1213	55/23	5-6	6/3	5	1-2	1	1	1	1	1	26

* - percent of rock volume
** - 82% groundmass
- 7 % phenocrysts
*** - includes pseudomorphed augite

from Jago,1980

TABLE 6
Mafic volcanic xenoliths - Modes

mineral / abundance in :	C170	C2050	C366B
plagioclase	65	-	3
alkali feldspar	-	11	14
amphibole	17	80	65
opaques	tr	tr	-
biotite	12	-	2
pyroxene	tr	tr	tr
quartz	-	tr	5
apatite and microlites	2	8	10
zircon	-	-	tr
fluorite	3	-	-
sericite/saussurite	tr	tr	tr

included in the amphibole. In another specimen, C2213, a trace amount of interstitial calcite is found.

3.5 Volcanic Xenoliths

Oligoclase basalt xenoliths are the major component of the Neys Lookout and Ashburton Lookout breccias. They contain the following primary minerals: alkali feldspar, quartz, plagioclase, pyroxene, amphibole, biotite, opaque minerals, fluorite, epidote, zircon, sphene, apatite. Secondary carbonate, hematite and sericite is evident in many volcanic xenoliths. Estimated modes (Jago, 1980) from some typical xenoliths are presented in Table 5. This study found a greater proportion of mafic minerals, constituting 40% to 80% of the mode (Table 6).

Petrographic study reveals that the majority of volcanic xenoliths are porphyritic, varying from unaltered examples with plagioclase microphenocrysts, to metasomatized rocks with porphyroblastic alkali feldspar completely replacing the plagioclase. Jago (1980) determined the plagioclase composition to be labradorite, whereas Mitchell and Platt, (1982a) suggest it is oligoclase. The dominant texture of the volcanic xenoliths is the development of biotite-rich ovoids.

Jago (1980) described subhedral to euhedral phenocrysts of labradorite that exhibit glomeroporphyritic and interpenetrant textures. These grains display rounded cores and are mantled and replaced by alkali feldspar. Inclusions of biotite, apatite and other groundmass minerals occur in the labradorite cores. Albite- and pericline-twinning is poorly developed in most instances. Strained extinction is common in the plagioclase grains. The laths have no preferred orientation. Plagioclase laths are moderately saussuritized and sericitized.

The porphyroblastic alkali feldspar may or may not exhibit perthitic

textures. Typically these phenocrysts are subhedral to corroded and strongly hematized and sericitized. Alteration, which is patchy, is most evident at crystal terminations. Euhedral braid perthitic alkali feldspar is rare, and is evident only where the plagioclase replacement is complete. Carlsbad twins may be found. Inclusions of fluorite, biotite, amphiboles and opaque minerals occur in the porphyroblasts. In the groundmass, corroded, anhedral plagioclase grains are intergrown with moderately hematized alkali feldspar.

Jago(1980) has observed phenocrysts of amphibole and amphibole pseudomorphs after augite up to 1.5 mm long.

In the groundmass, biotite ovoids give the volcanic xenoliths their characteristic hornfelsed, spotty texture. Up to 15% of the volume of the rock may be attributed to these biotite ovoids. These clusters are typically spherical to ovoid, with an irregular outer edge. Randomly oriented brown biotite constitutes the bulk of these ovoids, although pyroxene and opaque mineral grains have been found in them.

In the groundmass biotite occurs primarily as a replacement of amphibole. The pleochroic colours exhibited are: light brown to dark olive green, brown, greenish yellow to olive green, straw yellow to brown, and orange to brown.

Amphibole is interstitial to most phases and generally constitutes a few percent of the mode of the metavolcanic xenoliths. Grains are coloured: light brown to medium olive green, or light yellowish-green to dark green. The amphibole is ragged and is commonly partly replaced by biotite.

Pyroxene occurs in trace amounts, as colourless or pale green round grains. It is scattered throughout the groundmass, occurs as remnant phenocrysts and may be present within the biotite ovoids. Some pyroxene

crystals are concentrically zoned. Replacement of pyroxene by amphibole is commonly observed.

Skeletal and equant opaque grains are found in the mafic minerals and occur as discrete crystals throughout the groundmass.

A small amount of interstitial quartz is found in most specimens of volcanic xenoliths. Strained extinction is evident. Jago (1980) noted that a small amount of zircon may be observed in the volcanics, and it is extensively altered. Fluorite, sphene and epidote occur as very fine-grained, anhedral, disseminated grains. Jago states that fluorite may contain inclusions of quartz and alkali feldspar. Apatite forms microlites within alkali feldspar, and in the groundmass may form small clusters of parallel acicular crystals. Jago (1980) observed apatite in the biotite ovoids. He also observed carbonate with poikilitic inclusions of amphibole, quartz, alkali feldspar and plagioclase.

3.6 Metasedimentary Xenoliths

The typical metasediment occurring as xenoliths in Centre III syenites is a fine-grained, poorly sorted, turbiditic greywacke. Petrographic study reveals that the metasedimentary xenoliths may contain: quartz (45-85%), biotite (10-55%), plagioclase (1-2%), opaque minerals (1%), fluorite (nil to 2%), amphibole (nil to 5%), pyroxene (nil to 5%) and trace amounts of sericite and zircon. The typical grain size averages less than 0.5 mm and ovoids up to 1.5 mm have been found (Jago, 1980).

In relatively deformation free sedimentary specimens the quartz grains are rounded to subangular, corroded, equidimensional and poorly sorted (Jago, 1980). In deformed sediments, the quartz forms a recrystallized mosaic texture, interstitial to all other grains. Augen of

quartz may be developed.

Plagioclase exhibits albite- and pericline-twinning, and forms subhedral grains in a consertal texture with quartz. Minor sericitization of the plagioclase is ubiquitous.

Jago (1980) observed amphibole and pyroxene in some metasedimentary xenoliths. Both minerals form corroded, anhedral grains and blasts, and both may be replaced by biotite.

Biotite is yellow-green to brown, in anhedral plates which define a foliation. Discontinuous lenses of biotite wrap around the largest feldspar grains, possibly a remnant of earlier regional metamorphic effects (Jago, 1980). The biotite may alter to sericite, but is normally unaltered.

In metasedimentary xenoliths biotite ovoids may be observed. In the core, a grain of fluorite or magnetite may be found. Anhedral biotite laths are oriented perpendicular to the long axis of the blast (Jago, 1980). Inclusions of zircon and quartz are oriented with their long axes parallel to the long axis of the blast.

Fluorite is common in the metasedimentary xenoliths, forming anhedral grains in interstices. Opaque minerals are disseminated throughout the rock.

AMPHIBOLE COMPOSITIONAL VARIATION

4.1 Introduction

All of the compositional data presented in this thesis are new. The bulk of the analytical work was performed by the author at Dalhousie University. Additional amphibole data were obtained by Dr. R.H. Mitchell at Purdue University and at Cambridge University. Electron microprobe operating conditions are presented in Appendix I.

Altogether 71 specimens of Centre III syenite were utilized in the microprobe study of amphiboles. Specimens from all four syenite types and from the volcanic xenoliths were investigated. Amphiboles are ubiquitous in Centre III syenites from all of the study areas, and are generally unaltered, so there was no difficulty in obtaining representative compositions. Rock samples were prepared as circular, one-inch diameter polished thin sections. The author generally performed four spot analyses per thin section, and Dr. Mitchell typically made about ten spot analyses per thin section.

Representative amphibole compositions for the four Centre III syenite types and for the volcanic xenoliths are presented in Tables 7 to 11. A complete list of amphibole compositions is given in Appendix V.

The classification scheme and nomenclature used for amphiboles from the syenites and xenoliths is that recommended by the I.M.A. (Leake, 1978). Cations are allocated to Z, Y, X and A sites in the amphibole standard formula $A_{0-1}X_2Y_5Z_8O_{22}(OH,F,Cl)_2$. Neumann's (1976) method was used to determine structural formulae and the ferric iron content. (See Appendices II and III). The I.M.A. amphibole classification diagrams are given in Figure 13 to 19. The amphibole classification indicates that

TABLE 7

Microprobe analyses - Amphiboles from magnesio-hornblende syenite

	C178/3 core	C178/4 rim	C181/1	C2120/1	C2123/3	C2128/1	C2150/1 core	C2150/2 rim
SiO2	42.2	39.9	41.0	52.3	46.4	41.2	42.9	45.9
TiO2	1.88	0.62	1.86	-	1.1	1.97	2.50	1.33
Al2O3	9.21	9.05	8.93	0.57	6.25	9.54	9.49	6.72
FeO T	20.7	27.3	23.8	9.78	18.8	20.7	17.5	18.3
MnO	0.37	0.24	0.72	0.21	0.4	0.43	0.372	0.28
MgO	8.51	3.44	5.86	12.4	11.2	8.01	10.4	10.8
CaO	11.9	12.0	11.0	24.8	11.0	11.4	10.8	10.7
Na2O	1.98	1.69	2.48	0.2	1.57	2.1	2.32	1.31
K2O	0.84	1.32	1.25	-	0.60	1.3	1.15	0.781
Recalc	-----	-----	-----	-----	-----	-----	-----	-----
Fe2O3	2.63	-	1.43	-	6.80	2.21	4.03	6.53
FeO	18.3	27.3	22.5	9.78	12.7	18.7	13.9	12.4
Total	97.7	95.5	97.1	100.2	97.9	96.9	97.8	96.9
Si	6.47	6.55	6.48	8.52	6.91	6.41	6.46	6.90
Aliv	1.53	1.45	1.52	-	1.09	1.59	1.54	1.10
Alvi	0.137	0.300	0.148	0.110	0.010	0.163	0.139	0.088
Ti	0.217	0.077	0.221	-	0.123	0.230	0.283	0.150
Fe3+	0.304	-	0.171	-	0.762	0.258	0.456	0.739
Fe2+	2.35	3.75	2.98	1.33	1.58	2.43	1.75	1.56
Mn	0.048	0.033	0.096	0.029	0.050	0.057	0.047	0.036
Mg	1.95	0.843	1.38	3.00	2.48	1.86	2.33	2.43
Ca	1.95	2.11	1.87	4.33	1.75	1.91	1.74	1.72
Na	0.589	0.538	0.761	0.063	0.453	0.633	0.678	0.381
K	0.164	0.277	0.252	-	0.114	0.258	0.221	0.150
Mg#	0.454	0.184	0.317	0.692	0.611	0.433	0.571	0.608

TABLE 8

Microprobe analyses - Amphiboles from ferro-edenite syenite

C182/1	C333/1	C2001/1	C2053/6	C2101/3	C2190/2	C2223/5	C2233/3
SiO2	44.8	45.9	44.2	42.5	44.2	42.0	46.5	49.5
TiO2	1.22	0.18	0.59	2.10	1.48	2.18	1.24	0.66
Al2O3	4.66	2.91	6.98	7.23	4.42	8.73	2.67	1.16
FeO T	28.5	32.9	22.0	27.0	30.5	21.9	31.0	31.6
MnO	0.94	0.76	0.64	0.573	0.93	0.53	0.836	1.98
MgO	3.5	1.71	8.41	4.23	1.63	7.5	2.86	1.27
CaO	9.05	6.16	11.2	4.90	9.67	11.1	7.76	1.2
Na2O	1.96	4.4	2.19	2.48	3.04	2.31	2.74	7.91
K2O	0.92	1.21	1.34	1.24	0.90	1.05	0.96	0.64
Recalc	-----	-----	-----	-----	-----	-----	-----	-----
Fe2O3	4.59	6.01	3.19	16.6	-	2.54	5.45	6.83
FeO	24.4	27.4	19.2	12.0	30.5	19.6	26.1	25.5
Total	96.0	96.6	97.9	93.9	96.8	97.6	93.1	96.6
Si	7.18	7.44	6.81	6.74	7.26	6.51	7.42	7.91
Aliv	0.82	0.56	1.19	1.26	0.74	1.49	0.50	0.09
Alvi	0.06	-	0.080	0.094	0.112	0.103	-	0.123
Ti	0.147	0.022	0.068	0.250	0.183	0.254	0.149	0.079
Fe3+	0.554	0.734	0.370	1.98	-	0.297	0.655	0.822
Fe2+	3.27	3.73	2.47	1.59	4.18	2.54	3.48	3.41
Mn	0.128	0.104	0.084	0.077	0.129	0.070	0.113	0.268
Mg	0.837	0.414	1.93	1.00	0.399	1.73	0.679	0.302
Ca	1.56	1.07	1.84	0.833	1.70	1.84	1.33	0.205
Na	0.610	1.38	0.654	0.762	0.967	0.694	0.849	2.45
K	0.188	0.251	0.263	0.251	0.188	0.208	0.195	0.130
Mg#	0.204	0.100	0.439	0.386	0.087	0.405	0.163	0.082

TABLE 9

Microprobe analyses - Amphiboles from contaminated ferro-edenite syenite

	C2031/1	C2036/1	C2063/1	C2064/1	C2064/2	C2067/1	C2176/1	C2229/1
SiO2	43.3	40.4	44.5	43.4	45.5	43.1	42.9	41.4
TiO2	1.04	2.0	1.33	1.93	1.01	1.33	1.64	1.87
Al2O3	5.04	8.53	6.56	7.63	6.11	7.36	5.34	8.15
FeO T	29.3	26.7	23.2	23.0	20.8	23.7	27.5	25.2
MnO	1.12	0.77	0.59	0.43	0.41	0.58	1.39	0.67
MgO	3.38	4.2	6.81	7.7	9.18	6.65	3.19	5.09
CaO	10.2	10.6	11.1	10.9	11.4	11.8	9.14	11.4
Na2O	1.85	2.26	2.19	2.07	1.78	2.29	3.68	2.48
K2O	0.83	1.53	1.08	0.95	0.58	0.84	1.11	1.37
Recalc	-----	-----	-----	-----	-----	-----	-----	-----
Fe2O3	4.47	2.47	-	4.52	3.07	-	-	-
FeO	25.3	24.4	23.2	19.0	18.0	23.7	27.5	25.2
Total	96.4	97.3	97.4	98.5	97.1	97.7	95.9	97.6
Si	6.99	6.47	6.95	6.64	6.97	6.76	7.03	6.59
Aliv	0.96	1.53	1.05	1.36	1.03	1.24	0.97	1.41
Alvi	-	0.084	0.153	0.018	0.071	0.113	0.058	0.120
Ti	0.126	0.241	0.156	0.222	0.116	0.157	0.202	0.224
Fe3+	0.543	0.297	-	0.521	0.353	-	-	-
Fe2+	3.41	3.27	3.03	2.43	2.31	3.10	3.77	3.36
Mn	0.153	0.104	0.078	0.056	0.053	0.077	0.193	0.090
Mg	0.814	1.00	1.58	1.76	2.10	1.55	0.779	1.21
Ca	1.76	1.82	1.86	1.79	1.87	1.98	1.60	1.95
Na	0.580	0.701	0.663	0.614	0.528	0.695	1.17	0.766
K	0.171	0.312	0.215	0.185	0.113	0.168	0.232	0.278
Mg#	0.193	0.235	0.343	0.420	0.476	0.334	0.171	0.265

TABLE 10

Microprobe analyses - Amphiboles from quartz syenite

	C346/3	C367/4	C369/2	C2071/2	C2081/1	C2091/1	C2136/2	C2138/6
SiO2	46.7	51.2	44.6	40.7	49.5	41.9	48.2	46.3
TiO2	1.33	0.14	1.3	1.09	0.48	2.06	0.47	1.19
Al2O3	3.29	1.05	3.97	8.27	1.24	7.55	0.44	3.25
FeO T	33.7	34.1	32.0	25.4	12.6	25.9	27.0	32.3
MnO	0.7	1.16	0.73	1.02	0.6	0.82	0.86	0.618
MgO	1.21	0.32	2.31	4.6	9.45	4.61	1.47	1.86
CaO	7.27	2.3	8.87	11.0	21.2	10.1	19.1	8.14
Na2O	2.63	5.42	2.64	2.88	1.05	2.92	1.03	2.84
K2O	1.03	0.33	0.82	1.2	-	1.28	-	0.895
Recalc	-----	-----	-----	-----	-----	-----	-----	-----
Fe2O3	6.74	9.58	4.88	-	-	1.02	-	3.66
FeO	27.6	25.5	27.6	25.4	12.6	25.0	27.0	29.0
Total	98.5	97.0	97.7	96.1	96.1	97.3	98.6	97.7
Si	7.39	8.06	7.15	6.59	8.41	6.67	8.40	7.41
Aliv	0.61	-	0.75	1.41	-	1.33	-	0.59
Alvi	0.01	0.195	-	0.174	0.249	0.092	0.090	0.018
Ti	0.158	0.017	0.157	0.133	0.061	0.247	0.061	0.143
Fe3+	0.804	0.14	0.589	-	-	0.122	-	0.440
Fe2+	3.65	3.35	3.70	3.44	1.79	3.33	3.94	3.87
Mn	0.094	0.155	0.099	0.140	0.086	0.111	0.127	0.084
Mg	0.286	0.075	0.553	1.11	2.40	1.10	0.382	0.445
Ca	1.23	0.388	1.52	1.92	3.86	1.73	3.57	1.39
Na	0.807	1.65	0.821	0.906	0.35	0.902	0.348	0.879
K	0.208	0.066	0.168	0.248	-	0.260	-	0.183
Mg#	0.073	0.022	0.130	0.244	0.572	0.247	0.088	0.103

TABLE 11

Microprobe analyses - Amphiboles from xenoliths

	C2098/3	C170/1	C170/2	C170/3	C366B/1	C366B/2	C366B/3	C366B/4
SiO2	50.1	41.5	41.6	41.4	47.3	48.0	45.9	46.4
TiO2	0.08	1.51	1.84	1.4	1.22	0.49	1.37	1.47
Al2O3	0.17	10.2	10.0	10.5	5.27	4.51	6.14	6.19
FeO T	24.7	20.0	19.3	20.3	19.2	19.8	19.6	19.7
MnO	0.81	0.31	0.38	0.34	0.33	0.35	0.28	0.39
MgO	2.5	8.66	8.66	8.48	10.1	10.1	9.19	9.53
CaO	18.6	11.2	11.6	11.2	11.8	12.5	12.2	11.9
Na2O	2.06	3.64	3.51	3.48	1.65	0.89	1.58	1.86
K2O	-	0.73	0.7	0.76	0.44	0.3	0.6	0.58
Recalc	-----	-----	-----	-----	-----	-----	-----	-----
Fe2O3	-	0.94	-	1.74	0.36	1.12	-	-
FeO	24.7	19.1	19.3	18.7	18.9	18.8	19.6	19.7
	-----	-----	-----	-----	-----	-----	-----	-----
Total	99.0	97.8	97.6	98.1	97.4	97.0	96.9	98.0
Si	8.63	6.38	6.43	6.35	7.16	7.28	7.06	7.03
Aliv	-	1.62	1.57	1.65	0.84	0.72	0.94	0.85
Alvi	0.035	0.229	0.254	0.253	0.106	0.091	0.177	0.135
Ti	0.010	0.175	0.214	0.161	0.139	0.056	0.158	0.167
Fe3+	-	0.109	-	0.201	0.041	0.128	-	-
Fe2+	3.56	2.46	2.49	2.40	2.39	2.39	2.52	2.50
Mn	0.118	0.040	0.050	0.044	0.042	0.045	0.036	0.050
Mg	0.642	1.99	1.99	1.94	2.28	2.29	2.11	2.15
Ca	3.43	1.85	1.92	1.85	1.92	2.03	2.01	1.92
Na	0.688	1.09	1.05	1.03	0.485	0.262	0.471	0.546
K	-	0.143	0.138	0.149	0.085	0.058	0.118	0.112
Mg#	0.153	0.447	0.445	0.446	0.488	0.489	0.455	0.463

CALCIC AMPHIBOLES: $(Ca+Na_B) \geq 1.34$: $Na_B < 0.67$

FIG.13. $(Na+K)_A < 0.50$; $Ti < 0.50$

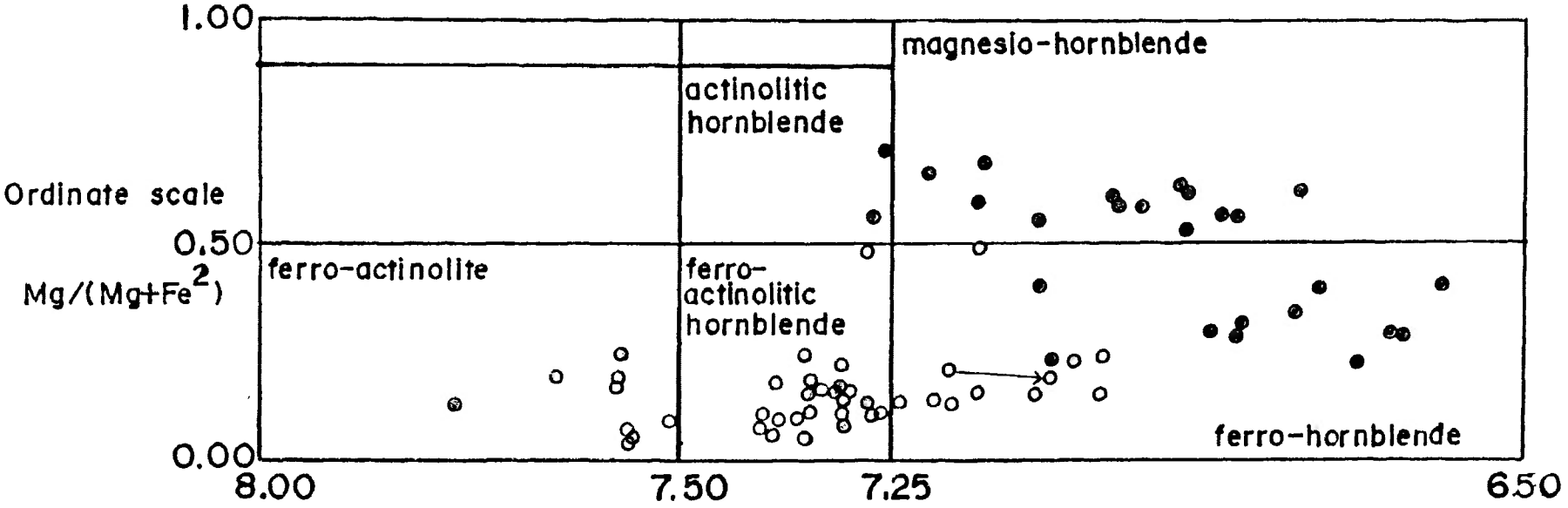

LITHOLOGICAL CODE *

- magnesio-hornblende syenite
- contaminated ferro-edenite syenite
- ferro-edenite syenite
- quartz syenite
- mafic volcanic xenolith

* This code is used throughout the thesis.

CALCIC AMPHIBOLES: $(Ca+Na)_B \geq 1.34$; $Na_B < 0.67$

FIG.14. $(Na+K)_A \geq 0.50$; $Ti < 0.50$; $Fe^{3+} \leq Al^{VI}$

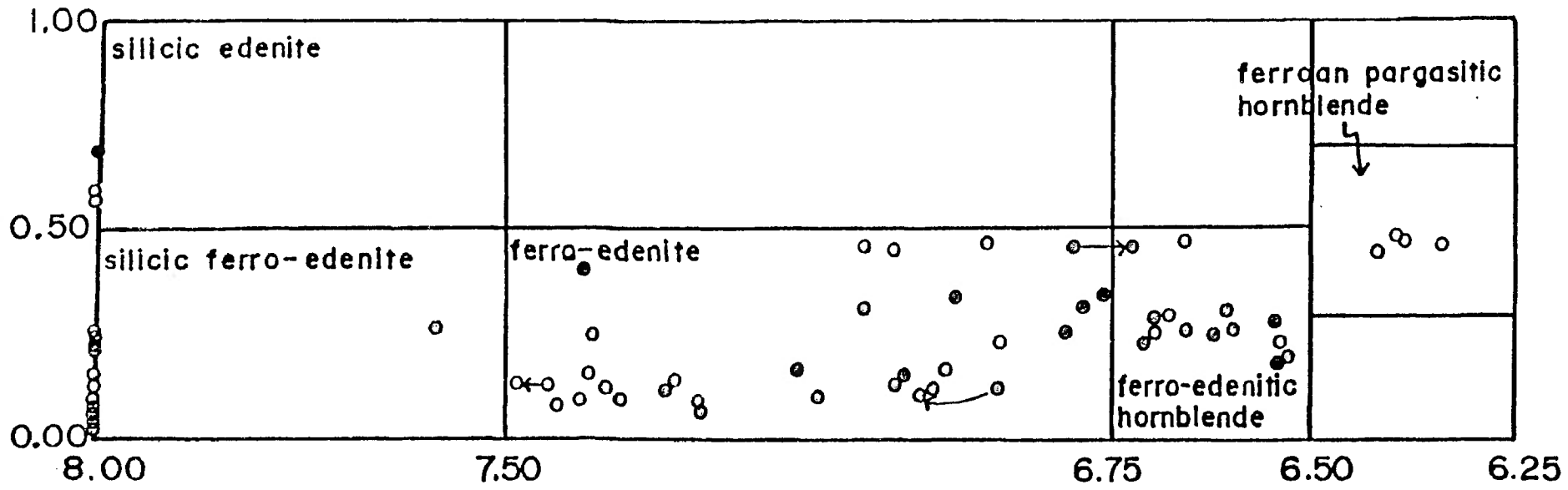

CALCIC AMPHIBOLES: $(Ca+Na)_B \geq 1.34$, $Na_B < 0.67$

FIG.15. $(Na+K)_A > 0.50$; $Ti < 0.50$; $Fe^{3+} > Al^{VI}$

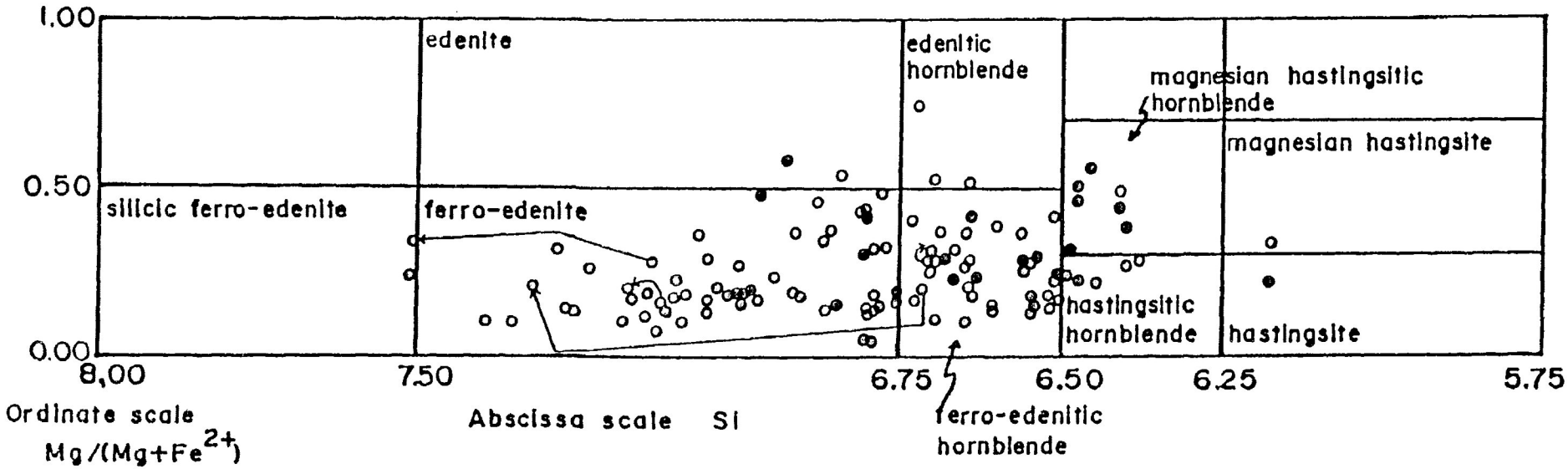

SODIC-CALCIC AMPHIBOLES: $(Ca+Na)_B \geq 1.34$; $0.67 < Na_B < 1.34$

FIG.17. $(Na+K)_A \geq 0.50$

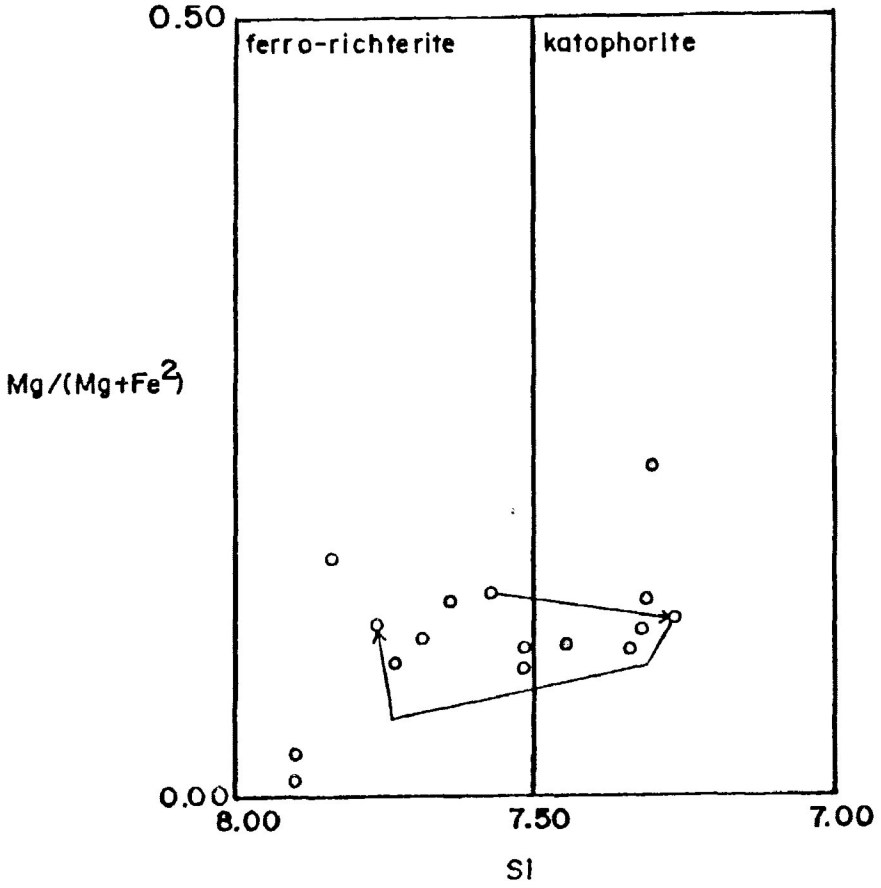

SODIC-CALCIC AMPHIBOLES: $(Ca+Na)_B \geq 1.34$; $0.67 < Na_B < 1.34$

FIG.16. $(Na+K)_A < 0.50$

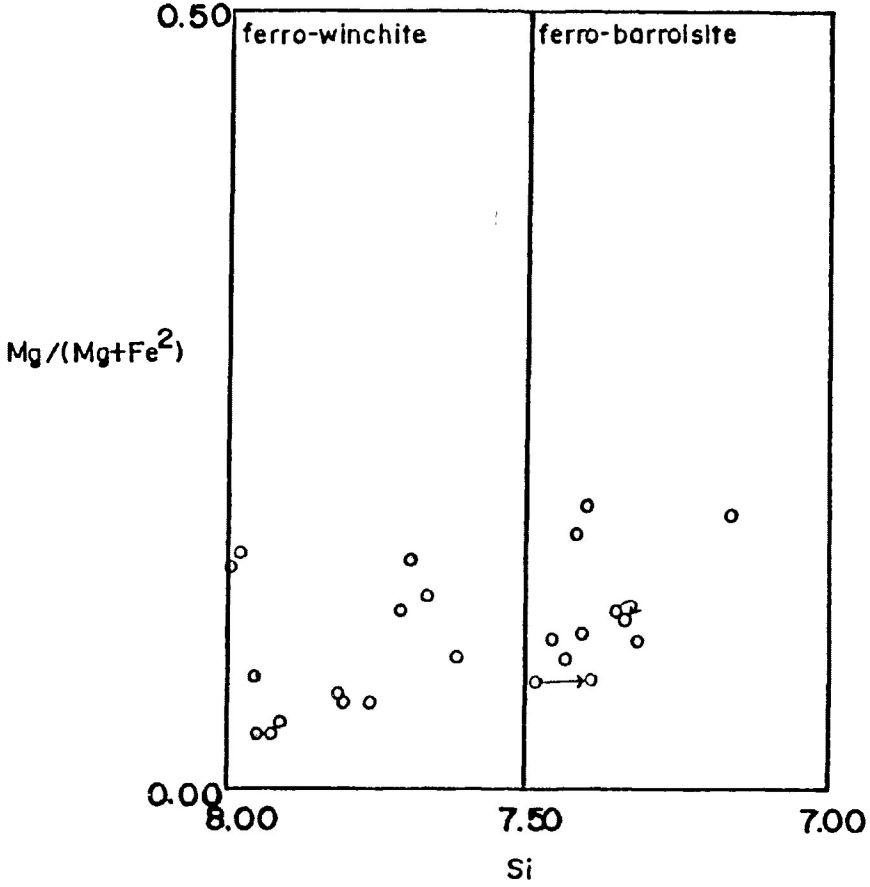

ALKALI AMPHIBOLES: $Na_B \geq 1.34$

FIG. 19. $(Na+K)_A < 0.50$

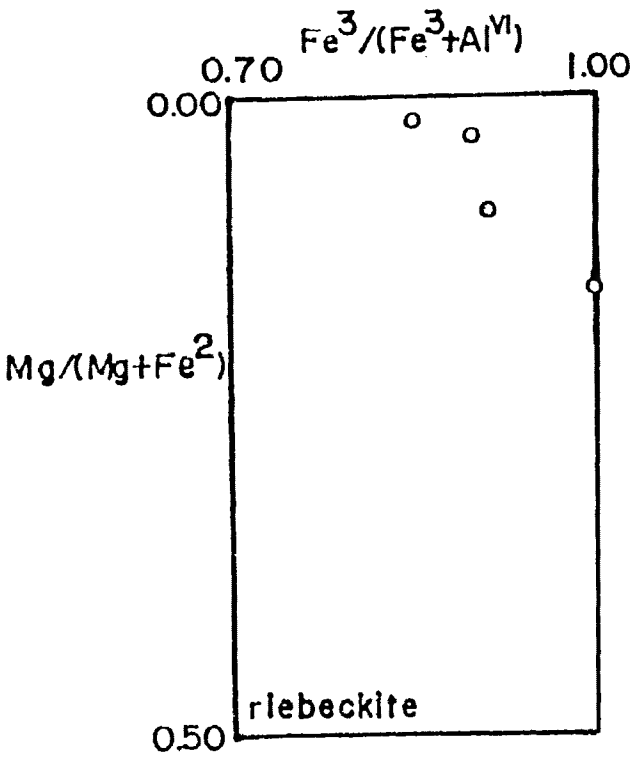

ALKALI AMPHIBOLES: $Na \geq 1.34$

FIG. 18. $(Na+K)_A \geq 0.50$

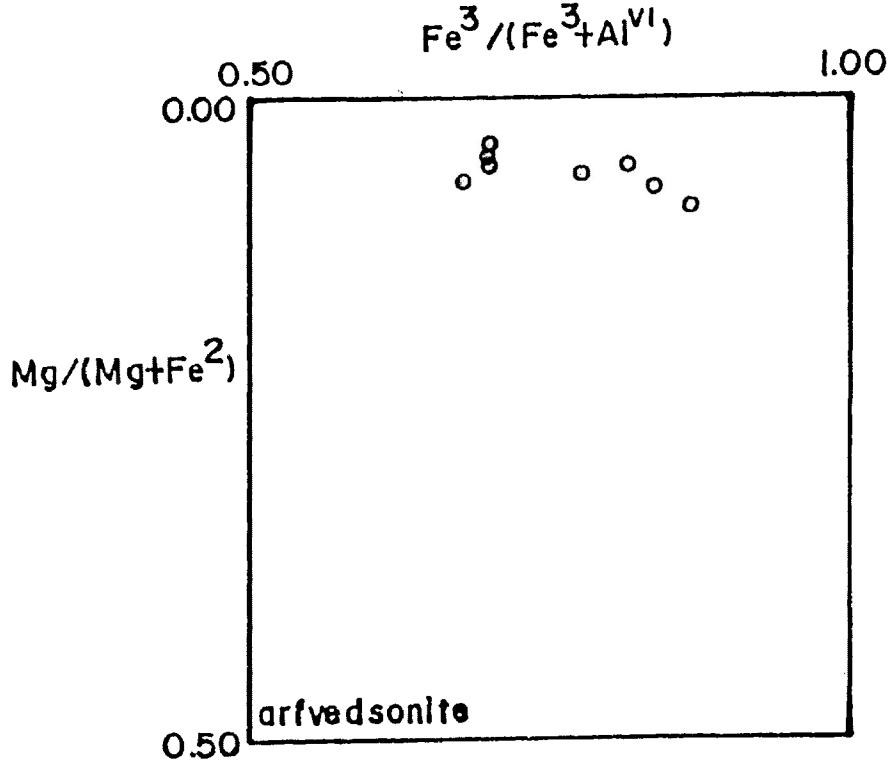

Centre III amphiboles show an exceptionally wide compositional range. Three of the four main amphibole categories are represented: alkalic, sodic-calcic and calcic, with the latter type predominating. The specific amphibole varieties range from magnesio-hornblende and magnesian hastingsite to arfvedsonite and riebeckite. Three of the four syenites have been named for the typical amphibole occurring in them., i.e. magnesio-hornblende syenite and the ferro-edenite syenites. The quartz syenites do not contain one dominant amphibole, rather, they range in composition from ferro-actinolitic hornblende to ferro-edenite to ferro-barroisite and ferro-winchite.

4.2 Magnesio-hornblende syenite

All of the amphiboles from magnesio-hornblende syenites are calcic. The compositional variation is illustrated in Figures 13 to 15. In Figure 13 the majority of compositions classify as actinolitic hornblende and ferro-hornblende. Together these compositions lie in a long, wide, linear trend. In Figure 14 amphibole compositions from this syenite type fall into the categories of: silicic edenite, edenite and ferro-edenitic hornblende. The anomalous silicic edenite composition represents the most silicic amphibole from the magnesio-hornblende syenites. In Figure 15 the majority of amphibole compositions form a small, oval cluster centred over the fields of magnesian hastingsitic hornblende and ferro-edenitic hornblende. Hastingsite and edenite were also determined in this category, but are minor. Figures 16 to 19 depict the classification of sodic-calcic and alkali amphiboles, and are not applicable to amphiboles from magnesio-hornblende syenites.

Figure 20, adapted from Giret et al. (1980) shows effectively the overall compositional trend for amphiboles from the magnesio-hornblende

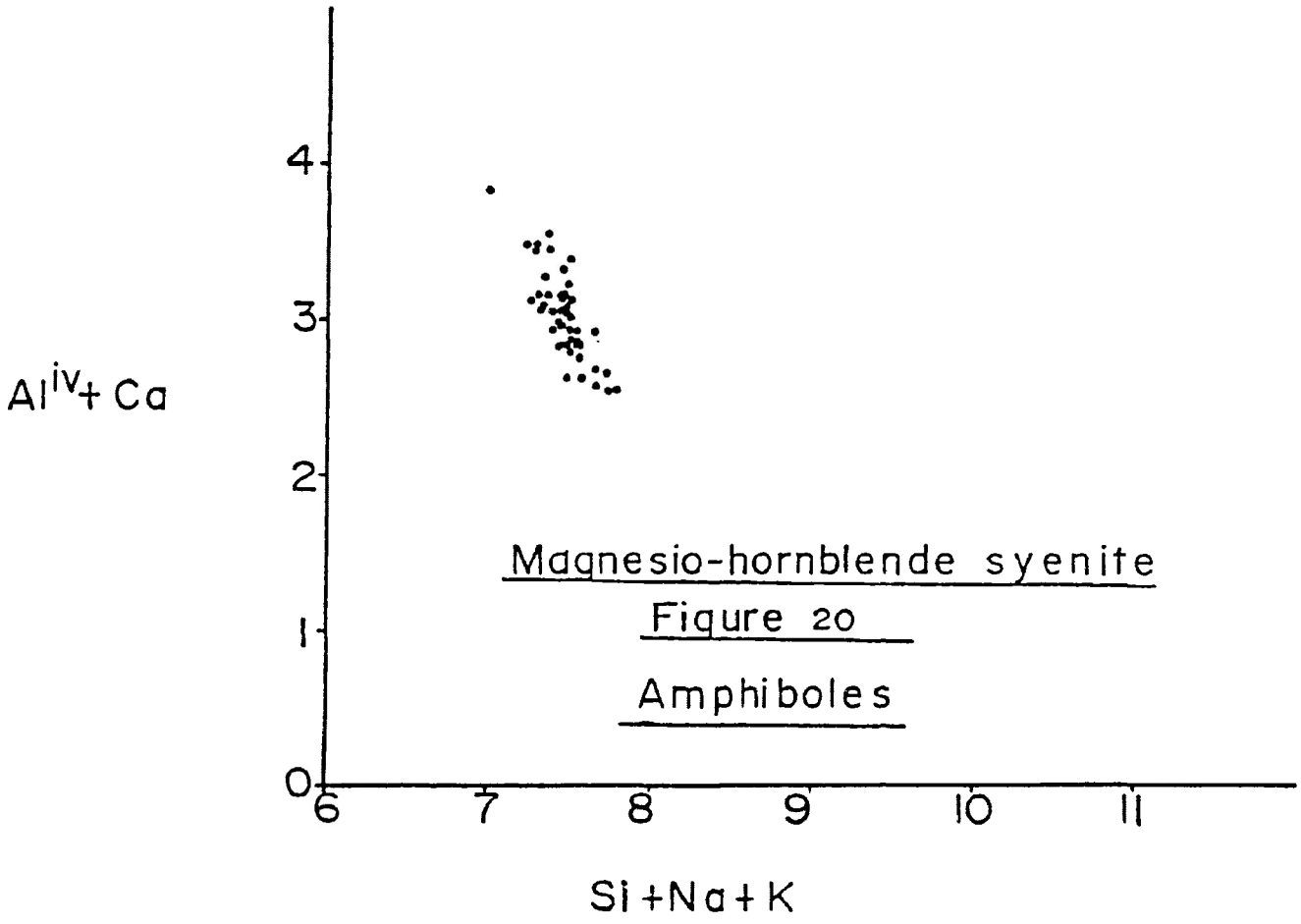

Magnesio-hornblende syenite

Figure 20

Amphiboles

syenites. The amphiboles evolve from hastingsite in the cores of zoned grains, to hornblende in the rims. The amphiboles that exhibit synneusis texture are the more evolved hornblende varieties, whereas discrete amphiboles in the groundmass are less evolved hastingsites. The predominant chemical evolutionary trend is to aluminum and sodium depletion, along with silica enrichment. This is verified with the relationships shown in Figure 21, a plot of Na+K/Na+K+Ca versus Si. A few compositions from this syenite type had mg numbers greater than 0.50 and are not plotted. The mg number for amphiboles from magnesio-hornblende syenites ranges from 0.18 to 0.70 ($Mg/(Mg+Fe^{2+})$). Within a single syenite specimen the range may be large, for example, from C2128, the mg numbers vary from 0.22 to 0.54.

Typical examples of the compositional zonation of amphiboles are discussed for two specimens. In C178, a green amphibole core is magnesian hastingsitic hornblende, whereas the blueish green rim is (potassian) ferro-edenitic hornblende. In specimen C2150 the zonation is from (titanian) magnesian hastingsitic hornblende (brown core) to magnesio-hornblende (green rim).

An example that serves to illustrate the difference between amphiboles that exhibit synneusis structure and those in the groundmass is specimen C181, in which the amphibole in the clusters is (ferrian, manganoan) ferro-hornblende, whereas the amphibole outside the clusters is (potassian) magnesian hastingsitic hornblende, and is considerably less silica-rich. In specimens C2128 and C2120, the amphiboles exhibiting synneusis structure are edenite and edenitic hornblende (C2128) and (silicic) silicic edenite (C2120). In the groundmass of both rocks, the green amphiboles are (potassian) magnesian hastingsitic hornblende, whereas the blue-green amphiboles are (potassian) hastingsite.

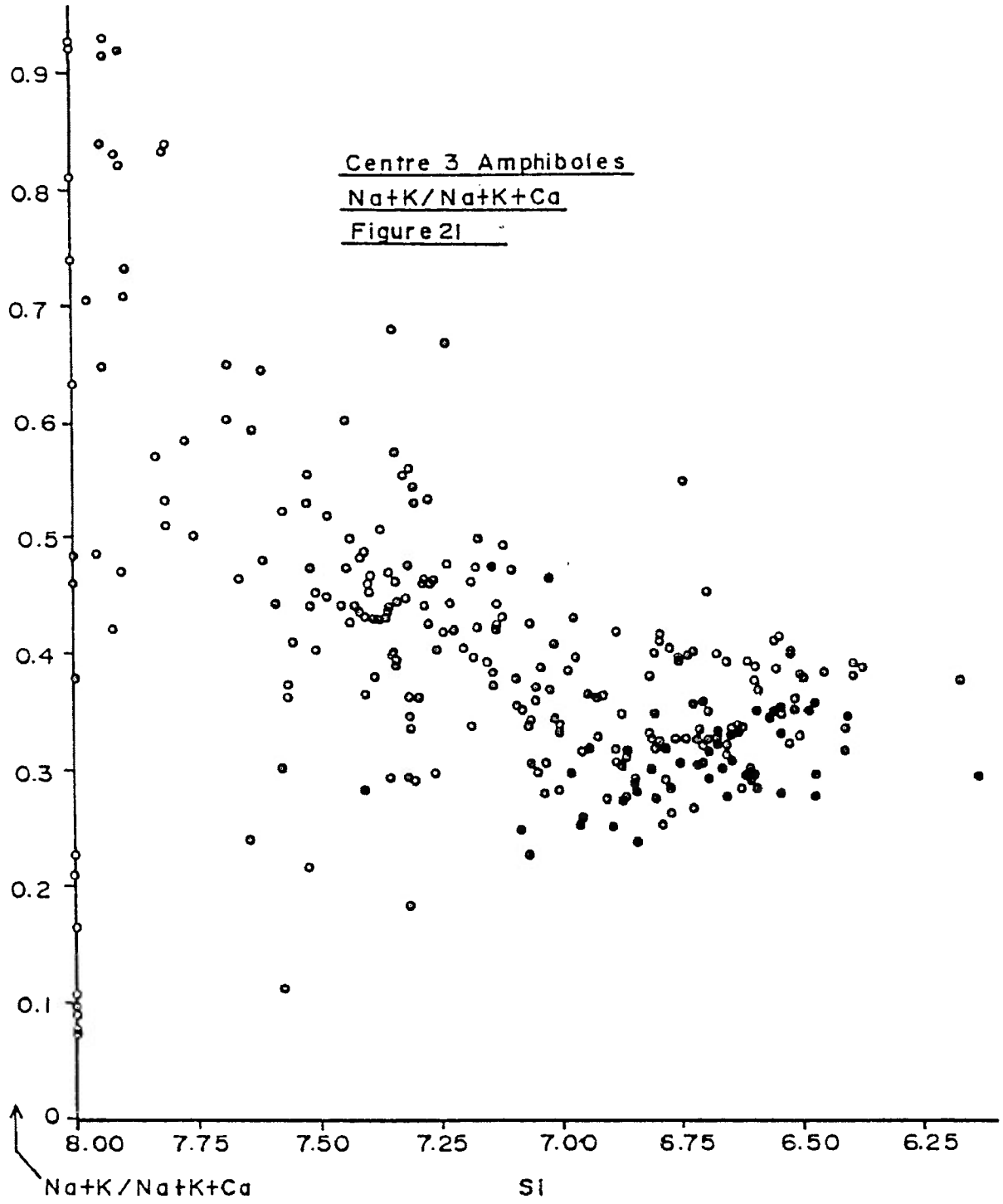
Centre 3 Amphiboles
Na+K/Na+K+Ca
Figure 21
0.9
0.8
0.7
0.6
0.5
0.4
0.3
0.2
0.1
0
8.00
7.75
7.50
7.25
7.00
6.75
6.50
6.25
Na+K/Na+K+Ca
Si

4.3 Ferro-edenite syenite

Amphiboles from ferro-edenite syenites are predominantly calcic, although sodic-calcic and alkali amphiboles may occur. These amphibole compositions are shown in Figures 13 to 19. The most common variety of amphibole from these syenites is the calcic amphibole, ferro-edenite, hence the name for this syenite type. From the classification diagrams for calcic amphiboles, Figures 13 to 15, the amphibole varieties found are: magnesian hastingsite, hastingsitic hornblende, ferro-edenitic hornblende, ferro-edenite, silicic ferro-edenite, ferro-hornblende, ferro-actinolitic hornblende, ferro-actinolite and silicic edenite. A wide, linear compositional trend is evident in all three diagrams. In Si content the amphiboles range from approximately 6.18 to >8.00. Some core to rim compositional trends are depicted with arrows in these diagrams, and in most cases the changes are very minor. The rims may be more or less silica-rich, than the core. Several core-rim pairs are not joined because the compositions plot in separate diagrams, although they may not be drastically different. The mg number for amphiboles from ferro-edenite syenites ranges from 0.60 to 0.03. The range in mg number within any one specimen is limited to less than 0.10. This is true for all of the amphiboles from ferro-edenite syenites. The sodic-calcic compositions are presented in Figures 16 and 17, and ferro-winchite, ferro-barroisite, ferro-richterite and katophorite varieties occur in the ferro-edenite syenite. From the alkali amphibole category, riebeckite and arfvedsonite compositions have been determined for this syenite (Figures 18 and 19).

In Figure 22, the compositions for amphiboles from ferro-edenite syenites form a well-defined, linear trend, indicating the dominant isomorphous substitution $Al^{3+}_{iv}+Ca^{2+} \rightleftarrows Si^{4+}+Na^{+}$. Simultaneously, throughout the evolution of magmatic amphiboles in these syenites, the substitution

Ferro-edenite syenite — Amphiboles

Figure 22

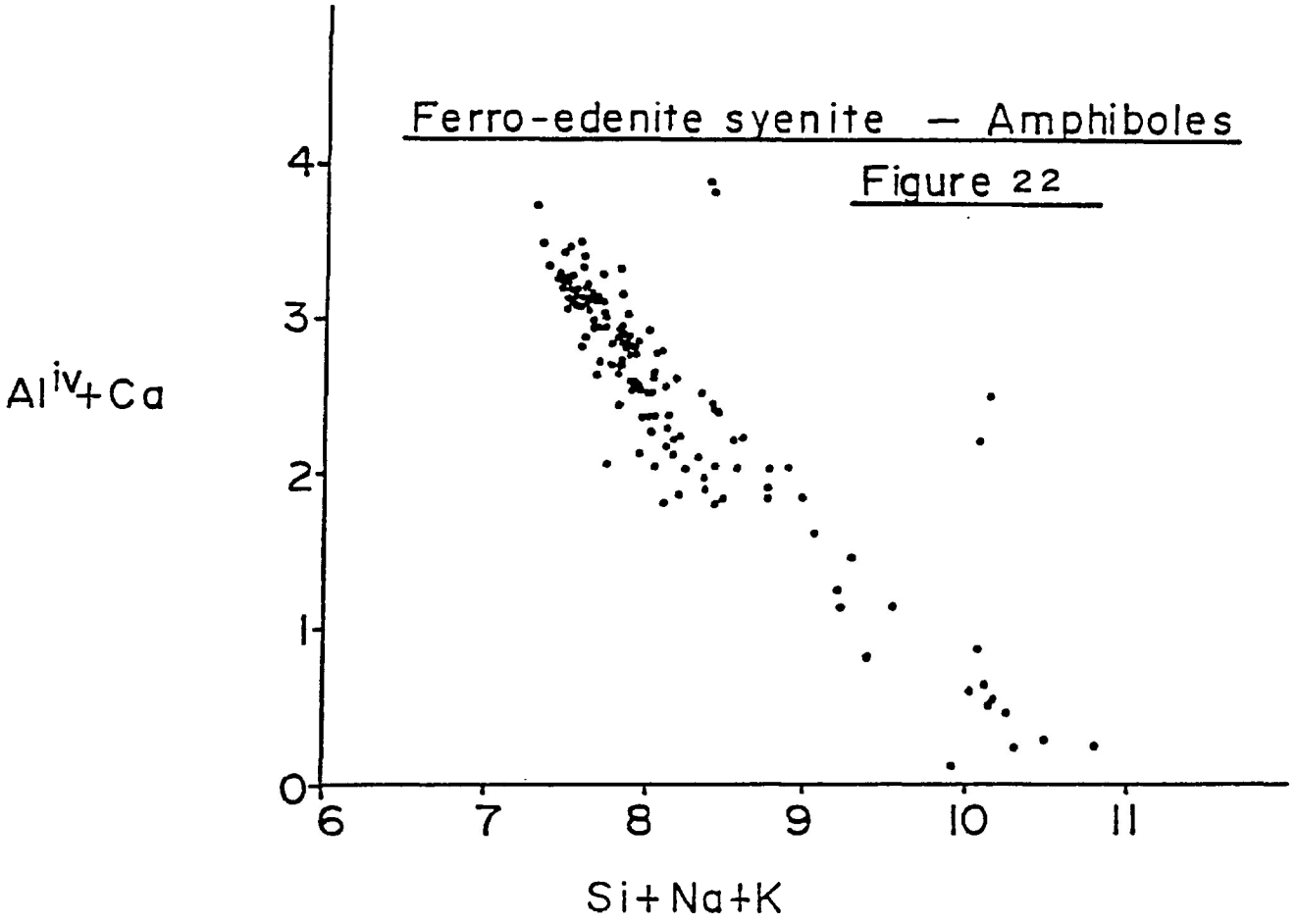

$Mg^{2+}_{vi} \rightleftarrows Fe^{2+}_{vi}$ prevails. Compositional zoning and textural evidence confirms that with evolution of this magma, the amphiboles become silica- and sodium-enriched. This trend is also indicated from the plot of Na+K/Na+K+Ca versus Si, in Figure 21. The main amphibole compositional trend, under reducing conditions, is referred to as the magmatic-subsolidus trend (Strong and Taylor, 1984). In this diagram, as in Figure 22, a very minor off-shoot of the main trend indicates a slight Na-depletion coupled with strong silica-enrichment. These are the riebeckites, which occur as a deuteric replacement of the calcic and sodic-calcic amphiboles. The riebeckites display depleted Na and K with respect to the arfvedsonites within the magmatic trend. Within a single syenite, where riebeckites are the most evolved members, these grains have relatively enriched Na, but still show relatively decreased values for K. Similar trends towards riebeckitic amphiboles have been noted by Ernst (1962, 1976), Giret et al. (1980), Strong and Taylor (1984) and Bonin and Giret (1985), and are referred as oxidation or hydrothermal trends. Ernst (1962, 1976) has determined that riebeckite is not a stable magmatic mineral, and is only stable under oxidizing conditions at low temperatures ($<500^{o}C$), where the oxygen fugacity is defined by the hematite-magnetite buffer, at 1 kbar of fluid pressure. The trend is not a result of silica depletion, but does reflect a decrease in alkali content and a substantial iron-enrichment, according to the relationship $(K, Na)_A Fe^{2+} \rightleftarrows Fe^{3+}$ (Strong and Taylor, 1984).

The sodic-calcic and alkali amphiboles in this syenite type are blue and commonly have a ragged or acicular texture. Many of these Na-amphiboles are adjacent to, or replacing more calcic varieties of amphibole, suggesting that they are subsolidus reaction products resulting from the reaction of juvenile hydrothermal solutions with

pre-existing amphiboles. In specimen C371 the olive green magmatic amphibole is silicic ferro-edenite, whereas the ragged blue grains are ferro-winchite. The ferro-winchite of specimen C322 is ragged and green, or less commonly blue. The more abundant blue amphibole in this particular specimen is riebeckite. Arfvedsonite and ferro-richterite are the blue-green amphiboles in specimen C2222 from Guse Point. Not all blue or blue-green amphiboles are sodic-calcic or alkali varieties, but in some cases are calcic ferro-edenites. (eg. C2218 , C2101, C2001).Thus petrographic identification is not always correct and it is necessary to analyze the amphiboles in order to classify them properly.

4.4 Contaminated ferro-edenite syenite

All amphiboles from contaminated ferro-edenite syenites are calcic and their compositions are presented in Figures 13 to 15. Ferro-edenite is the most common amphibole, as implied in the name of this syenite type. The varieties of amphibole found in these contaminated rocks include: hastingsitic hornblende, ferro-hornblende, ferro-actinolite, ferro-edenitic hornblende and ferro-edenite. Compositionally, these amphiboles trend from about Si=6.45 to 7.87, with mg numbers ranging from approximately 0.13 to 0.48. Within a single syenite specimen, the range in mg numbers of amphiboles is restricted to about 0.10. Overall, the compositional field is relatively narrow and linear, situated between the compositions for amphiboles from mafic volcanic xenoliths and from ferro-edenite syenites. This observation suggests that the ferro-edenite syenite magma was hybridized by the assimilation of more mafic rocks, namely the alkaline basalts and mafic metavolcanics. This conclusion is supported by macroscopic and microscopic textural evidence, presented in

sections 2.3.3. and 3.3. The incorporation of these xenoliths reduced the relative silica content of the syenite, by introducing relatively high levels of alkalis and MgO. Hence the amphiboles in this hybridized rock reflect these chemical changes, and have slightly elevated mg numbers and reduced silica content, compared to the contamination-free types.

The petrographic investigation revealed that amphiboles from contaminated ferro-edenite syenites are relatively small and generally do not exhibit optical zonation. Due to the fine grain size, it was difficult or impossible to perform more than one spot analysis with the microprobe on a single amphibole grain. No core to rim data were obtained, except for one specimen (C2031), where a zoned amphibole was observed within a biotite-rich ovoid. The core of this grain is ferro-edenite, whereas the rim is ferro-hornblende. A minute, buff-green inclusion within alkali feldspar is (subcalcic) ferro-actinolite. The majority of the tiny, green, euhedral amphiboles in the groundmass of C2031 though, are ferro-edenites. In some other specimens, euhedral, rectangular groundmass amphiboles have a (potassian) ferro-edenitic hornblende composition (C2036, C2229). In specimen C2176 the olive green groundmass amphiboles are (sodian) ferro-edenites. While it is rare to find amphibole grains in the ovoids, large enough to analyze, from the small amount of data obtained, it appears that amphibole compositions evolve during the hybridization process towards less alkalic and more calcic compositions.

Amphibole compositions from contaminated ferro-edenite syenite are presented in Figure 23, Al^{iv}+Ca versus Si+Na+K. A distinct cluster of points occurs at about Al^{iv}+Ca=3 and Si+Na+K=7.7. A weak trend towards higher silica contents is observed. In Figure 21, the plot of Na+K/Na+K+Ca versus Si, the compositions for these amphiboles are

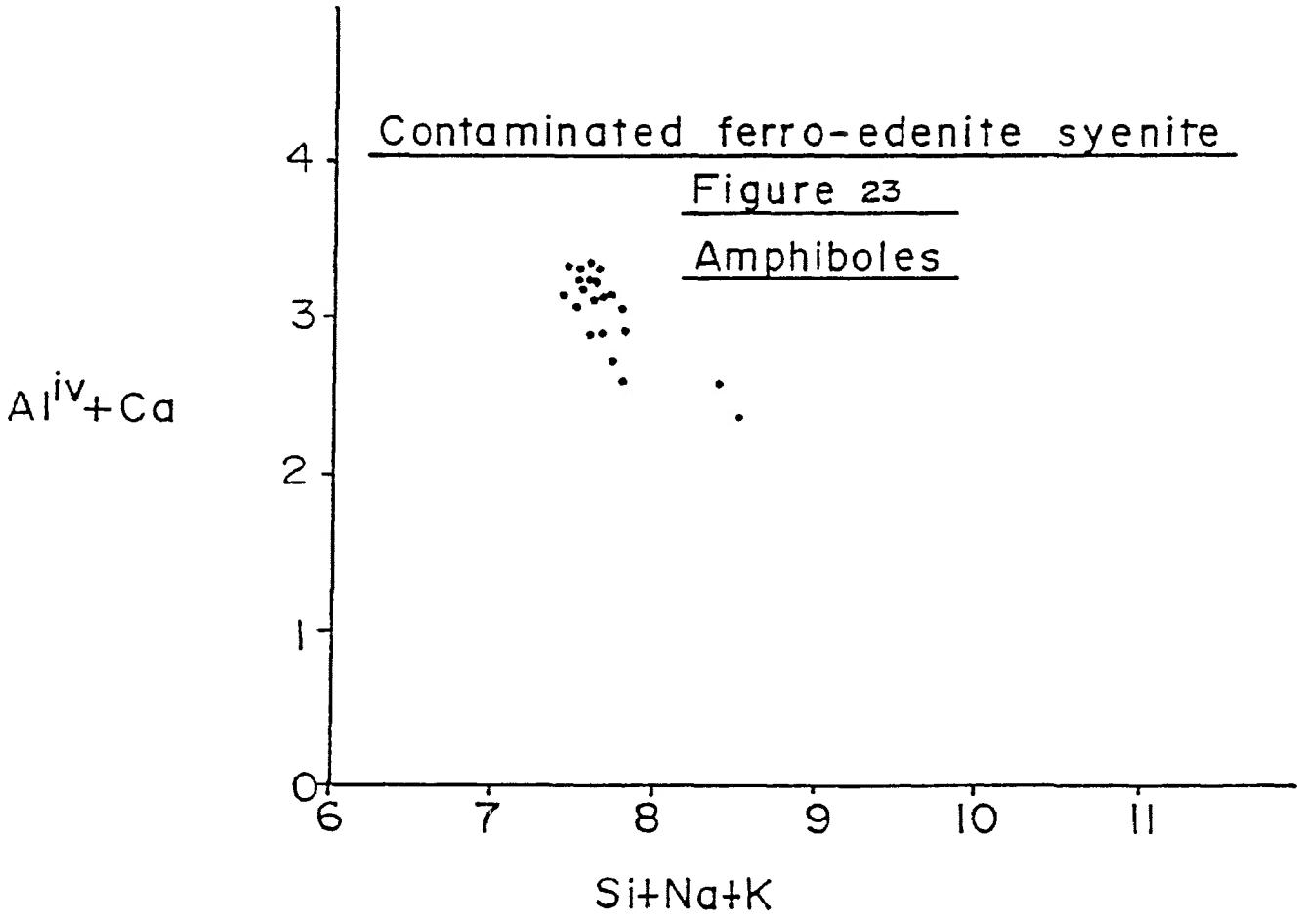
Contaminated ferro-edenite syenite
Amphiboles
$Al^{iv}+Ca$
0
1
2
3
4
6
7
8
9
10
11
Si+Na+K

Figure 23

situated between those for magnesio-hornblende syenites and ferro-edenite syenites. Otherwise no significant compositional trend is detected.

4.5 Quartz syenite

Amphiboles from quartz syenites have diverse compositions, covering the spectrum from calcic to alkali amphiboles. As indicated in Figures 13 to 17 and 19 the varieties include: ferro-hornblende, ferro-actinolitic hornblende, ferro-actinolite, ferro-edenitic hornblende, ferro-edenite, silicic ferro-edenite, silicic edenite, ferro-baroisite, ferro-winchite, katophorite, ferro-richterite and riebeckite. The composition of ferro-edenite dominates only slightly over other types. Figures 13, 14 and 15 show that amphiboles from quartz syenites are generally more evolved than those from ferro-edenite syenites, with higher silica contents and lower mg numbers. Figure 16 demonstrates that ferro-barroisite and ferro-winchite from quartz syenites have lower mg numbers than that occurring in ferro-edenite syenites. In Figure 17 this distinction is not apparent. The scarcity of compositions in Figure 19 makes it difficult to draw any conclusions about the riebeckites. Overall, the silica content varies from about 6.55 to greater than 8.00. The mg number ranges from 1.4 to 57.2 and within a single quartz syenite this range is very restricted, usually approximately 0.05.

Some core to rim compositional trends are indicated for amphiboles from quartz syenites, in Figures 14, 15, 16 and 17. An oscillatory zonation is indicated in Figure 17, for specimen C2153. The brown core and green rim are both ferro-richterite, whereas an intermediate zone has the composition katophorite. Other core to rim pairs were analyzed in this specimen. A brown katophorite core is surrounded by a greenish-brown ferro-winchite, that is in turn rimmed by green (ferrian) ferro-winchite.

Many of the brown amphibole cores in this specimen are (sodian, subcalcic, silicic) ferro-edenite. The green rims are riebeckite, ferro-richterite and, in one instance, (potassian) katophorite.

In specimen C346 two core to rim pairs were analyzed. One brown amphibole core is (ferrian) ferro-barroisite, which is rimmed by (subcalcic) ferro-actinolite, a distinctly different variety of amphibole. In the same specimen the zonation may be subtle, for example, a ferro-barroisite core engulfed by (ferrian) ferro-barroisite. Most of the unzoned grains in this specimen are (subcalcic and commonly ferrian) ferro-actinolitic hornblende. In specimen C367 there is little compositional difference between core and rim regions of amphibole grains. The cores tend to be (subcalcic, silicic) ferro-edenite, rimmed by (sodian, subcalcic, silicic) ferro-edenite. The other amphiboles in quartz syenite C367 are ferro-winchites and riebeckites, which occur as subhedral to anhedral deuteric laths.

The petrographic investigation of these quartz syenites reveals that pyroxene grains may be rimmed by amphibole. In C173 (subcalcic) ferro-actinolitic hornblende surrounds the pyroxene. Ferro-actinolite mantles pyroxene in specimen C2164. A (sodian, subcalcic, subsilicic) ferro-edenite encloses the pyroxenes of quartz syenite specimen C2091. A similar amphibole rims the pyroxenes in C2154.

For the majority of quartz syenites, no zonation or mantling is evident, and isolated, subhedral amphibole grains of one type are present. The brown amphiboles appear to be the most primitive, with compositions of (subcalcic) ferro-hornblende (C2164, C369, C367). Other brown to very dark green amphiboles are (potassian ± titanian) ferro-edenitic hornblende (C2091, C2051). Olive green or medium to light green amphiboles generally have a composition of ferro-edenite or ferro-

actinolite. Very bright medium green amphiboles are (silicic) silicic ferro-edenite (C369, C2071, C2098, C2136). The riebeckites of C367 and C2153 are blue, whereas blue-green amphiboles may be (subcalcic, silicic) silicic ferro-edenite (C2091) or ferro-winchites (C367).

Figure 24 gives an indication of the diversity of amphibole compositions which occur in the Coldwell quartz syenites. A distinct, major linear trend is paralled by a minor trend, covering the compositions of silicic ferro-edenite and silicic edenite. The major trend indicates amphiboles evolving from edenite → barroisite and katophorite → winchite and richterite → riebeckite. In Figure 24, the amphiboles from quartz syenites are observed falling in the same region as amphiboles from ferro-edenite syenites, but in general the former are more siliceous. Once again a minor trend towards calcium enrichment with silica enrichment is observed. As is the case with amphiboles from ferro-edenite syenites, the majority of amphiboles from quartz syenites show an increasing sodium content with increasing silica.

4.6 Alkaline basalt xenoliths

Amphiboles were analyzed from oligoclase basalt xenoliths contained within contaminated and xenolith-bearing ferro-edenite syenites. The compositions for these amphiboles are plotted as uncoloured circles in Figures 13, 14 and 15. The varieties represented are all calcic, being: ferro-hornblende, ferro-actinolitic hornblende, ferroan pargasitic hornblende, ferro-edenitic hornblende, ferro-edenite, magnesian hastingsitic hornblende, hastingsitic hornblende, edenitic hornblende and edenite. No distinct trend is noted, although these compositions fall between the regions occupied by amphibole from magnesio-hornblende syenites and the contaminated ferro-edenite syenites.

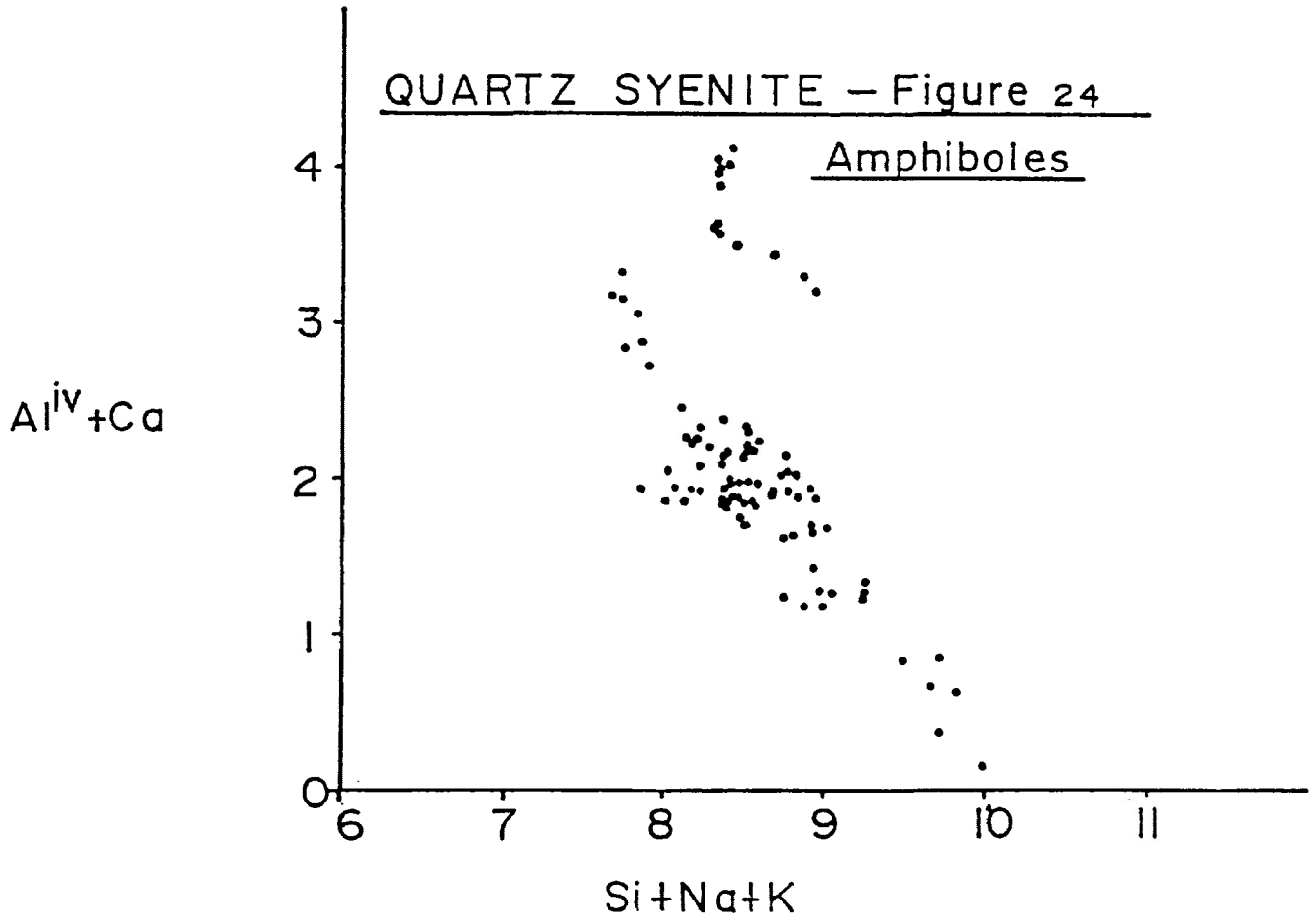
QUARTZ SYENITE — Figure 24
Amphiboles
$Al^{iv}+Ca$
4
3
2
1
0
6
7
8
9
10
11
Si+Na+K

Amphiboles within the groundmass of the alkaline basalt xenoliths in specimens C170, C172, C366B and C2077 are ferroan pargasitic hornblende, ferro-hornblende, ferro-actinolitic hornblende, ferro-edenite, and (potassian) edenitic hornblende. These amphibole grains are typically anhedral, light olive green to medium green and occur as relatively rare, discrete grains. This amphibole commonly replaces the outer margins of pyroxene grains. Within the biotite ovoids small quantities of subhedral, medium green ferro-edenite and ferro-edenitic hornblende are detected. Thus quite a large compositional range may be present between the amphiboles of the groundmass and the ovoids. Generally the amphiboles from the metasomatic ovoids are more evolved, with higher silica and iron contents.

In a few cases, (C2058, C2098, C2077, C2190) it was possible to analyse amphiboles from both xenoliths and host syenite. Both amphiboles have very similar compositions, suggesting that a homogenization of amphibole compositions has occurred during the hybridization process.

Little or no amphibole is preserved in the metamorphosed Archean mafic volcanic xenoliths, and thus no compositional data could be collected for these rock types.

4.7 Comparative data for Coldwell Complex rocks

Previous studies of Coldwell amphibole composition have been made by Mitchell and Platt (1978, 1982a) and Currie (1980). For discussion purposes, Currie's data will be referred to by two numbers, e.g. 3-1, indicating Table 3 - Analysis 1 in Currie (1980). These electron microprobe data have been interpreted with the aid of the amphibole classification program presented in Appendix III.

Some portions of the Centre I ferro-augite syenite have been

investigated by Mitchell and Platt (1978). These authors have divided one section of the intrusion into an upper and lower series. The lower series ferro-augite syenite exhibits igneous layering and amphiboles have crystallized from the intercumulus liquid. The amphiboles range in composition from (brown) ferro-hastingsitic hornblende to ferro-edenitic hornblende to (turquoise) ferro-actinolitic edenite. These compositions are shown on Leake's classification diagram, Figure 25. The upper series syenites generally do not exhibit well-developed layering, although the amphiboles have crystallized from intercumulus liquids. The compositions of these amphiboles vary from ferro-richteritic katophorite to ferro-richterite, as depicted in Figure 26. (Mitchell and Platt, 1978).

Currie's (1980) analysis 11-1 is of a (potassian) ferroan paragasite from a brown melasyenite in the Centre I intrusion. Four other analyses (5-7, 7-3, 7-9 and 11-4) are most likely from Centre I syenites, based upon their field locations and the presence of small amounts of quartz. These amphiboles are: ferro-edenite (5-7); (potassian, titanian, sodian) ferro-paragasitic hornblende (7-3); (potassian, titanian) hastingsite (7-9); and magnesian hastingsite (11-4). Their low alumina and low to moderate mg numbers suggest similar compositions to the amphiboles of the lower series syenites reported by Mitchell and Platt (1978).

Currie (1980) presented one amphibole composition from Centre I eastern border gabbro (9-4); a (potassian) magnesio-hastingsitic hornblende. This primitive amphibole has high Mg, low Si and Fe and forms brown poikilitic plates.

Centre II magmatic activity is represented by alkaline biotite gabbro and nepheline syenite. From Mitchell and Platt's (1982b) data, it is evident that amphiboles from nepheline syenites have moderate to high alumina contents and moderate to high mg numbers. These amphiboles vary

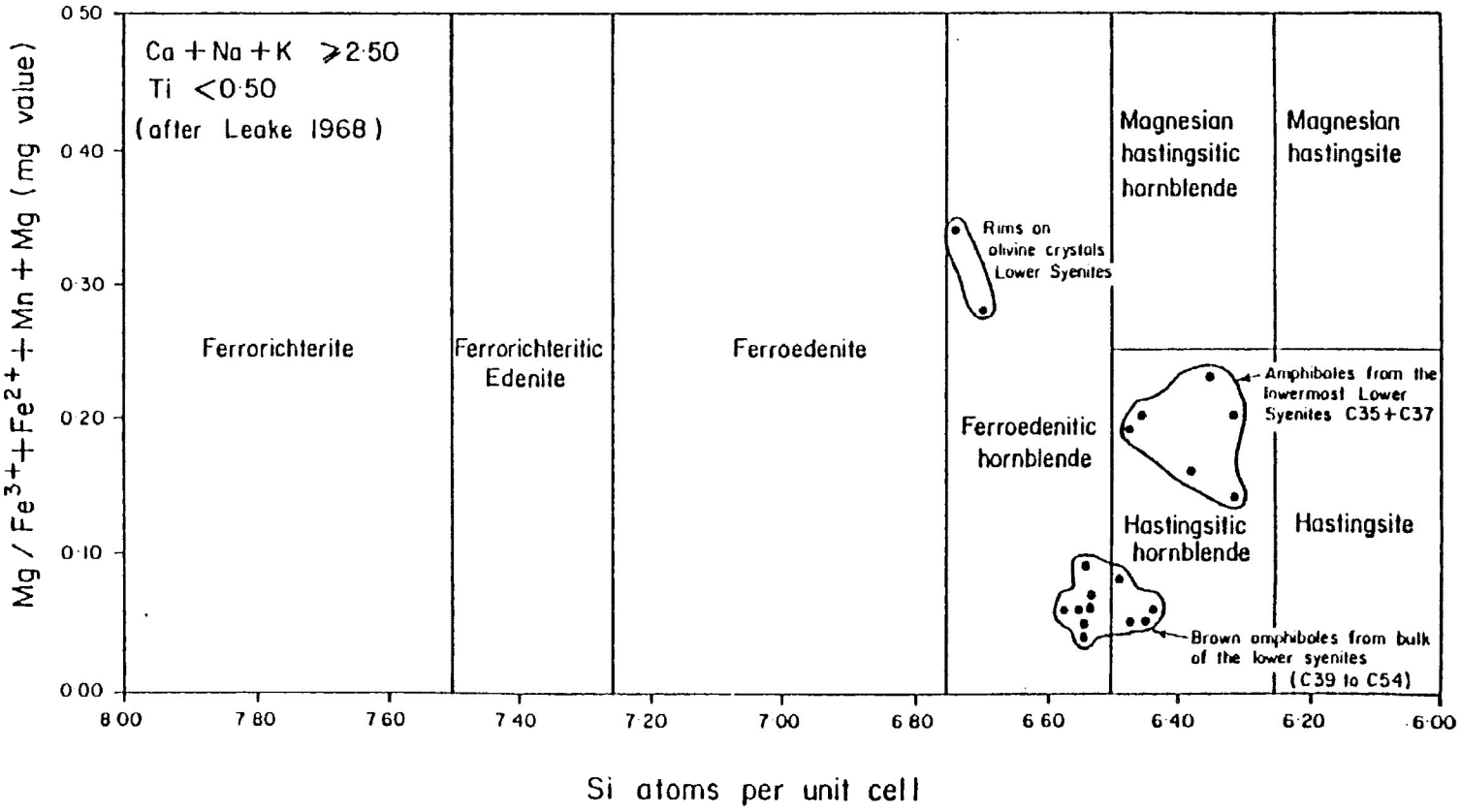

FIG.25. AMPHIBOLE COMPOSITIONAL DATA FOR FERRO-AUGITE SYENITE

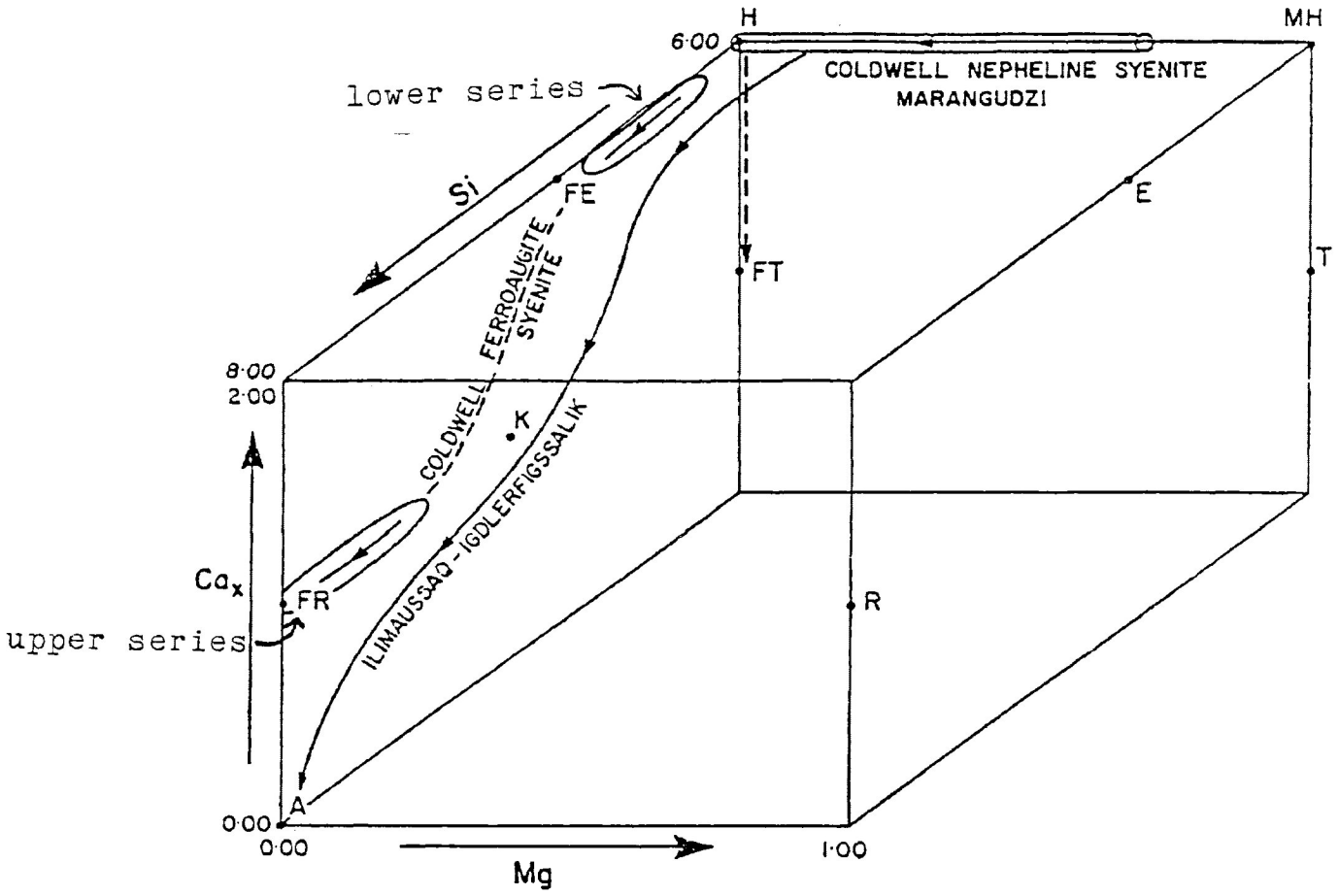

FIG. 26. AMPHIBOLE COMPOSITIONAL TRENDS FOR CENTRE I AND CENTRE II SYENITES – $Mg : Ca_x : Si$

A =arfvedsonite
E =edenite
FE=ferro-edenite
FR=ferro-richterite
FT=ferro-taramite
H =hastingsite
K =katophorite
MH=magnesio-hastingsite
R =richterite
T =taramite

in composition from magnesian hastingsitic hornblende to hastingsite to hastingsitic hornblende to ferro-edenitic hornblende. In deformation-free nepheline syenites, continuously zoned amphiboles have yellow-brown cores, through orange-green zones to dark green margins. These zones represent a wide compositional range, from magnesian hastingsitic hornblende to ferro-edenitic hornblende (Figure 27). A very wide range of mg numbers is represented, from 0.6 to 0.1. as the Fe is increased in these amphiboles, the Si and Ti values decrease and Mn increases. The least evolved of these zoned grains are titanian and potassian. Mitchell and Platt (1982b) indicate that the amphiboles from deformed nepheline syenites have similar compositions, but have a more restricted, intermediate range of mg numbers. This suggests that the zoned amphiboles were homogenized during the recrystallization process.

Currie (1980) presented three analyses of amphiboles from nepheline syenites. Sample 15-2 is a (potassian, titanian) magnesian hastingsitic hornblende from a leucocratic nepheline syenite. As expected, the amphibole from a melanocratic nepheline syenite is somewhat more Mg-rich, being (potassian, titanian) magnesio-hastingsitic hornblende. From a pegmatitic nepheline syenite the amphibole is slightly more evolved, analysis 15-12 being (potassian, titanian) ferroan paragasitic hornblende.

Currie (1980) presents one analysis (13-3) of (potassian) pargasitic hornblende from a Centre II gabbro dyke. This amphibole has a high mg number (0.74), relatively high Al, and forms large poikilitic plates that include olivine grains.

From Mitchell and Platt's (1982b) work it is evident that there is some overlap in composition between the least evolved amphiboles of the ferro-augite syenite and those of the nepheline syenite. Significant

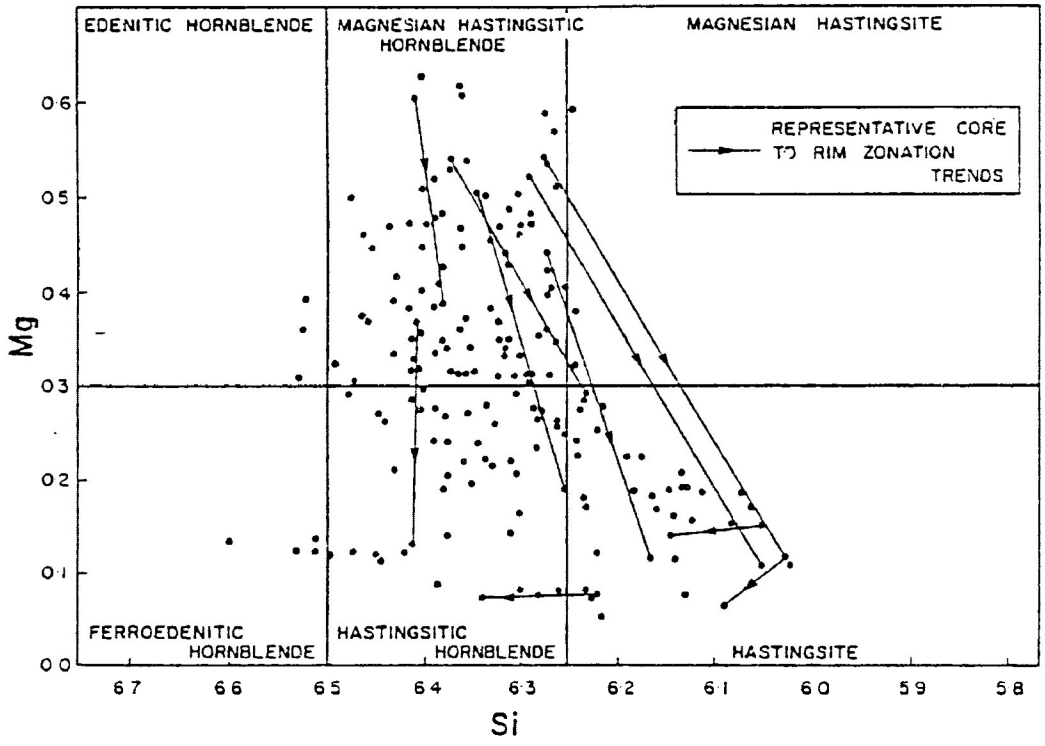

FIG 27. AMPHIBOLE COMPOSITIONAL DATA FOR NEPHELINE SYENITE

differences, though, are found. Centre I amphiboles generally have mg numbers less than 0.1. Amphiboles from Centre II syenites typically have mg numbers in the range 0.1-0.6. For Centre I specimens, increasing Fe content is matched with increasing Si, and (Na+K)/(Na+K+Ca), and decreasing Al. For amphiboles from Centre II, the increase in Fe is accompanied first by a decrease in Si and Ti and an increase in Mn, at a constant (Na+K)/(Na+K+Ca). (Mitchell and Platt, 1982b).

Currie (1980) reports one analysis of amphibole from an altered basalt xenolith, which is probably hosted in Centre III syenites. This (titanian) ferro-pargasite (3-4) is less siliceous and more iron-rich than the amphiboles analyzed in this study. Currie also presented the compositions for two arfvedsonites (3-1, 3-2) and a (sodian, subcalcic) ferro-edenite (3-3) from rocks that are probably Centre III syenites. The descriptions of the host rocks are not detailed enough to determine which syenite types are represented.

This study has found that evolutionary trends in amphiboles, from four Centre III syenite types, show a progression corresponding to their sequence of emplacement as indicated by field relationships. In the earliest syenite, the magnesio-hornblende syenite, the amphiboles are the most primitive. These amphiboles are all calcic, with moderate to high mg numbers (0.2-0.7). Little compositional zonation is observed, but where present, the trend is from hastingsite to hornblende, with alumina and sodium decreasing as silica increases. The amphiboles forming synneusis structures are typically edenites and edenitic hornblendes, whereas those of the groundmass are potassian varieties of magnesian hastingsitic hornblende and hastingsite.

The ferro-edenite syenites contain calcic, sodic-calcic and alkali amphiboles. Low to moderate mg numbers exist over this wide compositional

range. Evidence from zonation and other textures indicates that the evolutionary trend is towards increasing silica contents. This is accompanied by increasing sodium, at the expense of aluminum and calcium. The replacement of Mg by Fe^{2+} is the dominant change in these amphiboles. In the more evolved members there is a secondary trend, where Fe^{3+} substitutes for Na and Fe^{2+}.

The contaminated ferro-edenite syenites contain only calcic amphiboles, the majority of which are homogenized in composition with respect to the amphiboles of the basalt xenoliths, as a result of the hybridization event. The compositions of these amphiboles fall in between those for magnesio-hornblende syenites and ferro-edenite syenites. The trend is similar to that for ferro-edenite syenites, but the small number of analyses and lack of zoned graines precludes detailed documentation of the compositional evolution trend. The mg numbers for these grains range from about 0.13 to 0.5.

Field relationships indicate that the quartz syenite represents the latest Centre III magmatic activity. The constituent amphiboles are also the most evolved of all Centre III syenites. The amphiboles classify broadly into the calcic, sodic-calcic and alkali amphibole categories, generally following the same overall trend as for the ferro-edenite syenites, but typically exhibiting higher silica contents than the latter. The mg numbers vary from 0.01 to 0.58, but average in the high 0.30 range. The trend from the sodic-calcic to riebeckitic alkali varieties is continuous and largely reflects a relative K depletion.

Figures 28 to 32 are based upon the three-dimensional Figure 26, constructed by Mitchell and Platt (1982a). By comparing all of these figures, as in Figure 26, it becomes evident that the Centre III trends most clearly parallel those of Centre I. The most obvious difference is

Figure 28 – Amphiboles from magnesio - hornblende syenite

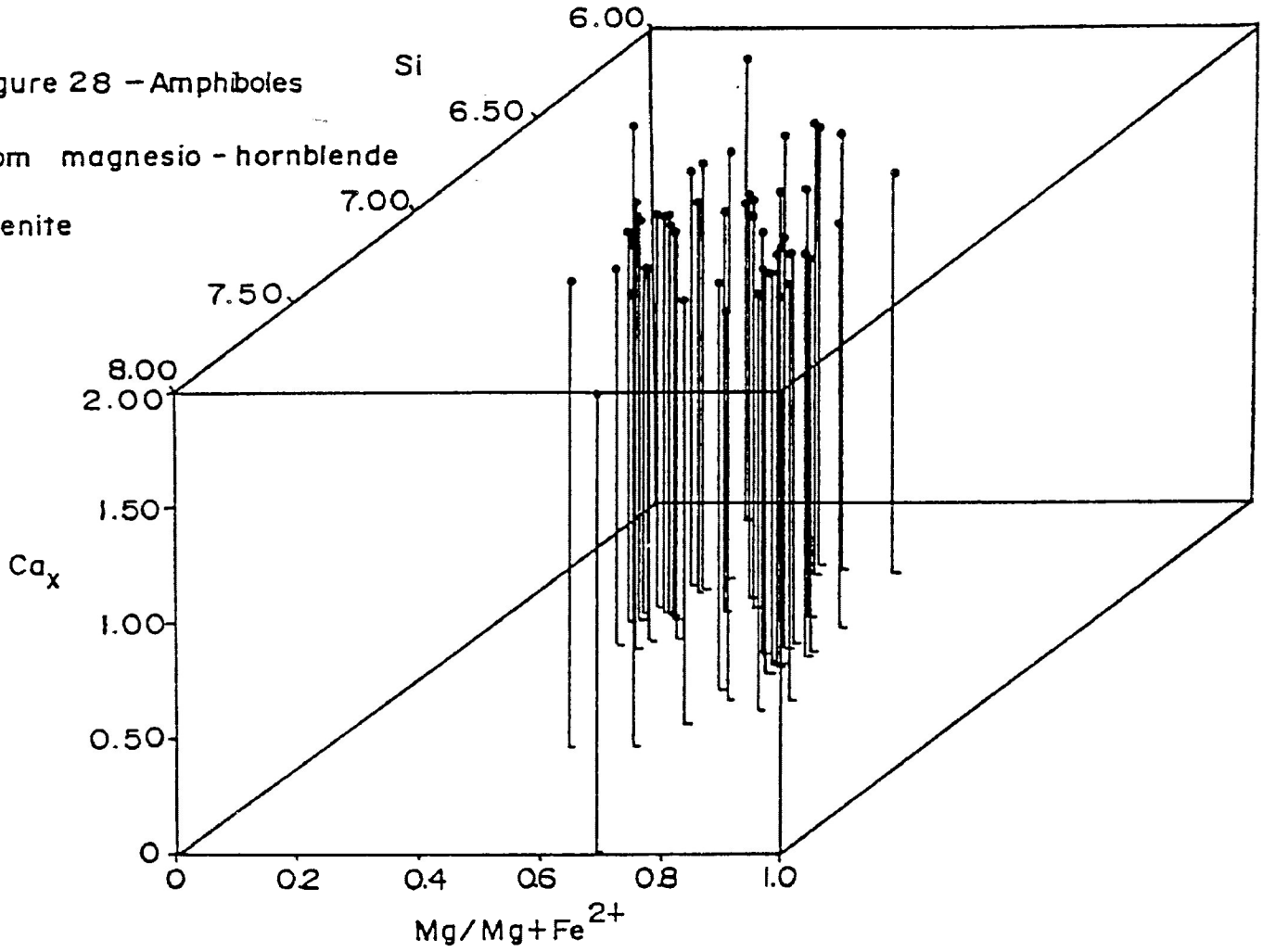

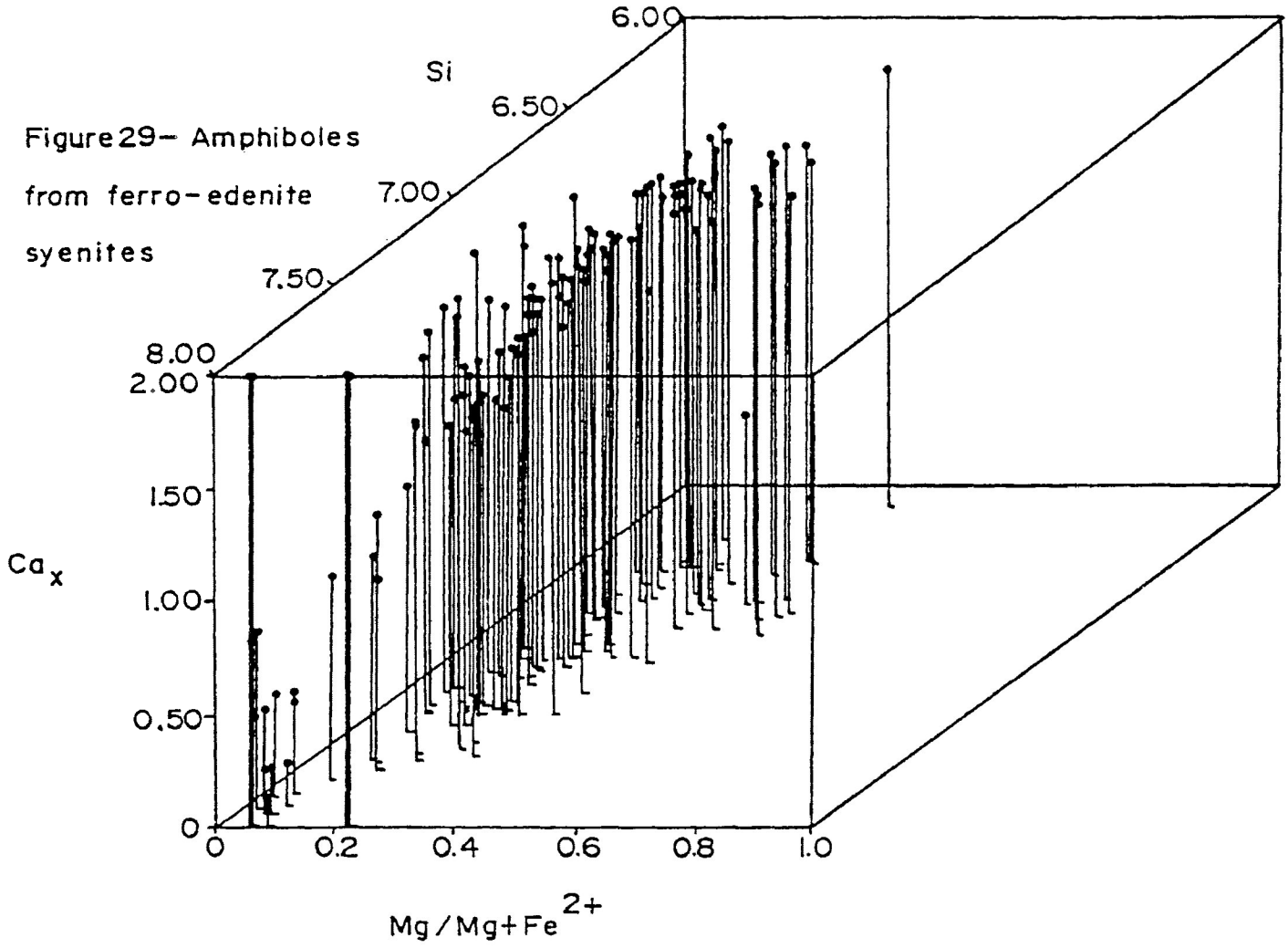

Figure 29– Amphiboles from ferro-edenite syenites

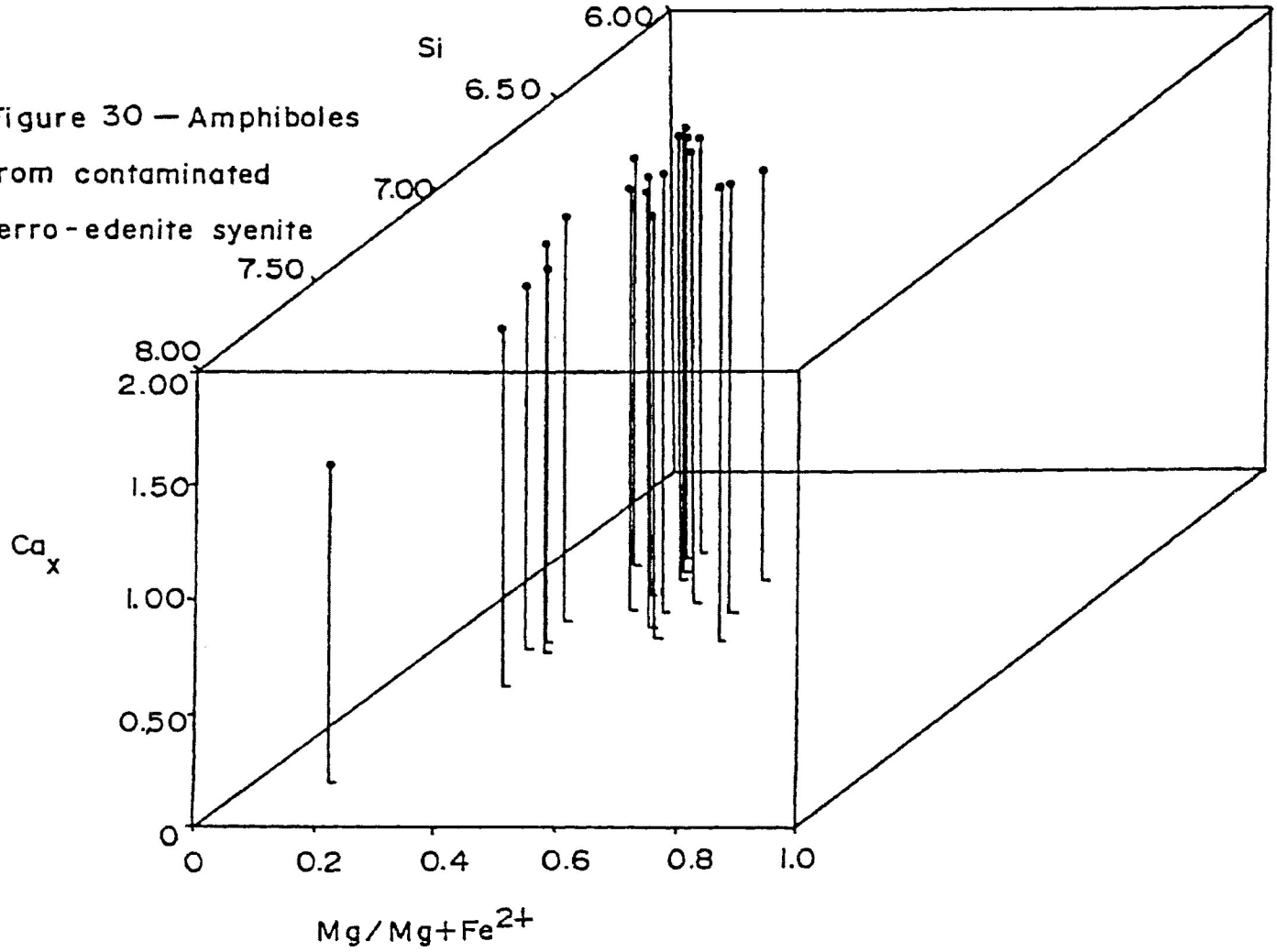

Figure 30 — Amphiboles from contaminated ferro-edenite syenite

Figure 31 -

Amphiboles from quartz syenites

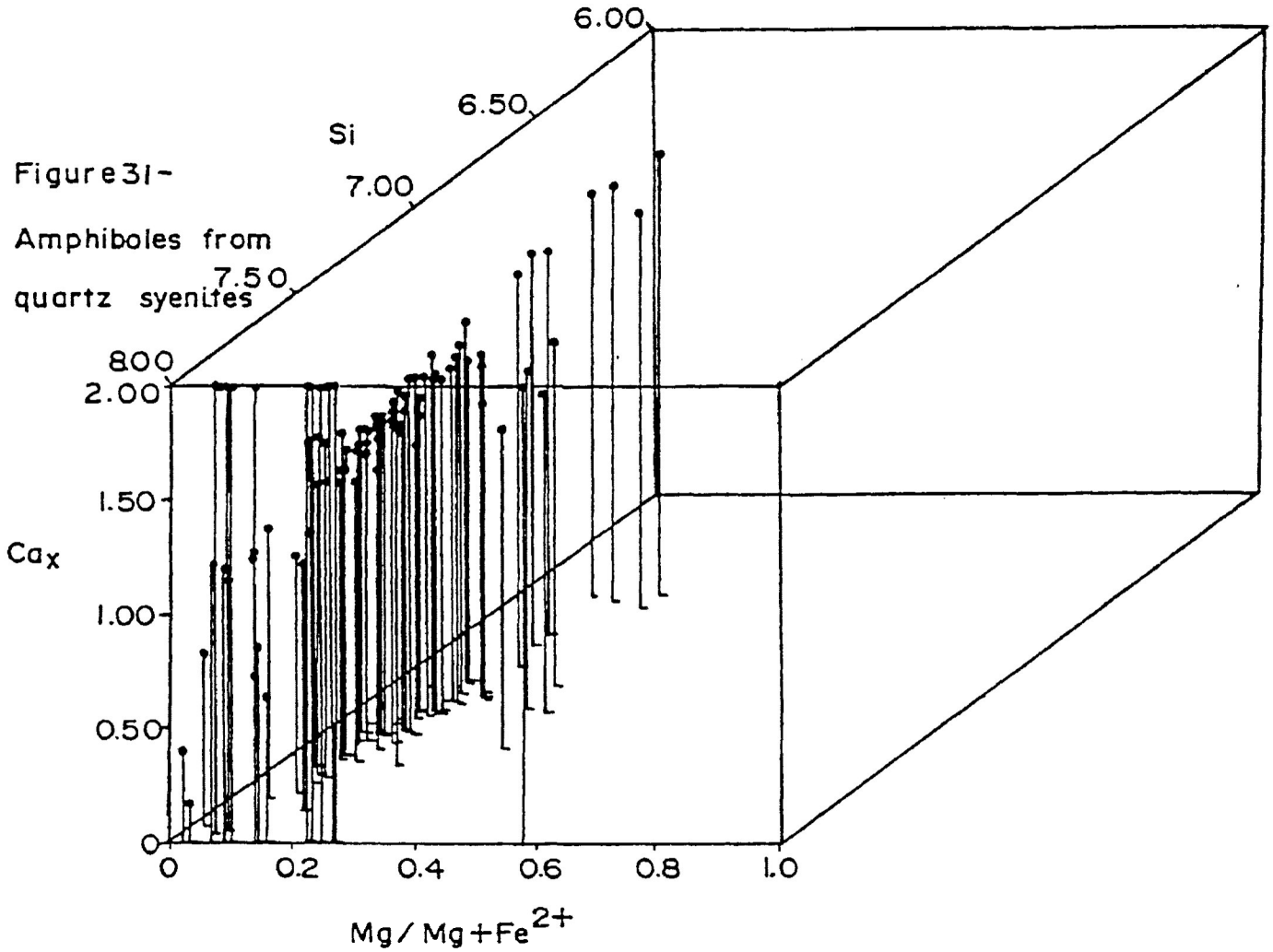

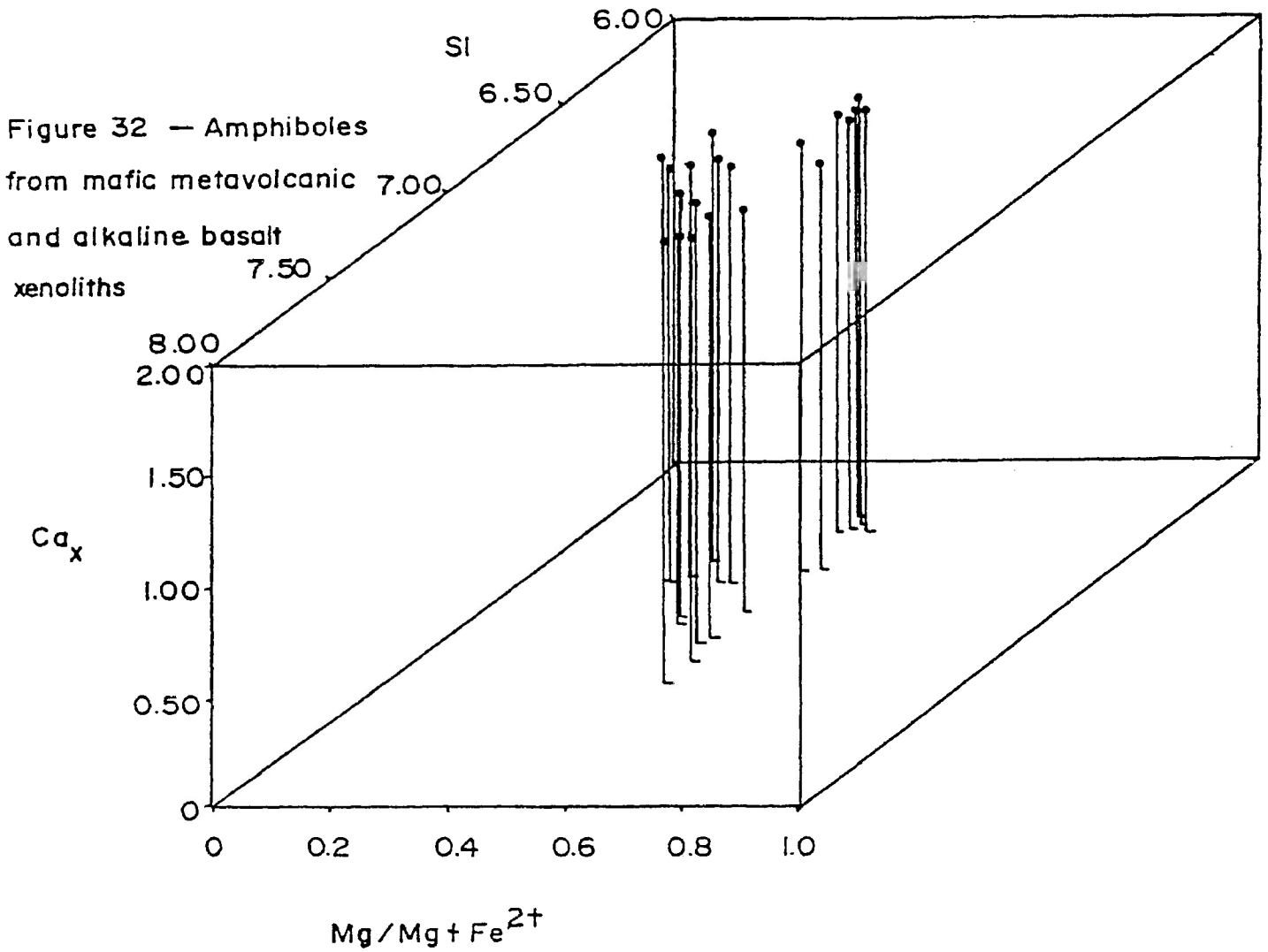

Figure 32 — Amphiboles from mafic metavolcanic and alkaline basalt xenoliths

that the amphiboles from magnesio-hornblende syenites have higher mg numbers than the lower series of Centre I ferro-augite syenites. The Centre II amphiboles from nepheline syenites generally exhibit trends which are contrary to those in Centre III, particularly in that with increasing Fe, the Si content is decreasing at a relatively constant Na value. In Centre III amphiboles Si, Na, and Fe contents all increase with evolution of the magma.

PYROXENE COMPOSITIONAL VARIATION

5.1 Introduction

Pyroxenes from all four syenite types and from basalt xenoliths have been analyzed by the author on the Dalhousie electron microprobe and by Dr. Mitchell, using the probe facilities at Purdue and Cambridge universities. The operating conditions for these investigations are as for amphiboles, described in Appendix I.

The ferrous:ferric iron ratio and structural formula for 62 pyroxenes were determined with the "Structure" computer program (Appendix IV). This program also calculates the ratio of acmite:hedenbergite:diopside, used in the pyroxene compositional trend diagram, Figure 33. The compositions of pyroxenes with greater than five percent $CaAl(SiAl)O_6$ or $CaTiAl_2O_6$ are not plotted in this figure and these pyroxenes with higher alumina contents are plotted in Figure 34. The end-members of this ternary system are: acmite-$NaFe^{3+}Si_2O_6$, Ti-pyroxene-$CaTiAl_2O_6$ and CATS or Ca-Tschermack's-$CaAl(SiAl)O_6$ molecule. Pyroxenes from C2153 and C2138 are very high in silica and low in alumina and their structural formulae and iron ratios were calculated on the basis of stoichiometry assuming 4 cations and 6 oxygens.

Representative pyroxene compositions for the four syenite types and for the volcanic xenoliths are presented in Tables 12 to 16. The remainder of the pyroxene data is found in Appendix VI. All but two of the compositions are clinopyroxenes. Two grains from quartz syenite C2138 may be orthopyroxene, ferrosilite. These two analyses are presented in Table 17. The presence of orthopyroxene suggests that the rock formed under high temperature (1130°C-1300°C) and very high pressure conditions (16.5kb-19kb) (Morse, 1980, and Lindsley et al 1968). This quartz syenite

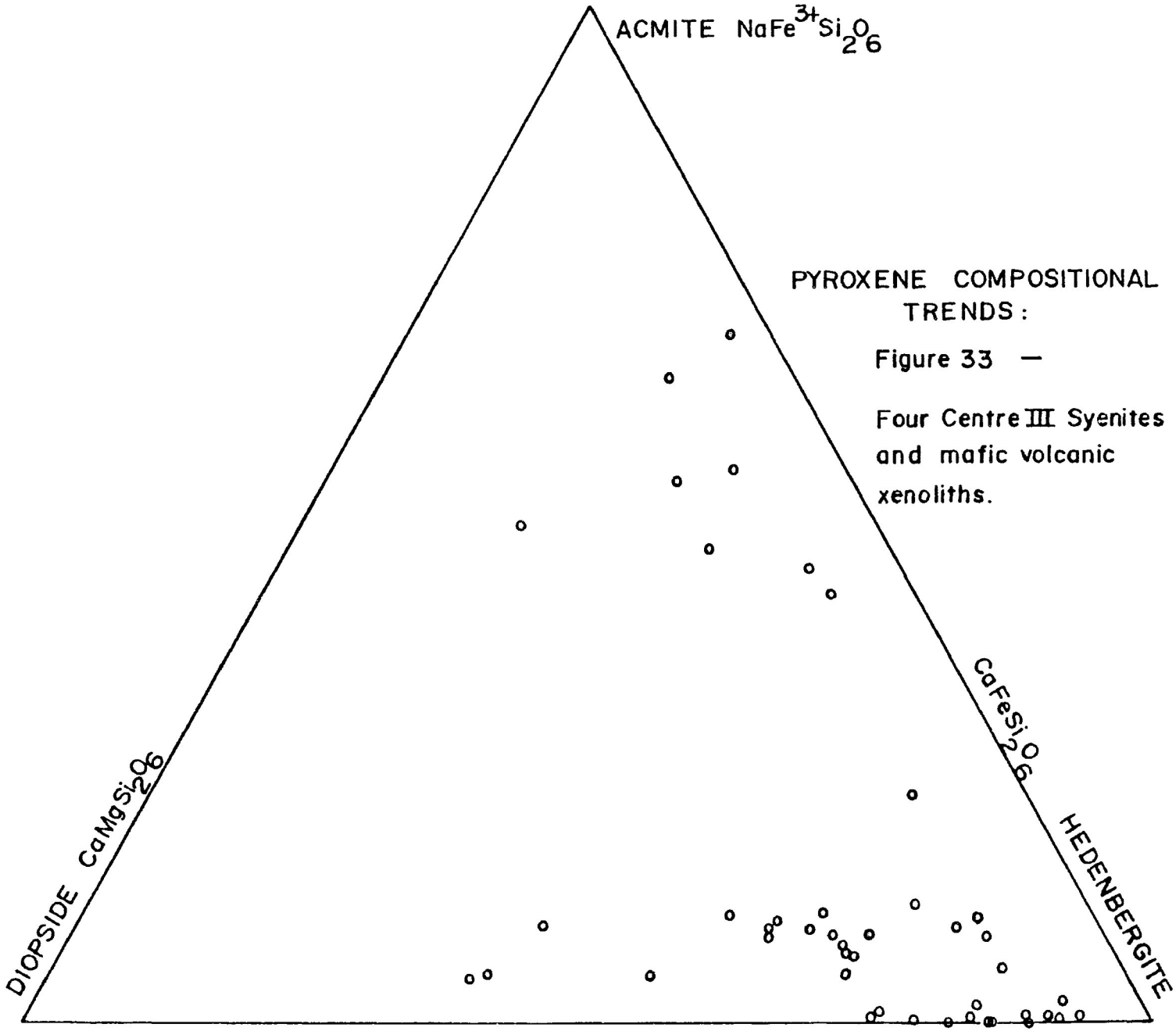

PYROXENE COMPOSITIONAL TRENDS:

Figure 33 —

Four Centre III Syenites and mafic volcanic xenoliths.

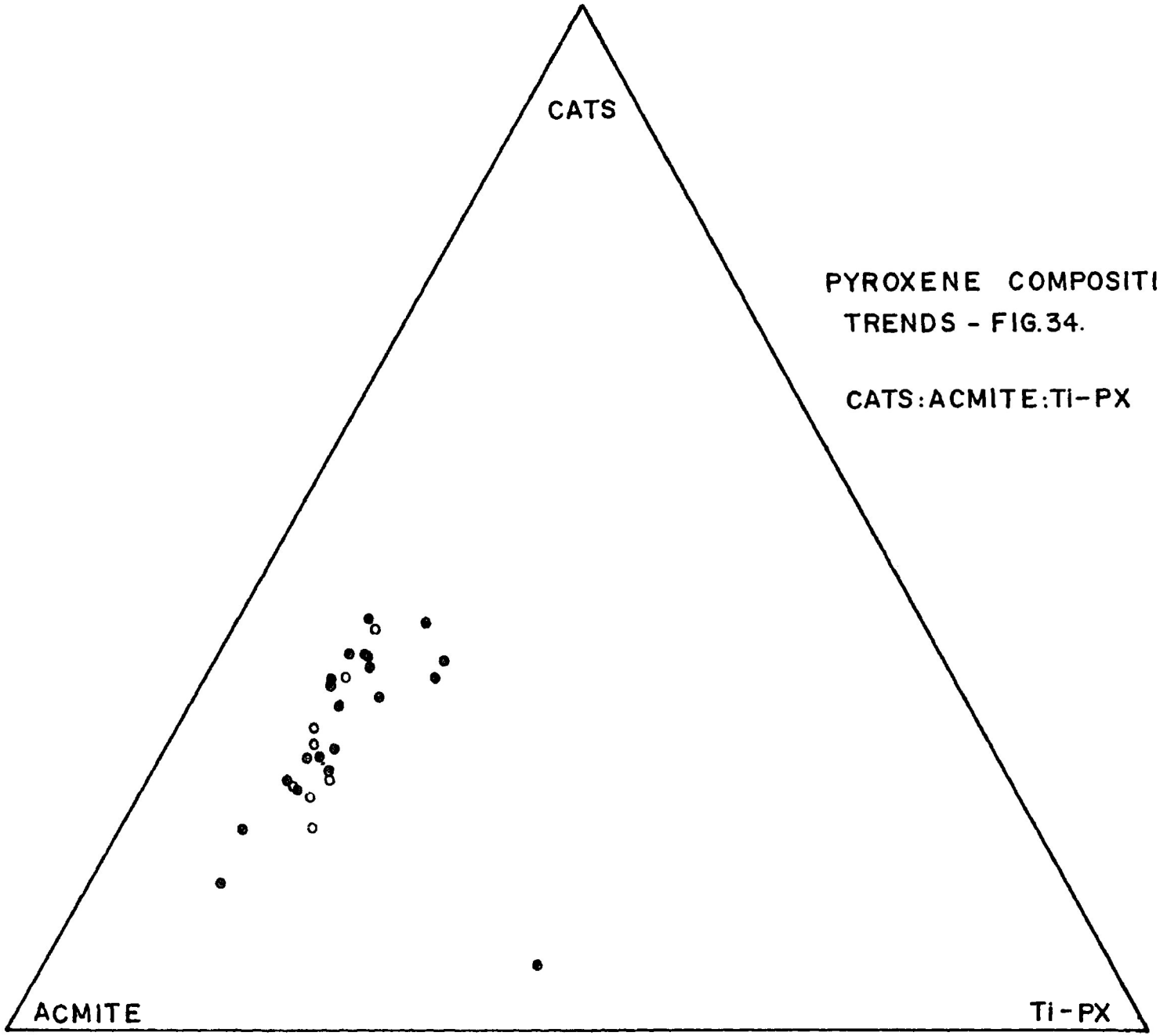

PYROXENE COMPOSITIONAL TRENDS - FIG.34.

CATS:ACMITE:Ti-PX

TABLE 12

Microprobe analyses - Pyroxenes from magnesio-hornblende syenite

	C181/1	C181/2	C181/3	C2123/1	C2123/2	C2123/3
SiO2	42.0	42.3	41.4	45.4	47.6	45.8
TiO2	1.34	1.34	1.34	1.36	1.35	1.36
Al2O3	9.2	9.2	9.26	6.32	5.04	5.32
Fe2O3	6.21	5.44	6.42	3.48	2.94	2.94
FeO	18.7	19.2	18.6	15.3	18.4	17.5
MnO	0.82	0.82	0.82	0.82	0.82	0.82
MgO	6.29	5.79	5.61	10.7	9.48	10.1
CaO	11.3	11.2	11.1	11.7	12.2	12.0
Na2O	2.41	2.11	2.49	1.35	1.14	1.14
Cr2O3	0.07	0.07	0.07	0.07	0.07	0.07
K2O	0.91	1.08	0.81	0.15	-	-
Total	99.3	98.6	97.8	96.6	99.0	97.0
Si	1.68	1.70	1.68	1.80	1.86	1.82
Aliv	0.321	0.299	0.321	0.201	0.145	0.177
Alvi	0.113	0.137	0.122	0.094	0.087	0.072
Fe3iv	-	-	-	-	-	-
Fe3vi	0.187	0.165	0.196	0.104	0.086	0.088
Fe2	0.626	0.646	0.630	0.508	0.599	0.584
Mn	0.028	0.028	0.028	0.028	0.027	0.028
Mg	0.375	0.347	0.340	0.632	0.551	0.597
Ca	0.482	0.482	0.481	0.496	0.511	0.510
Na	0.187	0.165	0.196	0.104	0.086	0.088
Ti	0.040	0.041	0.041	0.041	0.040	0.041
Cr	0.002	0.002	0.002	0.002	0.002	0.002
K	0.046	0.056	0.042	0.008	-	-

TABLE 13

Microprobe analyses - Pyroxenes from ferro-edenite syenite

	C333/2	C2127/1	C333/1	C2004/2	C2133/2	C2127/2	C2074/2
SiO2	49.4	49.1	46.4	42.2	42.9	44.2	47.8
TiO2	1.31	1.33	1.36	1.33	1.33	1.33	1.37
Al2O3	0.87	1.81	0.66	7.21	6.02	5.32	1.88
Fe2O3	13.7	9.28	6.62	5.13	6.16	8.73	2.76
FeO	19.5	19.1	18.0	25.0	24.4	20.5	17.4
MnO	0.81	0.82	0.82	0.81	0.81	0.81	0.82
MgO	1.27	4.51	1.52	2.74	3.25	3.58	4.59
CaO	4.47	7.72	17.6	9.92	10.2	8.72	20.6
Na2O	5.33	3.60	2.57	1.99	2.39	3.39	1.07
Cr2O3	0.06	0.06	0.07	0.06	0.06	0.06	0.07
K2O	0.99	0.39	-	0.76	0.27	0.66	-
Total	97.9	97.7	95.6	97.2	97.7	97.3	98.3
Si	2.01	1.97	1.95	1.76	1.78	1.82	1.92
Aliv	-	0.027	0.033	0.238	0.223	0.182	0.081
Alvi	0.053	0.059	-	0.117	0.071	0.076	0.009
Fe3iv	-	-	0.021	-	-	-	-
Fe3vi	0.421	0.280	0.189	0.161	0.192	0.270	0.083
Fe2	0.665	0.640	0.632	0.873	0.845	0.703	0.583
Mn	0.028	0.028	0.029	0.029	0.029	0.028	0.028
Mg	0.077	0.270	0.095	0.170	0.201	0.219	0.275
Ca	0.195	0.332	0.793	0.443	0.452	0.384	0.888
Na	0.421	0.280	0.209	0.161	0.192	0.270	0.083
Ti	0.040	0.040	0.043	0.042	0.042	0.041	0.041
Cr	0.002	0.002	0.002	0.002	0.002	0.002	0.002
K	0.051	0.020	-	0.040	0.014	0.035	-

TABLE 14

Microprobe analyses - Pyroxenes from contaminated ferro-edenite syenite

	C2036/1	C2036/2	C2036/3	C2064/1	C2064/2	C2064/3
SiO2	42.2	42.5	42.3	44.2	50.7	45.4
TiO2	1.34	1.34	1.34	1.35	1.39	1.35
Al2O3	8.81	6.84	7.15	6.91	2.19	6.89
Fe2O3	5.95	5.67	5.54	4.90	1.65	5.00
FeO	21.4	21.5	20.7	17.1	9.1	15.3
MnO	0.82	0.82	0.82	0.82	0.83	0.82
MgO	4.29	5.16	4.90	8.13	12.1	9.39
CaO	10.8	10.7	10.8	11.1	21.0	11.3
Na2O	2.31	2.20	2.15	1.90	0.64	1.94
Cr2O3	0.06	0.06	0.06	0.07	0.07	0.07
K2O	1.00	0.52	0.72	0.39	-	0.20
Total	99.0	97.3	96.5	96.9	99.7	97.7
Si	1.71	1.75	1.75	1.78	1.92	1.79
Aliv	0.292	0.251	0.249	0.224	0.084	0.212
Alvi	0.129	0.080	0.100	0.103	0.014	0.107
Fe3iv	-	-	-	-	-	-
Fe3vi	0.181	0.175	0.172	0.148	0.047	0.148
Fe2	0.726	0.738	0.717	0.576	0.287	0.503
Mn	0.028	0.029	0.029	0.028	0.027	0.027
Mg	0.259	0.316	0.302	0.487	0.680	0.551
Ca	0.466	0.472	0.477	0.476	0.851	0.478
Na	0.181	0.175	0.172	0.148	0.047	0.148
Ti	0.041	0.041	0.042	0.041	0.040	0.040
Cr	0.002	0.002	0.002	0.002	0.002	0.002
K	0.052	0.027	0.038	0.020	-	0.01

TABLE 15

Microprobe analyses - Pyroxenes from quartz syenite

	C2081/2	C369/4	C2138/1	C2138/9	C2136/2	C2154/2	C2071/1
SiO2	50.3	49.6	47.2	48.9	45.3	43.8	38.7
TiO2	1.39	0.12	0.39	0.13	1.32	1.32	1.34
Al2O3	0.80	0.84	0.46	0.21	3.86	4.50	8.44
Fe2O3	1.65	3.07	-	2.14	6.83	10.0	6.65
FeO	11.7	18.7	25.6	26.3	26.3	20.9	19.6
MnO	0.83	0.77	0.96	0.98	0.81	0.81	0.82
MgO	9.60	5.89	2.42	0.79	2.11	3.21	4.25
CaO	22.7	18.6	19.0	18.5	8.46	7.71	11.1
Na2O	0.64	1.19	-	0.83	2.65	3.89	2.58
Cr2O3	-	-	-	0.17	0.06	0.06	0.06
K2O	-	-	-	-	0.49	0.87	0.97
Total	99.8	98.8	98.0	99.0	98.2	97.1	94.5
Si	1.94	1.98	2.02	2.01	1.88	1.82	1.66
Aliv	0.036	0.023	-	-	0.125	0.182	0.344
Alvi	-	0.016	0.044	0.025	0.064	0.039	0.081
Fe3iv	0.027	-	-	-	-	-	-
Fe3vi	0.021	0.092	-	0.066	0.213	0.313	0.214
Fe2	0.378	0.625	0.881	0.906	0.909	0.727	0.699
Mn	0.027	0.026	0.033	0.034	0.028	0.029	0.030
Mg	0.551	0.350	0.148	0.049	0.130	0.199	0.271
Ca	0.938	0.795	0.836	0.817	0.375	0.343	0.508
Na	0.048	0.092	-	0.066	0.213	0.313	0.214
Ti	0.040	0.004	0.012	0.004	0.041	0.041	0.043
Cr	-	-	-	0.005	0.002	0.002	0.002
K	-	-	-	-	0.026	0.046	0.053

TABLE 16

Microprobe analyses - Pyroxenes from xenoliths

	C2164/1	C2164/2	C2006/1	C2006/2	C2006/3	C2059/1	C2059/2	C2059/3
SiO2	39.4	41.0	45.6	47.2	45.1	42.1	41.1	41.5
TiO2	1.32	1.32	1.34	1.34	1.35	1.35	1.36	1.35
Al2O3	7.98	7.72	5.13	4.64	4.47	9.33	6.69	9.7
Fe2O3	6.21	6.39	5.28	5.33	5.05	5.77	5.1	5.18
FeO	25.1	25.2	18.5	19.4	17.1	15.3	14.2	15.5
MnO	0.81	0.81	0.82	0.82	0.82	0.82	0.82	0.82
MgO	2.1	2.03	7.38	7.23	7.86	9.05	9.36	8.43
CaO	9.4	9.48	9.83	10.6	9.74	11.2	10.9	11.8
Na2O	2.41	2.48	2.05	2.07	1.96	2.24	1.98	2.01
Cr2O3	0.06	0.06	0.07	0.07	0.07	0.07	0.07	0.07
K2O	1.00	1.25	0.07	0.29	-	0.55	0.39	0.69
Total	95.8	97.8	96.0	99.1	93.5	97.6	92.0	97.1
Si	1.69	1.72	1.85	1.86	1.87	1.67	1.73	1.67
Aliv	0.309	0.280	0.152	0.136	0.133	0.325	0.267	0.333
Alvi	0.095	0.101	0.093	0.080	0.086	0.113	0.065	0.126
Fe3iv	-	-	-	-	-	-	-	-
Fe3vi	0.201	0.202	0.161	0.158	0.157	0.173	0.162	0.156
Fe2	0.900	0.884	0.625	0.641	0.591	0.508	0.501	0.521
Mn	0.024	0.029	0.028	0.027	0.029	0.028	0.029	0.028
Mg	0.134	0.127	0.446	0.425	0.485	0.537	0.588	0.504
Ca	0.432	0.426	0.427	0.448	0.432	0.476	0.493	0.508
Na	0.201	0.202	0.161	0.158	0.157	0.173	0.162	0.156
Ti	0.043	0.042	0.041	0.040	0.042	0.040	0.043	0.041
Cr	0.002	0.002	0.002	0.002	0.002	0.002	0.002	0.002
K	0.055	0.067	0.004	0.015	-	0.028	0.021	0.035

TABLE 17

Microprobe analyses - Orthopyroxenes from quartz syenite

	C2138/6	C2138/7
SiO2	48.6	46.0
TiO2	-	-
Al2O3	-	0.37
Fe2O3	-	-
FeO	44.9	42.3
MnO	2.6	2.47
MgO	0.27	-
CaO	0.25	0.45
Na2O	-	-
Cr2O3	-	-
K2O	-	0.1
Total	96.6	91.8
Si	2.12	2.11
Aliv	-	-
Alvi	-	0.132
Fe3iv	-	-
Fe3vi	-	-
Fe2	1.64	1.62
Mn	0.096	0.096
Mg	0.017	-
Ca	0.012	0.022
Na	-	-
Ti	-	-
Cr	-	-
K	-	0.006

may represent a xenolith of lower crustal materials or the orthopyroxenes themselves may be xenocrysts.

5.2 Magnesio-hornblende syenite

Clinopyroxenes were analyzed from two specimens of magnesio-hornblende syenite, C181 and C2123. These data are presented in Table 12, and in the $NaFe^{3+}Si_2O_6$:$CaTiSiAl_2O_6$:$CaAl_2SiO_6$ ternary in Figure 34. In both of these specimens the pyroxene occurs in trace to small amounts, forming tiny euhedral to subhedral, medium green grains. These pyroxenes are commonly found within the mafic synneusis clusters. These six compositions plot within a small region of the ternary diagram, as acmitic CATS-type pyroxene, and thus are amongst the most aluminous pyroxenes found in Centre III syenites. In common with other pyroxenes plotted on this diagram, there is only limited solid solution with the Ti-pyroxene $CaTiAl_2O_6$.

With respect to pyroxenes from other syenite types, pyroxenes from magnesio-hornblende syenite have: lower silica (41.4-47.6% SiO_2) and ferrous iron (15.3-19.2% FeO); and higher alumina (5.0-9.3% Al_2O_3) and magnesia (5.6-10.7% MgO). There are insufficient data to define evolutionary composition trends.

5.3 Ferro-edenite syenite

Representative analyses of clinopyroxenes from ferro-edenite syenites are given in Table 13 and the pertinent compositions are presented in Figures 33 and 34. In the acmite:hedenbergite:diopside system, four pyroxenes from ferro-edenite syenites are hedenbergitic and three are sodic hedenbergites. Three of the hedenbergitic compositions are from C2077, a rock that is texturally very similar to the quartz syenites, but

differs significantly in not having quartz in the mode. In terms of pyroxene composition, this syenite has more affinity to the quartz syenite pyroxenes.

Nine of the pyroxenes from ferro-edenite syenites plot on the acmite: Ti-pyroxene:CATS ternary diagram (Figure 34). A roughly linear trend parallels the acmite:CATS join, from about 37% CATS to 14% CATS. The pyroxenes from ferro-edenite syenites have a higher acmite component than those from magnesio-hornblende syenites and contaminated ferro-edenite syenites.

Distinct colour changes are observed in examination of thin sections, between the hedenbergitic/CATS-bearing pyroxenes, and those approaching acmitic compositions. The former, as exemplified by C2004, are light to medium green and may or may not be replaced along margins by amphibole. At a composition of approximately 36% acmite component the pyroxene is medium green. Towards the aegirine end member most of the pyroxenes are dark green, with the most highly evolved grains being dark olive green. At any point along this trend the pyroxene may be partly replaced by amphibole.

While most ferro-edenite syenites contain one pyroxene of uniform composition, the entire collection of pyroxenes from all ferro-edenite syenites show a wide compositional range. The major evolutionary composition trend is controlled by the substitution $NaFe^{3+} \rightleftarrows CaFe^{2+}$. The major elemental changes are increasing Si, Na, Fe^{3+} and K, with relative decreases in Al, Mg and Ca. The levels of Mn, Ti, Cr and Fe_T remain relatively constant throughout this evolution. Silica contents are moderate to high for the majority of these pyroxenes (SiO_2:41.6-49.4%). Alumina contents are highly variable, ranging from 0.66 to 7.23 wt.% Al_2O_3.

The majority of ferro-edenite syenites contain one pyroxene of uniform composition, namely sodic-hedenbergite. In one specimen though, C333, two quite different pyroxenes coexist; aegirine-hedenbergites and a sodic-hedenbergite with only 22% acmite content. The latter grain is quite ragged, but a fresh edge to this grain was analyzed.

5.4 Contaminated ferro-edenite syenite

Pyroxenes from contaminated ferro-edenite syenites have compositions depicted in Figure 34, the acmite: Ti-pyroxene:CATS diagram. The majority plot near the acmite:CATS join, where they form a crude line from about 50% to 60% acmite. One composition plots away from all others, having a significant Ti-pyroxene component. It is possible that this peculiar pyroxene is a xenocryst from a different variety of xenolith. In terms of chemical evolution, the pyroxenes from these syenites are compositionally between those of magnesio-hornblende syenite and the ferro-edenite syenite (Table 14). The silica content is typically low, approximately 42-43% SiO_2, but does reach 50.7% SiO_2 in one example. The alumina varies from 2.2% to 8.8% Al_2O_3, with only one pyroxene with less than 6.8% Al_2O_3. Otherwise these pyroxenes have no outstanding chemical characteristics.

5.5 Quartz Syenite

Pyroxenes are most common in the Centre III quartz syenites and it was possible to analyze many examples. The majority of these pyroxenes have compositions which plot within the acmite:hedenbergite:diopside triangle (Figure 33, Table 15). Many compositions plot on a line close and parallel to the diopside:hedenbergite join. These compositions range from 37% to 94% hedenbergite component. The major chemical change in this

group is the substitution $CaMg \rightleftarrows CaFe^{2+}$, with iron replacing magnesium in the more evolved pyroxenes. The magnesium content decreases from 10.2% to 0.8% MgO, while the iron content increases from about 12% to over 28% FeO. At the same time several elements decrease: SiO_2 (52.7-48.9%); TiO_2 (1.4-0.13%); Al_2O_3 (0.53-0.20%) and CaO (23.4-18.5%). The MnO and Na_2O remains relatively constant, at approximately 0.9% MnO and 0.8% Na_2O.

Within the acmite:hedenbergite:diopside triangle (Figure 33) five pyroxenes from quartz syenites plot considerably closer to the acmite end-member, than the majority of pyroxenes from quartz syenites. Four are sodic hedenbergites, C2136/1 and 2, C2154/2 and C2091/3. One anomalous composition C2091/2 plots at 47.8% acmite, 19.4% hedenbergite and 32.8% diopside. Three other pyroxene compositions are presented in the acmite: Ti-pyroxene:CATS diagram (Figure 34). They plot in the middle portion of the ferro-edenite syenite trend. They are in this system due to their elevated Al_2O_3 contents (e.g. 8.44%, 7.98% and 7.72%).

In summary, the pyroxenes from quartz syenites are compositionally distinct when compared with pyroxenes from other Centre III syenites. In the majority of cases, a negative correlation exists between silica content, which ranges from 52.7% SiO_2 to 38.7%, and sodium content, varying from nil to 3.9% Na_2O (eg. C2164/1 has 39.4% SiO_2 and 2.4% Na_2O). The main trend is that as sodium content increases, the total iron content also rises. In addition the ferric iron content increases, to levels of 10% Fe_2O_3 (in C2154/2). Simultaneously, the magnesia and lime levels drop, from 10.2% MgO and 23.4% CaO in the most primitive pyroxenes, to approximately 2% MgO and 7.7% CaO in the most highly evolved grains. Alumina shows a positive correlation with sodium and total iron, increasing from 0.53% to 8.4% Al_2O_3. Thus as magma evolution proceeds, pyroxene compositions show relative increases in Na, Fe_T, Fe^{3+}

and Al and decreasing Si, Mg and Ca.

5.6 Volcanic Xenoliths

Pyroxene is not common in volcanic xenoliths of Centre III syenites, thus only six grains were analyzed in xenoliths found in syenites C2006 and C2059. All of these compositions are plotted in the acmite: Ti-pyroxene:CATS diagram (Figure 34, Table 16). The points form a linear trend coincident with the analyses from all the syenites, in particular corresponding in their composition to the pyroxenes from contaminated ferro-edenite syenite. The silica content varies from approximately 41% SiO_2 to 47.2%. Alumina decreases as silica increases, from a high of 9.7% Al_2O_3 to 4.5%. Sodium contents remain approximately constant, varying between 2.0% Na_2O and 2.2%. While the total iron and proportion of ferrous iron increases along with increasing silica (14.2 to 19.4% FeO), the amount of ferric iron is constant (5.0 to 5.8% Fe_2O_3). The only other oxide to increase with silica is titania, increasing from 0.4% TiO_2 to 1.4%. Magnesia and lime contents decrease with proceeding evolution of pyroxene compositions. Magnesia varies from 9.4% to 7.2% MgO, and lime decreases from 11.82% to 9.7% CaO.

5.7 Summary of pyroxenes from all Coldwell Complex syenites

The pyroxenes from Centre I ferro-augite syenites have been described by Mitchell and Platt (1978). The pyroxenes of the lower series cumulus ferro-augite syenite are weakly pleochroic from light brown to greenish brown to pale green. Compositionally they vary between $Di_{50}Hd_{45}Ac_5$ and $Di_5Hd_{90}Ac_5$, and thus are largely ferro-augites. In the upper series syenites, pyroxenes from the acmite-hedenbergite join dominate, with compositions from $Di_5Hd_{50}Ac_{45}$ to $Ac_{50}Hd_{50}$. Petrographically these

pyroxenes range from pale green weakly pleochroic hedenbergite to dark green strongly pleochroic acmitic hedenbergite. The increase in intensity of green colour is a result of increasing iron content at a relatively constant Na_2O and CaO. In the upper series syenites the major chemical trend is defined by increasing Na_2O and Fe_2O_3 at constant MgO levels. The pyroxenes within the earliest, structurally lowest syenite are the most primitive. In more evolved pyroxenes the Al ion is replaced by Fe^{3+}. Continuously zoned pyroxenes have been used to characterize the chemical evolution. Within a single syenite the compositions represent only a segment of the entire trend, defined by the compositions of pyroxenes from all Centre I syenites.

Mitchell and Platt (1982a,b) investigated the pyroxenes of Centre II nepheline syenites. A wide range of compositions are found in these rocks, with the majority being augites and ferro-augites with less than 15% acmite component. In deformation free syenites pyroxene forms irregular cores surrounded by amphibole. A weak zonation, or some recrystallization may be observed. In deformed syenites the pyroxene occurs as cores to poikiloblastic amphiboles, or as equant grains mantled by amphibole. In late-stage pegmatites amphibole is replaced along cleavage planes and margins by a dark green acmitic pyroxene. The dominant chemical trend for pyroxenes from all of these syenites, is characterized by increasing relative proportions of Na_2O and FeO. In the more evolved pyroxenes the increasing Na_2O is coupled with increasing Fe_2O_3 and MnO. The Al_2O_3 and TiO_2 levels exhibit no obvious trend with respect to changing Mg/(Mg+Fe) ratios. Thus the Centre II pyroxene compositional trends are similar to those for Centre I. The main difference is that pyroxenes from nepheline syenites are more aluminous (0.4 to 3.1%) and more sodic at any particular mg numbers, than pyroxenes

from Centre I syenites (0.2-1.7% Al_2O_3). Also, the evolutionary trend for pyroxenes from nepheline syenites starts out at more magnesian compositions, i.e. more primitive, and does not exhibit the strong FeO enrichment of highly evolved Centre I pyroxenes. Instead, pyroxene compositions from nepheline syenites display early ferric iron enrichment, toward acmite via aegirine-augite.

The summary of Centre I, II and III pyroxene compositional trends is presented in Figure 35, the acmite:hedenbergite:diopside system. The trends for Centre I and II syenites are taken from Mitchell and Platt (1982a). The ferro-edenite syenite and quartz trends coincide with that for ferro-augite syenites near the hedenbergite end member, and overlap both Centre I and II trends in the more evolved sodic hedenbergites.

The pyroxenes of Centre III magnesio-hornblende syenites and contaminated ferro-edenites are highly aluminous, with low silica and ferrous iron values. Insufficient data preclude discussion of evolutionary trends, but it is evident that these pyroxenes are very different from those in Centre I and II syenites.

The ferro-edenite syenites have pyroxenes with highly variable compositions. Their evolution is similar to pyroxenes from ferro-augite syenites, although in the Centre III pyroxenes the MgO content decreases as Si and Na increases. The pyroxenes of the quartz syenite are dissimilar, due to decreasing silica content with progressing magma evolution. Otherwise the $CaMg \rightleftarrows NaFe^{3+}$ exchange controls the pyroxene crystallization sequence in quartz syenites, as in the ferro-edenite syenites.

Pyroxene compositional trends - Fig.35.

Coldwell syenites

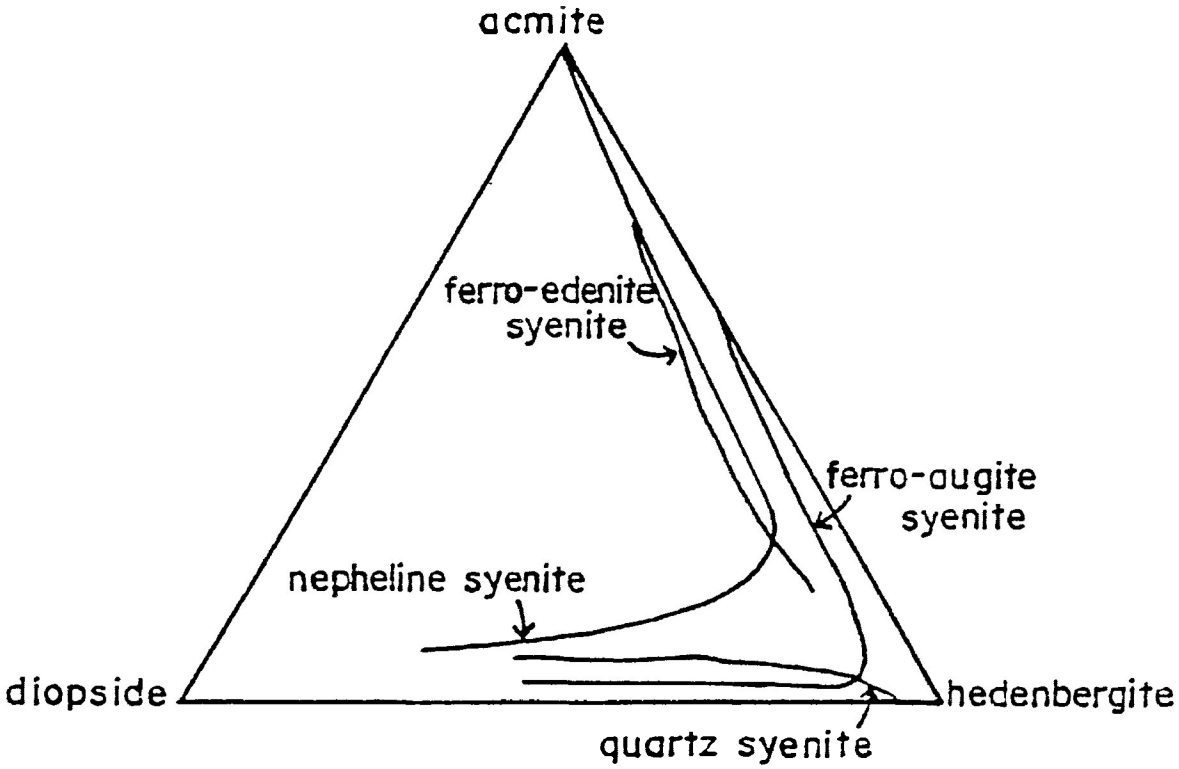

MICA COMPOSITIONAL VARIATION

6.1 Introduction

Micas from three syenite types have been analyzed with the microprobe:magnesio-hornblende syenite, ferro-edenite syenite and quartz syenite. The operating conditions were as for other minerals, described in Appendix I. The "Structure" program (Appendix IV) was utilized in determination of the structural formula, and the ratio of phlogopite: annite:manganophyllite. The structural formula was calculated on the basis of 22 oxygens. All mica compositions are presented in Tables 18 to 20.

Three diagrams are used in the discussion of results: a composite graph of Mn+Fe/Mn+Fe+Mg vs. Mn, Na+K, Si, Al and Ti (Figure 36); a plot of Fe^{2+}/Fe^{2+}+Mg vs. Si (Figure 37); and the ternary system phlogopite: annite:manganophyllite (Figure 38).

6.2 Magnesio-hornblende syenite

A total of seven micas have been analyzed from magnesio-hornblende syenites. As evident from Figure 36, (Table 18), the dominant chemical variation is the ratio of iron to magnesium. This change is highlighted by the wide range in Mn+Fe/Mn+Fe+Mg, from about 0.49 to 0.80. As the magma evolves, the micas crystallizing are enriched in iron (from 20.2% to 29.81% FeO) and manganese (from 0.14% to 0.31% MnO). The relative proportion of silicon (5.71 to 5.76 Si) and aluminum (2.26 to 2.35 Al) remains almost unchanged, whilst titanium increases initially (from 0.31 to 0.53 Ti) but decreases steadily to about 0.46 Ti for the most evolved mica from this syenite type.

The dominant trend of increasing iron and silica, with magma evolution, is also evident from the silica vs. $Fe^{2+}/Mg+Fe^{2+}$ diagram

TABLE 18

Microprobe analyses - Micas from magnesio-hornblende syenite

	C180/1	C180/2	C180/3	C180/4	C2150/1	C2150/2	C2150/3
SiO2	36.0	35.7	36.5	36.3	37.0	37.1	37.6
TiO2	4.00	3.79	4.08	4.09	2.57	4.59	4.43
Al2O3	12.0	12.2	12.4	12.3	12.6	12.5	12.7
FeO	29.1	29.8	28.9	29.2	20.2	21.0	21.1
MnO	0.31	0.24	0.28	0.27	0.14	0.20	0.21
MgO	5.11	4.29	5.29	5.40	11.8	10.6	10.5
CaO	-	-	-	0.12	-	-	-
K2O	8.97	8.99	8.89	9.05	9.14	9.16	9.33
Total	95.4	95.1	96.4	96.7	93.4	95.2	96.0
Si	5.76	5.76	5.76	5.74	5.71	5.71	5.74
Ti	0.482	0.460	0.485	0.486	0.306	0.532	0.509
Al	2.26	2.33	2.31	2.28	2.36	2.27	2.29
Fe2	3.90	4.03	3.82	3.857	2.68	2.71	2.70
Mn	0.042	0.033	0.038	0.036	0.019	0.026	0.027
Mg	1.22	1.03	1.25	1.27	2.77	2.43	2.39
Ca	-	-	-	0.020	-	-	-
K	1.83	1.85	1.79	1.82	1.85	1.80	1.82
Fe2#	0.76	0.80	0.76	0.75	0.49	0.47	0.47

TABLE 19

Microprobe analyses - Micas from ferro-edenite syenite

	C2224/1	C2053/1	C2053/2	C2221/1 core	C2221/2 rim	C2221/3	C2223/1
SiO2	31.6	37.0	37.5	34.9	33.9	35.5	36.2
TiO2	2.28	3.59	3.78	3.32	3.05	3.00	2.71
Al2O3	9.71	10.7	10.7	11.4	11.5	11.0	9.48
FeO	41.5	31.3	30.7	32.8	33.5	31.7	33.9
MnO	0.51	0.29	0.26	0.62	0.47	0.54	0.20
MgO	1.14	5.16	5.14	2.95	3.43	4.72	2.28
CaO	0.12	0.14	0.10	-	0.11	-	-
K2O	4.31	8.95	9.23	8.78	7.31	8.36	8.67
Total	91.2	97.2	97.4	94.8	93.3	94.8	93.5
Si	5.61	5.88	5.92	5.76	5.68	5.81	6.09
Ti	0.305	0.429	0.449	0.412	0.384	0.369	0.342
Al	2.04	2.00	1.98	2.23	2.27	2.11	1.88
Fe2	6.18	4.16	4.06	4.547	4.70	4.34	4.76
Mn	0.077	0.039	0.035	0.087	0.067	0.075	0.029
Mg	0.303	1.22	1.21	0.727	0.857	1.15	0.571
Ca	0.023	0.024	0.017	-	0.020	-	-
K	0.979	1.81	1.86	1.85	1.56	1.75	1.86
Fe2#	0.95	0.77	0.77	0.86	0.85	0.79	0.89

TABLE 20

Microprobe analyses - Micas from quartz syenite

	C2153/1	C2153/2	C367/1	C367/2	C346/1	C346/2	C2138/1
SiO2	36.4	35.6	36.5	36.4	35.4	36.2	35.3
TiO2	1.44	0.36	2.67	2.59	3.18	3.15	2.86
Al2O3	7.73	7.14	8.27	8.71	9.22	9.65	9.23
FeO	38.9	40.6	37.9	36.9	37.0	36.5	37.7
MnO	0.38	0.39	0.43	0.61	0.41	0.23	0.31
MgO	2.30	2.47	0.82	1.17	0.51	0.47	0.35
CaO	0.14	0.12	0.13	-	-	-	-
K2O	8.56	7.81	8.94	8.93	8.48	8.96	8.61
Total	95.9	94.5	95.6	95.3	94.2	95.1	94.3
Si	6.12	6.14	6.13	6.10	6.00	6.05	6.00
Ti	0.182	0.047	0.337	0.327	0.406	0.396	0.366
Al	1.53	1.45	1.64	1.72	1.85	1.90	1.85
Fe2	5.48	5.85	5.32	5.19	5.26	5.10	5.37
Mn	0.054	0.057	0.061	0.087	0.059	0.033	0.045
Mg	0.577	0.63	0.206	0.293	0.129	0.117	0.089
Ca	0.025	0.022	0.023	-	-	-	-
K	1.84	1.72	1.92	1.91	1.84	1.91	1.87
Fe2#	0.90	0.90	0.96	0.95	0.98	0.98	0.98

MICAS - Fe+Mn/Fe+Mn+Mg vs. Ti, Al, Si, Mn, Na+K - FIG. 36

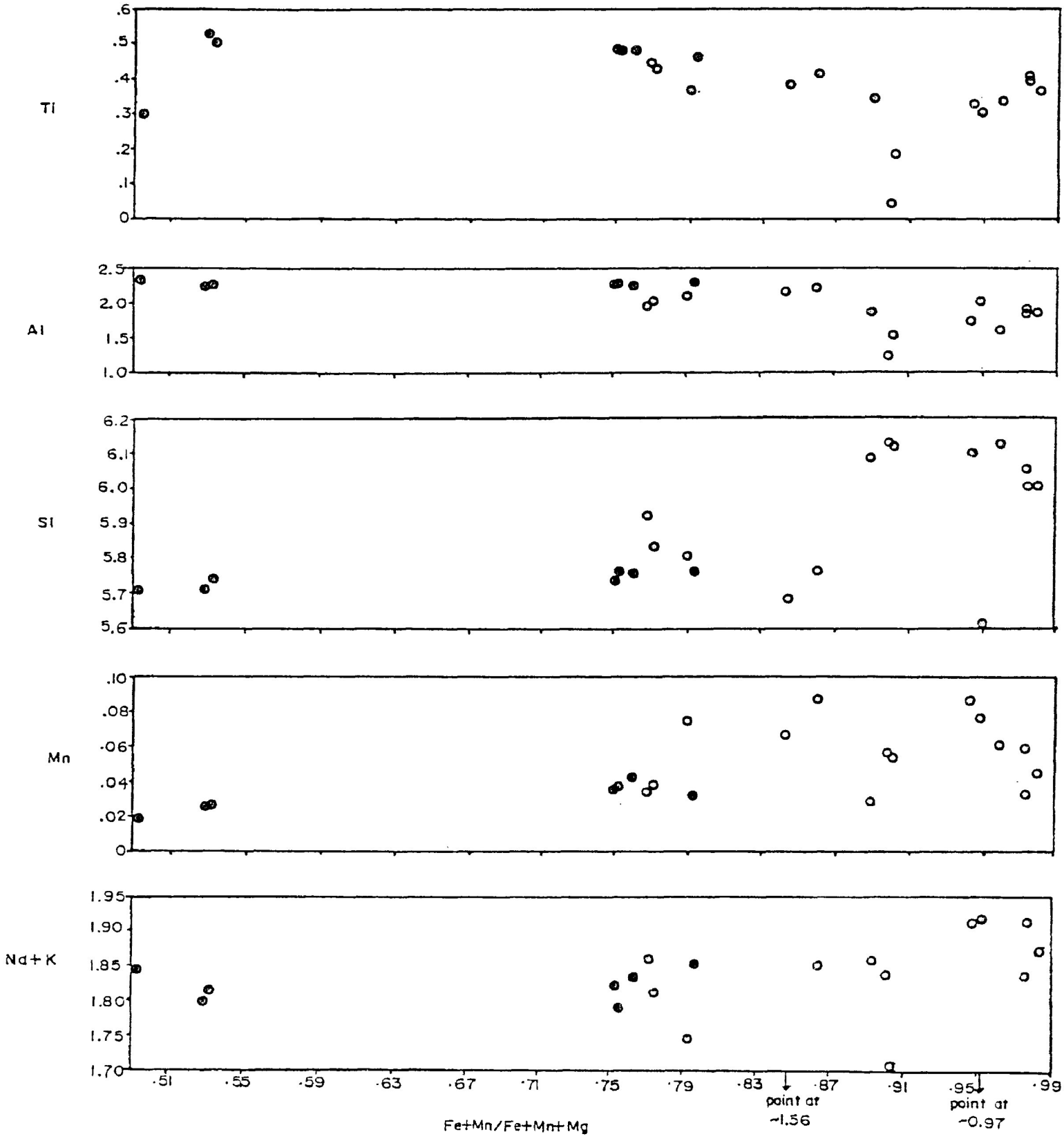

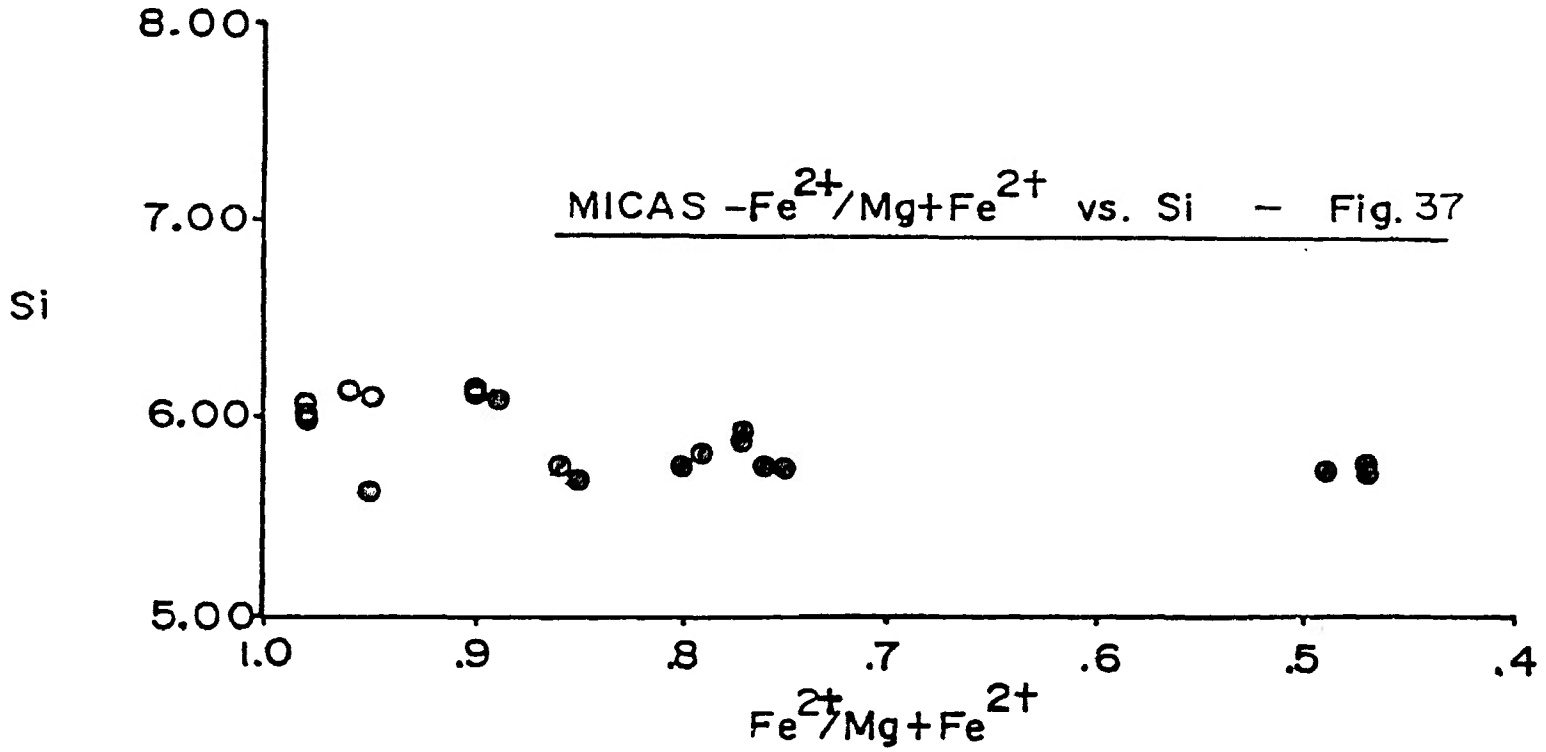
MICAS -Fe2+/Mg+Fe2+ vs. Si – Fig. 37
Si
8.00
7.00
6.00
5.00
1.0
.9
.8
.7
.6
.5
.4
Fe2+/Mg+Fe2+

MICAS FROM CENTRE

III SYENITES

Mg(Phlogopite): Fe(Annite): Mn(Manganophyllite)

Figure 38

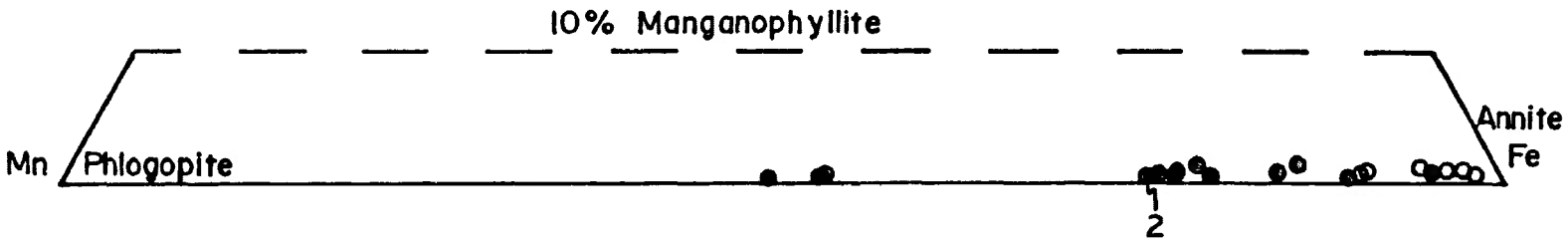

(Figure 36). In the ternary diagram (Figure 38) the seven analyses are parallel and very close to the phlogopite:annite join. These micas range in composition from Ann_{49} to Ann_{79}.

6.3 Ferro-edenite syenite

Seven micas from ferro-edenite syenites are compositionally similar, but slightly more evolved, than those from magnesio-hornblende syenites (Table 19). The most significant chemical difference is the slightly increased ratio Mn+Fe/Mn+Fe+Mg and Fe^{2+} number (Figures 36 and 37). Accompanying this change is increasing Si, K, Na, Mn and slightly decreasing Ti and Al. In the ternary plot, Figure 38, these micas display a range in composition from Ann_{76} to Ann_{95}.

6.4 Quartz syenite

Micas from quartz syenites exhibit the most evolved compositions (Table 20). These seven analyses show the highest iron and silica levels (Figures 36 and 37). With increasing iron, the Ti and Al contents increase, while remaining lower overall, than for micas from ferro-edenite syenites. The silicon content actually shows a decreasing trend, with increasing Mn+Fe/Mn+Fe+Mg, but is high when compared with micas from the other two syenites. Alkalis attain very high levels, up to 1.92 K in sample C367. Manganese contents are similar to those of micas in ferro-edenite syenites. The annite content of micas from quartz syenites ranges in composition from Ann_{79} to Ann_{99}.

6.5 Summary of mica compositions from all Coldwell syenites

Mitchell and Platt (1982a) indicate that biotite is a minor constituent of Centre I ferro-augite syenites. No compositional data are

available. Two micas are present in Centre II nepheline syenites, biotite in the melanocratic nepheline syenite and late stage primary and replacement muscovite (Mitchell and Platt, 1982b). The muscovite replaces primary nepheline. The biotite of the melanocratic nepheline syenite is zoned from yellow and red brown, to olive green margins. Incipient chloritization is evident at biotite margins and along cleavage planes, in the more evolved syenites. This alteration has reduced the K_2O contents in the nine micas analyzed. The micas are titaniferous biotites, ranging in composition from magnesian biotite to siderophyllite-annite. With progressive magma evolution the titanium level decreases, and iron and manganese contents increase. These compositions (Mitchell and Platt, 1982b) have been plotted in the ternary diagram $Mg:Fe^{2+}:Al$, by Platt and Wooley (1986). These compositions have been transferred to Figure 39, the ternary $Mg:Fe^{2+}:Al$, where they can be compared to Centre III micas. The micas from nepheline syenites evolve linearly from about $Mg_{50}Fe^{2+}_{20}Al_{30}$ to $Mg_6Fe^{2+}_{59}Al_{35}$.

Mica compositions from Centre III syenites are also depicted on this diagram. They evolve along a gently curved line from about $Mg_{35}Fe^{2+}_{35}Al_{30}$ to $Mg_5Fe^{2+}_{75}Al_{20}$. Compared to the micas from nepheline syenites, these micas are significantly less aluminous and in general, are more highly evolved with higher iron contents. The most highly evolved Centre II micas are enriched in alumina, compared to the most primitive Centre II micas. With Centre III micas the converse is true.

According to the classification scheme for micas recommended by Deer, Howie and Zussman (1978) the division between biotites and phlogopites is at a ratio Mg:Fe of 2:1. Thus, with the aid of Figure 37, all of the Centre III micas can be termed biotites, in particular, they are largely annites.

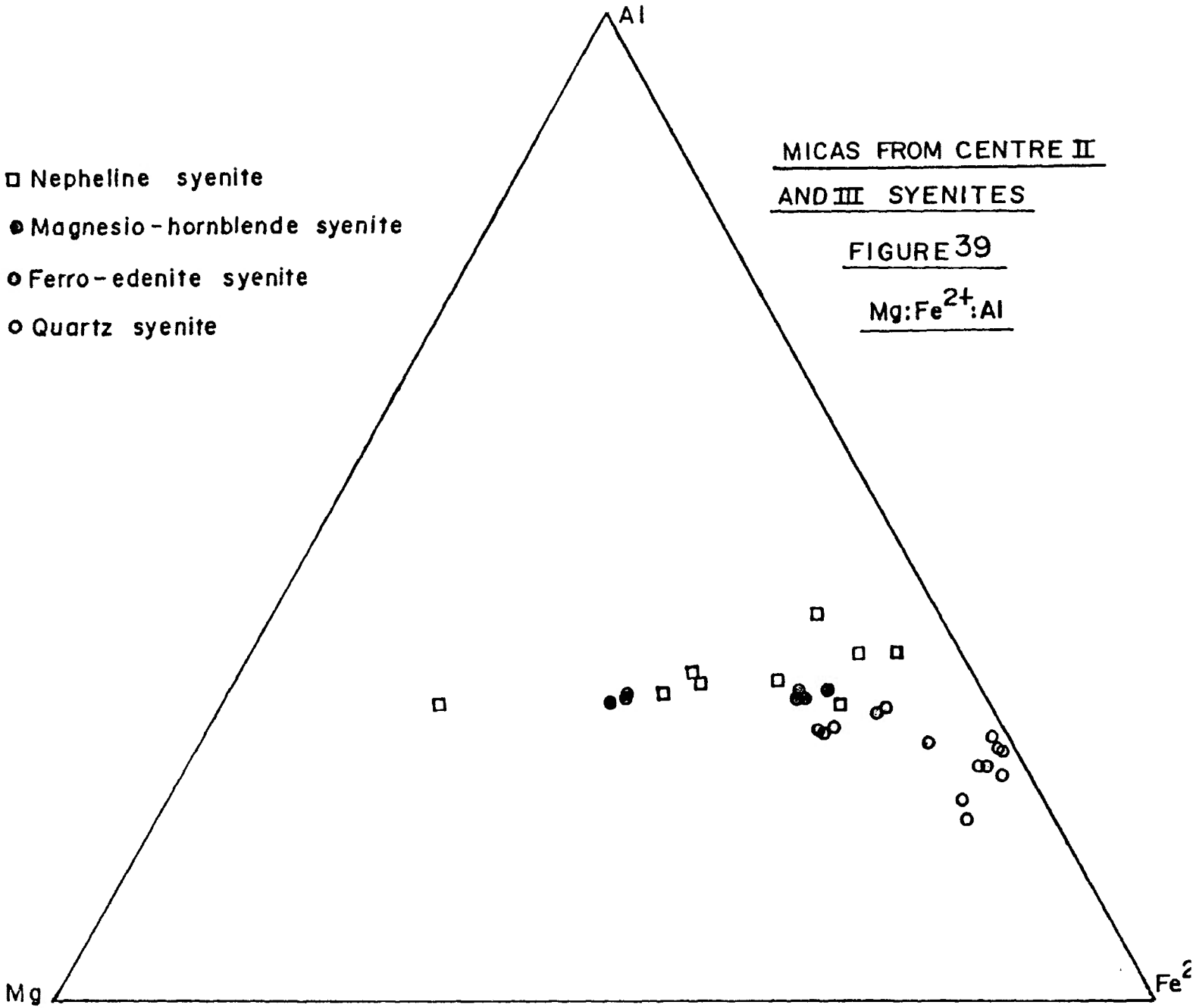

MICAS FROM CENTRE II AND III SYENITES

FIGURE 39

Mg:Fe^{2+}:Al

FELDSPAR COMPOSITIONAL VARIATION

7.1 Introduction

Feldspars from all four syenite types and from a basalt xenolith have been analyzed by the author on the Dalhousie electron microprobe and by Dr. Mitchell, using the probe facilities at Purdue and Cambridge universities. The operating conditions for these investigations are as for amphiboles described in Appendix I. No scans were performed, all data are spot analyses of homogeneous phases.

The structural formulae for 185 feldspars were determined with the "Structure" computer program (Appendix IV). This program also calculates two indices: celsian/anorthite/albite/orthoclase and anorthite/albite/orthoclase. The latter ratio was used in the composite diagram of Figure 40.

Representative feldspar compositions from the four syenite types and the basalt xenolith are presented in Tables 21 to 25. The remainder of the feldspar composition data are found in Appendix VIII. Where petrographically evident a distinction has been made between host and exsolved phases in perthites.

7.2 Magnesio-hornblende syenite

Twenty three analyses of feldspars were made from three magnesio-hornblende syenites, C178, C180 and C181. All compositions are depicted in Figure 40. Perthitic alkali feldspar grains are common as phenocrysts and groundmass constituents of magnesio-hornblende syenite, are generally altered, and exhibit patchy exsolution textures. Primary plagioclase occurs in small quantities in the groundmass. The coexistence of both feldspar types in magnesio-hornblende syenites is unique amongst Centre

FELDSPARS FROM CENTRE III SYENITES - An:Or:Ab
FIG. 40

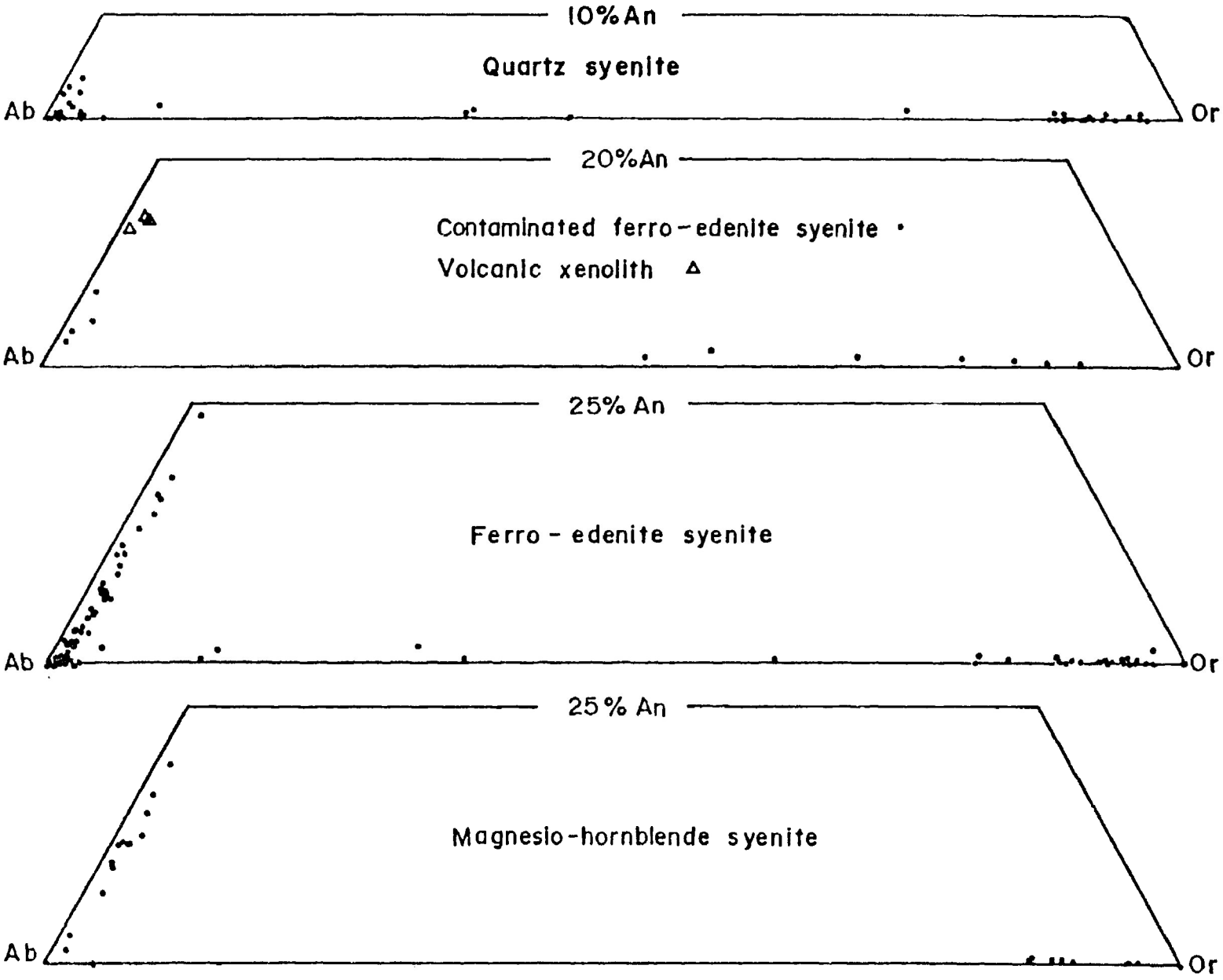

TABLE 21

Microprobe analyses - Feldspars from magnesio-hornblende syenite

	C180/4	C180/5	C180/7	C178/1	C178/2	C181/2	C181/3	C181/5
SiO2	62.0	67.1	65.5	64.1	69.5	67.2	65.2	66.9
Al2O3	17.7	19.1	22.1	22.6	20.2	21.1	18.2	20.6
FeO	0.17	0.20	0.42	0.33	0.23	0.32	0.26	0.3
MgO	-	-	-	0.03	0.03	-	0.03	0.05
CaO	-	0.15	2.89	3.82	0.49	2.7	0.08	2.38
Na2O	0.36	7.38	8.01	8.71	8.99	8.61	1.13	8.76
K2O	14.7	0.16	0.21	0.24	0.14	0.28	15.2	0.33
P2O5	-	0.17	-	-	-	-	-	-
BaO	0.48	-	-	0.05	-	0.04	0.28	-
Total	95.4	94.3	99.2	99.8	99.6	100.2	100.3	99.3
Si	2.99	3.05	2.89	2.83	3.01	2.93	3.00	2.94
Al	1.01	1.02	1.15	1.17	1.03	1.08	0.99	1.06
Fe	0.007	0.008	0.016	0.012	0.008	0.012	0.01	0.01
Mg	-	-	-	0.002	0.002	-	0.002	0.003
Ca	-	0.008	0.136	0.181	0.023	0.126	0.004	0.112
Na	0.034	0.650	0.684	0.746	0.756	0.728	0.101	0.747
K	0.904	0.009	0.012	0.014	0.008	0.016	0.890	0.019
P	-	0.007	-	-	-	-	-	-
Ba	0.009	-	-	0.001	-	0.001	0.005	-

TABLE 22

Microprobe analyses - Feldspars from ferro-edenite syenite

	C361/1	C2235/4	C2228/3	C2127/3	C2169/4	C1487/1	C2218/2	C2004/5
SiO2	68.7	65.5	70.2	65.0	65.5	69.4	65.6	66.4
Al2O3	20.1	18.5	19.8	17.5	20.3	18.8	17.9	17.6
FeO	0.35	0.83	0.45	0.43	-	0.39	0.21	0.31
MgO	0.01	0.04	-	-	-	-	-	-
CaO	0.89	0.08	0.20	0.04	1.20	0.18	0.04	0.08
Na2O	10.0	0.33	10.2	0.74	1.69	11.1	0.47	1.94
K2O	0.21	15.5	0.18	15.2	0.21	0.21	16.3	13.6
P2O5	-	-	-	-	-	-	-	-
BaO	-	0.09	-	0.04	-	-	0.06	-
Total	100.3	100.9	100.9	98.9	98.7	100.1	100.5	100.0
Si	2.98	2.99	3.02	3.02	2.92	3.02	3.01	3.03
Al	1.03	0.999	1.00	0.958	1.06	0.963	0.970	0.950
Fe	0.013	0.032	0.016	0.017	-	0.014	0.008	0.012
Mg	0.001	0.003	-	-	-	-	-	-
Ca	0.041	0.004	0.009	0.002	0.057	0.008	0.002	0.004
Na	0.845	0.029	0.849	0.067	1.00	0.941	0.042	0.172
K	0.012	0.906	0.009	0.902	0.012	0.012	0.955	0.794
P	-	-	-	-	-	-	-	-
Ba	-	0.002	-	0.001	-	-	0.001	-

TABLE 23

Microprobe analyses - Feldspars from contaminated ferro-edenite syenite

	C2063/1	C2063/2	C2036/2	C2036/3	C2036/4	C2067/1	C2067/2	C2067/3
SiO2	67.5	69.6	65.7	65.9	68.2	66.9	65.8	69.5
Al2O3	20.0	19.2	18.5	18.9	20.2	21.3	18.4	20.0
FeO	0.26	0.36	0.34	0.34	0.42	0.44	0.35	0.41
MgO	-	-	0.04	0.02	0.02	0.03	0.01	0.01
CaO	1.45	0.61	0.07	0.13	0.75	2.23	0.07	0.42
Na2O	10.3	9.89	1.25	1.99	9.09	8.78	0.93	10.2
K2O	0.18	0.17	14.6	13.28	0.33	0.18	15.1	0.19
P2O5	-	-	-	-	-	-	-	-
BaO	-	0.03	0.18	0.27	0.05	-	0.02	0.02
Total	99.7	99.9	100.8	100.8	99.0	99.9	100.6	100.8
Si	2.96	3.02	3.00	2.99	2.99	2.92	3.00	3.00
Al	1.03	0.985	0.995	1.01	1.04	1.10	0.99	1.01
Fe	0.010	0.013	0.013	0.013	0.015	0.016	0.013	0.015
Mg	-	-	0.003	0.001	0.001	0.002	0.001	0.001
Ca	0.068	0.028	0.003	0.006	0.035	0.104	0.003	0.019
Na	0.872	0.834	0.111	0.175	0.773	0.744	0.082	0.857
K	0.010	0.009	0.851	0.769	0.019	0.01	0.878	0.011
P	-	-	-	-	-	-	-	-
Ba	-	-	0.003	0.005	0.001	-	-	-

TABLE 24

Microprobe analyses - Feldspars from quartz syenite

	C2138/1	C346/6	C367/7	C2153/1	C2091/4	C2071/2	C369/4	C2164/1
SiO2	69.2	66.3	66.1	70.7	69.8	65.1	70.4	68.7
Al2O3	19.4	18.4	18.0	19.8	18.9	17.7	18.8	18.6
FeO	-	0.25	0.25	0.38	0.38	0.34	0.32	0.34
MgO	-	-	-	-	-	-	-	-
CaO	-	-	-	-	0.25	0.08	0.11	0.36
Na2O	10.8	0.74	0.63	11.9	9.77	1.15	9.4	9.09
K2O	0.17	14.9	15.2	0.13	0.21	15.3	0.16	0.07
P2O5	-	-	0.23	-	-	-	-	-
BaO	-	-	-	-	-	0.42	0.18	0.04
Total	99.5	100.5	100.4	102.9	99.3	100.1	99.3	97.3
Si	3.02	3.02	3.02	3.00	3.04	3.01	3.06	3.05
Al	0.995	0.987	0.967	0.992	0.972	0.963	0.962	0.975
Fe	-	0.010	0.010	0.014	0.014	0.013	0.012	0.013
Mg	-	-	-	-	-	-	-	-
Ca	-	-	-	-	0.012	0.004	0.005	0.017
Na	0.910	0.065	0.056	0.977	0.827	0.103	0.794	0.783
K	0.010	0.865	0.885	0.007	0.012	0.904	0.009	0.004
P	-	-	0.009	-	-	-	-	-
Ba	-	-	-	-	-	0.008	0.003	0.001

TABLE 25

Microprobe analyses - Feldspars
from volcanic xenoliths

	C366B/1	C366B/2	C366B/3
SiO2	65.7	65.3	65.6
Al2O3	21.2	20.8	21.1
FeO	0.27	0.31	0.21
MgO	0.01	-	0.03
CaO	2.7	2.96	2.64
Na2O	8.89	9.43	9.38
K2O	0.34	0.25	0.11
P2O5	-	-	-
BaO	0.09	-	0.04
Total	99.5	99.1	99.2
Si	2.90	2.89	2.90
Al	1.10	1.09	1.10
Fe	0.01	0.012	0.008
Mg	0.001	-	0.002
Ca	0.128	0.141	0.125
Na	0.763	0.811	0.804
K	0.019	0.014	0.006
P	-	-	-
Ba	0.002	-	0.001

III syenites.

From C178 two analyses of plagioclase have drastically different anorthite contents, 20% An (oligoclase) and 3% An (albite). Both grains are simple-twinned plagioclase. Sixteen analyses were made of feldspars from C180, six plotting near the orthoclase component and ten near the albite end members. Most grains are patch perthites with both orthoclase and albite compositions. About half of the non-perthitic grains are albitic and the other half are potassic. Five feldspars were analyzed from C181. A phenocryst with poor exsolution texture is albitic with about 11.5% An. In a patch perthite grain, the host phase is albitic whereas the exsolved phase is potassic. In a second perthitic grain, where it is unclear which is the exsolved phase, one phase is albitic and one is potassic.

In general, the potassic grains vary from about 87% to 100% Or and nil to 0.5% An. The albitic grains have higher anorthite contents, ranging from nil to about 20% An, and contain 1-2% Or component. Based on one example, the host phase of a patch perthite is albitic, and thus is, in fact antiperthite.

7.3 Ferro-edenite syenite

One hundred analyses were made of feldspars from twenty one specimens of ferro-edenite syenites. All compositions are presented in the relevant portion of Figure 40. In the typical situation the host phase of the feldspar is albite, whether the lamellae form patches or braids. Examples of antiperthites are found in specimens: C322, C361, C371, C1487, C2001, C2127, C2218, C2228 and C2235. The albite phase compositions range from about 89% Ab 9% An to nearly 100% Ab, with one anomalous composition at 66% Ab 1% An. The exsolved orthoclase phase varies from 84% Or to 100%

Or, with one anomalous composition at 64% Or. In two specimens, C361 and C2101, both perthites and antiperthites appear to coexist. In general, the non-perthitic feldspar grains have albitic compositions.

Mantled feldspars have plagioclase cores, with compositions ranging from 92-95% Ab in C2169, and 76-98% Ab in C2212. Other mantled feldspars have perthitic cores and rims. In the core and rim zones of a feldspar in C322, the host phase is albite. In C2004 the host phase of the core is albite, whereas the rim orthoclase appears to be the host phase. In those specimens where both perthite and anti-perthite appear to be present, some magma mixing may have occurred. The introduction of a second magma of different alkali content, during feldspar crystallization, could initiate formation of a second feldspar type.

7.4 Contaminated ferro-edenite syenite

Twelve analyses were made of feldspars from three specimens of contaminated ferro-edenite syenite (C2063, C2067 and C2036). Polysynthetically twinned feldspars present in the groundmass are albites, and one analysis of orthoclase gave an anomalous composition of 58% Or 1.5% An. In the perthitic phenocrysts it was not possible to distinguish the host from the exsolved lamellae. Another anomalous composition of 53% Or 1% An was found in one phase of the perthite of C2067.

7.5 Quartz Syenite

Forty seven analyses were made of feldspars from nine quartz syenites. The braid perthites are in fact antiperthites, in each case where the distinction between host and exsolved phase is clear. Analyzed samples containing braid antiperthites are: C369, C346, C367, C2153 and C2138. In specimens C2091, C2071 and C2164 the patch perthites also have

an albitic host. Generally the compositions plot close to the end-member compositions, in all specimens except C2213. This syenite is exposed as an isolated outcrop near Guse Point, in the midst of ferro-edenite syenites. Three anomalous feldspar compositions were analyzed from this rock, with the orthoclase varying in composition from 36.5% to 46% Or and also from about 88% to 93% Or.

7.6 Volcanic Xenolith

Three analyses were made from oligoclase basalt xenolith C366B. The compositions are all about 85% Ab 2% Or. The three grains analyzed have crystallized with apparently different twinning patterns: one is not twinned; one displays simple (Carlsbad) twinning; and a third is polysynthetically twinned. Thus only single-phase albite grains are present in this xenolith specimen.

7.7 Summary of Feldspar Mineralogy from Coldwell Complex Syenites

As implied by the name syenite, all of these lithologies consist largely of alkali feldspar as a primary, early crystallizing phase. Mitchell and Platt (1978) indicate that the Centre I ferro-augite syenite contains greater than 70% modal alkali feldspar. In both the lower and upper series syenites this feldspar is a cumulus phase, with no compositional trends evident throughout the sequence. Generally the alkali feldspar is homogeneous with Carlsbad twinning and no perthitic exsolutions. All grains have compositions with less than 5% An and vary from $Ab_{50-65}Or_{50-35}$. A minority of grains exhibit incipient exsolution.

Mitchell and Platt (1982b) describe the feldspars of Centre II nepheline syenites. Vein and patch perthite is present in the undeformed nepheline syenites. Some grains are twin-free and form an allotriomorphic

granular texture. Other tabular prisms exhibit Carlsbad twinning. Albitic plagioclase is also present in small quantities in the majority of nepheline syenites. In the nepheline syenites of Pic Island the alkali feldspars are generally homogeneous, with compositions ranging from $Or_{28}Ab_{68}An_4$ to $Or_{45}Ab_{53}An_1$. In the Redsucker Cove area, in more evolved nepheline syenites, the feldspar composition varies from $Or_{56}Ab_{42}An_2$ to $Or_{82}Ab_{18}$.

In deformed, recrystallized nepheline syenites alkali feldspars form homogeneous, granuloblastic, twin-free grains. Secondary albite is not present. In common with the deformation-free nepheline syenites, with progressing magma evolution, the alkali feldspars become more potassic. The general lack of microcline and the poorly developed exsolution textures suggest that the feldspars of Centre II nepheline syenites equilibrated at relatively high temperatures.

In all of the Centre III syenites, feldspar compositions are similar, with orthoclase ranging in composition from about 87% Or to 100% Or along the Ab-Or join. Generally this phase has nil to 0.5% An. There is no trend in orthoclase compositions between the four syenite types. The plagioclase compositions fall largely in the field of albite, generally with about 1-2% Or and from nil to 30% An. Typically the albite phase of perthitic grains has very low An contents, whereas the primary plagioclase laths (in magnesio-hornblende syenite) and secondary laths have the higher An compositions. All albitic phases analyzed from quartz syenites are restricted to less than 4% An.

Barium was determined in ninety-two feldspars, and ranges from nil to 0.42% BaO. The average level of barium for these feldspars is 0.07% BaO. There does not appear to be any difference in barium levels between the various syenites.

Most of the orthoclase and albite phases from perthites are compositionally close to pure end members, suggesting that the cooling history was long and final equilibration temperatures were relatively low. The presence of wide braid lamellae, and also occasional polysynthetic and microcline twinning also indicates a long period of slow cooling. This is in sharp contrast to Centre II nepheline syenites which appear to have cooled rapidly at relatively high temperatures.

IRON-TITANIUM OXIDE MINERALOGY

8.1 Introduction

Sixty-seven analyses have been made of iron-titanium oxides from Centre III syenites and xenoliths. This work was performed utilizing a microprobe under the operating conditions outlined in Appendix I. A computer program was used to calculate Fe_2O_3 contents, mole fractions and temperatures of crystallization. This program "OXTEMP" was devised by Stormer (1983) and a description is presented in Appendix IV. Representative compositions of ilmenite and magnetite from Centre III rocks are displayed in Tables 26 to 29. The remainder of the data are presented in Appendix VIII. All of the compositions appear in Figure 41, a ternary plot of mole percent $FeO:TiO_2:Fe_2O_3$.

8.2 Discussion

In many of the specimens, from all four syenite types, both magnetite and ilmenite are present. In the magnesio-hornblende syenite, discrete inclusions of anhedral magnetite and ilmenite occur within perthite, biotite and amphibole. Similar textures are observed in ferro-edenite syenite, where these oxides may also form clusters with apatite. In the contaminated ferro-edenite syenite the opaque phases may be concentrated in the biotite ovoids. In the quartz syenites, the iron-titanium oxides form discrete inclusions in mafic minerals, in some cases as a replacement texture. Anhedral to euhedral magnetite and/or ilmenite grains are also partly to completely included within late-stage fluorite. In general, the Fe-Ti oxide phases appear to be petrographically and chemically homogeneous. In specimens where both magnetite and ilmenite occur, separate, homogeneous grains of magnetite and ilmenite were

TABLE 26

Microprobe analyses - Fe-Ti oxides from magnesio-hornblende syenite

	C2123/1	C2123/2	C2123/3	C181/1	C181/2	C181/3	C179/1	C179/2
SiO2	0.09	0.11	0.06	0.12	0.08	0.12	0.16	0.07
TiO2	47.8	49.6	48.7	0.88	0.60	0.85	0.68	49.4
Al2O3	0.09	0.09	-	0.24	0.19	0.22	0.15	0.08
Fe2O3	7.85	5.79	6.17	66.7	66.8	65.6	66.7	5.05
FeO	40.6	42.2	41.4	31.9	31.2	31.5	31.6	41.5
MnO	2.22	2.33	2.28	0.09	0.12	0.04	0.22	2.85
MgO	0.07	0.04	0.10	0.04	0.07	-	-	0.06
CaO	0.03	0.06	0.02	0.01	0.01	-	0.05	-
Total	98.7	100.2	98.7	99.9	99.0	98.3	99.5	99.0
Si	0.002	0.003	0.002	0.005	0.003	0.005	0.006	0.002
Ti	0.921	0.941	0.939	0.025	0.018	0.025	0.020	0.949
Al	0.003	0.003	-	0.011	0.009	0.010	0.007	0.002
Fe3	0.152	0.110	0.119	1.93	1.95	1.93	1.94	0.097
Fe2	0.871	0.891	0.887	1.02	1.01	1.03	1.02	0.886
Mn	0.048	0.050	0.050	0.003	0.004	0.001	0.004	0.062
Mg	0.003	0.002	0.004	0.002	0.004	-	-	0.002
Ca	0.001	0.002	0.001	-	-	-	0.002	-

TABLE 27

Microprobe analyses- Fe-Ti oxides from ferro-edenite syenite

	C333/1	C2232/1	C294/4	C2235/2	C2074/1	C2226/2	C2190/1
SiO2	0.07	0.05	0.13	0.21	0.12	2.36	0.15
TiO2	50.0	47.3	4.01	4.60	3.99	0.09	0.67
Al2O3	0.06	0.04	0.11	0.17	0.84	0.06	0.25
Fe2O3	5.23	7.82	61.4	58.9	59.8	62.8	66.0
FeO	42.0	37.4	34.8	35.2	34.0	33.9	31.3
MnO	2.99	5.13	0.23	0.16	0.90	0.10	0.04
MgO	-	-	0.04	-	-	0.02	-
CaO	0.02	0.05	0.08	0.02	0.01	0.08	0.05
Total	100.3	97.8	100.8	99.3	99.7	99.4	98.5
Si	0.002	0.001	0.005	0.008	0.005	0.090	0.006
Ti	0.948	0.922	0.115	0.133	0.115	0.003	0.020
Al	0.002	0.001	0.005	0.008	0.038	0.003	0.012
Fe3	0.099	0.153	1.76	1.71	1.72	1.81	1.94
Fe2	0.885	0.809	1.11	1.14	1.09	1.09	1.02
Mn	0.064	0.113	0.007	0.005	0.029	0.003	0.001
Mg	-	-	0.002	-	-	0.001	-
Ca	0.001	0.001	0.003	0.001	-	0.003	0.002

TABLE 28

Microprobe analyses- Fe-Ti oxides from contaminated ferro-edenite syenite

	C2031/1	C2031/2	C2036/1	C2036/2	C2036/3	C2031/3	C2229/1	C2229/2
SiO2	0.18	0.09	0.14	0.04	0.05	0.19	0.11	0.21
TiO2	47.5	47.8	2.75	47.5	48.1	47.7	46.5	47.3
Al2O3	0.10	0.10	0.12	0.01	0.02	0.06	-	0.10
Fe2O3	6.98	5.10	63.4	6.72	4.95	4.79	8.48	6.54
FeO	40.4	40.7	33.5	40.2	38.9	40.4	36.3	24.5
MnO	2.36	2.17	0.36	2.37	4.16	2.51	5.43	17.8
MgO	0.07	0.04	0.03	0.03	-	0.04	0.01	0.02
CaO	-	0.09	0.01	0.06	0.12	0.04	0.06	0.15
Total	97.6	96.1	100.3	96.9	96.3	95.8	96.9	96.6
Si	0.005	0.003	0.005	0.001	0.001	0.005	0.003	0.006
Ti	0.926	0.946	0.079	0.933	0.950	0.947	0.914	0.929
Al	0.003	0.003	0.005	-	0.001	0.002	-	0.003
Fe3	0.136	0.101	1.83	0.132	0.098	0.095	0.167	0.129
Fe2	0.876	0.896	1.07	0.879	0.855	0.893	0.794	0.535
Mn	0.052	0.048	0.012	0.052	0.093	0.056	0.120	0.394
Mg	0.003	0.002	0.002	0.001	-	0.002	-	0.001
Ca	-	0.003	-	0.002	0.003	0.001	0.002	0.004

TABLE 29

Microprobe analyses- Fe-Ti oxides from quartz syenite

	C2098/3	C173/1	C2060/1	C2136/3	C2071/1	C369/1	C2081/3	C2154/1
SiO2	0.13	0.10	0.14	0.23	0.05	0.13	0.32	0.20
TiO2	47.7	49.2	2.53	0.63	2.56	0.92	1.25	15.9
Al2O3	0.01	0.08	0.50	0.04	0.57	0.06	0.07	0.05
Fe2O3	6.40	4.89	64.7	68.1	63.7	64.6	66.5	70.3
FeO	38.1	41.8	34.1	32.3	33.4	30.9	32.7	13.6
MnO	4.78	2.37	0.15	-	0.25	-	0.08	0.80
MgO	0.04	0.05	0.02	0.01	0.03	-	0.07	0.02
CaO	0.09	0.06	0.03	0.03	0.06	0.15	0.05	0.03
Total	97.3	98.5	102.1	101.4	100.6	96.8	101.0	100.9
Si	0.003	0.003	0.005	0.009	0.002	0.005	0.012	0.005
Ti	0.934	0.949	0.071	0.019	0.073	0.028	0.036	0.309
Al	-	0.002	0.022	0.002	0.026	0.003	0.003	0.002
Fe3	0.125	0.094	1.82	1.94	1.82	1.93	1.90	1.37
Fe2	0.828	0.897	1.07	1.02	1.06	1.03	1.04	0.295
Mn	0.105	0.052	0.005	-	0.008	-	0.003	0.018
Mg	0.002	0.002	0.001	0.001	0.002	-	0.004	0.001
Ca	0.003	0.002	0.001	0.001	0.002	0.006	0.002	0.001

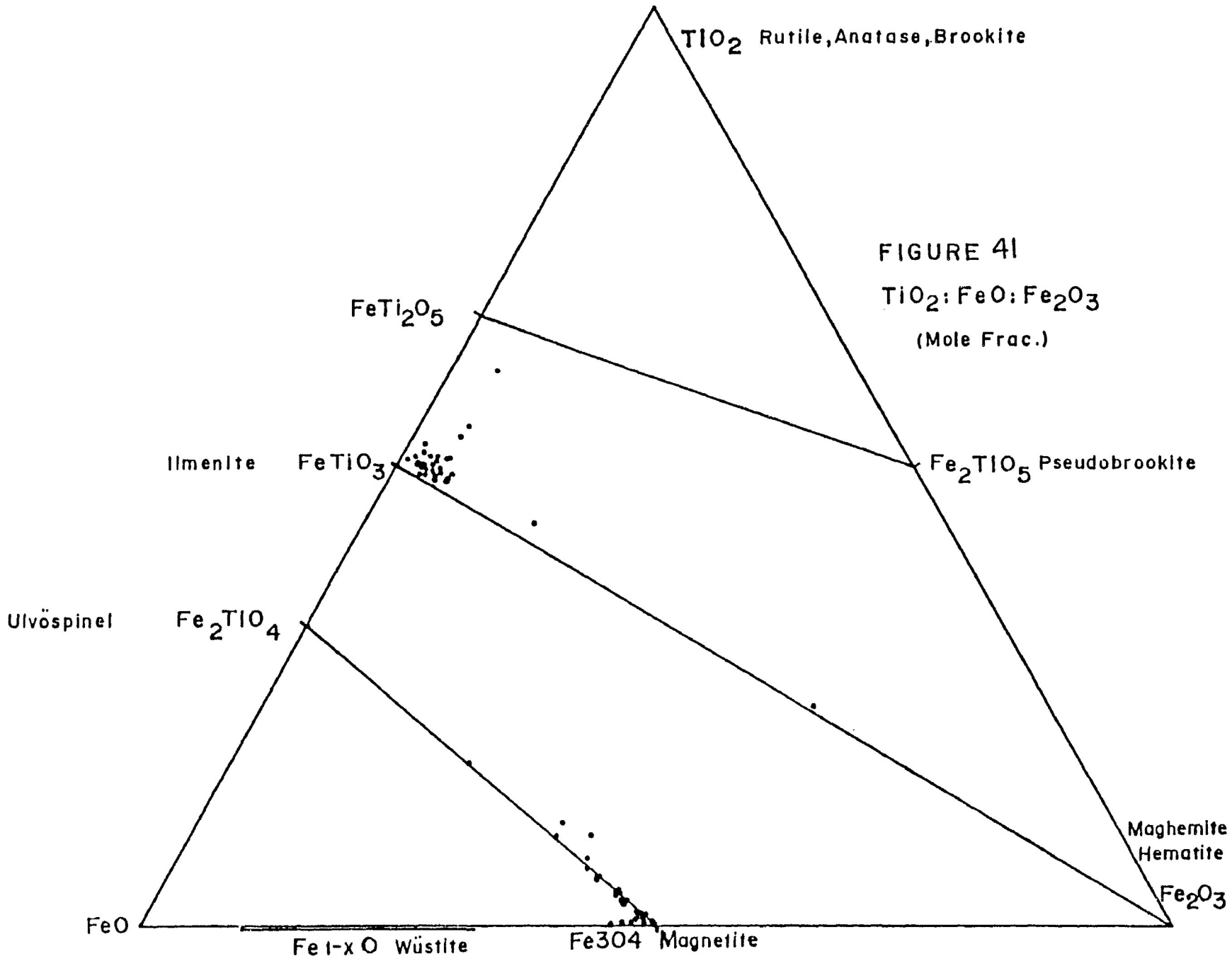

FIGURE 41

TiO_2: FeO: Fe_2O_3

(Mole Frac.)

analyzed. While not optically observed, it is possible that ilmenite has exsolved from magnetite on a submicroscopic scale, but these lamellae would be too thin to analyze separately with the microprobe. In only one ferro-edenite syenite, C294, is exsolution visible.

As shown in Figure 41 the majority of compositions plot in two separate, approximately linear clusters: one at the ilmenite end-member, and one at the magnetite composition. The ilmenite compositions fall near the ilmenite-hematite solid solution projection, whereas the magnetite compositions plot on the magnetite-ulvöspinel join. There is no apparent segregation of compositions with respect to syenite type. Considering only the syenite specimens from which both ilmenite and magnetite were analyzed, ilmenites which are relatively rich in hematite coexist with magnetite-rich members of the ulvöspinel-magnetite series. Alternatively, ulvöspinel-magnetite phases which are relatively rich in ulvöspinel coexist with relatively pure ilmenite.

Magnetite grains from Centre III rocks contain 0.06 to 13.45% TiO_2 and nil to 4.58% MnO. For ilmenite grains, the MnO content varies from 0.06 to 17.8% MnO, but is generally less than 5%. The three anomalous ilmenite compositions (Fig. 41), well off of the ilmenite-hematite join, contain 9 to 17.8% MnO. In more aluminous rocks, such as the contaminated ferro-edenite syenites, early ilmenite may oxidize in the presence of calcium and silica, to produce the observed sphene and magnetite or hematite. The relevant chemical relationships, as presented by Bonin and Giret (1985) are:

$$3\ \underset{\text{ilmenite}}{FeTiO_3} + (3CaO + 3SiO_2)_{liq} + \tfrac{1}{2}O_2 \rightarrow 3\underset{\text{sphene}}{CaTiSiO_5} + \underset{\text{magnetite}}{Fe_3O_4}\ ;$$

$$\text{or,}\ 2\ \underset{\text{ilmenite}}{FeTiO_3} + (2CaO + 2SiO_2)_{liq} + \tfrac{1}{2}O_2 \rightarrow 2\underset{\text{sphene}}{CaTiSiO_5} + \underset{\text{hematite}}{Fe_2O_3}\ .$$

A summary of equilibration temperatures and oxygen fugacities for several Fe-Ti oxide pairs is presented in Table 30. Discrepancies are evident between pairs from the same sample, suggesting that disequilibrium precludes the use of these data for precise temperature and fugacity determinations.

For Centre III syenites temperatures vary between 436±91^{o}C and 762±46^{o}C. Oxygen fugacities vary from $10^{-15.53\pm0.71}$ to $10^{-30.65\pm5.04}$. These determinations, calculated by the method of Stormer (1982) are presented in Figure 42, a plot of T(^{o}C) versus-logfo_2. Four of the analyses are considered to be out-of-range by Stormer's (1983) computer program, well outside of the accuracy limits of temperature (±30^{o}C) and fugacity (±0.50 units). These out-of-range samples are indicated with crosses. The curve labelled QFM is the quartz-fayalite-magnetite buffer, as determined by Wones and Gilbert (1969).

In the majority of Centre III syenites examined, the oxide minerals crystallized together with the silicate minerals, and not as subsolidus exsolutions or replacements. Thus these temperature and fugacity values may reflect the prevailing conditions at the time of crystallization of the magmas.

From the relatively small number of magnetite-ilmenite pairs analyzed, it is difficult to generalize about the distribution of points for different syenite types. As in the ternary plot of Figure 41, the data points in the temperature/fugacity plot are mixed, with respect to the four syenite types.

The oxygen fugacities decrease with decreasing temperature along a path which is closely parallel to that of the synthetic QFM oxygen buffer of Wones and Gilbert (1969). The analyses for Centre III syenites are slightly above this buffer curve, suggesting that these oxides crystallized under more oxidizing conditions than the QFM.

Table 30
OXCALC 2 - Fe-Ti Oxide Temperatures and Oxygen Fugacities

a) magnesio-hornblende syenite:

C179 -	551+/-48,-20.57+/-1.04	
	436+/-91,-30.65+/-5.04	out of range.

b) ferro-edenite syenite:

C2235 -	657+/-30,-17.51+/-0.72	
	762+/-46,-15.53+/-0.71	
C2190 -	577+/-45,-18.76+/-0.74	
	555+/-55,-19.15+/-0.76	
C2226 -	592+/-52,-16.86+/-0.48	out of range.
	602+/-46,-16.69+/-0.47	out of range.
	527+/-158,-17.99+/-.51	out of range.

c) contaminated ferro-edenite syenite:

C2036 -	635+/-30,-17.79+/-0.71	
	607+/-35,-19.43+/-0.97	

d) quartz syenite:

C2136 -	585+/-45,-18.02+/-0.63	
	590+/-45,-17.69+/-0.59	
C2081 -	507+/-58,-25.23+/-2.37	
	494+/-62,-25.53+/-2.39	
C369 -	596+/-38,-18.16+/-0.68	
	661+/-28,-17.06+/-0.64	

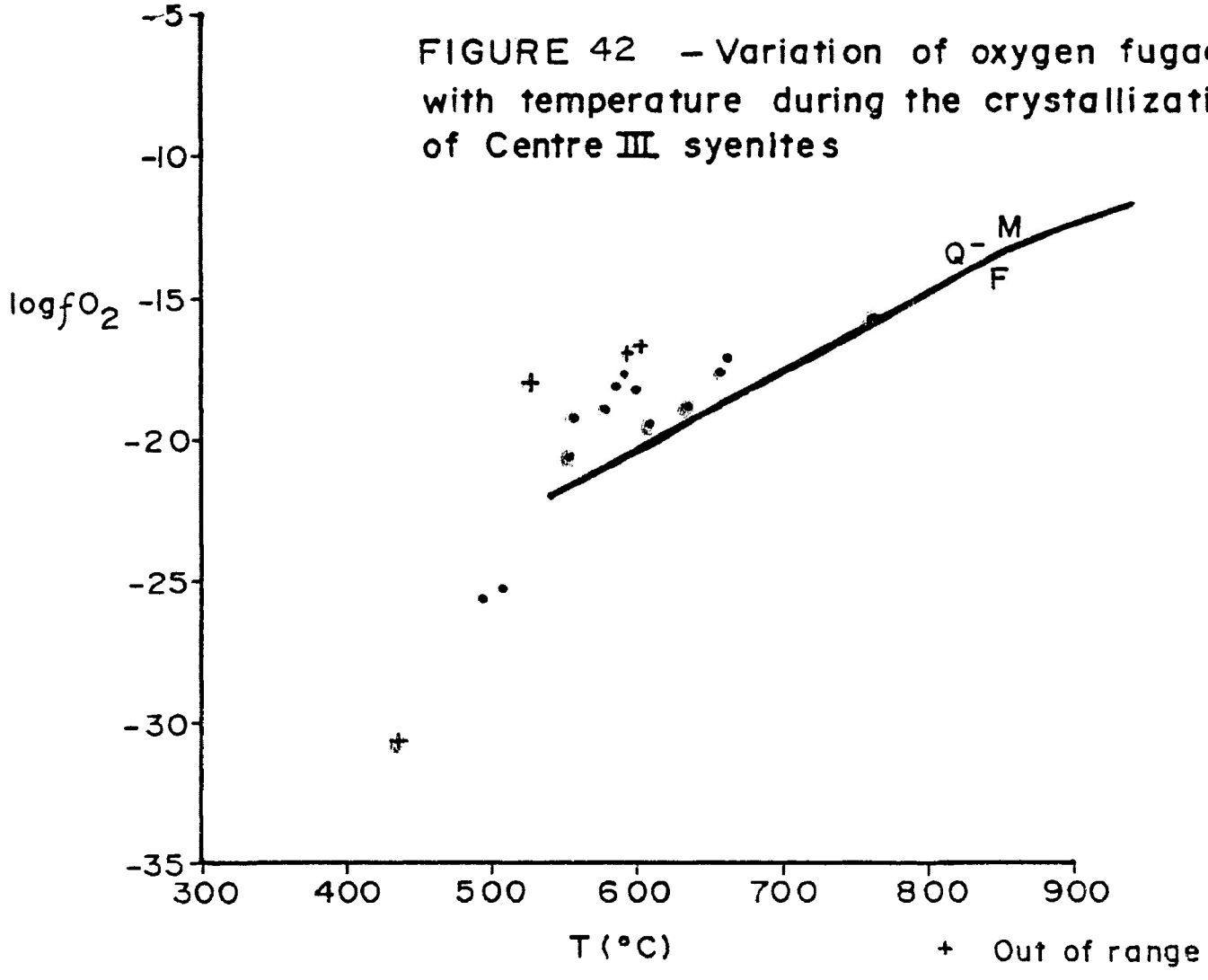

FIGURE 42 – Variation of oxygen fugacity with temperature during the crystallization of Centre III syenites

WHOLE ROCK CHEMISTRY

9.1 Introduction

Forty three whole rock samples have been analyzed for major and minor elements. The work was performed by the Centre in Mining and Mineral Exploration Research, at Laurentian University. The major oxide whole rock analyses were done by XRF methods on glass discs, as described by Norrish and Hutton (1969). The accuracy for major element analyses is approximately ±2%. The major oxides determined were: SiO_2, TiO_2, Al_2O_3, Fe_2O_3, MnO, CaO, MgO, Na_2O, K_2O and P_2O_5. The trace elements were determined using pressed whole rock powders, with an accuracy of better than ±10%. The trace elements measured are: Cr, Co, Ni, Cu, Zn, Pb, Zr, Y, Sr, Rb, Ba, Ce and La.

At Lakehead University the C, H and N contents were determined using a Control Equipment 240XA Elemental Analyzer. All samples were at, or below, the detection limits for these samples. The FeO content of these samples was also measured, at Lakehead University, by a titration method (accuracy approximately ±0.05). This FeO value was converted to Fe_2O_3 and this amount was subtracted from the original Fe_2O_3 analyses.

A computer program "ROCALC" written by Stormer (1985) was used to calculate: the norms (using the procedure of Barker, 1983); differentiation index; various normative ratios; and the parameters F', Q' and An, used in the Streckeisen and Lemaitre (1979) rock classification plot.

Tables 31 to 37 list compositions for the four syenite types together with metasedimentary and volcanic xenoliths, as well as normative indices used in constructing the diagrams. Two diagrams will be referred to, the Streckeisen and Lemaitre (1979) rock classification diagram (Figure 43),

TABLE 31

Whole rock analyses - Magnesio-hornblende syenite

	C2120	C2123	C178	C2150	C180
SiO2	52.1	53.2	55.6	56.1	60.5
TiO2	0.578	0.588	0.658	0.496	0.742
Al2O3	15.2	15.6	15.6	15.4	16.3
Fe2O3	2.27	3.61	4.48	2.53	6.28
FeO	5.96	5.04	4.44	4.52	1.80
MnO	0.158	0.218	0.169	0.155	0.165
MgO	6.50	5.45	4.02	4.66	1.27
CaO	9.12	6.98	5.66	5.82	3.07
Na2O	3.80	3.71	4.18	3.92	5.08
K2O	1.91	2.93	3.51	3.31	3.83
P2O5	0.338	0.298	0.326	0.147	0.258
CO2	0.48	0.15	0.77	0.26	0.29
H2O	1.07	2.68	2.32	1.96	1.61
NO2	-	-	-	0.13	0.13
Total	99.5	100.5	101.7	99.5	101.4
Cr	14.2	11.8	5.83	8.15	-
Co	39.9	51.0	53.0	36.2	31.8
Ni	79.5	53.6	31.9	52.6	7.94
Cu	99.2	81.8	15.0	56.3	22.6
Zn	81.8	105	114	89.3	109
Pb	13.0	12.8	13.7	11.6	19.8
Zr	259	335	506	369	306
Y	41.5	45.2	59.2	51.3	40.3
Sr	589	570	553	510	527
Rb	81.5	150	173	155	138
Ba	519	998	575	796	1377
Ce	170	200	277	216	240
La	93.2	115	157	127	138
Q'	-	-	3.80	3.25	11.3
F'	-	-	-	-	-
Anor	62.3	49.9	39.3	42.9	31.4
Q	-	-	4.67	4.12	12.9
Ab	74.0	64.5	60.1	60.3	57.1
Or	26.0	35.5	35.2	35.6	30.0

TABLE 32

Whole rock analyses - Perro-edenite syenite

	C182	C2158	C2225	C2025	C2221	C2236
SiO2	64.5	64.5	64.9	64.9	65.0	65.0
TiO2	0.321	0.35	0.45	0.294	0.256	0.394
Al2O3	15.6	16.4	15.4	16.1	16.8	16.2
Fe2O3	2.02	3.69	3.93	2.88	2.23	2.28
FeO	2.96	0.88	0.28	1.12	1.24	0.64
MnO	0.132	0.085	0.129	0.079	0.116	0.104
MgO	0.553	0.548	0.129	0.211	0.201	0.404
CaO	1.87	0.85	1.89	1.16	1.01	1.43
Na2O	5.22	5.36	5.24	5.77	5.46	5.31
K2O	5.18	6.27	5.47	5.29	5.67	5.81
P2O5	0.029	0.005	0.005	0.005	0.025	0.006
CO2	0.44	0.07	0.66	-	0.33	0.48
H2O	2.14	1.79	1.43	0.89	0.89	1.25
NO2	0.16	-	0.80	-	-	-
Total	101.0	100.8	100.7	98.7	99.2	98.7
Cr	4.84	1.61	6.23	10.7	6.44	10.1
Co	26.0	44.3	31.1	40.9	38.0	41.9
Ni	15.7	8.72	8.17	13.5	8.30	7.99
Cu	7.79	21.1	3.41	0.38	7.50	0.49
Zn	111	84.9	55.9	113	67.5	65.4
Pb	22.2	16.5	13.1	24.8	14.1	16.8
Zr	1074	480	319	1096	307	530
Y	83.0	45.5	40.0	79.9	27.1	38.6
Sr	81.5	29.3	29.2	53.8	50.1	170
Rb	189	183	161	362	166	194
Ba	213	156	233	220	211	1238
Ce	766	504	257	614	196	340
La	457	285	143	362	107	202
Q'	11.0	7.96	12.9	9.83	10.7	10.5
F'	-	-	-	-	-	-
Anor	10.8	5.25	6.68	7.51	7.60	8.73
Q	11.5	8.14	13.3	10.1	11.1	10.9
Ab	52.3	50.6	50.2	54.8	51.6	50.5
Or	36.3	41.3	36.6	35.1	37.4	38.6

TABLE 33

Whole rock analyses - Perro-edenite syenite

	C2133	C2040	C2222	C2135	C2129
SiO2	65.2	66.2	72.7	75.0	76.1
TiO2	0.376	0.322	0.134	0.072	0.128
Al2O3	15.4	15.7	13.2	12.4	10.7
Fe2O3	0.987	-	1.40	1.85	2.91
FeO	3.32	4.48	0.96	0.32	0.28
MnO	0.121	0.103	0.071	0.026	0.026
MgO	0.588	0.251	0.001	0.285	0.410
CaO	1.58	1.12	1.17	0.435	0.647
Na2O	4.37	4.86	4.62	3.71	3.18
K2O	6.26	5.67	4.22	5.15	4.47
P2O5	0.082	0.038	-	0.042	0.001
CO2	0.29	0.15	0.11	0.37	0.04
H2O	0.89	0.71	2.68	0.89	0.18
NO2	0.16	0.07	-	-	-
Total	99.6	99.7	101.2	100.6	99.2
Cr	7.05	17.8	13.1	16.0	27.4
Co	37.4	26.6	58.0	37.7	29.4
Ni	13.3	10.9	10.9	13.8	15.4
Cu	0.25	0.10	0.53	6.33	0.60
Zn	152	71.3	74.6	19.9	26.2
Pb	62.4	21.3	14.3	20.1	21.2
Zr	1151	772	667	306	1717
Y	66.0	56.9	59.9	104	166
Sr	86.5	62.8	29.1	48.7	36.0
Rb	235	303	188	203	228
Ba	376	344	138	221	124
Ce	507	333	295	180	177
La	299	194	166	97.2	95.4
Q'	12.1	11.7	29.3	35.3	41.3
F'	-	-	-	-	-
Anor	9.69	11.5	10.2	-	6.51
Q	12.7	12.3	30.2	35.2	42.2
Ab	43.6	48.3	42.6	32.9	29.2
Or	43.7	39.4	27.2	32.0	28.7

TABLE 34

Whole rock analyses - Perro-edenite syenite

	C2059	C2077	C2053	C2101	C2223	C2004
SiO2	54.7	56.7	61.7	63.4	63.9	64.1
TiO2	0.608	0.553	0.414	0.364	0.411	0.408
Al2O3	15.5	15.9	16.9	16.2	15.8	16.7
Fe2O3	2.58	3.74	2.31	2.71	1.13	1.88
FeO	5.36	3.84	2.84	2.28	1.76	2.36
MnO	0.157	0.171	0.162	0.127	0.129	0.145
MgO	4.17	3.33	0.478	0.242	0.483	0.288
CaO	7.02	5.84	1.62	1.38	2.09	1.207
Na2O	4.35	5.28	5.14	5.21	5.36	5.12
K2O	2.79	2.72	6.04	5.80	5.78	5.95
P2O5	0.366	0.348	0.099	0.058	0.008	0.059
CO2	0.18	0.15	0.29	0.66	1.47	0.22
H2O	1.79	1.43	1.07	1.25	1.07	1.61
NO2	-	0.26	0.10	-	-	0.07
Total	99.6	100.3	99.2	99.6	99.4	100.1
Cr	5.07	4.70	0.15	1.79	7.76	0.17
Co	37.1	48.8	25.2	20.8	35.9	16.9
Ni	43.2	37.1	10.5	11.0	8.59	9.81
Cu	49.7	41.3	20.12	3.72	0.04	-
Zn	134	133	90.5	80.7	52.3	84.0
Pb	20.9	17.2	21.1	16.5	12.7	22.5
Zr	358	483	481	977	776	945
Y	47.0	60.7	46.8	74.1	73.6	49.5
Sr	594	552	142	35.2	20.2	41.7
Rb	118	87.1	155	171	192	264
Ba	595	481	923	204	89.8	224
Ce	224	340	231	703	454	469
La	128	196	134	414	255	273
Q'	-	1.45	4.80	9.82	9.68	9.00
F'	-	-	-	-	-	-
Anor	46.6	41.9	12.8	6.22	2.84	10.7
Q	-	1.73	5.10	10.1	9.79	9.43
Ab	69.1	72.3	52.1	50.6	51.5	50.0
Or	31.0	26.0	42.8	39.4	38.8	40.6

TABLE 35

Whole rock analyses - Contaminated ferro-edenite syenite

	C2028	C2042	C2026	C2000	C2038	C2063
SiO2	66.4	65.8	61.0	60.9	58.7	59.3
TiO2	0.238	0.307	0.843	0.436	0.788	0.582
Al2O3	15.8	15.6	17.7	15.7	17.1	15.0
Fe2O3	2.50	2.71	2.70	2.77	2.29	1.99
FeO	0.96	1.08	1.72	2.92	4.04	5.28
MnO	0.087	0.103	0.136	0.14	0.184	0.156
MgO	0.211	0.414	1.28	1.805	1.195	2.478
CaO	1.23	1.63	3.02	3.63	3.00	4.35
Na2O	5.62	4.68	6.08	5.29	5.12	5.32
K2O	4.93	5.83	3.94	4.41	4.84	3.20
P2O5	0.002	0.004	0.268	0.188	0.302	0.306
CO2	0.29	0.11	0.04	0.29	0.33	0.37
H2O	0.71	0.89	1.96	1.25	1.07	1.25
NO2	-	-	-	0.03	0.03	0.03
Total	99.0	98.9	100.7	99.8	99.0	99.6
Cr	9.12	6.10	10.0	19.4	-	-
Co	48.4	48.2	29.4	29.7	21.3	38.2
Ni	12.6	9.05	15.9	21.6	10.1	24.8
Cu	0.29	0.26	0.06	2.78	9.85	27.9
Zn	61.1	75.2	82.0	120	134	137
Pb	32.0	30.5	23.5	18.0	22.1	25.4
Zr	1127	1085	608	694	547	590
Y	103	88.7	55.3	91.3	52.9	65.6
Sr	84.5	88.7	512	309	479	372
Rb	312	219	165	142	177	122
Ba	206	255	1462	395	1527	453
Ce	575	757	363	399	372	318
La	337	444	219	226	215	179
Q'	13.9	14.3	4.39	5.87	2.60	4.97
F'	-	-	-	-	-	-
Anor	10.2	11.3	28.7	19.3	24.8	28.4
Q	14.4	15.0	4.91	6.35	2.92	5.52
Ab	53.1	45.4	65.4	59.2	58.5	66.5
Or	32.5	39.6	29.7	34.4	38.6	28.0

TABLE 36

Whole rock analyses - Quartz syenite

	C2138	C2153	C2091	C2044	C2071	C2060	C2072
SiO2	64.3	63.0	60.9	59.1	59.9	57.7	52.3
TiO2	0.378	0.441	0.604	0.582	0.501	0.729	1.09
Al2O3	16.5	16.0	16.4	18.0	15.8	14.4	11.9
Fe2O3	2.18	2.56	3.13	4.04	5.04	7.17	12.3
FeO	1.72	3.16	3.4	1.72	4.08	4.24	7.28
MnO	0.098	0.173	0.194	0.147	0.274	0.326	0.591
MgO	0.571	0.357	0.812	0.707	0.608	0.778	1.19
CaO	1.00	1.59	1.86	2.29	2.14	4.03	4.24
Na2O	5.20	5.40	5.29	5.08	4.79	4.74	3.97
K2O	5.96	5.86	5.6	6.40	5.51	5.18	4.23
P2O5	0.007	0.016	0.158	0.09	0.208	0.1	0.232
CO2	0.15	0.29	0.15	0.26	0.73	0.26	0.29
H2O	1.25	0.89	1.07	1.43	1.96	1.07	1.25
NO2	0.23	0.26	0.23	-	0.33	-	-
Total	99.5	99.9	99.8	99.8	101.6	100.6	100.9
Cr	2.65	0.01	0.01	5.19	-	1.44	0.15
Co	17.1	22.7	26.1	22.7	43.6	26.4	36.9
Ni	9.00	8.05	7.79	9.83	7.94	7.93	5.02
Cu	7.99	15.9	22.4	9.86	33.4	21.3	38.7
Zn	41.1	105	118	80.5	129	147	302
Pb	11.8	11.1	11.3	23.2	18.7	17.7	23.4
Zr	495	307	215	287	216	189	248
Y	45.4	33.8	31.4	34.9	35.9	34.8	61.0
Sr	33.5	33.7	64.1	311	148	72.8	124
Rb	148	150	149	162	168	131	116
Ba	227	158	346	1616	998	253	783
Ce	586	183	187	199	223	177	302
La	338	98.1	100	121	133	95.4	164
Q'	9.00	6.14	4.20	0.47	7.88	5.36	8.70
F'	-	-	-	-	-	-	-
Anor	10.1	5.61	12.0	16.4	12.4	7.82	8.28
Q	9.41	6.28	4.43	0.51	8.33	5.56	9.00
Ab	50.4	53.3	54.9	52.9	50.8	53.6	52.2
Or	40.2	40.4	40.6	46.6	40.8	40.9	38.8

TABLE 37

Whole rock analyses - Xenoliths

	C366B vol	C2050 vol	C2128 vol	C2043 sed	C2027 sed	C2052 sed	C2056 sed
SiO2	52.4	49.3	49.8	59.1	61.1	49.4	53.8
TiO2	0.672	1.02	0.629	0.856	0.662	1.87	1.45
Al2O3	16.6	16.6	16.0	16.3	15.9	17.3	14.8
Fe2O3	1.47	5.47	5.27	1.59	1.85	7.22	3.59
FeO	6.8	6.28	4.4	6.72	4.56	3.28	6.92
MnO	0.163	0.236	0.173	0.127	0.156	0.216	0.191
MgO	4.51	4.59	5.87	5.02	3.68	3.46	3.48
CaO	8.28	8.95	10.2	3.60	2.37	5.17	6.23
Na2O	4.41	4.33	3.62	3.82	5.77	5.26	4.48
K2O	2.03	1.74	1.56	1.92	1.98	3.04	2.71
P2O5	0.433	0.902	0.402	0.151	0.121	1.25	0.477
CO2	0.33	0.29	0.11	0.11	-	0.15	0.04
H2O	2.32	2.32	2.14	1.61	1.43	3.04	1.96
NO2	-	-	-	0.26	-	-	-
Total	100.4	100.0	100.2	101.2	99.6	100.6	100.1
Cr	16.7	0.07	25.9	339	187	0.03	15.0
Co	49.3	64.6	40.3	52.4	45.0	37.2	48.1
Ni	50.9	37.3	65.8	124	80.8	9.83	17.2
Cu	69.7	140	63.4	98.6	20.5	17.5	32.1
Zn	122	208	91.2	102	120	144	132
Pb	18.6	23.9	15.8	16.0	13.9	18.9	17.9
Zr	176	250	190	117	152	364	312
Y	34.7	43.9	32.8	22.8	16.4	47.5	46.2
Sr	824	1020	745	460	547	1522	555
Rb	223	131	61.1	86.9	167	97.1	109
Ba	680	873	652	648	521	1952	1071
Ce	186	251	156	64.3	92.0	332	242
La	108	133	87	25.9	48.7	191	134
Q'	-	-	-	14.93	8.91	-	0.02
F'	0.97	6.28	-	-	-	3.70	-
Anor	61.8	66.8	71.2	58.7	48.3	45.0	43.4
Q	-	-	-	19.4	10.4	-	0.03
Ab	75.1	73.9	76.9	59.7	72.3	68.7	70.3
Or	24.9	26.1	23.1	21.0	17.4	31.3	29.7

NORMATIVE An vs. Q':F'

Figure 43

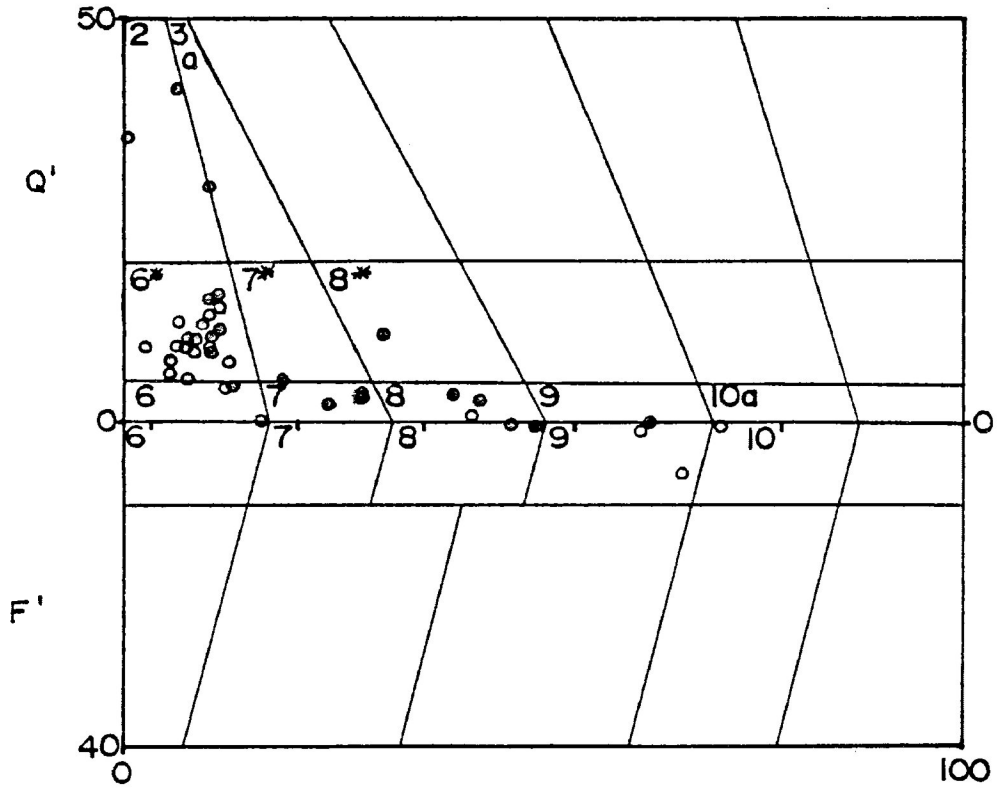

2 alkali feldspar granite
3a granite
6 alkali feldspar syenite
6* alkali feldspar quartz syenite
6' foid-bearing alkali feldspar syenite
7 syenite
7* quartz syenite
8 monzonite
8* quartz monzonite
8' foid-bearing monzonite
9 monzodiorite/monzogabbro
9' foid-bearing monzodiorite/monzogabbro
10 diorite/gabbro/anorthosite
10' foid-bearing diorite/gabbro/anorthosite

and the ternary Q:Ab:Or system (Figure 44).

9.2 Magnesio-hornblende syenite

Five samples of magnesio-hornblende syenite have been analyzed: C178, C180, C2120, C2123 and C2150 (Table 31). Three specimens are quartz-normative (C178, C180 and C2150), with silica ranging from 55.6 to 60.5% SiO_2. The other two samples contain 52.1 and 53.2% SiO_2. The differentiation index increases from 43.4 to 75.3 as silica increases. This value is under 60 for four of the specimens analyzed. Alumina ranges from 15.2 to 16.3% Al_2O_3, increasing along with silica in the five specimens. While the total iron content remains approximately constant, the FeO content decreases (5.96 to 1.80% FeO) and Fe_2O_3 increases (2.3 to 6.3% Fe_2O_3) as silica content increases. The sodium content is elevated in the most siliceous sample, varying in these magnesio-hornblende syenites from 3.7 to 5.1% Na_2O. The potassium levels increase progressively with increasing silica, from 1.9 to 3.8% K_2O. Both CaO and MgO have an inverse relationship with silica, decreasing from 9.1 to 3.1% CaO and 6.5 to 1.3% MgO. Titania appears to increase with increasing silica, varying from 0.50 to 0.74% TiO_2. The remainder of oxides occur at very low levels with no apparent trends evident: average MnO=0.18%; average P_2O_5=0.28%; average H_2O=1.93% and average CO_2=0.39%. Two samples had detectable NO_2 at about 0.13%.

With regards to the trace elements, with proceeding magma evolution, i.e. increasing silica content, the levels of these elements rise: Pb, Zn, Rb, Ba, Ce and La. Significant decreases are noted with: Cr, Ni, Cu and Sr.

In Figure 43, the Streckeisen and Lemaitre (1979) rock classification plot, the two most primitive syenites plot on the Q'/F'=0 line, in the

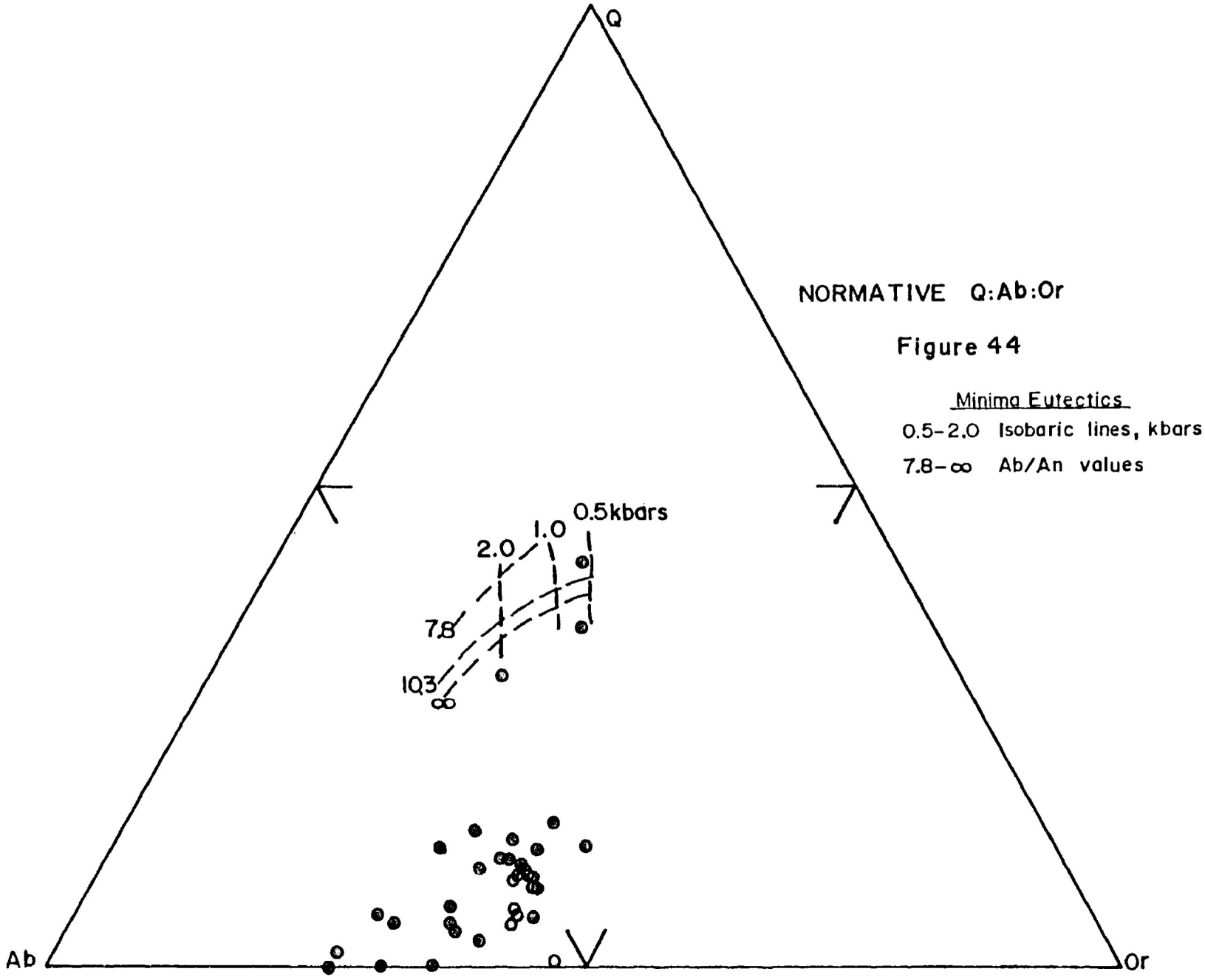

NORMATIVE Q:Ab:Or

Figure 44

Minima Eutectics

0.5-2.0 Isobaric lines, kbars

7.8-∞ Ab/An values

range of monzodiorite/monzogabbro and monzonite. The three others are quartz normative and plot as monzonites (2) and quartz monzonite (1).

9.3 Ferro-edenite syenite

Seventeen specimens of ferro-edenite syenite were analyzed and representative data are presented in Tables 32-34. Sixteen specimens are quartz-normative, while one is neither quartz- nor nepheline-normative. Silica content ranges overall from 54.7 to 76.1% SiO_2, with concentrations of compositions at three levels: 55%, 64% and 74% SiO_2. The differentiation index increases from 53.4 to 95.3 in ferro-edenite syenites, with all but two specimens with differentiation index over 83.

As the silica content increases, alumina decreases from highs of 16.9% to 10.7% Al_2O_3. While the total iron content and FeO decreases (5.4 to 0.3% FeO), the amount of Fe_2O_3 shows no trend, varying between nil and 3.9% Fe_2O_3. The soda and potash decrease slightly as silica content rises, with the ranges being: 5.8 to 3.2% Na_2O and 6.3 to 2.7% K_2O. The MgO and CaO concentrations highlight the anomalous chemistry of samples C2059 and C2077. As well as having the lowest silica content for ferro-edenite syenites, they also have unusually high MgO and CaO, and low K_2O. Disregarding these two specimens, there are no discernable trends for the MgO and CaO contents of the rest of these syenites. Very slight decreasing trends are noted for the TiO_2, MnO and P_2O_5 values, all of which are present at levels of less than one percent. No trends are evident for the low volatile contents in these syenites. Of note is one analysis of 1.47% CO_2 from the Guse Point syenite C2223.

In the ferro-edenite syenites the trends in trace element abundances are not well defined. With increasing relative silica content, slight increases are noted in the levels of Cr, Zr, Y and Rb. Five elements are

observed to decrease: Ni, Cu, Zn, Sr and Ba. Elements that remain approximately constant are Co, Pb, Ce and La. Of particular note are: the relatively high zirconium contents, varying between 307 ppm and 1717 ppm Zr; and high Ce and La, up to 766 ppm Ce and 457 ppm La.

Two specimens of ferro-edenite syenite, C2059 and C2077 plot in the monzonite field of Figure 43, the rock classification diagram. The former is neither quartz- nor nepheline-normative, and the latter is slightly quartz-normative. The majority of ferro-edenites plot in a tight cluster in the field of alkali feldspar quartz syenite. One sample borders the alkali feldspar syenite region. Three samples are distinctly more silica-saturated, plotting in the field of alkali feldspar granite (C2129, C2135 and C2222). These three separate clusters of ferro-edenite syenites form part of an accurate trend in Figure 43.

9.4 Contaminated ferro-edenite syenite

Six specimens of contaminated ferro-edenite syenite were analyzed and the results are presented in Table 35. All samples are quartz-normative, plotting in the fields of syenite, quartz syenite and alkali feldspar quartz syenite (Figure 43). Silica contents range from 59.3 to 66.4% SiO_2. As the silica proportion increases, there are simultaneous increases in alumina (15 to 17.7% Al_2O_3), ferric iron (1.99 to 2.77% Fe_2O_3) and potash (3.2 to 5.8% K_2O). Oxides which show a relative drop in proportion are: TiO_2, FeO (5.28 to 1.0%), MnO, MgO (2.5 to 0.2% MgO), CaO (4.3 to 1.2%), P_2O_5 and H_2O. Sodium, carbon and nitrogen, remain at approximately constant levels throughout.

While some of the trends in major oxides are not well-developed, the majority of minor elements display steady, linear changes. Elements which increase with silica include: Cr, Co, Pb, Zr, Y, Rb, Ce and La. In

particular, Zr (1127 ppm), Y (103 ppm), Ce (575 ppm) and La (337 ppm) attain relatively high concentrations. Barium is also significant in a couple of samples (up to 1527 ppm), but shows more of a decreasing trend with silica enrichment. Other elements that behave inversely to silica are: Ni, Cu, Zn and Sr.

9.5 Quartz syenite

Seven representative samples of Centre III quartz syenite were analyzed for major and minor elements. The analyses are presented in Table 36. All specimens are quartz-normative and plot in a small region of Figure 43. They are alkali feldspar syenites and alkali feldspar quartz syenites. Silica ranges from about 52.3 to 64.3%. The other oxides which increase as magma differentiation proceeds are: Al_2O_3, Na_2O and K_2O. The alumina ranges from 11.9 to 18.0% Al_2O_3. The soda content rises from about 4.0 to 5.2% Na_2O, with a high of 5.4% Na_2O (C2153). The highest potash value is 6.4% K_2O in quartz syenite C2044, and the lowest analyzed concentration is 4.2% K_2O.

The total iron content fell dramatically as this quartz syenite evolved, from about 19.5% combined Fe_2O_3 and FeO in C2072, to 3.9% in C2138. Individually both ferrous and ferric iron concentrations also decrease with differentiation. Manganese, phosphorus and titanium occur in small amounts and show an inverse relationship to silica. Similarly the magnesia and lime show decreases from 1.2 to 0.6% MgO and 4.2 to 1.0% CaO. The volatiles CO_2, H_2O and NO_2 all occur in very small amounts, at approximately constant levels throughout this magma type.

Some of the trace elements that appear to rise in proportion with progressing differentiation are Rb and Zr, the latter attaining a high of about 495 ppm. Rubidium varies between 116 and 168 Rb. Lanthanum and

cerium are relatively abundant in the quartz syenites with up to 586 ppm Ce and 338 ppm La in the most evolved quartz syenite analyzed, C2138. Both chromium and yttrium do not show progressive trends, with nil to 5.2 ppm Cr and 31 to 61 ppm Y. The relative abundances of six elements decrease with differentiation: Co, Cu, Zn, Pb, Sr and Ba. Of note are some elevated barium concentrations of 783 to 1616 ppm Ba, and strontium at 311 ppm in C2044 and 302 ppm Zn in C2072.

9.6 Xenoliths

Seven whole rock analyses were made of xenoliths found in Centre III rocks. Four specimens are metasedimentary xenoliths: C2043, C2027, C2052 and C2056. Three are analyses of volcanic xenoliths: C366B, C2050 and C2128. These data are presented in Table 37. The analyses for volcanic xenoliths are also represented on the classification plot, Figure 43, falling in the range of silica-undersaturated basalt and andesite.

The chemical analyses for volcanic xenoliths show a small range in composition. Silica varies between 47.3 and 52.4% SiO_2. Alumina is found in concentrations of 16.0 to 16.6% Al_2O_3. Ferric iron ranges from 1.5 to 5.5% Fe_2O_3 whereas ferrous iron occurs at levels of 4.4 to 6.8% FeO. High levels of calcium are detected in these volcanic xenoliths, from 8.3 to 10.2% CaO. Magnesia is in the range 4.6 to 5.9% MgO. Low levels of manganese oxide (0.2% MnO) and titania (0.6 to 1.0 TiO_2) are found. Alkalis and phosphorous show a small range in concentration, with 3.6 to 4.4% Na_2O, 1.6 to 2.0% K_2O and 0.4 to 0.9% P_2O_5. While water content seems high (2.1 to 2.3% H_2O) relative to most of the syenites, there is no detectable nitrogen and only 0.1 to 0.35% CO_2.

No particularly significant trace element abundances are observed for the volcanic xenoliths. Zinc is present at the 100 to 200 ppm level.

Zirconium exhibits concentrations of 176 to 249 ppm Zr. Cerium ranges from 156 to 251 ppm Ce and lanthanum exhibits abundances of 87 to 133 ppm La.

In the sedimentary xenoliths the oxide and trace element abundances show a wider range than in the volcanic xenoliths. Silica ranges from 49.4 to 61.1% SiO_2 and alumina lies between 14.8 and 17.3% Al_2O_3 and 3.3 to 6.9% FeO. Titania ranges from 0.7 to 1.9% TiO_2. Magnesia varies between 3.5 and 5.0% MgO, while the lime content changes from 2.4 to 6.0% CaO. Soda ranges from 3.8 to 5.3% Na_2O and potash falls in the range 1.9 to 3.0% K_2O. The amount of water shows a wider range than in the volcanic xenoliths, varying between 1.43 and 3.04% H_2O.

The chromium ranges up to about 339 ppm Cr, in C2043. Zirconium varies between 117 and 364 ppm Zr and barium exhibits concentrations of 648 to 1952 ppm Ba.

9.7 Summary of whole rock chemistry of Centre III syenites

The Centre III syenites are all silica-saturated and -oversaturated. According to the Streckeisen-Lemaitre scheme (Figure 43) the rocks range from monzodiorites, through monzonites and syenites, to alkali feldspar granites. The alkalinity of these syenites can be measured from the molar ratio $(K_2O+Na_2O)/Al_2O_3$. Peralkaline rocks have total alkalis in greater quantity than alumina. All Centre III syenites are subalkaline, with no alumina deficiences. About half of the rocks analyzed in this study are metaluminous or peraluminous. Metaluminous rocks are defined as those with molecular proportions of CaO, Na_2O and K_2O less than Al_2O_3, but which have Al_2O_3 less than Na_2O plus K_2O.

The chemistry of the four Centre III syenite types is similar, with most of the oxide abundances overlapping. The differentiation index may

be used to help define the minor differences in chemistry. This index measures the weight percent of oxides versus the sum of salic normative constituents, namely Ne, Ab, Q, Lc, Ks and Or. Wide ranges in differentiation index are observed for the four Centre III syenite types. The magnesio-hornblende syenite has D.I. ranging from 43.4 to 75.3. A very wide range is observed for the ferro-edenite syenite from 53.4 to 95.3 D.I. The specimens at the upper end of this series are the most felsic, evolved syenites in Centre III. The contaminated ferro-edenite syenite exhibits a much more restricted range in differentiation index, from 67.7 to 89.6 D.I. The quartz syenites also have a similar range, from 64.4 to 87.5 D.I.

Within each of the four syenite series trends in oxide abundances are noted with respect to increasing silica content and differentiation index. The most interesting observation is that for the ferro-edenite syenite series, alumina decreases as silica content rises. In the three other syenite types the alumina increases along with silica. In the ferro-edenite syenite the Na_2O and Fe_2O_3 content remains constant with differentiation, whereas in the other three types Na_2O, Fe_2O_3 and K_2O contents generally increases. This tendency is an indication of alkaline conditions. As expected, in the four syenite series FeO, MgO and CaO contents always decreases with increasing differentiation. Except for the magnesio-hornblende syenite series (where these oxides remain constant), the TiO, MnO and P_2O_5 contents generally decrease.

The trace element abundances show more variety between the four syenite types. Rubidium increases with magma differentiation in all series, while copper and strontium always decrease with progressive

silica enrichment. Zinc, nickel and barium generally decrease, while simultaneously zirconium, yttrium; cerium and lanthanum increase. It is notable that all Centre III syenites have anomalous levels of zirconium, yttrium, cerium and lanthanum, relative to the volcanic and sedimentary xenoliths. These rare-earth elements may occur in the carbonates, sphene, apatite, fluorite, zircon and the rare parrisite, synchisite, bastnesite and other REE-carbonates present in these Centre III rocks.

The whole rock chemistry for Centre III syenites may be summarized with reference to the normative Q-Ab-Or ternary diagram (Figure 44). The dashed isobaric lines and Ab/An values found in this ternary diagram are after Winkler (1979), James and Hamilton (1969) and von Platten (1965) (Table 38). Not shown on this diagram is a thermal minimum situated between the fields of sodic and potassic alkali feldspar. It trends from approximately $Ab_{70}Or_{30}$ towards the ternary eutectic region. This minimum is not a true cotectic, since only one phase is crystallizing in that temperature range.

For many of the analyzed Centre III syenites this phase diagram well represents bulk compositions, because greater than 80% of the mode consists of quartz and alkali feldspars. All of the Centre III compositions are situated in a wide zone along the feldspar thermal minimum, and on the orthoclase side of this line. The monzonitic magnesio-hornblende syenites and the hybridized contaminated ferro-edenite syenites plot near the alkali feldspar minimum, at $Ab_{70}Or_{30}$. The most highly evolved ferro-edenite syenites plot near the thermal minimum in the region of the feldspar-silica field boundary. The quartz syenites lie between the magnesio-hornblende syenites and the majority of the ferro-edenite syenite compositions.

The position of the eutectic in this system depends upon pressure and

TABLE 38

Minima Eutectics

P_{H2O}(kb)	T(^{o}C)	Q	Ab	Or	Ab/An	Reference
0.5	770	39	30	31		Winkler,1979
1.0	720	37	34	29		"
1.0	730±5-10	38	31	28	10.3	James & Hamilton,69
2.0	670	35	40	25		Winkler,1979
2.0	675	40	38	22	7.8	von Platten,1965

the Ab/An ratios. As demonstrated by Manning (1981), the fluorine content may also vary the eutectic composition, for example, at 1 kb the fluorine-free system reached the solidus at 730°C at $Qz_{37}:Ab_{34}:Or_{29}$, whereas with 4% added fluorine, the eutectic point is shifted to $Qz_{15}Ab_{58}:Or_{27}$ and a temperature of 630°C. Although fluorine was not analyzed for in the Centre III syenites, its ubiquitous presence in the mode, as fluorite (CaF_2), suggests it may have had an important effect on the position of the eutectic. For Centre III syenites a P_{H_2O} of 0.5 to 1.0 kbars is realistic, because these are shallow-level bodies (Mitchell and Platt, 1982b). The Centre III feldspar compositions, as determined by microprobe, have little or no anorthite content, and thus the Ab/An ratio may be considered as infinite. The three ferro-edenite syenite compositions plotting in the eutectic region crystallized alkali feldspar and quartz, and represent the composition of the last remaining liquid. While all liquids evolve, through fractional crystallization, towards the minimum point, the composition of the final liquid still depends on the original magma composition (Ehlers, 1972). The few magmas that undergo prolonged fractional crystallization to yield finally some liquid of the minima composition are known as ideal granites (Hughes, 1982).

The compositions which plot away from the ternary minimum, but near the alkali feldspar minimum represent the majority of Centre III syenites. In some cases the original magma composition has a mafic mineral content too high to be represented adequately by a simple ternary system. Ehlers (1972) indicates that some felsic rock compositions plotting in this region may have crystallized under higher pressures, than those in the ternary minimum region. The majority of the felsic rocks in this region probably did not undergo extensive fractional crystallization, and cooling may have been slow enough to allow early-

formed crystals to re-equilibrate with the changing liquid compositions. Systems which evolve under non-equilibrium conditions have liquids that are more likely to attain eutectic compositions (Ernst, 1972). This suggests that equilibrium conditions may have predominated during the crystallization of some of these Centre III syenite compositions. The compositional variety of these syenites (which plot away from the eutectic region), may be in response to formation of diverse initial liquids, produced by partial fusion. Barker (1983) suggests that for quartz-normative rocks, partial fusion of continental crustal rocks may give rise to the parental liquids. Several of the Centre III syenites have nil to very low normative quartz levels, indicative of a source rock low in silica. Upper crustal rocks are generally high in silica, thus it is more likely that Centre III syenites originated from lower crustal sources.

A variety of factors, apart from original compositional differences, affected the history of each of the syenite types. Diverse pressure and temperature conditions may have had a significant impact, but the most obvious factor was the hybridization of the ferro-edenite syenites. Stoping of xenoliths, magma mixing, and the periodic, pulsating magmatism has all combined to create a diverse suite of syenites.

SYNTHESIS AND DISCUSSION

Field relationships, petrography and mineral chemistry were utilized in defining four main Centre III lithologies: magnesio-hornblende syenite; ferro-edenite syenite; contaminated ferro-edenite syenite and quartz syenite. Amphiboles were most useful in characterizing the lithological types, primarily because of their wide compositional variation. All but the contaminated ferro-edenite syenite represent distinct magma types. Compositional trends found in the whole rock major and minor element analyses serve to highlight the differences between the three main magma suites.

The earliest Centre III magmatism is represented by magnesio-hornblende syenite, which exhibits a major synneusis texture. Typical constituents include: patch antiperthite, albite, magnesio-hornblende, aluminous pyroxene, biotite, apatite, quartz, zircon, magnetite, ilmenite and fluorite.

Multiple intrusions of ferro-edenite syenite follow, constituting the predominant Centre III lithology. Generally this is a porphyritic rock with: braid antiperthite, calcic to alkali amphibole, annite, aluminous hedenbergitic pyroxene to acmitic hedenbergite, quartz, zircon, apatite, fluorite, magnetite and ilmenite.

During the waning stages of Coldwell magmatism quartz syenites were emplaced. These coarse-grained, massive rocks contain braid antiperthite and abundant quartz, with calcic to alkali amphibole, hedenbergite, annite, magnetite, ilmenite, fluorite, apatite, sphene and the highest proportions of incompatible element-bearing minerals, such as zircon, chevkinite, synchisite-bastnesite, parrisite, niobian rutile and aeschylite.

Alkaline basalts and Archean country rocks were brecciated by, and incorporated into, the ferro-edenite syenites. The repetitious nature of ferro-edenite syenite injection has resulted in brecciation of early syenites by later ones. Thus xenoliths of basalt and metasediments, as well as autoliths of ferro-edenite syenite, served to hybridize this magma suite. Various degrees of digestion and assimilation of all of these blocks has produced an almost infinite array of syenites. The result of extensive to complete assimilation of basaltic and sedimentary xenoliths is a distinctive contaminated ferro-edenite syenite: purple, porphyritic, with metasomatic biotite ovoids.

The Centre III syenites appear to be A-type felsic intrusions, as defined by Loiselle and Wones (1979), Wones (1979), Peck et al. (1980), Motzer (1981), Sillitoe (1981), Stern and Wyllie (1981), Collins et al. (1982), Pitcher (1982), Spulber and Rutherford (1983), O'Halloran (1985) and Whalen et al. (1987). A synthesis of these studies indicates that A-type granites are anorogenic melts produced from the fusion of lower crustal rocks. The resulting plutons typically form multiple-centred cauldron complexes and plutons of relatively small volume. These granites are emplaced at shallow levels (Whalen et al., 1987), typically less than 5 km from the surface. These A-type granites are centred over rifts, transcurrent faults or subduction zones (Whalen et al., 1987) and the doming and uplift of stable continental crust is observed (O'Halloran, 1985). Extensional stresses may result from the positioning of stable crust over a mantle plume or hot spot, creating a rifting basin. Lower crustal melting could have given rise to the typical A-type lithologic association: alkaline to peralkaline granite and syenite with associated carbonatites. All of these tectonic considerations are plausible in the Centre III Coldwell situation.

Mineralogical and textural characteristics of Centre III syenites also confirm their A-type affinity. The dominance of perthitic alkali feldspar, quartz and albite is documented (O'Halloran, 1985 and Whalen et al., 1987). The latter study also recognized that the mafic minerals characteristically crystallized late in the solidification history, forming interstitial grains or clots. These mafic minerals are typically: annite, brown to green and F-rich; alkalic types of amphiboles; and sodic pyroxenes. Minor and accessory minerals common to A-type granites and the Centre III syenites include: magnetite, sphene, ilmenite, zircon, fluorite and rare olivine.

The similarity between Centre III syenites and A-type granites may be extended to whole rock chemistry, note: high SiO_2, Na_2O+K_2O, Fe/Mg, Zr, Y, Ce (Whalen et al., 1987), and high K_2O/Na_2O and Zr. Whalen et al., include high Nb, Ga and Ga/Al as characteristics of A-type granites. Low values for CaO, MgO, Al_2O_3, Cr, Ni and Sr are also observed in Centre III rocks, as in other A-type suites. While most A-type granites are peralkaline, alkaline, peraluminous or metaluminous (O'Halloran, 1985), subalkaline examples have been recognized (Whalen et al., 1987).

The magmatic centres for Coldwell intrusive activity have migrated from Centre I in the east, to Centre III in the west. A common feature of alkaline magmatism is the long-lived nature of the igneous activity. Centre I border gabbro and ferro-augite syenite have differentiated in situ, resulting in the layered ferro-augite cumulate sequences. The Centre II biotite gabbro and nepheline syenite may have been produced by fractional crystallization of an alkali basalt parent (Platt and Mitchell, 1982). Volumetrically, Centre III rocks may be very significant, under Lake Superior, and in the northwest portion of the complex. Mineralogically and chemically Centre III ferro-edenite syenites

are most similar to the most evolved ferro-augite syenites.

The majority of Centre III syenites crystallized under relatively dry, hypersolvus conditions, evident in the late crystallization of hydrous phases, which are found in very small proportions. Some Centre III rocks though, underwent textural and mineralogical changes, to appear as subsolvus types. These rocks are situated at the periphery of exposed Centre III intrusions, particularly in the Guse Point-Pic Island area. In response to deformation of the cooling intrusions (along zones of weakness or due to contraction of a cooling body), hydrothermal fluids have altered the syenites. Recrystallization and alteration textures occur along the frequent shear zones of Pic Island exposures.

Each centre of Coldwell magmatism may represent a major cauldron subsidence event (Mitchell and Platt, 1982a, Currie, 1980). The different levels of intrusion exposed by erosion, across the complex, attest to the presence of block-faulting. In many cauldron systems, subsidence and resurgence is a well-established phenomena. Repeated magmatism results in the earliest intrusions being thermally re-equilibrated during later events. Erosion of the Proterozoic Coldwell complex reveals only the inner core of the cauldron system, the intrusive rocks.

Most of the Centre III exposures are of high-level intrusions. Evidence for this conclusion exists in the form of: intrusions which are limited in size and commonly discordant; pegmatites and miarolitic cavities; abundance of xenoliths and breccia zones; and the evidence from mineral stabilty data, particularly the dominance of mesoperthitic alkali feldspar. The stoped and spalled xenoliths originated at the top and sides of the syenite magma chamber. While angular basalt xenoliths indicate consolidation of the mafic volcanic unit prior to brecciation, many blocks have rounded and convoluted shapes. This texture suggests

either, that the invaded volcanic cap rock was still plastic, or that assimilation processes worked unevenly on these blocks.

Many cauldron subsidences are associated with rift zones, where the accumulation of mafic melts in the upper mantle causes increases in the geothermal gradient. This in turn initiates partial fusion of the lower crust, which may form the source magmas. Block faults or transcurrent faults may then act as major conduits for rising magmas. This is a likely scenario for the Coldwell Complex, of the Lake Superior Basin.

The petrogenesis of Centre III syenites can be summarized in a general way. The presence of primary albite in the magnesio-hornblende syenite and relict albite cores in some ferro-edenite syenites suggest relatively high pressure origins for this magma. The experimental work of Steiner et al., (1975) shows that, for a liquid formed by partial fusion of crustal rocks, the first feldspars to crystallize are sodic, and successive crystals become more sodic, prior to changing rapidly to a potassic trend. This is true for a system at equilibrium at elevated pressure (at 4 kb), with low to moderate water content. Even with perfect fractional crystallization, early sodic feldspars are followed by more potassic crystals (Steiner et al., 1975). With progressing crystallization of the magnesio-hornblende and ferro-edenite syenites, the plagioclase was partly or completely resorbed and superceded by potassic alkali feldspar crystallization. The mantled feldspars may be the product of magma mixing, which could drastically alter the composition of the liquid, or cause heterogeneity and disequilibrium in the system.

Throughout the differentiation of the three Centre III magma types, the oxygen fugacity approximated that defined by the QFM buffer. The relatively low oxygen fugacity may have prevented the widespread

crystallization of acmite. As the iron-poor potassic alkali feldspar and calcic pyroxene fractionated, the residual liquid became progressively more iron-rich. The drop in oxygen fugacity with differentiation is evident from the increasing $Fe^{2+}/(Mg+Fe^{2+})$ trends for the mafic minerals.

Amphibole and biotite could only begin crystallizing once approximately 3% water was concentrated in the liquid (Burnham, 1979). Textural evidence from Centre III syenites indicates that this stage was reached after the bulk of alkali feldspar crystallization. This suggests that the magmas were generally anhydrous, attaining water saturation late in the magmatic process. While the hydrous mafic minerals were forming, the water content of the magma remained relatively constant. The crystallization of calcic amphiboles dominated the late stage of Centre III syenite differentiation. Their formation caused the silica saturation of residual liquids (Bonin and Giret, 1985). Exsolution of the alkali feldspar probably began once the hydrous minerals had crystallized, aided by the presence of excess water (Buddington, 1939). In the case of the ferro-edenite syenites, once the magma became saturated in the volatiles, decreases in total pressure caused the volatiles to separate as bubbles (Burnham, 1979) and form miarolitic cavities near the tops of intrusions.

Contamination of ferro-edenite syenites is a significant factor in creating a diversity of compositions. Due to the great chemical differences between syenite and basaltic or sedimentary xenoliths, the degree of hybridization can be great. The mafic volcanic xenoliths are not readily assimilated because the engulfing syenite is already saturated in those minerals composing the basalt. Through diffusion and metasomatism the minerals of the basalt approach the compositions found in the syenite, leading eventually to a common mineral suite. Biotite, the most common phase in the volcanic xenoliths, represents the end

product of the reaction series of mafic minerals. The biotite ovoids may have formed as replacements of pyroxene or amphibole phenocrysts.

A few recommendations are presented for further research on these Centre III syenites. A study of the complex feldspars would help to unravel the petrogenetic processes at work. Preliminary cathodo-luminescence studies (by Dr. Mitchell) indicate that some ferro-edenite syenites contain two compositionally different primary feldspars. X-ray structural studies of feldspars would also prove beneficial.

Many whole rock samples from Centre III syenites are currently being analyzed for REE content (Dr. Mitchell). Initial data indicate that the syenites have REE distribution patterns similar to other A-type granitoids with strongly developed negative europium anomalies. In particular gallium analyses would prove beneficial, to be used in the various Ga/Al plots of Whalen et al., 1987.

Many of the Centre III syenites contain abundant fluid inclusions and research would help to define physical and chemical parameters of emplacement. Oxygen and hydrogen isotope research would define the contribution of surface-derived groundwater that has reacted with the intrusive rocks.

References

Anderson,A.T.,1968,"Oxidation of the LaBlanche Lake titaniferous magnetite deposit,Quebec",Journal of Geology.76,528-547.

Aubut,A.J.,1977,The Geology of the Southwest Margin of Coldwell Complex.HBSc. thesis.Lakehead University, Thunder Bay.115p.

Baer,A.J.,Frarey,M.J. and Ayres,L.D.,1972,Field Excursion A35-C35 : The Geology of the Canadian Shield between Winnipeg and Montreal.International Geological Congress,Montreal.

Barker,D.S.,1983,Igneous Rocks.Prentice-Hall Inc.: Englewood Cliffs,New Jersey,417p.

Bell,K.,Blenkinsop,J. and Watkinson,D.H.,1979,"Rb/Sr geochronology of alkalic complexes,Ontario",Ontario Geological Survey,Miscellaneous Paper 87,69-78.

Bence,A.E. and Albee,A.L.,1968,"Empirical correction factors for the electron microanalysis of silicates and oxides",Journal of Geology, 76, 382-403.

Billings,M.D.,1974,"Survey of the Geology and Geomorphology of Neys Provincial Park and Adjacent Areas, District of Thunder Bay,Ontario",Neys Provincial Park,Environmental Planning Series,Earth Science Report 1974.Ministry of Natural Resources.

Blenkinsop,J. and Bell,K.,1980,"Ages and initial $^{87}Sr-^{86}Sr$ ratios from alkalic complexes of Ontario", Ontario Geological Survey,Miscellaneous Paper 93. 16-23.

Bonin,B. and Giret,A.,1985,"Contrasting roles of rock-forming minerals in alkaline ring complexes", Journal of African Earth Sciences.3,no.1/2,41-49.

Buddington,A.F.,1939,"Adirondack igneous rocks and their metamorphism",Geological Society of America, Memoir 7.354p.

Burnham,C.W.,1979,"Magmas and Hydrothermal Fluids",in, Geochemistry of Hydrothermal Ore Deposits,Second Edition.(ed.by H.L.Barnes),John Wiley and Sons:New York,71-136.

Card,K.D.,Church,W.R.,Franklin,J.M.,Frarey,M.J.,Robertson,J.A.,West,G.F. and Young,G.M.,1972,"The Southern Province", in,Variations in Tectonic Styles in Canada.(ed. by R.A.Price and R.J.Douglas) Geological Association of Canada,Special Paper 11. 335-380.

Carmichael,I.S.E.,1967,"The mineralogy and Petrology of the volcanic rocks from the Leucite Hills,Wyoming", Contributions to Mineralogy and Petrology.15,24-66.

Cerny,P.,Smith,J.V.,Mason,R.A. and Delaney,J.S.,1984, "Geochemistry and petrology of Feldspar Crystallization in the Vezna Pegmatite,Czechoslovakia",Canadian Mineralogist.22,631-651.

Chaudhuri,S.,Brookins,D.G. and Fenton,M.D.,1971,"Rubidium-strontium whole rock and mineral ages of the Coldwell,Ontario syenites",Geological Society of America,North-central Meeting,Lincoln,NE,Abstracts with Programs,255.

Collins,W.J.,Beams,S.D.,White,A.J.R. and Chappell,B.W., 1982,"Nature and origin of A-type granites with particular reference to southeastern Australia",Contributions to Mineralogy and Petrology.80,189-200.

Currie,K.L.,1976,The Alkaline Rocks of Canada.Geological Survey of Canada,Bulletin 239.228p.

Currie,K.L.,1980,"A contribution to the Petrology of the Coldwell Alkaline Complex,Northern Ontario",Geological Survey of Canada,Bulletin 287,43p.

Deer,W.A.,Howie,R.A. and Zussman,J.,1978,An Introduction to the Rock Forming Minerals.Longman Group Ltd.:London,528p.

Didier,J.,1973,Granites and their Enclaves.Elsevier: Amsterdam,393p.

Ehlers.E.G.,1972,The Interpretation of Geological Phase Diagrams.W.H.Freeman and Company:San Francisco,280p.

Ernst,W.G.,1962,"Synthesis,stability relations,and occurrence of riebeckite and riebeckite-arfvedsonite solid solutions",Journal of Geology.70,689-736.

Ernst,W.G.,1976,Petrologic Phase Equilibria.W.H.Freeman and Company:San Francisco,333p.

Giret,A.,Bonin,B. and Leger,J.-M.,1980,"Amphibole compositional trends in oversaturated and undersaturated alkaline plutonic ring-complexes", Canadian Mineralogist.18,481-495.

Heaman,L.M. and Machado,N.,1987,"Isotope geochemistry of the Coldwell Alkaline Complex,I - U-Pb studies on accessory minerals",Geological Assoc. of Canada and Mineralogical Assoc. of Canada Joint Annual Meeting,Program with Abstracts,vol.12.

Hoshino,M.,1986,"Amphiboles and coexisting ferromagnesian silicates in granitic rocks in Mahe,Seychelles",Lithos.19,11-25.

Hughes,C.J.,1982,Igneous Petrology.Elsevier Scientific Publishing Co.:Amsterdam,551p.

Jago,B.C.,1980,The Geology of a Portion of the Western Contact Margin : The Coldwell Complex.HBSc thesis,Lakehead University.93p.

James.R.S. and Hamilton,D.L.,1969,"Phase relations in the system $NaAlSi_3O_8$-$KAlSi_3O_8$-$CaAl_2Si_2O_8$-SiO_2 at 1 kilobar water vapour pressure",Contributions to Mineralogy and Petrology.21,111-161.

Kerr,H.L.,1910,"Nepheline syenites of Port Coldwell", Ontario Bureau of Mines.19,part 1,194-232,map 196.

Klasner,J.S.,Cannon,W.F. and van Schmus,W.R.,1982,"The pre-Keweenawan tectonic history of southern Canadian Shield and its influence on formation of the Midcontinent Rift",Geological Society of America, Memoir 156,Geology and Tectonics of the Lake Superior Basin. 27-46.

Laderoute,D.,1985,personal communication while on field trip through Coldwell Complex in October 1985.

Leake,B.E.,1978,"Nomenclature of amphiboles",American Mineralogist.63,1023-1052.

Lindsley,D.H.,Speidel,D.H. and Nafziger,R.H.,1968,"P-T-f_{O2} relations for the system Fe-O-SiO_2",American Journal of Science.226,342-360.

Lindsley,D.H. and Spencer,K.J.,1982,"Fe-Ti oxide geothermometry : reducing analyses of coexisting Ti-magnetite(Mt) and ilmenite(Ilm)",Transactions of the American Geophysical Union.63,471.

Loiselle,M.C. and Wones,D.R.,1979,"Characteristics and origins of anorogenic granites",Geological Society of America,Abstracts with programs.11,no.7,468.

Manning,D.A.C.,1981,"The effect of fluorine on liquidus phase relationships in the system Qz-Ab-Or with excess water at 1 kb",Contributions to Mineralogy and Petrology.76,206-215.

McGill,M.R.,1980,The Coldwell Complex Western Margin - Petrology and Intrusive Relationships.HBSc.thesis,Lakehead University.98p.

Mitchell,R.H. and Platt,R.G.,1978,"Mafic mineralogy of ferroaugite syenite from the Coldwell Alkaline Complex, Ontario,Canada",Journal of Petrology.19,part 4,627-651.

Mitchell,R.H. and Platt,R.G.,1982a,"Field guide to aspects of the geology of the Coldwell Alkaline Complex",Geological Assoc. of Canada and Mineralogical Assoc. of Canada,Joint Annual Meeting.34p.

Mitchell,R.H. and Platt,R.G.,1982b,"Mineralogy and petrology of nepheline syenites from the Coldwell Alkaline Complex,Ontario,Canada",Journal of Petrology.186-214.

Mitchell,R.H.,Platt,R.G. and Cheadle,S.P.,1983,"A gravity study of the Coldwell Complex,northwestern Ontario and its petrological significance",Canadian Journal of Earth Sciences,20,1631-1638.

Morse,S.A.,1980,Basalts and Phase Diagrams.Springer-Verlag : New York,493p.

Motzer,W.E.,1981,"Tertiary epizonal plutonic rocks of the Selway-Bitterroot Wilderness,Idaho",Geological Society of America,Abstracts with programs.13,no. 4,220.

Neumann,E.R.,1976,"Two refinements for the calculation of structural formulae for pyroxenes and amphiboles",Norsk Geologisk Tidsskrift.56,1-6

Norrish,K. and Hutton,J.T.,1969,"An accurate X-ray spectrographic method for the analysis of a wide range of geological samples",Geochimica et Cosmochimica Acta.33,431-453.

O'Halloran,D.A.,1985,"Ras ed Dom migrating ring complex : A-type granites and syenites from the Bayuda Desert,Sudan",Journal of African Sciences.13,no.1/2, 61-75.

Peck,D.L. and Wones,D.R.,1980,"Penrose conference report,granite I : origin and evolution of granitic magmas",Geology.8,452-453.

Pitcher,W.S.,1982,"Granite type and tectonic environment",in,Mountain Building Processes.(ed. by K.Hsu),Academic Press,19-42.

Platt,R.G. and Mitchell,R.H.,1982,"Rb-Sr geochronology of the Coldwell Complex,northwestern Ontario,Canada", Canadian Journal of Earth Sciences.19,1796-1801.

Puskas,F.P.,1967,"The geology of the Port Coldwell area, district of Thunder Bay",Open File Report 5014.Ontario Department of Mines,114p.

Rock,N.M.S. and Leake,B.E.,1984,"The International Mineralogical Association amphibole nomenclature scheme : computerization and its consequences",Mineralogical Magazine.48,211-227.

Sage,R.D.,1978a,"Radioactive diatremes north of Lake Superior",Miscellaneous Paper 82.Ontario Department of Mines,no.9,53-66.

Sage,R.D.,1978b,"Diatremes and shock features in Precambrian rocks of the Slate Islands,northeastern Lake Superior",Geological Society of America.89,1529-1540.

Sillitoe,R.H.,1981,"Ore deposits in cordilleran and island arc settings",in,Relations of Tectonics to Ore Deposits in the Southern Cordillera.(ed. by W.R.Dickinson and W.D.Payne),Arizona Geological Digest.14,49-69.

Spencer,K.J. and Lindsley,D.H.,1981,"A solution model for coexisting iron-titanium oxides",American Mineralogist.66,1189-1201.

Spulber,S.D. and Rutherford,M.J.,1983,"The origin of rhyolite and plagiogranite in oceanic crust : an experimental study",Journal of Petrology.24,part 1,1-25.

Statham,P.J.,1976,"A comparative study of techniques for quantitative analysis of the X-ray spectra obtained with a Si(Li) detector",X-ray Spectrometry.5,16-28.

Steiner,J.C.,Jahns,R.H. and Luth,W.C.,1975,"Crystallization of alkali feldspar and quartz in the haplogranite system $NaAlSi_3O_8$-$KAlSi_3O_8$-SiO_2-H_2O at 4 kb",Geological Society of America,Bulletin 86.83-98.

Stern,C.R. and Wyllie.P.J.,1981,"Phase relationships of I-type granite with H_2O to 35 kilobars : the Dinkey Lakes Biotite-Granite from the Sierra Nevada batholith",Journal of Geophysical Research.86,no.B11,10412-10422.

Stormer,J.C.,1982,"The recalculation of multicomponent Fe-Ti oxide analyses for geothermometry : a quasi-thermodynamic model",Transactions of the American Geophysical Union.63,471.

Strong,D.F. and Taylor,R.P.,1984,"Magmatic-subsolidus and oxidation trends in composition of amphiboles from silica-saturated peralkaline igneous rocks",Tschermaks Mineralogische und Petrographische Mitteilungen.32,211-222.

Sweatman,T.R. and Long,J.V.P.,1969,"Quantitative electron-probe microanalysis of rock-forming minerals",Journal of Petrology.10,332-379.

Tuttle.O.F. and Bowen,N.L.,1958,"Origin of granite in the light of experimental studies in the system $NaAlSi_3O_8$-$KAlSi_3O_8$-SiO_2-H_2O",Geological Society of America,Memoir 74.153p.

von Platten,H.,1965,"Kristallisation granitscher schnelzen",Contributions to Mineralogy and Petrology.11,334-381.

Walker,J.W.B.,1967,"Geology of the Jackfish-Middleton area",Ontario Department of Mines Geological Report 50.38p.,maps 2107,2112.

Whalen,J.B.,Currie,K.L. and Chappell,B.W.,1987,"A-type granites : geochemical characteristics, discrimination and petrogenesis",Contributions to Mineralogy and Petrology.95,no.4,407-419.

Winkler,H.G.F.,1979,Petrogenesis of Metamorphic Rocks.Springer-Verlag : New York,5th ed.,348p.

Wones,D.R.,1979,"Intensive parameters during the crystallization of granitic plutons",Geological Association of America,Abstracts with programs.11, no.7,543.

Wones,D.R. and Gilbert,M.C.,1969,"The fayalite-magnetite-quartz assemblage between 600° and 800°C",American Journal of Science.267A,480-488.

APPENDIX I

MINERAL CHEMISTRY-MICROPROBE ANALYSES

Conditions of Analysis-Dalhousie

Circular, one-inch diameter, polished thin sections were studied utilizing a fully automated JEOL-733 Electron Microprobe at Dalhousie University, Halifax, Nova Scotia. The microprobe has four wavelength spectrometers and a Tracor Northern Si(Li) energy dispersive detector. Operating conditions employed an accelerating voltage of 15KV and a beam current of 5 nanoamperes. The spot size was approximately one micron. Geological materials were used as standards. An on-line matrix correction program utilizes a Tracor Northern ZAF procedure. The accuracy for major elements is approximately 1 to 2 percent.

Conditions of Analysis-Cambridge

Circular, one-inch diameter, polished thin sections were utilized in the automated energy dispersive electron microprobe, constructed at Cambridge University, United Kingdom. Operating conditions employed an accelerating voltage of 20 KV and a beam current of 45 nanoamperes. The spot size was one micron. Full ZAF corrections were applied as given by Sweatman and Long (1969) and Statham (1976).

Conditions of Analysis-Purdue

Circular, one-inch diameter, polished thin sections were utilized in the automated wavelength dispersive MAC 500 at Purdue University, Indiana. Operating conditions employed an accelerating voltage of 15 KV and a beam current of 25 nanoamperes. The spot size was one micron. Natural and synthetic standards were used. The ZAF procedure as outlined by Bence and Albee (1968) was followed.

APPENDIX II

AMPHIBOLE-STRUCTURAL FORMULAE

Amphibole compositions were recalculated to determine the structural formula and to assess the amount of Fe^{2+} and Fe^{3+}, by assuming stoichiometry, as outlined by Neumann, (1976). This method calculates the structural formula based upon the number of cations, and for alkaline and silicic rocks the relation is: (Si+Al+Ti+Mg+Fe+Mn)=13.0 cations. A computer program was developed to perform these calculations, and to classify the amphiboles, according to the system recommended by the I.M.A. (Leake, 1978; Rock and Leake, 1984). This calculation is based on a formula having thirteen cations in the Y and Z sites combined (i.e. Si, Al^{iv}, Al^{vi}, Ti, Fe, Mn and Mg; and excluding [Ca+Na+K] and adjusting the Fe^{2+}/Fe^{3+} to form 23 oxygen in the unit cell. The computer program also calculates various petrological ratios and indices. (see Appendix III).

APPENDIX III

AMCAL - Basic computer program to calculate structural formulae and classify amphiboles.

```
 1 si = 42.49
 2 ti = 2.04
 3 al = 8.04
 4 fe = 25.51
 5 mn = .55
 6 mg = 5.04
 7 ca = 10.03
 8 na = 2.13
 9 k = .95
10 s$ = "C180\14"
11 d$ = "East Bank Granite"
12 ly = si+ti+al+mn+mg+ca+na+k
15 PRINT "AMPHIBOLE"
20 PRINT s$
30 PRINT d$
39 PRINT "Weight % Oxides"
40 PRINT "Si02="; si
41 PRINT "Ti02="; ti
42 PRINT "Al203="; al
43 PRINT "FeO="; fe
44 PRINT "MnO="; mn
45 PRINT "MgO="; mg
46 PRINT "CaO="; ca
47 PRINT "Na2O="; na
48 PRINT "K2O="; k
51 k1 = si/60.08
52 k2 = ti/79.9
53 k3 = al/101.96
54 k4 = fe/71.85
55 k5 = mn/70.94
56 k6 = mg/40.3
57 k7 = ca/56.08
58 k8 = na/61.98
59 k9 = k/94.2
72 t1 = k1+k2+(2*k3)+k4+k5+k6
74 x = 13/t1
76 p1 = k1*2*x
78 p2 = k2*2*x
80 p3 = k3*2*1.5*x
82 p4 = k4*x
84 p5 = k5*x
86 p6 = k6*x
100 s1 = k1*2
102 s2 = k2*2
104 s3 = k3*3
106 s4 = k4
108 s5 = k5
110 s6 = k6
112 s7 = k7
114 s8 = k8
116 s9 = k9
136 t2 = s1+s2+s3+s4+s5+s6+s7+s8+s9
138 y = 23/t2
142 u1 = s1*y
144 u2 = s2*y
146 u3 = s3*y
148 u4 = s4*y
150 u5 = s5*y
152 u6 = s6*y
154 u7 = s7*y
156 u8 = s8*y
158 u9 = s9*y
180 v1 = u1*.5
182 v2 = u2*.5
184 v3 = u3*(2/3)
186 v4 = u4
188 v5 = u5
```

```
190 v6 = u6
192 v7 = u7
194 v8 = u8*2
196 v9 = u9*2
216 z2 = v1+v2+v3+v4+v5+v6
218 z3 = 13/z2
220 ca = v7*z3
222 na = v8*z3
224 k = v9*z3
226 z1 = p1+p2+p3+p4+p5+p6+ca+(na/2)+(k/2)
227 IF z1 > 23 THEN  z1 = 23
228 f3 = (23-z1)*2
230 f2 = p4-f3
232 si = p1/2
234 ti = p2/2
236 al = p3*(2/3)
238 mn = p5
240 mg = p6
250 fs = f3/(f3+f2)*fe*1.111
260 PRINT "WT% Fe2O3= ", fs
270 fc = fe-(fs/1.111)
280 PRINT "WT% FeO= ", fc
281 lx = ly+fs+fc
282 PRINT "Total wt%="; lx
283 ft = f3+f2
290 PRINT "Struct.form.13 Cations,23 Oxygens"
295 PRINT "Si="; si
297 PRINT "Ti="; ti
299 PRINT "Al="; al
301 PRINT "Fe3+="; f3
303 PRINT "Fe2+="; f2
305 PRINT "Mn="; mn
307 PRINT "Mg="; mg
309 PRINT "Ca="; ca
311 PRINT "Na="; na
312 IF si > 8 THEN  si = 8
313 PRINT "K="; k
314 PRINT "use Si="; si
315 t = si+al+f3+ti
317 IF t > 8 THEN  qt = t-8
318 IF t <= 8 THEN  qt = 0
319 c = qt+mg+f2+mn
321 IF c > 5 THEN  qc = c-5
322 IF c <= 5 THEN  qc = 0
323 b = qc+ca+na
324 IF b > 2 THEN  qb = b-2
325 IF b <= 2 THEN  qb = 0
326 IF ca < 2-qc THEN  cb = ca
327 IF ca >= 2-qc THEN  cb = 2
329 nb = na-qb
331 an = qb
333 cn = ca+nb
335 nk = qb+k
337 mf = mg/(mg+f2)
338 is = 8-si
339 xw = al-is
340 ac = is+ca
342 IF xw < 0 THEN  e$ = "No ALvi present"
343 ad = (na+k)/al
344 xy = f3/(f3+si+al-8)
345 ae = si+na+k
346 PRINT "Plotting Parameters"
347 PRINT "Na^B="; nb
349 PRINT "Na^A="; an
351 PRINT "(Ca+Na)B="; cn
353 PRINT "(Na+K)A="; nk
355 PRINT "Mg/(Mg+Fe2)="; mf
```

```
  357 PRINT "8-Si="; is
  358 PRINT "Aliv="; am; " and Aliv + Ca="; am+ca
  359 PRINT "(8-Si)+Ca="; ac
  360 PRINT "Alvi="; xw
  361 PRINT "(Na+K)/Al="; ad
  362 PRINT "Si+Na+K="; ae
  363 PRINT "Fe3/(Fe3+Alvi)="; xy
  364 PRINT e$
  365 IF cn < 1.34 THEN  z$ = "Iron-magnesium-manganese"
  367 IF cn >= 1.34 AND nb < .67 THEN  z$ = "Calcic"
  369 IF cn >= 1.34 AND nb >= .67 AND nb < 1.34 THEN  z$ = "Sodic-calcic"
  371 IF nb >= 1.34 THEN  z$ = "Alkali"
  373 PRINT "Sample "; s$; " is "; z$; " Amphibole"
  400 IF cn >= 1.34 AND nb < 1.34 AND xw >= 1 THEN  l$ = "Alumino"
  402 IF cn >= 1.34 AND nb < .67 AND na >= 1 THEN  k$ = "Sodian"
  404 IF cn >= 1.34 AND nb < .67 AND ca < 1.5 THEN  j$ = "Subcalcic"
  406 IF cn >= 1.34 AND nb < .67 AND si > 7.25 AND nk >= .5 THEN  i$ = "Silicic"

  408 IF nb >= 1.34 AND ca >= .5 THEN  h$ = "Calcian"
  410 IF nb < 1.34 AND f3 >= 1 THEN  v$ = "Ferri*"
  412 IF nb < 1.34 AND f3 >= .75 AND f3 <= .99 THEN  v$ = "Ferrian*"
  414 IF mn >= 1 THEN  t$ = "Manganese"
  416 IF mn >= .25 AND mn <= .99 THEN  t$ = "Manganoan"
  418 IF k >= .5 THEN  q$ = "Potassium"
  420 IF nb < 1.34 AND k <= .49 AND k >= .25 THEN  q$ = "Potassian"
  422 IF si < 5.75 THEN  o$ = "Subsilicic"
  424 IF ti >= 1 THEN  n$ = "Titanium**"
  426 IF ti >= .25 AND ti <= .99 THEN  n$ = "Titanian**"
  428 IF cn >= 1.34 AND nb < .67 AND nk >= .5 AND ti < .5 AND f3 <= xw AND si <
5.5 THEN  a$ = "Sadanagaite"
  430 IF nb >= 1.34 AND nk >= .5 AND f3 <= xw AND si < 7.5 THEN  b$ = "Nyboite"
  432 IF nb >= 1.34 AND nk >= .5 AND f3 >= xw AND si < 7.5 THEN  c$ = "Anophorit
e"
  440 PRINT "This "; z$; " Amphibole is also "; v$; t$; q$; o$; n$; l$; k$; j$;
i$; h$; a$; b$; c$
  450 PRINT "* excluding hastingsite,** ex. kaersutite"
  570 nz = na+ca+k
  572 nl = 100*(na/nz)
  574 nc = 100*(ca/nz)
  576 nn = 100*(k/nz)
  578 PRINT "Na:CA:K="; nl; ":"; nc; ":"; nn
  580 kn = na+k
  582 PRINT "Na+K="; kn
  584 PRINT "Ca X="; cb
  586 PRINT "Ca+Na+K="; nz
  588 ny = kn/nz
  590 PRINT "NA+K/Na+K+Ca="; ny
  592 nx = 100*(ca/nz)
  594 PRINT "100Ca/(Ca+Na+K)="; nx
  596 nv = kn+al+ca
  598 nu = 100*(kn/nv)
  600 nt = 100*(al/nv)
  602 ns = 100*(ca/nv)
  604 PRINT "Na+K:Al:Ca="; nu; ":"; nt; ":"; ns
  606 nr = mg+ft+mn+kn
  608 nq = 100*(mg/nr)
  610 np = 100*((ft+mn)/nr)
  612 no = 100*(kn/nr)
  614 PRINT "Mg:FeT+Mn:Na+K="; nq; ":"; np; ":"; no
  616 nm = 100*(ft/(ft+mg))
  618 PRINT "100 FeT/(FeT+Mg)="; nm
  620 nj = 100*(f3/ft)
  622 PRINT "100 Fe3/(Fe3+Fe2)="; nj
  624 ni = 100*(mg/(mg+ft+mn))
  626 PRINT "100 Mg/(Mg+FeT+Mn)="; ni
  628 nf = mg/(mg+ft)
  630 PRINT "Mg/(Mg+FeT)="; nf
```

APPENDIX IV

OTHER MINERALS - STRUCTURAL FORMULAE

Several APL routines ("STRUCTURE") developed by Dr. Mitchell were utilized to calculate structural formulae for pyroxene, biotite, feldspar and olivine. For pyroxenes the Fe_2O_3 was calculated by assigning all the Na_2O to acmite. Magnetite and ilmenite recalculations utilized the OXTEMP and OXCALC2 routines written by Stormer (1983). These routines are based upon the work of Stormer (1982), Anderson (1968), Carmichael (1967), and Lindsley and Spencer (1982). Stormer's routines calculate the mole fractions of ulvospinel and ilmenite components from analyses of Fe-Ti oxides. Temperatures are calculated using the model of Spencer and Lindsley (1981).

APPENDIX V

Microprobe analyses - Amphiboles from magnesio-hornblende syenite

	C178/1	C178/2	C179/1	C179/2	C179/3	C180/1	C180/2	C180/3
SiO2	42.6	42.7	42.9	41.7	41.6	42.8	44.3	43.6
TiO2	1.92	1.47	2.13	2.51	2.43	2.57	1.45	1.46
Al2O3	9.44	0.42	7.63	8.65	8.65	8.6	7.04	6.62
FeO T	19.1	21.3	26.3	24.2	24.5	22.9	26.1	26.6
MnO	0.39	0.12	0.69	0.56	0.56	0.38	0.43	0.55
MgO	9.45	8.53	4.69	5.61	5.22	6.72	5.59	4.85
CaO	11.8	11.5	10.9	11.1	10.6	10.4	10.1	9.85
Na2O	2.18	2.06	2.05	2.25	2.35	1.4	1.6	1.52
K2O	0.86	0.72	0.89	1.21	1.1	1.33	0.89	0.86
Recalc	-----	-----	-----	-----	-----	-----	-----	-----
Fe2O3	2.30	-	1.71	0.71	1.45	4.72	6.23	6.04
FeO	17.0	21.3	24.7	23.6	23.2	18.7	20.5	21.2
Total	98.0	88.8	98.3	97.8	97.1	97.6	98.1	96.5
Si	6.48	7.41	6.72	6.54	6.56	6.60	6.84	6.87
Aliv	1.52	0.086	1.28	1.46	1.44	1.40	1.16	1.13
Alvi	0.167	-	0.124	0.141	0.172	0.157	0.121	0.101
Ti	0.219	0.192	0.251	0.296	0.288	0.298	0.168	0.173
Fe3+	0.263	-	0.202	0.084	0.173	0.547	0.724	0.717
Fe2+	2.16	3.09	3.24	3.09	3.06	2.40	2.64	2.79
Mn	0.050	0.018	0.091	0.074	0.075	0.050	0.056	0.073
Mg	2.14	2.21	1.09	1.31	1.23	1.54	1.29	1.14
Ca	1.92	2.14	1.83	1.86	1.79	1.71	1.66	1.66
Na	0.64	0.693	0.622	0.684	0.719	0.418	0.479	0.463
K	0.167	0.159	0.178	0.242	0.221	0.261	0.175	0.173
Mg#	0.498	0.417	0.253	0.298	0.286	0.391	0.316	0.290

APPENDIX V

Microprobe analyses - Amphiboles from magnesio-hornblende syenite

	C180/12	C180/13	C180/14	C180/15	C180/16	C181/2	C181/3	C2120/2
SiO2	43.1	42.4	42.5	43.5	42.6	46.0	41.1	48.6
TiO2	2.63	2.44	2.04	1.42	2.37	0.13	2.0	0.03
Al2O3	8.39	8.31	8.04	7.09	8.13	4.92	9.26	5.65
FeO T	22.5	22.8	25.5	25.4	22.9	25.7	22.7	15.8
MnO	0.35	0.35	0.55	0.44	0.41	2.06	0.73	0.23
MgO	7.2	6.79	5.04	5.38	6.66	6.28	6.94	13.2
CaO	10.7	10.2	10.0	10.5	10.4	10.4	11.2	11.4
Na2O	1.54	1.57	2.13	1.67	1.99	1.37	2.34	1.91
K2O	1.31	1.28	0.95	0.99	1.26	0.52	1.37	0.15
Recalc	-----	-----	-----	-----	-----	-----	-----	-----
Fe2O3	3.93	4.87	4.05	3.37	3.11	8.43	2.78	4.96
FeO	19.0	18.4	21.9	22.4	20.1	18.1	20.2	11.4
Total	98.1	96.6	97.2	96.8	97.1	98.2	97.9	97.4
Si	6.60	6.61	6.67	6.85	6.64	7.08	6.40	7.15
Aliv	1.40	1.39	1.33	1.15	1.36	0.89	1.60	0.85
Alvi	0.12	0.13	0.158	0.16	0.133	-	0.102	0.128
Ti	0.303	0.286	0.241	0.168	0.278	0.015	0.234	-
Fe3+	0.454	0.570	0.478	0.399	0.364	0.977	0.326	0.550
Fe2+	2.43	2.39	2.87	2.95	2.62	2.33	2.63	1.40
Mn	0.045	0.046	0.073	0.059	0.054	0.269	0.096	0.029
Mg	1.65	1.58	1.18	1.26	1.55	1.44	1.61	2.89
Ca	1.75	1.70	1.69	1.77	1.73	1.72	1.86	1.80
Na	0.458	0.474	0.648	0.510	0.601	0.409	0.706	0.545
K	0.256	0.254	0.190	0.199	0.250	0.102	0.272	0.028
Mg#	0.404	0.397	0.291	0.300	0.371	0.382	0.380	0.674

APPENDIX V

Microprobe analyses - Amphiboles from magnesio-hornblende syenite

	C180/4	C180/5	C180/6	C180/7	C180/8	C180/9	C180/10	C180/11
SiO2	42.9	42.4	42.5	42.1	42.1	41.9	42.9	42.7
TiO2	0.92	2.3	2.42	2.01	2.56	2.37	2.53	2.31
Al2O3	7.48	8.48	8.16	8.02	8.24	8.52	8.25	8.0
FeO T	25.0	26.2	26.3	26.8	24.5	25.7	22.5	26.0
MnO	0.51	0.51	0.57	0.56	0.47	0.54	0.4	0.52
MgO	5.75	4.43	4.22	3.87	5.03	5.04	7.18	4.9
CaO	10.3	10.2	10.2	9.86	10.2	10.2	10.7	10.3
Na2O	1.63	1.97	1.87	1.7	1.59	2.25	1.71	1.45
K2O	0.93	1.18	1.22	1.08	1.25	1.21	1.29	1.13
Recalc	-----	-----	-----	-----	-----	-----	-----	-----
Fe2O3	5.64	3.32	2.69	4.28	2.86	3.93	3.43	4.77
FeO	19.9	23.2	23.9	22.9	22.0	22.2	19.4	21.7
Total	96.0	98.0	97.6	96.4	96.3	98.2	97.7	97.8
Si	6.77	6.63	6.68	6.70	6.67	6.55	6.61	6.66
Aliv	1.23	1.37	1.32	1.30	1.33	1.45	1.39	1.34
Alvi	0.165	0.197	0.191	0.203	0.210	0.116	0.109	0.13
Ti	0.109	0.271	0.286	0.240	0.304	0.278	0.293	0.271
Fe3+	0.671	0.392	0.318	0.512	0.340	0.461	0.398	0.560
Fe2+	2.63	3.04	3.14	3.05	2.90	2,90	2.50	2.83
Mn	0.068	0.068	0.076	0.075	0.063	0.071	0.052	0.069
Mg	1.35	1.03	0.990	0.918	1.19	1.17	1.65	1.14
Ca	1.74	1.70	1.71	1.68	1.72	1.70	1.77	1.72
Na	0.499	0.598	0.570	0.524	0.488	0.681	0.511	0.438
K	0.187	0.236	0.245	0.219	0.252	0.241	0.253	0.225
Mg#	0.340	0.254	0.240	0.231	0.290	0.288	0.398	0.287

APPENDIX V

Microprobe analyses - Amphiboles from magnesio-hornblende syenite

	C2120/3	C2123/1	C2123/2	C2128/2	C2128/3	C2128/4	C2150/3	C2150/4
SiO2	46.6	46.7	45.2	38.7	43.3	44.3	48.4	46.7
TiO2	1.29	1.21	1.2	0.34	0.53	0.72	0.767	1.23
Al2O3	7.01	5.87	6.64	11.2	6.67	7.98	4.81	5.18
FeO T	16.4	18.3	19.3	28.2	18.1	20.2	18.0	18.2
MnO	0.25	0.43	0.41	0.41	0.41	0.51	0.336	0.264
MgO	11.8	11.2	10.9	3.62	10.2	9.71	11.1	10.5
CaO	11.6	11.2	10.9	11.7	11.6	11.4	11.4	10.8
Na2O	2.15	1.53	1.73	1.38	1.69	2.18	1.36	0.764
K2O	0.44	0.52	0.64	1.96	0.51	0.6	0.569	0.55
Recalc	-----	-----	-----	-----	-----	-----	-----	-----
Fe2O3	1.76	5.30	7.76	5.37	3.11	5.04	2.10	5.14
FeO	14.8	13.5	12.3	23.4	15.3	15.6	16.1	13.6
Total	97.7	97.4	97.7	98.1	93.3	98.1	96.9	94.8
Si	6.94	6.98	6.78	6.17	6.85	6.70	7.28	7.15
Aliv	1.06	1.02	1.17	1.83	1.15	1.30	0.72	0.85
Alvi	0.167	0.017	-	0.276	0.090	0.118	0.129	0.088
Ti	0.144	0.136	0.135	0.041	0.063	0.082	0.087	0.142
Fe3+	0.197	0.597	0.876	0.645	0.370	0.573	0.238	0.592
Fe2+	1.84	1.69	1.54	3.12	2.02	1.97	2.02	1.74
Mn	0.032	0.055	0.052	0.055	0.055	0.065	0.043	0.034
Mg	2.62	2.51	2.44	0.861	2.40	2.19	2.48	2.41
Ca	1.85	1.79	1.75	2.00	1.97	1.85	1.84	1.77
Na	0.621	0.444	0.503	0.427	0.519	0.639	0.397	0.227
K	0.084	0.099	0.122	0.399	0.103	0.116	0.109	0.107
Mg#	0.587	0.597	0.613	0.216	0.543	0.526	0.551	0.581

APPENDIX V

Microprobe analyses - Amphiboles from magnesio-hornblende syenite

	C2150/5	C2150/6	C2150/7	C2150/8	C2150/9	C2150/10	C2150/11	C2150/12
SiO2	45.7	46.5	45.9	46.4	46.2	45.6	49.0	50.0
TiO2	1.37	1.36	1.42	1.56	1.23	1.33	0.173	-
Al2O3	6.67	5.75	6.87	5.53	6.2	6.87	5.29	4.65
FeO T	19.5	19.1	19.3	18.6	19.2	19.6	16.3	15.6
MnO	0.278	0.266	0.287	0.32	0.399	0.306	0.237	0.273
MgO	10.1	10.8	10.3	10.2	10.4	10.2	12.8	13.9
CaO	11.2	10.8	10.9	10.8	10.5	10.5	11.5	11.6
Na2O	1.52	1.52	1.72	1.52	1.54	1.81	1.20	1.34
K2O	0.833	0.736	0.866	0.694	0.762	0.907	0.583	0.535
Recalc	-----	-----	-----	-----	-----	-----	-----	-----
Fe2O3	4.16	5.65	5.27	3.00	6.26	6.18	4.78	5.64
FeO	15.7	14.0	14.6	15.9	13.5	14.1	12.0	10.5
	-----	-----	-----	-----	-----	-----	-----	-----
Total	97.6	97.4	98.1	96.0	97.1	97.8	97.6	98.5
Si	6.90	6.99	6.86	7.09	6.96	6.85	7.22	7.26
Aliv	1.10	1.01	1.14	0.912	1.04	1.15	0.78	0.74
Alvi	0.081	0.003	0.076	0.084	0.060	0.061	0.135	0.054
Ti	0.156	0.154	0.160	0.179	0.139	0.150	0.019	-
Fe3+	0.473	0.638	0.593	0.345	0.710	0.698	0.530	0.616
Fe2+	1.98	1.75	1.83	2.03	1.71	1.77	1.47	1.28
Mn	0.036	0.034	0.036	0.041	0.051	0.039	0.030	0.034
Mg	2.27	2.42	2.31	2.32	2.33	2.28	2.81	3.02
Ca	1.82	1.74	1.74	1.77	1.70	1.70	1.81	1.80
Na	0.446	0.441	0.498	0.448	0.449	0.528	0.342	0.378
K	0.160	0.141	0.165	0.135	0.146	0.174	0.109	0.099
Mg#	0.534	0.579	0.558	0.533	0.578	0.563	0.656	0.702

APPENDIX V

Microprobe analyses - Amphiboles from ferro-edenite syenite

	C172/1 xeno	C172/3	C182/2	C182/3	C182/4	C182/5	C182/6	C182/7
SiO2	41.7	38.9	43.4	43.4	43.5	43.5	44.3	43.8
TiO2	1.04	1.06	1.74	1.32	1.36	1.55	1.53	1.71
Al2O3	10.2	11.0	6.2	5.42	6.08	6.4	5.52	5.91
FeO T	19.3	21.3	28.7	28.3	28.9	28.6	29.2	28.9
MnO	0.46	0.63	0.88	0.91	0.68	0.87	0.63	0.61
MgO	9.26	7.27	3.21	3.35	2.86	3.26	2.96	3.22
CaO	11.5	11.3	9.61	9.42	10.1	9.44	9.32	9.61
Na2O	3.28	2.76	2.22	2.02	1.54	2.18	2.13	2.72
K2O	1.16	1.52	1.22	1.06	1.03	1.2	1.07	1.17
Recalc	-----	-----	-----	-----	-----	-----	-----	-----
Fe2O3	1.33	2.79	3.08	3.46	2.79	3.77	3.02	1.32
FeO	18.1	18.8	26.0	25.2	26.4	25.2	26.5	27.7
	-----	-----	-----	-----	-----	-----	-----	-----
Total	98.0	96.1	97.6	96.1	96.3	97.4	97.0	97.8
Si	6.39	6.18	6.92	7.07	7.01	6.92	7.08	6.98
Aliv	1.61	1.82	1.08	0.93	0.99	1.08	0.92	1.02
Alvi	0.226	0.241	0.082	0.10	0.16	0.123	0.12	0.090
Ti	0.120	0.127	0.208	0.160	0.165	0.185	0.184	0.205
Fe3+	0.154	0.333	0.369	0.419	0.338	0.451	0.363	0.159
Fe2+	2.32	2.49	3.46	3.40	3.56	3.35	3.54	3.70
Mn	0.060	0.085	0.119	0.124	0.093	0.117	0.085	0.082
Mg	2.12	1.72	0.762	0.804	0.687	0.773	0.705	0.765
Ca	1.89	1.92	1.64	1.63	1.74	1.61	1.60	1.64
Na	0.976	0.849	0.685	0.631	0.481	0.672	0.660	0.841
K	0.227	0.308	0.248	0.218	0.212	0.243	0.218	0.238
Mg#	0.477	0.408	0.181	0.191	0.162	0.187	0.166	0.171

APPENDIX V

Microprobe analyses - Amphiboles from ferro-edenite syenite

	C182/8	C182/9	C182/10	C294/2	C294/3	C294/4	C322/1	C322/2
SiO2	43.7	44.1	44.6	44.4	44.3	45.7	45.6	51.2
TiO2	1.54	1.58	1.26	1.42	1.39	1.33	0.86	0.05
Al2O3	5.27	5.59	5.77	4.3	4.77	3.84	2.09	0.73
FeO T	29.0	29.1	28.6	28.9	29.1	29.8	30.4	33.1
MnO	0.86	0.87	0.57	1.17	1.19	1.12	1.24	0.48
MgO	3.03	3.21	3.29	3.38	3.64	2.89	1.78	1.26
CaO	9.28	9.3	9.53	9.17	9.2	8.83	4.92	0.83
Na2O	2.14	2.25	2.25	2.55	2.62	2.26	4.53	6.29
K2O	1.12	1.13	1.03	0.91	0.94	0.81	0.65	-
Recalc	-----	-----	-----	-----	-----	-----	-----	-----
Fe2O3	3.42	3.68	2.17	3.27	4.65	3.95	6.22	11.9
FeO	25.9	25.7	26.6	26.0	24.9	26.3	24.8	22.4
	-----	-----	-----	-----	-----	-----	-----	-----
Total	96.3	97.5	97.1	96.6	97.6	97.0	92.7	95.1
Si	7.05	7.02	7.10	7.15	7.04	7.30	7.61	8.11
Aliv	0.95	0.98	0.90	0.82	0.89	0.70	0.39	-
Alvi	0.052	0.068	0.182	-	-	0.02	0.023	0.136
Ti	0.187	0.189	0.151	0.172	0.166	0.160	0.108	0.005
Fe3+	0.415	0.440	0.260	0.396	0.557	0.474	0.782	1.41
Fe2+	3.50	3.42	3.55	3.50	3.32	3.50	3.47	2.97
Mn	0.118	0.117	0.077	0.159	0.160	0.151	0.175	0.064
Mg	0.729	0.761	0.781	0.811	0.863	0.688	0.443	0.298
Ca	1.60	1.58	1.63	1.58	1.57	1.51	0.881	0.141
Na	0.669	0.694	0.695	0.796	0.808	0.699	1.47	1.93
K	0.231	0.229	0.209	0.187	0.191	0.165	0.139	-
Mg#	0.172	0.182	0.180	0.188	0.206	0.164	0.113	0.091

APPENDIX V

Microprobe analyses - Amphiboles from ferro-edenite syenite

	C322/3	C333/2	C333/3	C341/1	C341/2	C341/3	C361/1	C361/2
SiO2	48.4	47.7	45.4	50.1	47.8	45.0	43.4	43.7
TiO2	0.97	1.47	1.59	0.17	1.76	1.7	1.54	1.14
Al2O3	1.82	1.36	3.52	0.19	1.95	3.69	7.08	6.7
FeO T	31.1	31.6	31.2	26.9	30.4	30.1	24.9	24.9
MnO	1.29	1.13	1.14	0.88	0.96	0.83	0.62	0.61
MgO	2.39	1.6	1.7	0.94	2.47	2.41	5.81	6.0
CaO	4.94	5.17	6.99	14.6	6.48	7.69	10.6	10.9
Na2O	4.7	4.91	4.6	4.93	4.53	4.36	2.11	1.94
K2O	0.55	1.33	1.01	-	1.22	1.09	1.1	1.05
Recalc	-----	-----	-----	-----	-----	-----	-----	-----
Fe2O3	6.95	2.47	1.49	-	0.48	0.02	2.52	2.46
FeO	24.8	29.4	29.9	26.9	30.0	30.1	22.7	22.7
	-----	-----	-----	-----	-----	-----	-----	-----
Total	96.9	96.5	97.3	98.7	97.6	96.9	97.4	97.2
Si	7.68	7.73	7.34	8.67	7.64	7.30	6.80	6.87
Aliv	0.32	0.26	0.66	-	0.36	0.70	1.20	1.13
Alvi	0.022	-	0.014	0.039	0.007	0.009	0.108	0.112
Ti	0.116	0.179	0.193	0.022	0.212	0.207	0.182	0.135
Fe3+	0.830	0.302	0.182	-	0.057	-	0.297	0.290
Fe2+	3.29	3.98	4.04	3.90	4.01	4.08	2.97	2.98
Mn	0.173	0.155	0.156	0.129	0.130	0.114	0.082	0.081
Mg	0.565	0.387	0.410	0.243	0.589	0.583	1.36	1.41
Ca	0.840	0.898	1.21	2.70	1.11	1.34	1.79	1.83
Na	1.45	1.54	1.44	1.65	1.40	1.37	0.641	0.591
K	0.111	0.275	0.208	-	0.249	0.226	0.220	0.210
Mg#	0.146	0.088	0.092	0.059	0.128	0.125	0.314	0.321

APPENDIX V

Microprobe analyses - Amphiboles from ferro-edenite syenite

	C361/3	C361/4	C371/1	C371/2	C371/3	C1487/1	C1487/2	C1487/3
SiO2	42.7	42.1	49.8	50.2	49.8	44.0	45.0	43.6
TiO2	1.69	1.5	0.37	0.41	0.2	1.07	0.87	1.13
Al2O3	7.47	7.1	0.29	0.62	0.63	4.94	5.29	5.74
FeO T	25.2	25.2	25.9	27.0	34.3	27.5	26.7	27.5
MnO	0.69	0.49	0.94	0.89	1.41	0.97	0.87	0.93
MgO	5.53	5.69	0.91	1.01	0.59	4.73	5.36	4.4
CaO	11.0	10.6	13.3	12.1	4.54	9.77	9.89	10.1
Na2O	2.2	2.14	6.29	6.33	4.54	2.24	2.59	2.48
K2O	1.23	1.09	-	-	0.21	0.95	1.0	1.08
Recalc	-----	-----	-----	-----	-----	-----	-----	-----
Fe2O3	1.35	3.24	-	-	7.80	4.59	3.39	2.76
FeO	23.9	22.2	25.9	27.0	27.3	23.4	23.6	25.0
Total	97.8	96.1	97.8	98.5	96.9	96.6	97.8	97.2
Si	6.72	6.71	8.72	8.57	7.95	7.02	7.05	6.95
Aliv	1.28	1.29	-	-	0.05	0.93	0.95	1.05
Alvi	0.102	0.045	0.060	0.125	0.065	-	0.030	0.026
Ti	0.200	0.180	0.049	0.053	0.024	0.128	0.103	0.135
Fe3+	0.159	0.389	-	-	0.938	0.551	0.400	0.332
Fe2+	3.15	2.97	3.80	3.86	3.64	3.12	3.10	3.33
Mn	0.092	0.066	0.139	0.129	0.191	0.131	0.116	0.126
Mg	1.30	1.35	0.237	0.257	0.140	1.12	1.25	1.05
Ca	1.85	1.81	2.49	2.21	0.777	1.67	1.66	1.72
Na	0.671	0.662	2.13	2.10	1.41	0.693	0.788	0.767
K	0.247	0.222	-	-	0.043	0.193	0.200	0.220
Mg#	0.292	0.313	0.059	0.062	0.037	0.265	0.288	0.239

APPENDIX V

Microprobe analyses - Amphiboles from ferro-edenite syenite

	C1488/1	C1488/2	C1488/3	C1495/1	C1495/2	C1495/3	C2001/2	C2001/3
SiO2	40.5	44.0	40.4	40.5	39.9	39.5	44.2	42.9
TiO2	1.75	1.85	1.69	1.76	1.85	2.05	1.22	1.33
Al2O3	8.46	9.72	8.85	8.55	9.43	8.98	6.17	7.11
FeO T	26.7	24.0	26.9	26.1	26.3	26.4	24.0	24.1
MnO	0.83	0.84	0.84	0.88	0.94	0.84	0.61	0.54
MgO	3.91	5.25	4.05	4.4	4.19	3.93	7.18	6.33
CaO	10.5	10.0	10.9	10.6	10.5	10.6	10.9	11.1
Na2O	2.9	3.62	2.8	2.69	2.77	2.65	1.97	2.06
K2O	1.48	1.38	1.36	1.34	1.37	1.43	1.18	1.41
Recalc	-----	-----	-----	-----	-----	-----	-----	-----
Fe2O3	0.47	-	1.17	1.76	2.50	1.61	3.48	1.19
FeO	26.2	24.0	25.9	24.5	24.1	25.0	20.9	23.0
Total	97.1	100.6	98.0	96.9	97.6	96.5	97.7	97.0
Si	6.53	6.69	6.46	6.50	6.37	6.39	6.86	6.77
Aliv	1.47	1.31	1.54	1.50	1.63	1.61	1.13	1.23
Alvi	0.136	0.435	0.123	0.113	0.145	0.109	-	0.094
Ti	0.212	0.212	0.203	0.212	0.222	0.250	0.143	0.158
Fe3+	0.057	-	0.140	0.213	0.300	0.196	0.407	0.141
Fe2+	3.54	3.05	3.46	3.29	3.21	3.38	2.71	3.04
Mn	0.113	0.108	0.114	0.120	0.127	0.115	0.080	0.072
Mg	0.940	1.19	0.964	1.05	0.997	0.949	1.66	1.49
Ca	1.82	1.63	1.86	1.82	1.80	1.84	1.81	1.88
Na	0.907	1.07	0.867	0.837	0.857	0.832	0.594	0.631
K	0.305	0.268	0.277	0.274	0.279	0.296	0.234	0.284
Mg#	0.210	0.281	0.218	0.243	0.237	0.219	0.380	0.329

APPENDIX V

Microprobe analyses - Amphiboles from ferro-edenite syenite

	C2004/1	C2004/2	C2004/3	C2006/1 xeno	C2006/2	C2006/3	C2053/1	C2053/2
SiO2	42.6	42.8	40.9	45.0	45.6	44.9	42.5	42.8
TiO2	1.31	1.3	1.6	1.31	1.34	1.36	1.90	2.22
Al2O3	5.93	6.25	6.96	6.13	5.22	5.93	7.49	7.27
FeO T	30.8	30.2	29.4	24.2	24.5	23.8	28.8	29.0
MnO	1.47	1.35	1.14	0.6	0.64	0.59	0.63	0.563
MgO	2.61	2.74	2.89	7.06	6.69	6.32	3.12	3.07
CaO	10.0	9.92	9.96	10.7	10.0	11.1	9.80	9.78
Na2O	2.02	2.09	2.02	2.23	2.31	1.97	2.75	2.83
K2O	0.88	0.84	1.16	0.98	0.75	1.02	1.23	1.14
Recalc	-----	-----	-----	-----	-----	-----	-----	-----
Fe2O3	6.13	5.75	5.52	3.02	3.54	-	2.15	1.75
FeO	25.3	25.1	24.4	21.5	21.3	23.8	26.9	27.5
Total	98.3	98.1	96.6	98.4	97.4	96.9	98.4	98.9
Si	6.80	6.81	6.63	6.92	7.07	7.06	6.74	6.76
Aliv	1.11	1.17	1.33	1.08	0.93	0.94	1.26	1.24
Alvi	-	-	-	0.037	0.029	0.155	0.134	0.108
Ti	0.157	0.156	0.195	0.152	0.156	0.161	0.226	0.264
Fe3+	0.736	0.689	0.674	0.350	0.413	-	0.256	0.208
Fe2+	3.37	3.34	3.31	2.76	2.77	3.12	3.56	3.62
Mn	0.199	0.182	0.157	0.078	0.084	0.079	0.084	0.075
Mg	0.621	0.651	0.699	1.62	1.55	1.48	0.737	0.722
Ca	1.71	1.69	1.73	1.76	1.66	1.86	1.66	1.65
Na	0.625	0.645	0.635	0.666	0.695	0.601	0.845	0.865
K	0.179	0.171	0.240	0.193	0.149	0.205	0.249	0.228
Mg#	0.156	0.163	0.174	0.370	0.359	0.322	0.171	0.116

APPENDIX V

Microprobe analyses - Amphiboles from ferro-edenite syenite

	C2053/3	C2053/4	C2053/7	C2053/8	C2053/9	C2053/10	C2053/11	C2053/12
SiO2	43.8	43.1	42.6	41.9	43.6	43.2	42.3	42.5
TiO2	1.00	1.83	1.65	1.57	1.47	1.63	1.27	2.05
Al2O3	5.86	6.71	7.24	7.46	6.36	7.12	5.77	7.38
FeO T	28.6	29.0	28.9	28.0	30.0	29.4	29.6	27.7
MnO	0.837	0.885	0.795	0.838	0.678	0.564	0.616	0.66
MgO	3.39	3.43	3.03	2.92	2.31	2.48	2.25	3.83
CaO	9.20	9.80	9.62	9.36	9.30	9.65	10.1	9.88
Na2O	2.77	3.09	2.81	2.6	3.07	2.99	2.47	2.91
K2O	1.13	1.22	1.24	1.37	1.23	1.32	1.56	1.15
Recalc	-----	-----	-----	-----	-----	-----	-----	-----
Fe2O3	3.05	2.05	2.52	2.48	0.80	0.14	-	1.82
FeO	25.9	27.2	26.7	25.8	29.3	29.3	29.6	26.1
Total	96.9	99.3	98.2	96.3	98.0	98.4	95.9	98.3
Si	7.02	6.79	6.77	6.78	6.98	6.88	6.99	6.72
Aliv	0.98	1.21	1.23	1.22	1.02	1.12	1.01	1.28
Alvi	0.125	0.036	0.131	0.197	0.178	0.220	0.108	0.099
Ti	0.121	0.217	0.197	0.191	0.177	0.196	0.158	0.244
Fe3+	0.368	0.244	0.302	0.302	0.097	0.017	-	0.217
Fe2+	3.47	3.58	3.54	3.49	3.92	3.90	4.09	3.45
Mn	0.114	0.118	0.107	0.115	0.078	0.076	0.086	0.088
Mg	0.808	0.805	0.719	0.704	0.552	0.588	0.554	0.904
Ca	1.58	1.65	1.64	1.62	1.59	1.65	1.78	1.67
Na	0.860	0.944	0.867	0.816	0.953	0.924	0.790	0.892
K	0.231	0.245	0.252	0.283	0.252	0.269	0.328	0.231
Mg#	0.189	0.184	0.169	0.168	0.124	0.130	0.119	0.208

APPENDIX V

Microprobe analyses - Amphiboles from ferro-edenite syenite

	C2053/13	C2053/14	C2058/1	C2058/2	C2058/3 xeno	C2058/4 xeno	C2059/1	C2059/2
SiO2	46.4	42.6	42.2	43.3	41.2	43.6	44.2	44.4
TiO2	0.889	2.03	1.75	1.21	2.06	1.22	1.15	1.28
Al2O3	3.57	7.35	8.72	7.46	8.65	8.38	7.81	6.99
FeO T	29.6	28.1	22.3	22.4	19.6	19.6	19.6	18.8
MnO	0.848	0.613	0.65	0.56	0.49	0.46	0.4	0.27
MgO	3.77	3.43	7.52	7.65	9.25	9.37	9.2	9.44
CaO	8.11	9.65	10.7	11.0	11.4	11.9	11.3	11.7
Na2O	3.30	2.70	2.53	2.09	2.33	2.03	2.24	2.1
K2O	1.26	1.19	1.2	1.33	1.24	1.42	0.52	0.54
Recalc	-----	-----	-----	-----	-----	-----	-----	-----
Fe2O3	3.94	2.25	3.79	2.61	3.10	1.16	2.39	-
FeO	26.0	26.1	18.9	20.0	16.8	18.5	17.5	18.8
Total	98.1	97.9	98.0	97.3	96.6	98.1	96.6	95.5
Si	7.33	6.76	6.51	6.74	6.41	6.66	6.78	6.91
Aliv	0.66	1.24	1.49	1.26	1.59	1.34	1.22	1.09
Alvi	-	0.134	0.101	0.103	-	0.167	0.193	0.187
Ti	0.106	0.242	0.203	0.142	0.241	0.140	0.133	0.150
Fe3+	0.468	0.268	0.441	0.306	0.363	0.133	0.277	-
Fe2+	3.44	3.46	2.44	2.60	2.19	2.37	2.24	2.44
Mn	0.113	0.082	0.085	0.074	0.065	0.059	0.052	0.036
Mg	0.887	0.811	1.73	1.77	2.15	2.13	2.11	2.19
Ca	1.37	1.64	1.77	1.84	1.90	1.94	1.86	1.95
Na	1.01	0.830	0.757	0.630	0.703	0.601	0.667	0.633
K	0.253	0.240	0.236	0.264	0.246	0.277	0.102	0.107
Mg#	0.205	0.190	0.415	0.405	0.495	0.474	0.484	0.473

APPENDIX V

Microprobe analyses - Amphiboles from ferro-edenite syenite

	C2059/3	C2059/4	C2074/2	C2074/3	C2077/1	C2077/2	C2077/3 xeno	C2077/4 xeno
SiO2	43.5	42.8	49.3	45.9	41.8	41.7	42.0	45.1
TiO2	1.45	1.50	0.43	0.47	1.1	1.67	1.3	1.42
Al2O3	8.21	8.24	1.05	0.89	7.48	7.39	6.81	6.53
FeO T	18.4	18.8	22.6	22.4	27.5	27.9	20.3	20.3
MnO	0.24	0.35	1.09	0.98	0.85	0.96	0.49	0.56
MgO	8.95	8.81	3.76	3.54	3.99	3.8	9.27	9.27
CaO	12.1	12.0	21.3	19.8	10.7	10.6	10.8	11.2
Na2O	1.98	2.02	1.22	1.19	2.29	1.88	2.18	2.14
K2O	0.61	0.67	-	-	1.36	1.37	1.3	1.18
Recalc	-----	-----	-----	-----	-----	-----	-----	-----
Fe2O3	-	-	-	-	2.06	3.33	4.59	1.74
FeO	18.4	18.8	22.6	22.4	25.6	24.9	16.1	18.7
Total	95.4	95.2	100.7	95.2	97.3	97.7	94.9	97.9
Si	6.79	6.72	8.40	8.27	6.70	6.66	6.64	6.89
Aliv	1.21	1.28	-	-	1.30	1.34	1.27	1.11
Alvi	0.304	0.248	0.211	0.189	0.111	0.046	-	0.061
Ti	0.170	0.177	0.055	0.064	0.133	0.200	0.155	0.163
Fe3+	-	-	-	-	0.248	0.400	0.547	0.200
Fe2+	2.41	2.47	3.22	3.37	3.44	3.32	2.13	2.39
Mn	0.032	0.047	0.157	0.150	0.115	0.130	0.066	0.072
Mg	2.08	2.06	0.956	0.951	0.954	0.904	2.19	2.11
Ca	2.03	2.02	3.88	3.83	1.84	1.82	1.83	1.83
Na	0.569	0.615	0.403	0.416	0.712	0.581	0.669	0.634
K	0.122	0.134	-	-	0.278	0.279	0.262	0.230
Mg#	0.464	0.455	0.229	0.220	0.217	0.214	0.506	0.469

APPENDIX V

Microprobe analyses - Amphiboles from ferro-edenite syenite

	C2101/1	C2101/2	C2101/4	C2127/1	C2127/2	C2127/3	C2133/1	C2133/2
SiO2	45.4	44.0	44.3	45.6	45.0	48.3	43.5	46.0
TiO2	1.34	1.51	1.46	1.51	1.51	1.21	1.3	0.1
Al2O3	3.79	4.74	4.36	4.5	5.14	2.91	5.63	2.86
FeO T	30.7	30.4	30.7	27.0	27.5	27.6	29.5	26.5
MnO	0.81	1.01	0.75	0.73	0.75	0.78	0.69	0.77
MgO	1.92	2.14	1.92	3.97	4.36	4.79	2.68	4.53
CaO	9.09	9.54	9.44	7.68	8.95	8.21	11.1	11.5
Na2O	3.27	3.22	3.24	3.79	3.63	3.33	2.21	0.37
K2O	0.81	0.97	0.87	1.5	1.17	1.2	0.78	0.68
Recalc	-----	-----	-----	-----	-----	-----	-----	-----
Fe2O3	-	-	-	0.52	0.73	1.44	-	-
FeO	30.7	30.4	30.7	26.5	26.8	26.3	29.5	26.5
Total	97.1	97.6	97.0	96.3	98.0	98.5	97.4	93.2
Si	7.37	7.13	7.22	7.30	7.11	7.52	7.04	7.57
Aliv	0.63	0.87	0.78	0.70	0.89	0.48	0.96	0.43
Alvi	0.091	0.039	0.062	0.151	0.067	0.052	0.109	0.126
Ti	0.164	0.184	0.179	0.182	0.179	0.142	0.158	0.012
Fe3+	-	-	-	0.063	0.087	0.169	-	-
Fe2+	4.17	4.12	4.19	3.56	3.54	3.42	3.99	3.64
Mn	0.111	0.139	0.104	0.099	0.100	0.103	0.095	0.107
Mg	0.465	0.517	0.467	0.948	1.03	1.11	0.646	1.11
Ca	1.58	1.66	1.65	1.32	1.51	1.37	1.92	2.02
Na	1.03	1.01	1.02	1.18	1.11	1.00	0.693	0.118
K	0.168	0.200	0.181	0.307	0.256	0.238	0.161	0.143
Mg#	0.100	0.111	0.100	0.210	0.225	0.245	0.139	0.234

APPENDIX V

Microprobe analyses - Amphiboles from ferro-edenite syenite

	C2133/3	C2133/4	C2190/1	C2190/3 xeno	C2190/4 xeno	C2190/5 xeno	C2190/6 xeno	C2218/1
SiO2	42.8	40.5	41.9	43.8	42.3	40.5	41.5	42.2
TiO2	1.47	0.57	1.92	1.28	1.43	0.96	1.46	1.56
Al2O3	6.3	3.17	8.56	7.09	8.01	6.97	7.94	7.71
FeO T	27.3	26.9	22.4	22.4	24.8	25.6	25.1	25.8
MnO	0.69	0.81	0.57	0.57	0.58	0.6	0.59	0.83
MgO	3.55	2.8	6.97	7.0	5.55	4.83	4.8	5.15
CaO	11.4	10.5	11.0	11.3	11.1	10.6	11.1	10.8
Na2O	2.33	0.97	2.18	2.24	2.33	2.17	2.32	3.09
K2O	0.91	0.53	1.08	0.85	0.97	0.83	0.97	1.15
Recalc	-----	-----	-----	-----	-----	-----	-----	-----
Fe2O3	-	0.15	1.98	-	1.29	3.00	-	0.43
FeO	27.3	26.7	20.6	22.4	23.6	22.9	25.1	25.4
Total	96.7	86.7	96.6	96.5	97.1	93.3	95.9	98.3
Si	6.96	7.31	6.58	6.88	6.68	6.70	6.69	6.66
Aliv	1.04	0.69	1.42	1.12	1.32	1.30	1.31	1.34
Alvi	0.162	0.011	0.162	0.194	0.171	0.063	0.203	0.093
Ti	0.180	0.077	0.227	0.151	0.170	0.120	0.177	0.185
Fe3+	-	0.020	0.234	-	0.154	0.373	-	0.051
Fe2+	3.70	4.04	2.71	2.94	3.12	3.17	3.39	3.35
Mn	0.095	0.124	0.076	0.076	0.078	0.084	0.081	0.111
Mg	0.860	0.754	1.59	1.64	1.31	1.19	1.15	1.21
Ca	1.98	2.03	1.85	1.91	1.87	1.87	1.92	1.82
Na	0.734	0.340	0.664	0.683	0.714	0.696	0.725	0.946
K	0.189	0.122	0.216	0.170	0.196	0.175	0.199	0.232
Mg#	0.188	0.157	0.370	0.358	0.295	0.273	0.254	0.266

APPENDIX V

Microprobe analyses - Amphiboles from ferro-edenite syenite

	C2218/2 xeno	C2218/3	C2218/4	C2221/1	C2221/2	C2221/3	C2221/4	C2221/5
SiO2	41.3	46.9	48.4	40.9	42.1	42.0	40.5	40.5
TiO2	1.91	1.2	0.92	1.96	1.17	1.25	1.89	2.05
Al2O3	8.46	4.1	2.46	8.44	7.20	6.92	8.35	8.42
FeO T	23.4	25.6	26.3	27.0	29.4	29.6	29.1	28.5
MnO	0.69	0.96	0.98	0.89	1.11	1.09	1.07	1.04
MgO	5.73	5.13	5.46	4.12	2.31	2.47	2.26	2.90
CaO	11.3	9.56	8.9	9.87	9.39	9.28	9.64	9.84
Na2O	3.11	3.37	3.37	2.51	2.63	2.68	2.76	2.47
K2O	1.3	0.96	0.83	1.35	1.31	1.42	1.45	1.33
Recalc	-----	-----	-----	-----	-----	-----	-----	-----
Fe2O3	-	-	-	4.44	3.15	3.72	2.73	3.92
FeO	23.4	25.6	26.3	23.0	26.6	26.2	26.6	24.9
Total	97.2	97.8	97.7	97.5	97.0	97.1	97.4	97.4
Si	6.60	7.39	7.58	6.51	6.81	6.79	6.55	6.51
Aliv	1.40	0.61	0.42	1.49	1.19	1.21	1.45	1.49
Alvi	0.190	0.147	0.037	0.087	0.179	0.109	0.146	0.099
Ti	0.230	0.142	0.108	0.235	0.142	0.151	0.229	0.248
Fe3+	-	-	-	0.531	0.384	0.453	0.332	0.473
Fe2+	3.12	3.38	3.45	3.05	3.59	3.54	3.60	3.35
Mn	0.093	0.128	0.130	0.120	0.152	0.149	0.146	0.141
Mg	1.37	1.21	1.27	0.975	0.555	0.594	0.545	0.693
Ca	1.94	1.61	1.49	1.68	1.63	1.61	1.67	1.69
Na	0.964	1.03	1.02	0.772	0.824	0.838	0.867	0.770
K	0.265	0.193	0.166	0.273	0.271	0.292	0.300	0.272
Mg#	0.304	0.263	0.270	0.242	0.134	0.144	0.131	0.172

APPENDIX V

Microprobe analyses - Amphiboles from ferro-edenite syenite

	C2222/4	C2222/5	C2222/6	C2223/1	C2223/2	C2223/3	C2223/4	C2223/6
SiO2	49.7	47.2	49.4	46.0	46.3	45.8	46.4	45.8
TiO2	0.73	0.719	0.731	1.32	1.32	1.28	1.22	0.923
Al2O3	2.01	1.54	1.61	3.48	3.34	3.50	3.05	3.39
FeO T	32.8	30.8	32.2	30.2	30.4	30.5	30.5	31.1
MnO	1.68	1.97	1.85	0.801	0.817	0.833	0.92	0.81
MgO	0.859	0.519	0.617	3.09	3.12	2.87	3.00	2.62
CaO	2.48	4.37	2.76	8.11	7.99	8.14	7.82	8.14
Na2O	6.72	6.22	6.71	2.92	2.69	1.73	2.59	2.25
K2O	0.899	0.87	0.867	1.05	1.04	0.978	0.982	0.961
Recalc	-----	-----	-----	-----	-----	-----	-----	-----
Fe2O3	6.59	-	4.20	4.08	5.28	7.28	5.86	6.27
FeO	26.9	30.8	28.4	26.5	25.7	23.9	25.2	25.5
Total	98.5	94.0	97.2	97.4	97.6	96.3	97.0	96.6
Si	7.81	7.89	7.91	7.33	7.34	7.32	7.38	7.34
Aliv	0.19	0.11	0.09	0.65	0.62	0.66	0.57	0.64
Alvi	0.179	0.198	0.210	-	-	-	-	-
Ti	0.087	0.090	0.088	0.158	0.158	0.154	0.146	0.111
Fe3+	0.779	-	0.506	0.489	0.629	0.876	0.702	0.757
Fe2+	3.53	4.30	3.80	3.53	3.40	3.20	3.36	3.41
Mn	0.223	0.279	0.251	0.108	0.110	0.113	0.124	0.110
Mg	0.201	0.129	0.147	0.733	0.738	0.684	0.711	0.625
Ca	0.418	0.783	0.472	1.38	1.36	1.39	1.33	1.40
Na	2.05	2.02	2.08	0.902	0.827	0.535	0.799	0.699
K	0.180	0.166	0.177	0.213	0.209	0.199	0.199	0.196
Mg#	0.054	0.029	0.037	0.172	0.178	0.176	0.175	0.155

APPENDIX V

Microprobe analyses - Amphiboles from ferro-edenite syenite

	C2221/6	C2221/7	C2221/8	C2221/9	C2221/10	C2222/1	C2222/2	C2222/3
SiO2	41.3	40.6	40.7	40.6	41.2	49.4	49.5	50.3
TiO2	1.99	1.4	1.96	1.74	1.87	0.72	0.658	0.85
Al2O3	8.58	8.31	8.41	8.53	8.66	1.98	1.47	1.71
FeO T	26.0	29.3	27.7	29.3	28.2	32.4	31.8	32.2
MnO	0.85	1.06	0.963	1.01	0.91	1.73	1.94	1.62
MgO	4.49	2.56	3.39	2.37	3.06	0.96	0.72	0.879
CaO	10.2	9.63	9.83	9.73	9.81	2.68	2.49	2.59
Na2O	2.10	2.82	2.71	2.62	2.49	6.98	6.87	6.79
K2O	1.42	1.43	1.41	1.50	1.40	0.83	0.81	0.83
Recalc	-----	-----	-----	-----	-----	-----	-----	-----
Fe2O3	3.64	4.10	3.14	3.54	3.66	5.28	4.25	4.55
FeO	22.7	25.6	24.8	26.1	25.0	27.6	27.9	28.1
Total	97.3	97.6	97.4	97.7	98.0	98.2	96.7	98.2
Si	6.55	6.54	6.53	6.53	6.55	7.81	7.95	7.91
Aliv	1.45	1.46	1.47	1.47	1.45	0.19	0.05	0.09
Alvi	0.146	0.122	0.116	0.145	0.174	0.178	0.224	0.232
Ti	0.237	0.170	0.236	0.210	0.223	0.085	0.079	0.101
Fe3+	0.433	0.497	0.379	0.428	0.437	0.628	0.513	0.539
Fe2+	3.01	3.45	3.33	3.51	3.32	3.65	3.75	3.71
Mn	0.115	0.145	0.131	0.137	0.123	0.232	0.264	0.216
Mg	1.06	0.615	0.810	0.568	0.726	0.227	0.173	0.206
Ca	1.74	1.66	1.69	1.68	1.67	0.454	0.427	0.437
Na	0.645	0.879	0.842	0.819	0.768	2.14	2.14	2.07
K	0.287	0.294	0.288	0.307	0.284	0.168	0.166	0.167

APPENDIX V

Microprobe analyses - Amphiboles from ferro-edenite syenite

	C2223/7	C2223/8	C2224/1	C2224/3	C2224/4	C2226/1	C2226/2	C2226/3
SiO2	47.0	48.0	47.9	44.5	44.3	45.5	44.5	44.5
TiO2	1.13	0.493	1.21	1.50	1.65	1.02	1.41	1.39
Al2O3	2.75	2.35	5.31	5.82	5.69	3.15	4.31	4.14
FeO T	30.9	31.4	27.5	28.2	28.1	29.1	30.4	30.8
MnO	0.895	0.634	0.617	0.447	0.451	1.01	0.93	0.81
MgO	3.17	2.97	4.07	3.85	4.05	3.8	3.18	2.74
CaO	7.69	8.59	9.02	9.89	9.69	9.19	9.14	8.69
Na2O	2.71	1.58	1.44	1.49	2.02	2.09	2.48	2.36
K2O	0.873	0.721	0.968	0.96	0.998	0.72	0.87	0.78
Recalc	-----	-----	-----	-----	-----	-----	-----	-----
Fe2O3	6.61	6.37	4.03	4.04	3.59	4.57	5.03	5.87
FeO	24.9	25.7	23.9	24.6	24.9	25.0	25.8	25.5
Total	97.7	97.4	98.4	97.2	96.5	96.0	97.7	96.9
Si	7.42	7.58	7.35	7.04	7.01	7.32	7.09	7.14
Aliv	0.51	0.42	0.65	0.96	0.99	0.60	0.81	0.78
Alvi	-	0.016	0.315	0.123	0.069	-	-	-
Ti	0.134	0.058	0.140	0.179	0.196	0.123	0.169	0.168
Fe3+	0.786	0.756	0.466	0.480	0.427	0.553	0.604	0.710
Fe2+	3.29	3.39	3.07	3.25	3.29	3.36	3.44	3.43
Mn	0.120	0.085	0.080	0.060	0.060	0.138	0.126	0.110
Mg	0.746	0.698	0.931	0.906	0.955	0.911	0.756	0.656
Ca	1.30	1.45	1.48	1.67	1.64	1.58	1.56	1.49
Na	0.829	0.483	0.429	0.457	0.619	0.652	0.767	0.735
K	0.176	0.145	0.190	0.193	0.201	0.148	0.177	0.160

APPENDIX V

Microprobe analyses - Amphiboles from ferro-edenite syenite

	C2232/1	C2232/2	C2232/3	C2233/1	C2233/2	C2235/1	C2235/2	C2235/3
SiO2	45.0	44.3	44.7	49.1	48.2	45.3	48.6	45.1
TiO2	1.2	1.37	1.35	0.74	0.66	1.35	0.21	0.78
Al2O3	3.61	4.62	4.29	1.28	1.37	3.33	1.66	3.66
FeO T	30.7	31.3	31.6	31.6	30.6	30.4	30.8	32.1
MnO	1.14	1.07	1.17	1.54	1.81	1.19	1.54	1.31
MgO	2.43	2.46	2.3	1.04	1.05	2.56	3.31	1.5
CaO	8.18	8.43	8.35	1.21	1.14	8.55	8.95	9.7
Na2O	2.85	2.87	3.01	7.16	8.53	2.19	1.56	1.87
K2O	0.83	0.88	0.81	0.64	0.68	0.79	-	0.53
Recalc	-----	-----	-----	-----	-----	-----	-----	-----
Fe2O3	4.79	5.98	5.65	7.50	3.48	4.96	7.36	3.40
FeO	26.4	25.9	26.5	24.8	27.4	26.0	24.2	29.0
	-----	-----	-----	-----	-----	-----	-----	-----
Total	96.5	97.8	83.3	95.0	94.4	96.2	97.4	96.9
Si	7.27	7.07	7.12	7.93	7.94	7.31	7.64	7.31
Aliv	0.69	0.87	0.81	0.07	0.06	0.63	0.31	0.69
Alvi	-	-	-	0.177	0.202	-	-	0.014
Ti	0.146	0.164	0.162	0.090	0.082	0.164	0.025	0.095
Fe3+	0.582	0.719	0.678	0.913	0.431	0.603	0.871	0.415
Fe2+	3.57	3.45	3.53	3.36	3.76	3.51	3.17	3.93
Mn	0.156	0.145	0.158	0.211	0.252	0.163	0.205	0.180
Mg	0.585	0.585	0.546	0.251	0.258	0.616	0.775	0.363
Ca	1.42	1.44	1.43	0.210	0.201	1.48	1.51	1.68
Na	0.893	0.888	0.930	2.25	2.72	0.686	0.475	0.588
K	0.171	0.179	0.165	0.132	0.143	0.163	-	0.110
Mg#	0.141	0.145	0.134	0.069	0.064	0.327	0.169	0.084

APPENDIX V

Microprobe analyses - Amphiboles from quartz syenite

	C173/1	C173/2	C173/3	C330/1	C330/2	C330/3	C346/1	C346/2
SiO2	45.9	43.9	45.2	46.4	46.3	46.3	46.6	47.4
TiO2	1.39	1.44	1.39	1.39	1.36	1.41	1.01	1.32
Al2O3	3.19	4.58	3.32	3.64	3.27	3.74	3.64	2.93
FeO T	32.3	31.3	32.7	29.4	29.5	29.3	33.7	33.6
MnO	0.87	0.78	0.89	0.74	0.88	0.79	0.67	0.69
MgO	1.83	2.18	1.81	2.7	2.56	2.98	1.1	1.24
CaO	8.01	9.08	8.42	8.60	7.91	8.98	7.77	7.22
Na2O	2.81	2.69	2.64	3.81	4.03	3.89	2.01	2.62
K2O	0.93	0.86	0.7	0.75	1.05	0.8	0.94	0.97
Recalc	-----	-----	-----	-----	-----	-----	-----	-----
Fe2O3	4.47	3.48	5.39	-	-	-	7.26	6.18
FeO	28.2	28.1	27.8	29.4	29.5	29.3	27.2	28.0
	-----	-----	-----	-----	-----	-----	-----	-----
Total	97.7	97.2	97.6	97.4	96.9	98.2	98.1	98.5
Si	7.36	7.10	7.26	7.45	7.49	7.40	7.38	7.48
Aliv	0.60	0.87	0.63	0.553	0.51	0.60	0.62	0.52
Alvi	-	-	-	0.136	0.109	0.101	0.06	0.03
Ti	0.167	0.175	0.168	0.168	0.165	0.704	0.120	0.157
Fe3+	0.538	0.423	0.651	-	-	-	0.866	0.735
Fe2+	3.78	3.80	3.74	3.95	3.99	3.91	3.60	3.69
Mn	0.118	0.107	0.121	0.101	0.120	0.107	0.090	0.092
Mg	0.437	0.525	0.433	0.647	0.617	0.710	0.260	0.293
Ca	1.37	1.57	1.45	1.48	1.37	1.54	1.32	1.22
Na	0.872	0.842	0.822	1.19	1.26	1.20	0.618	0.802
K	0.190	0.177	0.143	0.154	0.216	0.163	0.190	0.195
Mg#	0.073	0.121	0.104	0.141	0.134	0.153	0.067	0.073

APPENDIX V

Microprobe analyses - Amphiboles from contaminated ferro-edenite syenite

	C2031/2	C2031/3	C2031/4	C2036/2	C2036/3	C2064/3	C2067/2	C2067/3
SiO2	44.1	42.5	48.2	40.5	41.5	44.3	43.2	42.7
TiO2	0.97	1.19	0.95	2.11	1.83	1.63	1.53	1.38
Al2O3	4.66	5.93	5.37	8.44	7.9	6.77	6.6	6.99
FeO T	29.0	29.7	25.7	26.0	27.0	22.3	24.7	24.0
MnO	1.19	1.12	0.83	0.77	0.83	0.51	0.62	0.66
MgO	3.71	2.89	2.19	4.3	4.52	8.13	6.14	6.2
CaO	9.92	10.3	8.15	10.7	10.6	11.4	11.4	11.3
Na2O	1.91	2.0	2.08	2.27	2.2	1.92	2.17	2.33
K2O	0.78	0.92	0.75	1.63	1.48	0.77	0.86	0.89
Recalc	-----	-----	-----	-----	-----	-----	-----	-----
Fe2O3	4.94	3.88	-	1.07	3.40	2.72	0.80	0.55
FeO	24.6	26.2	25.7	25.0	24.0	19.8	23.9	23.5
	-----	-----	-----	-----	-----	-----	-----	-----
Total	96.8	96.8	94.1	96.8	98.2	98.0	97.2	96.5
Si	7.07	6.87	7.77	6.51	6.56	6.80	6.81	6.78
Aliv	0.88	1.13	0.23	1.49	1.44	1.20	1.19	1.22
Alvi	-	-	0.786	0.113	0.031	0.026	0.039	0.091
Ti	0.117	0.145	0.115	0.255	0.218	0.188	0.182	0.165
Fe3+	0.596	0.472	-	0.129	0.405	0.314	0.095	0.065
Fe2+	3.29	3.54	3.46	3.37	3.17	2.54	3.16	3.12
Mn	0.161	0.153	0.113	0.105	0.111	0.066	0.083	0.089
Mg	0.886	0.697	0.526	1.03	1.07	1.86	1.44	1.47
Ca	1.70	1.78	1.41	1.85	1.80	1.88	1.93	1.92
Na	0.593	0.627	0.650	0.708	0.674	0.571	0.664	0.717
K	0.159	0.190	0.154	0.335	0.299	0.151	0.173	0.180
Mg#	0.212	0.165	0.132	0.235	0.251	0.422	0.314	0.320

APPENDIX V

Microprobe analyses - Amphiboles from contaminated ferro-edenite syenite

	C2176/4	C2229/2	C2229/3	C2229/4	C2063/2	C2063/3
					---xenoliths---	
SiO2	44.3	41.7	42.0	42.9	43.0	42.7
TiO2	1.52	1.98	1.76	1.84	1.51	1.43
Al2O3	5.04	7.83	7.74	7.67	7.81	7.07
FeO T	27.3	25.4	25.7	25.1	23.9	23.9
MnO	1.44	0.68	0.67	0.63	0.62	0.55
MgO	3.45	5.01	4.66	4.76	6.65	6.96
CaO	8.78	11.4	10.8	11.0	11.5	11.2
Na2O	3.68	2.5	2.49	2.41	2.44	2.08
K2O	1.13	1.33	1.26	1.26	1.14	1.21
Recalc	-----	-----	-----	-----	-----	-----
Fe2O3	-	-	0.04	-	0.89	2.81
FeO	27.3	25.4	25.7	25.1	23.1	21.4
	-----	-----	-----	-----	-----	-----
Total	96.7	97.8	97.0	97.5	98.7	97.4
Si	7.15	6.63	6.70	6.81	6.67	6.69
Aliv	0.85	1.37	1.30	1.19	1.33	1.31
Alvi	0.105	0.098	0.158	0.243	0.102	-
Ti	0.184	0.237	0.211	0.220	0.176	0.169
Fe3+	-	-	0.005	-	0.104	0.332
Fe2+	3.68	3.38	3.43	3.33	3.00	2.80
Mn	0.197	0.092	0.091	0.085	0.081	0.073
Mg	0.829	1.19	1.11	1.13	1.54	1.63
Ca	1.52	1.95	1.84	1.87	1.90	1.88
Na	1.15	0.771	0.771	0.742	0.734	0.632
K	0.232	0.270	0.257	0.255	0.226	0.242
Mg#	0.184	0.260	0.245	0.253	0.231	0.367

APPENDIX V

Microprobe analyses - Amphiboles from quartz syenite

	C346/4	C346/5	C346/6	C346/7	C346/8	C346/9	C346/10	C346/11
SiO2	46.8	47.6	47.3	46.3	45.8	46.8	46.3	47.3
TiO2	1.26	1.26	0.91	1.25	1.25	1.06	1.34	1.07
Al2O3	3.04	3.11	3.18	4.29	4.75	3.85	3.55	3.09
FeO T	33.3	32.4	32.7	32.1	31.2	32.7	33.6	32.5
MnO	0.62	0.69	0.6	0.54	0.54	0.51	0.68	0.63
MgO	1.43	1.3	1.57	2.1	2.56	1.7	1.08	1.82
CaO	7.44	8.36	8.25	8.18	8.74	8.07	7.55	7.82
Na2O	2.47	2.65	2.51	2.86	2.62	2.69	2.08	2.83
K2O	0.98	0.946	0.88	1.08	1.07	1.05	1.04	0.95
Recalc	----	-----	-----	-----	-----	-----	-----	-----
Fe2O3	6.45	1.19	3.47	4.34	3.96	4.37	7.32	3.52
FeO	27.5	31.3	29.6	28.2	27.6	28.8	27.1	29.3
	-----	-----	-----	-----	-----	-----	-----	-----
Total	98.0	98.4	98.3	99.2	99.0	98.9	98.0	98.2
Si	7.43	7.56	7.51	7.28	7.20	7.38	7.36	7.51
Aliv	0.57	0.44	0.49	0.72	0.80	0.62	0.64	0.49
Alvi	0.002	0.14	0.11	0.07	0.08	0.09	0.03	0.09
Ti	0.151	0.151	0.109	0.148	0.148	0.126	0.16	0.128
Fe3+	0.772	0.143	0.414	0.513	0.469	0.519	0.875	0.420
Fe2+	3.65	4.16	3.92	3.70	3.63	3.79	3.59	3.89
Mn	0.083	0.093	0.081	0.072	0.072	0.068	0.091	0.085
Mg	0.339	0.308	0.371	0.492	0.600	0.399	0.256	0.383
Ca	1.27	1.42	1.40	1.38	1.47	1.36	1.28	1.33
Na	0.761	0.816	0.772	0.871	0.798	0.822	0.641	0.871
K	0.199	0.192	0.178	0.216	0.214	0.211	0.211	0.192
Mg#	0.085	0.069	0.087	0.117	0.142	0.095	0.066	0.090

APPENDIX V

Microprobe analyses - Amphiboles from quartz syenite

	C346/12	C367/1	C367/2	C367/3	C367/5	C367/6	C367/7	C367/8
SiO2	46.8	46.3	45.5	47.5	46.0	46.7	48.9	48.7
TiO2	1.08	1.26	1.06	1.05	1.27	1.1	-	0.65
Al2O3	3.2	3.86	3.75	3.01	3.84	4.4	2.08	2.75
FeO T	34.0	31.2	30.7	31.7	31.6	31.0	33.4	31.2
MnO	0.60	0.67	0.64	0.65	0.7	0.61	1.31	0.71
MgO	1.26	1.95	1.73	1.53	1.92	1.9	1.04	2.34
CaO	7.47	7.99	7.72	7.2	7.88	7.91	6.93	7.75
Na2O	1.72	3.21	3.56	3.11	3.18	3.49	3.36	3.09
K2O	0.985	1.0	1.04	0.88	1.03	1.06	0.78	0.98
Recalc	-----	-----	-----	-----	-----	-----	-----	-----
Fe2O3	9.04	2.03	0.773	2.80	3.10	1.04	4.67	2.11
FeO	25.8	29.4	30.0	29.1	28.8	30.0	29.2	29.3
	-----	-----	-----	-----	-----	-----	-----	-----
Total	98.0	97.6	95.8	96.9	97.7	98.2	98.3	98.3
Si	7.41	7.40	7.44	7.61	7.35	7.41	7.75	7.67
Aliv	0.59	0.60	0.56	0.39	0.65	0.59	0.25	0.33
Alvi	0.002	0.122	0.158	0.18	0.075	0.230	0.14	0.18
Ti	0.128	0.151	0.130	0.126	0.153	0.131	-	0.077
Fe3+	1.08	0.244	0.095	0.338	0.373	0.124	0.558	0.250
Fe2+	3.41	3.93	4.11	3.90	3.85	3.98	3.88	3.85
Mn	0.080	0.091	0.089	0.088	0.095	0.082	0.176	0.095
Mg	0.297	0.465	0.422	0.365	0.458	0.449	0.246	0.549
Ca	1.27	1.37	1.35	1.24	1.35	1.34	1.18	1.31
Na	0.527	0.995	1.13	0.966	0.986	1.07	1.03	0.943
K	0.199	0.204	0.217	0.180	0.210	0.214	0.158	0.197
Mg#	0.080	0.106	0.093	0.086	0.106	0.101	0.060	0.125

APPENDIX V

Microprobe analyses - Amphiboles from quartz syenite

	C367/9	C367/10	C367/11	C367/12	C367/13	C367/14	C369/1	C369/2
SiO2	49.9	51.6	49.6	49.5	50.1	49.6	44.9	44.6
TiO2	-	0.13	0.22	0.15	-	0.16	1.31	1.3
Al2O3	1.69	0.85	1.62	1.72	1.43	1.56	3.95	3.97
FeO T	33.0	35.2	33.3	33.2	32.4	32.7	31.7	32.0
MnO	1.70	0.6	1.66	1.63	1.38	1.9	0.81	0.73
MgO	0.65	0.48	1.09	1.08	1.24	0.73	2.39	2.51
CaO	6.78	0.96	6.59	6.46	6.55	6.45	8.67	8.87
Na2O	2.21	6.44	3.29	3.57	2.95	2.72	2.64	2.64
K2O	0.79	0.24	0.82	0.76	0.72	0.7	0.83	0.82
Recalc	-----	-----	-----	-----	-----	-----	-----	-----
Fe2O3	5.80	11.9	5.26	4.97	4.62	5.69	5.12	4.88
FeO	27.8	24.5	28.5	28.7	28.3	27.6	27.1	27.6
	-----	-----	-----	-----	-----	-----	-----	-----
Total	97.3	97.7	98.7	98.6	97.3	97.1	97.6	97.7
Si	7.92	8.05	7.82	7.81	7.95	7.90	7.18	7.15
Aliv	0.08	-	0.18	0.19	0.05	0.10	0.74	0.75
Alvi	0.24	0.156	0.12	0.13	0.22	0.20	-	-
Ti	-	0.015	0.026	0.018	-	0.019	0.158	0.157
Fe3+	0.693	1.40	0.623	0.590	0.551	0.682	0.617	0.589
Fe2+	3.69	3.19	3.76	3.79	3.75	3.67	3.62	3.70
Mn	0.229	0.079	0.221	0.218	0.185	0.256	0.110	0.099
Mg	0.154	0.112	0.256	0.249	0.293	0.173	0.570	0.553
Ca	1.15	0.160	1.11	1.09	1.11	1.10	1.49	1.52
Na	0.680	1.95	1.00	1.09	0.908	0.840	0.819	0.821
K	0.160	0.048	0.165	0.153	0.146	0.142	0.169	0.168
Mg#	0.040	0.034	0.064	0.062	0.073	0.045	0.136	0.130

APPENDIX V

Microprobe analyses - Amphiboles from quartz syenite

	C369/3	C2051/1	C2051/2	C2051/3	C2060/1	C2060/2	C2060/3	C2071/1
SiO2	49.4	43.9	39.9	42.9	48.6	48.1	48.2	48.6
TiO2	0.18	1.38	2.2	1.57	0.42	0.53	0.5	0.31
Al2O3	0.2	5.41	7.25	5.91	0.97	0.99	0.92	0.88
FeO T	27.3	29.6	27.6	30.5	22.3	22.9	23.2	21.2
MnO	1.13	0.82	0.75	0.8	0.87	0.96	0.78	1.12
MgO	1.71	3.21	3.08	2.61	3.97	3.66	3.85	3.88
CaO	19.2	10.1	10.1	9.95	21.4	21.9	21.7	22.0
Na2O	1.3	2.18	2.31	2.16	0.99	0.98	1.03	1.25
K2O	-	1.07	1.48	1.15	-	-	-	-
Recalc	-----	-----	-----	-----	-----	-----	-----	-----
Fe2O3	-	2.73	1.41	3.63	-	-	-	-
FeO	27.3	27.1	26.3	27.2	22.3	22.9	23.2	21.2
	-----	-----	-----	-----	-----	-----	-----	-----
Total	100.4	97.9	94.8	97.9	99.5	100.0	100.2	99.2
Si	8.44	7.00	6.62	6.87	8.38	8.33	8.30	8.50
Aliv	-	1.00	1.38	1.12	-	-	-	-
Alvi	0.040	0.017	0.032	-	0.197	0.202	0.187	0.181
Ti	0.023	0.165	0.274	0.189	0.054	0.069	0.065	0.041
Fe3+	-	0.328	0.176	0.438	-	-	-	-
Fe2+	3.90	3.62	3.65	3.65	3.22	3.32	3.34	3.10
Mn	0.163	0.111	0.105	0.109	0.127	0.141	0.114	0.166
Mg	0.435	0.763	0.761	0.624	1.02	0.944	0.989	1.01
Ca	3.51	1.72	1.79	1.71	3.95	4.06	4.00	4.12
Na	0.430	0.674	0.742	0.671	0.331	0.329	0.344	0.424
K	-	0.218	0.313	0.235	-	-	-	-
Mg#	0.100	0.174	0.173	0.146	0.241	0.222	0.228	0.246

APPENDIX V

Microprobe analyses - Amphiboles from quartz syenite

	C2071/3	C2091/2	C2091/3	C2091/4	C2098/1	C2098/2	C2136/1	C2136/3
SiO2	48.9	46.4	45.1	48.0	48.9	49.4	48.1	48.3
TiO2	0.4	0.08	0.12	0.42	0.23	0.06	0.22	0.2
Al2O3	0.92	4.16	4.87	2.9	0.1	0.08	0.26	0.24
FeO T	20.8	26.2	27.3	24.8	26.9	25.2	27.5	27.2
MnO	0.98	0.9	0.9	0.82	1.1	1.0	1.17	0.81
MgO	4.25	5.9	5.12	6.68	1.09	2.22	1.21	1.65
CaO	21.7	8.48	8.95	8.45	17.1	17.6	19.4	19.4
Na2O	1.19	3.29	3.17	3.16	2.79	2.61	0.92	0.93
K2O	-	1.12	1.25	1.12	-	-	-	-
Recalc	-----	-----	-----	-----	-----	-----	-----	-----
Fe2O3	-	4.78	4.39	2.93	-	-	-	-
FeO	20.8	21.9	23.3	22.2	26.9	25.2	27.5	27.2
	-----	-----	-----	-----	-----	-----	-----	-----
Total	99.1	97.0	97.2	96.7	98.2	98.2	98.7	98.7
Si	8.49	7.28	7.14	7.51	8.57	8.59	8.41	8.41
Aliv	-	0.72	0.86	0.49	-	-	-	-
Alvi	0.188	0.054	0.048	0.040	0.021	0.016	0.054	0.049
Ti	0.052	0.001	0.014	0.049	0.030	0.001	0.029	0.026
Fe3+	-	0.565	0.523	0.344	-	-	-	-
Fe2+	3.02	2.87	3.09	2.90	3.93	3.67	4.02	3.96
Mn	0.144	0.120	0.121	0.109	0.163	0.147	0.173	0.120
Mg	1.10	1.38	1.21	1.56	0.285	0.575	0.315	0.429
Ca	4.03	1.43	1.52	1.42	3.20	3.29	3.63	3.62
Na	0.40	1.00	0.973	0.958	0.947	0.880	0.312	0.314
K	-	0.224	0.252	0.223	-	-	-	-
Mg#	0.267	0.325	0.281	0.349	0.067	0.136	0.073	0.098

APPENDIX V

Microprobe analyses - Amphiboles from quartz syenite

	C2138/1	C2138/2	C2138/3	C2138/4	C2138/5	C2153/1	C2153/2	C2153/3
SiO2	46.8	45.1	47.4	45.8	46.8	44.8	49.2	45.5
TiO2	1.23	0.932	0.625	1.19	0.804	1.67	0.578	1.80
Al2O3	3.11	3.84	2.68	3.83	2.83	4.73	1.06	4.18
FeO T	32.4	32.1	33.4	31.1	33.1	30.8	31.1	29.2
MnO	0.587	0.619	0.616	0.79	0.555	0.78	0.667	0.56
MgO	1.74	2.67	1.35	2.13	0.991	2.49	2.84	3.01
CaO	7.67	7.23	8.29	8.57	8.15	8.40	6.36	8.62
Na2O	2.76	2.36	2.23	2.68	2.07	3.81	4.20	3.38
K2O	0.972	0.862	0.81	0.945	0.748	1.14	0.717	1.13
Recalc	-----	-----	-----	-----	-----	-----	-----	-----
Fe2O3	4.54	11.1	4.45	2.80	4.11	1.72	3.20	-
FeO	28.3	22.1	29.4	28.6	29.4	29.3	28.2	29.2
	-----	-----	-----	-----	-----	-----	-----	-----
Total	97.7	96.9	97.9	97.4	96.5	98.9	97.0	97.4
Si	7.45	7.18	7.56	7.34	7.57	7.12	7.84	7.29
Aliv	0.55	0.72	0.44	0.66	0.43	0.88	0.16	0.71
Alvi	0.039	-	0.067	0.065	0.109	0.009	0.034	0.078
Ti	0.147	0.112	0.075	0.144	0.098	0.200	0.069	0.217
Fe3+	0.544	1.33	0.535	0.338	0.500	0.206	0.384	-
Fe2+	3.78	2.94	3.92	3.84	3.98	3.89	3.75	3.91
Mn	0.079	0.083	0.083	0.107	0.076	0.105	0.090	0.076
Mg	0.414	0.633	0.320	0.510	0.235	0.589	0.674	0.720
Ca	1.31	1.23	1.416	1.47	1.41	1.43	1.08	1.48
Na	0.852	0.729	0.689	0.831	0.648	1.17	1.30	1.05
K	0.198	0.175	0.165	0.193	0.154	0.231	0.146	0.231
Mg#	0.099	0.177	0.075	0.117	0.057	0.131	0.152	0.155

APPENDIX V

Microprobe analyses - Amphiboles from quartz syenite

	C2153/4	C2153/5	C2153/6	C2153/7	C2153/8	C2153/9	C2153/10	C2153/11
SiO2	47.2	46.1	51.3	51.8	52.2	48.0	45.7	49.2
TiO2	1.24	1.41	0.307	0.253	0.137	0.822	1.57	0.764
Al2O3	3.02	3.88	0.345	-	-	2.57	4.50	1.62
FeO T	31.5	31.7	32.4	33.2	33.2	31.3	30.7	32.1
MnO	0.9	0.579	0.545	0.815	0.635	1.01	0.668	0.819
MgO	1.85	2.04	2.59	2.70	2.81	2.45	2.20	2.10
CaO	7.24	7.50	5.14	4.22	3.86	7.25	7.54	6.26
Na2O	3.89	4.46	4.47	5.31	5.77	3.78	4.08	4.13
K2O	0.971	1.12	0.765	0.630	0.581	0.964	1.05	1.18
Recalc	-----	-----	-----	-----	-----	-----	-----	-----
Fe2O3	1.72	1.07	5.50	7.71	7.44	3.08	1.71	3.04
FeO	29.9	30.8	27.5	26.2	26.5	28.5	29.2	29.3
	-----	-----	-----	-----	-----	-----	-----	-----
Total	97.9	98.9	98.5	99.6	99.9	98.5	98.2	98.4
Si	7.53	7.33	8.00	7.97	8.01	7.58	7.27	7.77
Aliv	0.47	0.67	-	-	-	0.42	0.73	0.23
Alvi	0.094	0.053	0.063	-	-	0.056	0.114	0.068
Ti	0.149	0.168	0.036	0.029	0.016	0.098	0.187	0.091
Fe3+	0.206	0.128	0.645	0.893	0.859	0.366	0.205	0.362
Fe2+	3.99	4.09	3.58	3.38	3.39	3.77	3.88	3.88
Mn	0.122	0.078	0.072	0.106	0.082	0.134	0.090	0.110
Mg	0.441	0.484	0.601	0.621	0.643	0.577	0.522	0.494
Ca	1.24	1.28	0.859	0.697	0.634	1.23	1.28	1.06
Na	1.20	1.37	1.35	1.58	1.72	1.16	1.26	1.27
K	0.198	0.226	0.152	0.124	0.114	0.194	0.212	0.237
Mg#	0.100	0.106	0.144	0.155	0.159	0.133	0.119	0.113

APPENDIX V

Microprobe analyses - Amphiboles from quartz syenite

	C2153/12	C2153/13	C2153/14	C2153/15	C2153/16	C2153/17	C2153/18	C2154/1
SiO2	48.7	46.5	46.8	45.7	46.7	45.5	48.1	44.7
TiO2	1.00	1.49	1.36	1.72	1.58	1.63	0.795	1.71
Al2O3	1.15	4.18	2.96	4.29	3.94	4.32	1.93	4.32
FeO T	33.5	30.1	31.5	29.8	31.3	30.4	32.3	28.9
MnO	1.21	0.669	0.874	0.605	0.83	0.645	0.635	0.96
MgO	0.234	2.52	1.64	2.79	2.57	2.80	0.935	3.09
CaO	4.28	8.24	6.98	8.53	7.12	8.58	6.07	8.7
Na2O	5.03	3.97	4.10	3.29	4.13	3.35	4.45	3.56
K2O	1.18	1.16	1.11	1.13	1.37	1.12	1.02	1.16
Recalc	-----	-----	-----	-----	-----	-----	-----	-----
Fe2O3	3.61	-	1.27	0.70	2.89	0.65	3.47	0.72
FeO	30.3	30.1	30.4	29.2	28.7	29.8	29.2	28.2
	-----	-----	-----	-----	-----	-----	-----	-----
Total	96.6	98.8	97.4	97.9	99.6	98.1	97.5	97.4
Si	7.89	7.37	7.52	7.27	7.32	7.26	7.68	7.17
Aliv	0.11	0.63	0.48	0.73	0.68	0.72	0.32	0.82
Alvi	0.113	0.151	0.084	0.077	0.046	0.074	0.045	-
Ti	0.219	0.178	0.164	0.206	0.186	0.195	0.096	0.206
Fe3+	0.441	-	0.154	0.083	0.341	0.079	0.417	0.817
Fe2+	4.10	3.99	4.09	3.89	3.76	3.97	3.90	3.79
Mn	0.166	0.090	0.119	0.082	0.110	0.087	0.086	0.117
Mg	0.057	0.595	0.392	0.661	0.553	0.594	0.460	0.811
Ca	0.743	1.40	1.20	1.45	1.20	1.47	1.04	1.49
Na	1.58	1.22	1.28	1.01	1.26	1.04	1.38	1.11
K	0.243	0.243	0.227	0.230	0.275	0.227	0.208	0.237
Mg#	0.014	0.130	0.088	0.145	0.128	0.074	0.106	0.176

APPENDIX V

Microprobe analyses - Amphiboles from quartz syenite

	C2154/2	C2154/3	C2164/1	C2164/2	C2164/3	C2213/1	C2213/2	C2213/3
SiO2	44.8	45.6	47.0	41.6	40.5	46.4	45.4	45.1
TiO2	1.33	0.9	0.27	1.05	1.61	1.37	1.37	1.49
Al2O3	4.4	4.61	2.11	6.82	7.64	3.06	3.18	3.99
FeO T	29.2	25.9	29.3	29.2	29.2	32.6	31.8	30.6
MnO	0.73	0.8	1.58	0.88	0.81	0.951	0.95	0.791
MgO	3.45	5.24	3.46	2.49	2.56	1.98	1.85	2.47
CaO	8.26	8.68	9.54	9.58	10.1	7.63	7.37	8.43
Na2O	3.74	3.61	1.4	2.53	2.7	2.66	2.86	2.68
K2O	1.26	1.23	0.11	1.11	1.37	0.972	0.99	1.02
Recalc	-----	-----	-----	-----	-----	-----	-----	-----
Fe2O3	1.95	1.12	5.25	3.17	1.97	6.62	5.89	3.63
FeO	27.4	24.9	24.6	26.4	27.5	26.6	26.5	27.3
	-----	-----	-----	-----	-----	-----	-----	-----
Total	97.3	96.7	95.4	95.6	96.8	98.2	96.4	96.9
Si	7.18	7.24	7.57	6.82	6.61	7.35	7.34	7.25
Aliv	0.82	0.76	0.40	1.18	1.39	0.57	0.61	0.75
Alvi	0.010	0.100	-	0.134	0.079	-	-	-
Ti	0.160	0.107	0.033	0.129	0.197	0.163	0.166	0.180
Fe3+	0.831	0.134	0.636	0.391	0.242	0.790	0.717	0.755
Fe2+	3.67	3.31	3.31	3.61	3.75	3.53	3.59	3.68
Mn	0.099	0.108	0.215	0.122	0.112	0.128	0.130	0.108
Mg	0.824	1.24	0.830	0.608	0.623	0.467	0.447	0.591
Ca	1.42	1.48	1.65	1.68	1.77	1.30	1.28	1.45
Na	1.16	1.11	0.437	0.804	0.85	0.818	0.896	0.836
K	0.258	0.249	0.023	0.232	0.285	0.197	0.204	0.209
Mg#	0.183	0.273	0.201	0.144	0.143	0.117	0.111	0.139

APPENDIX V

Microprobe analyses - Amphiboles from quartz syenite

	C2213/4	C2213/5	C2213/6	C2213/7	C2213/8
SiO2	46.9	45.9	45.0	44.4	46.0
TiO2	1.27	1.32	1.58	1.60	1.12
Al2O3	2.85	3.43	4.19	4.81	3.21
FeO T	33.1	32.6	31.6	32.1	33.6
MnO	1.03	0.971	0.855	0.807	0.942
MgO	1.69	1.67	2.09	1.43	1.54
CaO	6.94	7.62	8.18	8.42	7.88
Na2O	2.95	2.82	3.13	2.73	1.23
K2O	0.95	0.955	1.16	1.13	0.856
Recalc	-----	-----	-----	-----	-----
Fe2O3	7.59	6.03	3.75	3.74	10.8
FeO	26.3	27.1	28.2	28.7	24.0
	-----	-----	-----	-----	-----
Total	98.4	97.8	98.1	97.7	97.5
Si	7.41	7.32	7.19	7.13	7.31
Aliv	0.53	0.65	0.79	0.87	0.60
Alvi	-	-	-	0.044	-
Ti	0.150	0.158	0.189	0.193	0.133
Fe3+	0.903	0.724	0.451	0.911	1.29
Fe2+	3.47	3.62	3.77	3.86	3.18
Mn	0.138	0.131	0.116	0.110	0.127
Mg	0.398	0.396	0.498	0.343	0.364
Ca	1.17	1.30	1.40	1.45	1.34
Na	0.903	0.871	0.971	0.850	0.378
K	0.191	0.194	0.236	0.233	0.173
Mg#	0.103	0.099	0.117	0.082	0.103

APPENDIX VI

Microprobe analyses - Pyroxenes from ferro-edenite syenite

	C333/2	C2127/3	C2074/1	C2074/3	C2133/1	C2133/3	C2004/1
SiO2	49.4	44.3	48.1	47.7	42.4	42.3	41.6
TiO2	1.31	1.33	1.37	1.36	1.33	1.33	1.33
Al2O3	0.87	4.68	1.66	1.15	6.65	5.64	5.72
Fe2O3	13.7	8.66	2.81	2.81	6.24	5.13	4.20
FeO	19.5	21.3	17.0	21.1	21.7	25.8	24.8
MnO	0.81	0.81	0.82	0.82	0.83	0.81	0.81
MgO	1.27	3.70	4.49	3.43	4.11	2.99	3.14
CaO	4.47	8.9	20.8	21.7	10.5	9.76	10.3
Na2O	5.33	3.36	1.09	1.09	2.42	1.99	1.63
Cr2O3	0.06	0.06	0.07	0.07	0.06	0.06	0.06
K2O	0.99	0.31	-	-	0.56	0.64	0.12
Total	97.8	97.3	98.3	101.2	96.8	96.4	93.7
Si	2.01	1.82	1.93	1.90	1.76	1.79	1.80
Aliv	-	0.176	0.068	0.054	0.241	0.212	0.205
Alvi	0.053	0.051	0.010	-	0.085	0.070	0.087
Fe3iv	-	-	-	0.043	-	-	-
Fe3vi	0.421	0.268	0.085	0.041	0.195	0.163	0.137
Fe2	0.665	0.733	0.570	0.702	0.753	0.911	0.898
Mn	0.028	0.028	0.028	0.028	0.029	0.029	0.030
Mg	0.077	0.227	0.269	0.204	0.254	0.188	0.202
Ca	0.195	0.393	0.896	0.926	0.467	0.442	0.477
Na	0.421	0.268	0.085	0.084	0.195	0.163	0.137
Ti	0.040	0.041	0.041	0.041	0.042	0.042	0.043
Cr	0.002	0.002	0.002	0.002	0.002	0.002	0.002
K	0.051	0.016	-	-	0.030	0.035	0.007

APPENDIX VI

Microprobe analyses - Pyroxenes from ferro-edenite and quartz syenite

	C2004/3 f-e	C1487/1 f-e	C2081/1 qz	C2081/3 qz	C369/1 qz	C369/2 qz	C2138/2 qz
SiO2	41.8	41.9	50.3	49.7	48.9	48.8	49.7
TiO2	1.33	1.33	1.39	1.38	0.42	0.20	-
Al2O3	6.76	7.23	0.80	1.12	0.75	0.25	0.22
Fe2O3	5.18	6.75	1.65	1.47	1.39	3.09	1.45
FeO	26.5	22.6	11.7	15.8	22.3	24.4	26.4
MnO	0.81	0.81	0.83	0.83	0.76	1.06	0.85
MgO	2.59	3.94	9.6	7.05	4.34	1.73	1.15
CaO	10.5	9.76	22.7	21.6	20.2	19.4	18.6
Na2O	2.01	2.62	0.64	0.57	0.54	1.2	0.56
Cr2O3	0.06	0.06	0.07	0.07	0.04	0.04	0.13
K2O	0.63	1.15	-	-	-	-	-
Total	98.1	98.2	99.8	99.6	99.7	100.1	99.1
Si	1.74	1.73	1.94	1.95	1.97	1.98	2.03
Aliv	0.256	0.272	0.036	0.052	0.035	0.012	-
Alvi	0.077	0.079	-	-	0.001	-	0.044
Fe3iv	-	-	0.027	0.003	-	0.005	-
Fe3vi	0.163	0.210	0.021	0.040	0.042	0.090	0.045
Fe2	0.926	0.780	0.378	0.517	0.749	0.828	0.905
Mn	0.029	0.028	0.027	0.028	0.026	0.037	0.030
Mg	0.161	0.242	0.551	0.411	0.260	0.105	0.070
Ca	0.468	0.431	0.938	0.906	0.870	0.844	0.818
Na	0.163	0.210	0.048	0.043	0.042	0.095	0.045
Ti	0.042	0.041	0.040	0.041	0.013	0.006	-
Cr	0.002	0.002	0.002	0.002	0.001	0.001	0.004
K	0.034	0.061	-	-	-	-	-

APPENDIX VI

Microprobe analyses - Pyroxenes from quartz syenite

	C2138/3	C2138/4	C2138/5	C2138/8	C2136/1	C2136/3	C2154/1
SiO2	45.9	49.0	49.0	49.6	45.2	49.2	48.6
TiO2	0.14	0.20	0.14	0.14	1.32	1.35	1.37
Al2O3	0.32	0.24	0.22	0.25	3.97	0.27	0.69
Fe2O3	2.02	1.72	1.59	1.37	7.52	2.55	3.07
FeO	24.9	25.5	25.8	26.0	25.8	24.9	18.8
MnO	0.81	0.94	0.87	0.95	0.81	0.82	0.82
MgO	2.12	1.94	1.46	1.89	2.58	1.98	4.81
CaO	18.9	18.7	18.8	18.6	8.52	19.8	19.9
Na2O	0.78	0.67	0.62	0.53	2.92	0.99	1.19
Cr2O3	0.12	-	0.12	-	0.51	0.07	0.07
K2O	-	-	-	-	0.06	-	-
Total	99.6	98.9	98.6	99.4	99.2	101.9	99.3
Si	2.01	2.01	2.02	2.02	1.85	1.96	1.94
Aliv	-	-	-	-	0.147	0.013	0.033
Alvi	0.024	0.020	0.026	0.034	0.045	-	-
Fe3iv	-	-	-	-	-	0.026	0.025
Fe3vi	0.062	0.053	0.049	0.042	0.232	0.050	0.068
Fe2	0.845	0.874	0.890	0.885	0.884	0.831	0.629
Mn	0.028	0.033	0.030	0.033	0.028	0.028	0.028
Mg	0.128	0.119	0.090	0.115	0.158	0.118	0.287
Ca	0.822	0.118	0.831	0.813	0.374	0.845	0.852
Na	0.062	0.821	0.049	0.042	0.232	0.077	0.092
Ti	0.004	0.006	0.004	0.004	0.041	0.041	0.041
Cr	0.004	-	0.004	-	0.002	0.002	0.002
K	-	-	-	-	0 027	-	-

APPENDIX VI

Microprobe analyses - Pyroxenes from quartz syenite

	C2154/3	C2071/2	C2071/3	C2091/1	C2091/2	C2091/3	C2153/1
SiO2	49.2	48.8	48.0	50.8	51.6	47.5	49.7
TiO2	1.37	1.37	1.37	1.38	1.35	1.33	0.38
Al2O3	0.51	0.82	0.97	1.15	1.11	3.37	-
Fe2O3	3.5	2.81	2.89	3.04	9.87	9.51	1.62
FeO	19.3	20.2	18.9	13.0	11.3	19.5	23.4
MnO	0.82	0.82	0.82	0.83	0.82	0.81	0.93
MgO	3.91	4.03	4.18	8.73	10.7	5.49	2.94
CaO	21.2	21.5	20.6	20.8	7.87	7.52	19.5
Na2O	1.36	1.09	1.12	1.18	3.83	3.69	0.63
Cr2O3	0.07	0.07	0.07	0.07	0.07	0.06	-
K2O	-	-	-	-	-	0.60	-
Total	101.3	101.5	98.9	100.9	98.6	99.4	99.1
Si	1.94	1.93	1.93	1.94	1.98	1.89	2.01
Aliv	0.024	0.038	0.046	0.052	0.024	0.112	-
Alvi	-	-	-	-	0.026	0.046	-
Fe3iv	0.036	0.035	0.022	0.009	-	-	-
Fe3vi	0.068	0.048	0.066	0.079	0.284	0.284	0.050
Fe2	0.637	0.666	0.635	0.413	0.362	0.648	0.794
Mn	0.027	0.027	0.028	0.027	0.027	0.027	0.032
Mg	0.230	0.237	0.251	0.497	0.612	0.325	0.178
Ca	0.897	0.908	0.890	0.849	0.323	0.32	0.846
Na	0.104	0.083	0.088	0.087	0.284	0.284	0.050
Ti	0.041	0.041	0.042	0.040	0.039	0.040	0.012
Cr	0.002	0.002	0.002	0.002	0.002	0.002	-
K	-	-	-	-	-	0.030	-

Microprobe analyses - Pyroxenes from quartz syenite

	C2153/2	C2153/3	C2153/4	C2153/5	C2153/6	C2153/7	C2153/8
SiO2	49.8	50.1	49.6	50.3	50.3	50.6	50.6
TiO2	0.16	-	0.25	0.14	0.20	-	-
Al2O3	-	-	0.22	-	0.24	0.25	0.25
Fe2O3	3.13	4.78	2.75	1.57	2.82	2.07	4.62
FeO	24.6	22.9	24.4	26.8	24.7	22.2	22.8
MnO	1.06	0.89	1.01	1.03	0.97	0.98	0.99
MgO	1.54	0.87	2.22	1.42	1.99	3.54	0.98
CaO	18.9	17.3	18.9	18.2	18.7	19.9	17.5
Na2O	1.21	1.86	1.07	0.61	1.09	0.80	1.79
Cr2O3	-	-	0.15	-	-	0.13	0.13
K2O	-	-	-	-	-	-	-
Total	100.4	98.7	100.6	100.0	101.0	100.5	99.6
Si	2.01	2.04	2.00	2.04	2.01	2.01	2.04
Aliv	-	-	0.004	-	-	-	-
Alvi	-	-	0.007	-	0.023	0.023	0.052
Fe3iv	-	-	-	-	-	-	-
Fe3vi	0.095	0.147	0.083	0.048	0.085	0.062	0.140
Fe2	0.829	0.78	0.821	0.907	0.825	0.738	0.767
Mn	0.063	0.031	0.035	0.035	0.033	0.033	0.034
Mg	0.093	0.053	0.133	0.086	0.118	0.21	0.059
Ca	0.817	0.757	0.813	0.791	0.801	0.849	0.755
Na	0.095	0.147	0.083	0.048	0.085	0.062	0.140
Ti	0.005	-	0.075	0.004	0.006	-	-
Cr	-	-	0.005	-	-	0.004	0.004
K	-	-	-	-	-	-	-

APPENDIX VI

Microprobe analyses - Pyroxenes from quartz syenite

	C2153/9	C2153/10	C2098/1	C2098/2	C2098/3
SiO2	51.3	50.6	48.9	49.5	48.5
TiO2	-	-	1.37	1.36	1.37
Al2O3	-	0.24	0.95	0.97	0.95
Fe2O3	1.29	4.86	2.14	2.34	2.04
FeO	23.0	20.9	20.7	20.7	20.1
MnO	0.89	1.07	0.82	0.82	0.82
MgO	3.57	2.34	3.9	3.95	3.76
CaO	20.2	18.9	21.4	20.8	21.2
Na2O	0.50	1.89	0.83	0.91	0.79
Cr2O3	0.14	0.17	0.07	0.07	0.07
K2O	-	-	-	-	-
Total	100.8	101.0	101.1	101.4	99.6
Si	2.03	2.01	1.93	1.95	1.94
Aliv	-	-	0.044	0.045	0.045
Alvi	-	0.018	-	-	-
Fe3iv	-	-	0.021	0.009	0.011
Fe3vi	0.038	0.145	0.042	0.061	0.050
Fe2	0.76	0.692	0.685	0.68	0.674
Mn	0.030	0.036	0.028	0.027	0.028
Mg	0.211	0.139	0.230	0.232	0.225
Ca	0.855	0.804	0.909	0.878	0.909
Na	0.038	0.145	0.064	0.069	0.061
Ti	-	-	0.041	0.040	0.041
Cr	0.004	0.005	0.002	0.002	0.002
K	-	-	-	-	-

APPENDIX VII

Microprobe analyses - Feldspars from magnesio-hornblende syenite

	C180/8	C180/9	C180/10	C180/12	C180/13	C180/14	C180/15	C180/16
SiO2	65.6	68.6	65.7	65.8	69.4	65.3	67.5	66.8
Al2O3	18.7	20.9	18.8	18.7	20.2	18.8	21.2	21.8
FeO	0.24	0.21	0.12	0.29	0.46	-	0.11	0.17
MgO	-	-	-	-	-	-	-	-
CaO	0.12	1.1	-	-	0.33	-	1.76	2.27
Na2O	1.32	8.05	0.96	0.96	8.88	0.46	8.92	9.22
K2O	14.0	0.21	14.5	14.4	0.12	15.5	0.17	0.27
P2O5	-	-	-	-	-	-	0.19	-
BaO	-	-	-	0.29	-	0.35	-	-
Total	100.0	99.1	100.0	100.4	99.4	100.4	99.8	100.5
Si	3.00	2.99	3.00	3.00	3.01	2.99	2.94	2.90
Al	1.01	1.07	1.01	1.00	1.03	1.02	1.09	1.12
Fe	0.009	0.008	0.005	0.011	0.017	-	0.004	0.006
Mg	-	-	-	-	-	-	-	-
Ca	0.006	0.051	-	-	0.015	-	0.082	0.106
Na	0.117	0.680	0.085	0.085	0.749	0.041	0.753	0.778
K	0.819	0.012	0.845	0.839	0.007	0.908	0.009	0.015
P	-	-	-	-	-	-	0.007	-
Ba	-	-	-	0.005	-	0.006	-	-

APPENDIX VII

Microprobe analyses - Feldspars from ferro-edenite syenite

	C2053/2	C2053/3	C2053/4	C2222/1	C2222/2	C2222/3	C2222/4	C322/1
SiO2	68.8	64.7	64.9	65.3	68.9	65.4	69.2	70.1
Al2O3	19.4	18.4	18.5	18.1	19.3	18.4	18.9	18.9
FeO	0.14	0.16	-	0.20	0.27	0.15	0.46	0.34
MgO	-	-	-	-	-	-	-	-
CaO	0.08	-	-	-	-	-	-	0.18
Na2O	11.4	1.46	0.57	0.30	11.4	0.63	11.4	10.4
K2O	0.17	14.2	15.4	15.7	-	15.3	0.13	0.17
P2O5	-	-	-	-	-	-	-	-
BaO	-	-	-	-	-	-	-	-
Total	100.0	99.0	99.3	99.6	99.9	99.9	100.2	100.0
Si	3.00	2.99	3.00	3.01	3.00	3.00	3.01	3.04
Al	0.999	1.01	1.01	0.987	0.994	0.998	0.972	0.966
Fe	0.005	0.006	-	0.008	0.010	0.006	0.017	0.012
Mg	-	-	-	-	-	-	-	-
Ca	0.004	-	-	-	-	-	-	0.008
Na	0.963	0.131	0.051	0.027	0.965	0.056	0.966	0.875
K	0.010	0.838	0.906	0.927	-	0.899	0.007	0.009
P	-	-	-	-	-	-	-	-
Ba	-	-	-	-	-	-	-	-

APPENDIX VII

Microprobe analyses - Feldspars from magnesio-hornblende syenite

	C181/1	C181/4	C180/1	C180/2	C180/11	C180/3	C180/6
SiO2	66	65.8	66.0	62.9	67.1	66.2	63.2
Al2O3	20.3	18.3	21.2	18.2	21.4	21.1	18.2
FeO	0.35	0.28	0.23	0.23	0.38	0.22	0.24
MgO	0.01	-	-	-	-	-	-
CaO	2.36	0.07	2.15	-	1.73	1.86	-
Na2O	9.8	1.25	8.99	-	9	7.64	1.31
K2O	0.29	15.5	0.13	15.3	0.2	0.13	13.2
P2O5	-	-	-	-	-	-	-
BaO	-	0.21	-	0.41	-	-	0.29
Total	99.1	101.4	98.7	97.0	99.8	97.2	96.4
Si	2.92	3.00	2.91	2.99	2.93	2.95	2.99
Al	1.06	0.982	1.10	1.02	1.10	1.11	1.02
Fe	0.013	0.011	0.009	0.009	0.014	0.008	0.010
Mg	0.001	-	-	-	-	-	-
Ca	0.112	0.003	0.102	-	0.081	0.089	-
Na	0.843	0.111	0.771	-	0.763	0.660	0.12
K	0.016	0.901	0.007	0.930	0.011	0.007	0.795
P	-	-	-	-	-	-	-
Ba	-	0.004	-	0.008	-	-	0.005

APPENDIX VII

Microprobe analyses - Feldspars from ferro-edenite syenite

	C2223/1	C2223/2	C2223/3	C2223/4	C2223/5	C2223/6	C2224/1	C2053/1
SiO2	69.3	65.2	68.5	63.6	69.3	65.6	69.0	68.0
Al2O3	19.2	17.9	18.8	17.3	18.9	17.6	19.4	19.9
FeO	0.16	0.32	0.18	0.54	0.26	0.41	0.23	0.12
MgO	-	-	-	-	-	-	-	-
CaO	0.09	-	-	-	-	-	0.29	0.28
Na2O	10.8	-	10.6	0.52	11.0	0.36	11.0	11.4
K2O	0.28	16.2	0.42	14.6	0.18	15.4	0.17	0.21
P2O5	-	-	-	-	-	-	-	-
BaO	-	-	-	-	-	-	-	-
Total	99.9	99.7	98.5	96.5	99.6	99.5	100.0	99.9
Si	3.02	3.02	3.02	3.02	3.02	3.03	3.00	2.97
Al	0.987	0.977	0.979	0.967	0.972	0.960	0.997	1.03
Fe	0.006	0.012	0.007	0.022	0.010	0.016	0.008	0.004
Mg	-	-	-	-	-	-	-	-
Ca	0.004	-	-	-	-	-	0.014	0.013
Na	0.912	-	0.910	0.048	0.935	0.032	0.925	0.964
K	0.016	0.956	0.024	0.887	0.01	0.910	0.009	0.012
P	-	-	-	-	-	-	-	-
Ba	-	-	-	-	-	-	-	-

APPENDIX VII

Microprobe analyses - Feldspars from ferro-edenite syenite

	C322/2	C322/3	C2169/8	C2212/1	C2212/2	C2212/3	C2212/4	C2212/5
SiO2	66.0	71.1	65.9	66.5	63.7	64.5	62.6	65.7
Al2O3	17.8	18.8	20.4	20.5	22.7	22.2	23.1	20.7
FeO	0.27	0.52	-	-	-	-	-	-
MgO	0.02	0.01	-	-	-	-	-	-
CaO	0.07	0.07	1.5	0.98	3.31	3.06	3.88	1.52
Na2O	0.44	8.26	11.5	11.4	9.8	9.7	9.52	10.9
K2O	15.9	1.95	0.31	0.2	0.48	0.38	0.34	0.23
P2O5	-	-	-	-	-	-	-	-
BaO	0.05	0.01	-	-	-	-	-	-
Total	100.5	100.7	99.7	99.6	99.9	99.8	99.4	99.1
Si	3.02	3.07	2.91	2.93	2.81	2.84	2.78	2.91
Al	0.961	0.956	1.06	1.07	1.18	1.15	1.21	1.08
Fe	0.010	0.019	-	-	-	-	-	-
Mg	0.001	0.001	-	-	-	-	-	-
Ca	0.003	0.003	0.071	0.05	0.157	0.145	0.185	0.072
Na	0.039	0.691	0.989	0.976	0.840	0.830	0.822	0.938
K	0.930	0.107	0.018	0.011	0.027	0.021	0.019	0.013
P	-	-	-	-	-	-	-	-
Ba	0.001	-	-	-	-	-	-	-

APPENDIX VII

Microprobe analyses - Feldspars from ferro-edenite syenite

	C2212/6	C2212/7	C2212/8	C2212/9	C2212/10	C2212/11	C2212/12	C2212/13
SiO2	66.0	65.5	67.8	65.3	64.5	64.6	61.8	64.9
Al2O3	20.8	21.6	19.5	21.5	21.9	21.9	23.6	22.0
FeO	-	-	-	-	-	-	-	-
MgO	-	-	-	-	-	-	-	-
CaO	1.67	2.38	0.44	2.11	2.22	2.37	5.05	2.74
Na2O	11.0	11.2	11.6	10.8	10.4	10.6	8.66	9.69
K2O	0.22	0.18	0.18	0.3	0.3	0.31	0.26	0.27
P2O5	-	-	-	-	-	-	-	-
BaO	-	-	-	-	-	-	-	-
Total	99.7	100.8	99.4	100.0	99.2	99.8	99.3	99.5
Si	2.91	2.86	2.98	2.87	2.86	2.85	2.75	2.86
Al	1.08	1.12	1.01	1.11	1.14	1.14	1.24	1.14
Fe	-	-	-	-	-	-	-	-
Mg	-	-	-	-	-	-	-	-
Ca	0.079	0.112	0.021	0.10	0.106	0.112	0.242	0.130
Na	0.937	0.948	0.988	0.924	0.891	0.912	0.749	0.830
K	0.012	0.010	0.010	0.017	0.017	0.018	0.015	0.015
P	-	-	-	-	-	-	-	-
Ba	-	-	-	-	-	-	-	-

APPENDIX VII

Microprobe analyses - Feldspars from ferro-edenite syenite

	C371/4	C2001/1	C2001/2	C2001/3	C2001/4	C2001/5	C361/2
SiO2	65.1	66.7	65.8	69.5	69.6	67.7	65.7
Al2O3	18.3	21.0	18.7	20.2	20.4	19.5	18.5
FeO	0.44	0.49	0.32	0.3	0.37	0.37	0.3
MgO	-	0.03	0.03	-	0.04	0.01	-
CaO	0.08	1.77	0.04	0.6	0.56	0.27	0.02
Na2O	0.54	10.0	1.68	10.0	9.86	7.21	0.96
K2O	16.1	0.32	14.1	0.12	0.21	5.21	14.4
P2O5	-	-	-	-	-	-	-
BaO	-	-	0.11	-	0.04	0.18	0.19
Total	100.6	100.4	100.8	100.8	101.0	100.5	100.0
Si	2.99	2.91	2.99	2.99	2.99	2.99	3.01
Al	0.990	1.08	1.00	1.03	1.03	1.02	0.997
Fe	0.017	0.018	0.012	0.011	0.013	0.014	0.012
Mg	-	0.002	0.002	-	0.003	0.001	-
Ca	0.004	0.083	0.002	0.028	0.026	0.013	0.001
Na	0.048	0.848	0.148	0.840	0.823	0.618	0.085
K	0.946	0.018	0.815	0.007	0.012	0.294	0.844
P	-	-	-	-	-	-	-
Ba	-	-	0.002	-	0.001	0.003	0.003

APPENDIX VII

Microprobe analyses - Feldspars from ferro-edenite syenite

	C361/3	C361/4	C2235/1	C2235/2	C2235/3	C2228/1	C2228/2
SiO2	65.7	69.4	63.0	69.7	70.2	67.7	65.8
Al2O3	18.3	20.0	17.6	19.7	19.8	19.3	18.1
FeO	0.33	0.3	0.26	0.34	0.38	0.39	0.51
MgO	0.03	-	-	-	-	-	0.02
CaO	0.08	0.27	0.29	0.17	0.17	0.11	0.07
Na2O	1.17	9.24	0.22	10.7	9.74	7.03	0.73
K2O	15.1	0.56	14.8	0.17	0.13	6.15	14.8
P2O5	-	-	-	-	-	-	-
BaO	-	0.1	-	0.01	0.02	0.25	0.09
Total	100.7	99.9	96.2	100.8	100.5	100.9	100.2
Si	3.00	3.01	3.01	3.01	3.02	2.99	3.01
Al	0.987	1.02	0.992	1.00	1.01	1.01	0.978
Fe	0.013	0.011	0.010	0.01	0.014	0.014	0.020
Mg	0.002	-	-	-	-	-	0.001
Ca	0.004	0.013	0.015	0.008	0.008	0.005	0.003
Na	0.104	0.779	0.020	0.893	0.814	0.603	0.065
K	0.878	0.031	0.899	0.009	0.007	0.347	0.868
P	-	-	-	-	-	-	-
Ba	-	-	-	-	-	0.004	0.002

APPENDIX VII

Microprobe analyses - Feldspars from ferro-edenite syenite

	C2228/4	C322/4	C322/5	C322/6	C322/7	C2127/1	C2127/2
SiO2	64.7	65.8	70.7	71.5	70.6	67.4	70.3
Al2O3	18.1	17.2	18.8	18.6	18.9	18.1	19.1
FeO	0.46	0.51	0.47	0.58	0.58	0.36	0.35
MgO	0.01	0.04	-	-	0.01	0.02	0.02
CaO	0.11	0.07	-	-	0.05	0.03	0.14
Na2O	0.54	0.53	9.44	9.25	9.33	3.88	9.67
K2O	14.6	15.6	0.08	0.1	0.2	10.5	0.2
P2O5	-	-	-	-	-	-	-
BaO	-	-	0.02	0.02	-	0.1	0.01
Total	98.5	99.7	99.5	100.1	99.7	100.4	99.8
Si	3.01	3.04	3.06	3.08	3.06	3.03	3.05
Al	0.992	0.935	0.963	0.945	0.966	0.960	0.974
Fe	0.018	0.020	0.017	0.021	0.021	0.014	0.013
Mg	0.001	0.003	-	-	0.001	0.001	0.001
Ca	0.006	0.004	-	-	0.002	0.001	0.007
Na	0.049	0.048	0.795	0.773	0.785	0.338	0.813
K	0.865	0.919	0.004	0.006	0.011	0.604	0.011
P	-	-	-	-	-	-	-
Ba	-	-	-	-	-	0.002	-

APPENDIX VII

Microprobe analyses - Feldspars from ferro-edenite syenite

	C2233/1	C2233/2	C2233/3	C2233/4	C371/1	C371/2	C371/3
SiO2	68.5	70.1	70.0	69.7	64.7	69.5	68.3
Al2O3	18.9	19.3	18.8	19.1	18.1	18.6	18.7
FeO	0.79	0.94	0.85	0.84	0.72	1.17	0.46
MgO	-	0.02	-	0.02	0.04	0.04	-
CaO	0.08	0.04	0.09	0.04	0.08	0.02	0.1
Na2O	9.57	9.94	9.4	10.9	0.55	10.0	10.1
K2O	0.22	0.21	0.2	0.15	16.4	0.16	0.09
P2O5	-	-	-	-	-	-	-
BaO	-	0.22	-	-	-	-	-
Total	98.1	100.8	99.4	100.8	100.5	99.8	97.8
Si	3.03	3.03	3.05	3.01	2.98	3.03	3.03
Al	0.987	0.982	0.967	0.975	0.984	0.969	0.980
Fe	0.029	0.034	0.031	0.030	0.028	0.043	0.017
Mg	-	0.001	-	0.001	0.003	0.003	-
Ca	0.004	0.002	0.004	0.002	0.004	0.001	0.005
Na	0.821	0.833	0.795	0.915	0.049	0.848	0.870
K	0.012	0.012	0.011	0.008	0.965	0.009	0.005
P	-	-	-	-	-	-	-
Ba	-	0.004	-	-	-	-	-

APPENDIX VII

Microprobe analyses - Feldspars from ferro-edenite syenite

	C2101/1	C2101/2	C2101/3	C2101/4	C2221/1	C2221/2	C2221/3	C2221/4
SiO2	70.8	66.2	66.1	68.3	67.1	66.3	69.4	66.2
Al2O3	18.9	17.8	17.4	18.3	19.6	18.2	19.7	18.2
FeO	0.46	0.41	0.47	0.48	0.19	-	0.16	-
MgO	-	-	0.02	0.01	-	-	-	-
CaO	0.04	0.06	0.03	0.01	0.56	-	0.58	-
Na2O	10.0	1.09	0.76	8.55	9.22	-	9.4	0.31
K2O	0.07	15.2	16.0	2.02	0.22	16.3	0.2	16.1
P2O5	-	-	-	-	-	-	-	-
BaO	0.09	-	-	-	-	-	-	-
Total	100.3	100.8	100.8	97.6	96.9	100.8	99.4	100.8
Si	3.05	3.02	3.03	3.05	3.00	3.02	3.02	3.02
Al	0.959	0.956	0.941	0.961	1.03	0.981	1.01	0.978
Fe	0.017	0.016	0.018	0.018	0.007	-	0.006	-
Mg	-	-	0.001	0.001	-	-	-	-
Ca	0.002	0.003	0.002	0.001	0.027	-	0.027	-
Na	0.840	0.097	0.068	0.741	0.800	-	0.794	0.027
K	0.004	0.885	0.932	0.115	0.013	0.949	0.011	0.936
P	-	-	-	-	-	-	-	-
Ba	0.002	-	-	-	-	-	-	-

APPENDIX VII

Microprobe analyses - Feldspars from ferro-edenite syenite

	C2169/1	C2169/2	C2169/3	C2169/5	C2169/6	C2169/7	C2218/1	C2218/3
SiO2	65.5	65.3	65.3	65.6	66.3	65.4	70.3	69.4
Al2O3	20.8	20.5	20.5	20.9	20.6	20.6	18.9	19.6
FeO	-	-	-	-	-	-	0.42	0.31
MgO	-	-	-	-	-	-	0.01	-
CaO	1.48	1.05	1.08	1.53	1.35	1.56	0.03	0.57
Na2O	10.6	11.2	11.1	11.1	10.8	10.8	9.34	10.1
K2O	0.3	0.24	0.34	0.23	0.39	0.16	0.13	0.32
P2O5	-	-	-	-	-	-	-	-
BaO	-	-	-	-	-	-	0.03	0.16
Total	98.6	98.2	98.4	99.4	99.4	98.51	99.2	100.4
Si	2.91	2.92	2.91	2.90	2.92	2.91	3.06	3.01
Al	1.09	1.08	1.08	1.09	1.07	1.08	0.97	1.00
Fe	-	-	-	-	-	-	0.015	0.011
Mg	-	-	-	-	-	-	0.001	-
Ca	0.071	0.050	0.052	0.073	0.064	0.075	0.001	0.027
Na	0.914	0.967	0.962	0.951	0.923	0.930	0.789	0.848
K	0.017	0.014	0.019	0.013	0.022	0.009	0.007	0.018
P	-	-	-	-	-	-	-	-
Ba	-	-	-	-	-	-	0.001	0.003

APPENDIX VII

Microprobe analyses - Feldspars from ferro-edenite syenite

	C2218/4	C2218/5	C2004/1	C2004/2	C2004/3	C2004/4	C2004/6	C2190/1
SiO2	64.4	69.6	65.6	69.6	69.6	66.3	70.4	65.1
Al2O3	16.6	19.3	17.8	18.9	19.3	18.2	19.1	21.9
FeO	2.33	0.3	0.27	0.29	0.3	0.21	0.28	0.47
MgO	0.22	-	-	-	-	-	-	0.01
CaO	0.04	0.26	0.05	0.09	0.36	0.15	0.15	3.24
Na2O	0.65	9.77	1.19	9.73	9.46	1.88	10.2	9.05
K2O	14.4	0.18	14.8	0.13	0.06	13.3	0.11	0.3
P2O5	-	-	-	-	-	-	-	-
BaO	0.10	0.24	-	-	-	0.13	-	0.09
Total	98.6	99.6	99.6	98.7	99.0	100.1	100.2	100.1
Si	3.02	3.03	3.02	3.05	3.03	3.02	3.04	2.86
Al	0.917	0.991	0.964	0.976	0.992	0.975	0.972	1.13
Fe	0.092	0.011	0.010	0.011	0.011	0.008	0.010	0.017
Mg	0.016	-	-	-	-	-	-	0.001
Ca	0.002	0.012	0.003	0.004	0.017	0.007	0.007	0.153
Na	0.059	0.825	0.106	0.827	0.801	0.166	0.856	0.772
K	0.862	0.01	0.867	0.007	0.003	0.774	0.006	0.017
P	-	-	-	-	-	-	-	-
Ba	0.002	0.004	-	-	-	0.002	-	0.002

APPENDIX VII

Microprobe analyses - Feldspars from ferro-edenite syenite

	C2190/2	C2190/3	C1487/2	C1487/3	C1487/4	C2006/1	C2006/2
SiO2	62.1	62.1	65.3	70.6	66.0	68.1	69.1
Al2O3	17.1	17.1	17.8	18.4	17.5	19.0	19.4
FeO	0.43	0.35	0.21	0.49	0.45	0.36	0.29
MgO	0.01	0.01	0.02	0.01	-	-	0.04
CaO	0.14	0.23	0.08	-	0.03	0.62	0.42
Na2O	1.14	7.51	0.41	9.41	1.05	10.8	10.8
K2O	14.3	1.91	15.8	0.06	14.6	0.24	0.25
P2O5	-	-	-	-	-	-	-
BaO	0.22	0.04	0.24	-	0.07	-	0.08
Total	95.5	89.2	99.8	99.0	99.7	99.1	100.3
Si	3.00	3.03	3.02	3.08	3.03	3.00	3.00
Al	0.975	0.985	0.969	0.946	0.949	0.988	0.992
Fe	0.017	0.014	0.008	0.018	0.017	0.013	0.011
Mg	0.001	0.001	0.001	0.001	-	-	0.003
Ca	0.007	0.012	0.004	-	0.002	0.029	0.020
Na	0.107	0.712	0.037	0.796	0.094	0.923	0.907
K	0.880	0.119	0.933	0.003	0.856	0.014	0.014
P	-	-	-	-	-	-	-
Ba	0.004	0.001	0.004	-	0.001	-	0.001

APPENDIX VII

Microprobe analyses - Feldspars from ferro-edenite syenite and contaminated f-e syenite.

	C2127/3 f-e	C2127/4 f-e	C2063/3 con	C2067/3 con	C2067/4 con	C2036/1 con
SiO2	65	70.9	68.5	66.0	64.2	66.4
Al2O3	17.5	19.0	18.8	18.8	18.5	18.5
FeO	0.43	0.37	0.35	0.27	1.35	0.36
MgO	-	0.04	0.01	-	0.02	0.05
CaO	0.04	0.05	0.25	0.18	0.16	0.1
Na2O	0.74	9.38	4.4	3.06	4.96	1.51
K2O	15.2	0.16	9.6	11.9	8.57	13.9
P2O5	-	-	-	-	-	-
BaO	0.04	-	0.14	0.07	0.1	0.25
Total	98.9	99.9	102.1	100.2	97.8	101.1
Si	3.02	3.06	3.02	2.99	2.97	3.00
Al	0.958	0.967	0.978	1.00	1.01	0.989
Fe	0.017	0.013	0.013	0.010	0.052	0.014
Mg	-	0.003	0.001	-	0.001	0.003
Ca	0.002	0.002	0.012	0.009	0.008	0.005
Na	0.067	0.786	0.376	0.269	0.445	0.133
K	0.902	0.009	0.54	0.688	0.506	0.806
P	-	-	-	-	-	-
Ba	0.001	-	0.002	0.001	0.002	0.004

APPENDIX VII

Microprobe analyses - Feldspars from quartz syenite

	C2213/4	C2213/5	C2213/6	C2213/7	C2138/2	C346/1	C346/2
SiO2	69.3	65.4	69.3	67.6	65.3	66.2	65.6
Al2O3	19.1	17.6	18.8	18.8	17.7	18.3	18.3
FeO	0.28	1.31	0.3	0.26	0.12	0.26	0.24
MgO	-	-	-	-	-	-	-
CaO	0.19	0.1	0.1	-	-	-	-
Na2O	9.81	0.66	6.72	5.72	0.33	0.96	1.04
K2O	0.29	14.5	5.92	7.37	15.5	14.9	14.8
P2O5	-	-	-	-	-	-	-
BaO	-	-	-	-	-	-	-
Total	98.9	99.6	101.1	99.8	99.0	100.6	99.9
Si	3.03	3.02	3.03	3.02	3.03	3.01	3.01
Al	0.986	0.957	0.968	0.991	0.968	0.982	0.989
Fe	0.010	0.051	0.011	0.010	0.005	0.010	0.009
Mg	-	-	-	-	-	-	-
Ca	0.009	0.005	0.005	-	-	-	-
Na	0.834	0.059	0.571	0.495	0.030	0.085	0.093
K	0.016	0.854	0.331	0.420	0.919	0.864	0.864
P	-	-	-	-	-	-	-
Ba	-	-	-	-	-	-	-

APPENDIX VII

Microprobe analyses - Feldspars from quartz syenite

	C346/3	C346/4	C346/5	C346/7	C346/8	C346/9	C367/1	C367/2
SiO2	67.0	70.3	65.8	69.9	66.4	70.2	65.5	68.8
Al2O3	18.4	19.8	18.1	19.8	18.3	19.5	18.1	19.1
FeO	2.22	0.48	0.24	0.23	0.22	0.28	0.22	0.36
MgO	-	-	-	-	-	-	-	-
CaO	0.08	-	-	-	-	-	-	-
Na2O	9.24	8.2	1.14	8.7	0.86	10.0	0.95	10.6
K2O	0.14	0.16	14.8	0.13	15.1	0.14	14.9	0.13
P2O5	-	-	-	-	-	-	0.21	0.18
BaO	-	-	-	-	-	-	-	-
MnO	-	-	0.11	-	-	-	-	-
Total	97.1	99.0	100.2	98.8	100.9	100.1	99.9	99.2
Si	3.01	3.05	3.01	3.04	3.02	3.03	3.01	3.01
Al	0.975	1.01	0.978	1.01	0.981	0.991	0.978	0.987
Fe	0.084	0.017	0.009	0.008	0.008	0.010	0.008	0.013
Mg	-	-	-	-	-	-	-	-
Ca	0.004	-	-	-	-	-	-	-
Na	0.807	0.691	0.101	0.735	0.076	0.842	0.085	0.897
K	0.008	0.009	0.862	0.007	0.873	0.008	0.871	0.007
P	-	-	-	-	-	-	0.008	0.007
Ba	-	-	-	-	-	-	-	-
Mn	-	-	0.004	-	-	-	-	-

APPENDIX VII

Microprobe analyses - Feldspars from quartz syenite

	C367/3	C367/4	C367/5	C367/6	C367/8	C2164/2	C2164/3	C2164/4
SiO2	65.6	69.1	68.6	65.4	69.7	68.9	65.0	69.2
Al2O3	18.1	19.4	19.3	18.2	19.3	19.1	18.2	19.4
FeO	0.33	0.33	0.42	0.24	0.3	0.85	0.32	0.31
MgO	-	-	-	-	-	0.11	0.03	0.01
CaO	-	-	-	-	-	0.2	0.08	0.36
Na2O	0.4	11.5	9.4	1.03	8.89	8.86	0.38	10.3
K2O	15.6	0.14	0.28	14.8	0.15	1.44	16.1	0.2
P2O5	-	-	-	-	0.21	-	-	-
BaO	-	-	-	-	-	0.02	0.11	-
Total	100.0	100.4	98.0	99.6	98.6	99.5	100.1	99.7
Si	3.02	3.00	3.03	3.01	3.04	3.02	3.00	3.01
Al	0.979	0.991	1.01	0.987	0.992	0.988	0.988	0.996
Fe	0.013	0.012	0.016	0.009	0.011	0.031	0.012	0.011
Mg	-	-	-	-	-	0.007	0.002	0.001
Ca	-	-	-	-	-	0.009	0.004	0.017
Na	0.036	0.969	0.805	0.092	0.753	0.754	0.034	0.868
K	0.913	0.008	0.016	0.870	0.008	0.081	0.946	0.011
P	-	-	-	-	0.008	-	-	-
Ba	-	-	-	-	-	-	0.002	-

APPENDIX VII

Microprobe analyses - Feldspars from quartz syenite

	C369/1	C369/2	C369/3	C2091/1	C2091/2	C2091/3	C2071/1	C2071/3
SiO2	70.7	65.7	65.5	69.5	66.4	65.7	69.6	66.6
Al2O3	18.6	17.5	17.3	19.3	17.7	18.4	19.6	17.9
FeO	0.33	0.43	0.38	0.29	0.25	0.41	0.28	0.26
MgO	0.04	0.02	0.05	0.57	0.07	0.18	0.01	0.04
CaO	0.04	0.05	0.1				0.03	0.02
Na2O	8.75	0.86	0.37	10.0	0.47	2.75	9.67	1.13
K2O	0.19	15.1	15.6	0.1	15.9	13.0	0.19	14.0
P2O5	-	-	-	-	-	-	-	-
BaO	0.03	-	-	-	0.14	0.07	0.06	0.23
Total	98.6	99.7	99.3	99.8	100.8	100.5	100.2	100.3
Si	3.08	3.03	3.03	3.02	3.03	2.99	3.01	3.03
Al	0.957	0.953	0.947	0.990	0.950	0.988	1.00	0.963
Fe	0.012	0.017	0.015	0.011	0.010	0.016	0.010	0.010
Mg	-	0.001	0.004	-	-	-	0.001	0.003
Ca	0.002	0.003	0.005	0.027	0.003	0.009	0.034	0.006
Na	0.741	0.077	0.033	0.845	0.042	0.243	0.813	0.100
K	0.011	0.888	0.924	0.006	0.924	0.758	0.011	0.811
P	-	-	-	-	-	-	-	-
Ba	0.001	-	-	-	0.003	0.001	0.001	0.004

APPENDIX VII

Microprobe analyses - Feldspars from quartz syenite

	C2071/4	C2153/2	C2153/3	C2153/4	C2153/5	C2213/1	C2213/2	C2213/3
SiO2	69.6	64.8	69.1	65.6	69.2	66.5	69.8	68.0
Al2O3	18.9	18.2	19.1	18.2	19.4	17.6	18.5	18.9
FeO	0.24	1.36	0.41	0.19	0.32	0.37	1.12	0.21
MgO	-	-	-	-	-	-	-	-
CaO	0.45	-	-	-	-	-	0.11	0.18
Na2O	9.15	0.92	11.4	0.87	11.5	1.21	8.71	6.68
K2O	0.23	14.8	0.57	15.3	0.93	14.2	0.14	6.07
P2O5	-	-	-	-	-	-	-	-
BaO	0.05	-	-	-	-	-	-	-
Total	98.5	100.0	100.7	100.2	101.3	99.9	98.4	100.0
Si	3.05	2.99	3.00	3.01	2.99	3.04	3.07	3.01
Al	0.975	0.989	0.979	0.986	0.989	0.948	0.957	0.988
Fe	0.009	0.053	0.015	0.007	0.012	0.014	0.041	0.008
Mg	-	-	-	-	-	-	-	-
Ca	0.021	-	-	-	-	-	0.005	0.009
Na	0.779	0.082	0.965	0.077	0.967	0.107	0.742	0.575
K	0.013	0.868	0.032	0.895	0.051	0.831	0.008	0.344
P	-	-	-	-	-	-	-	-
Ba	0.001	-	-	-	-	-	-	-

APPENDIX VIII

Microprobe analyses- Fe-Ti oxides from magnesio-hornblende syenite (1) and ferro-edenite syenite

	C179/3 mag-hor	C2074/2	C2074/3	C2235/2	C294/1	C294/3	C2232/2	C2232/3
SiO2	0.11	0.02	0.23	0.08	1.51	0.15	0.06	0.04
TiO2	51.8	5.34	2.05	47.8	7.86	1.19	47.6	47.0
Al2O3	0.03	0.36	0.77	0.01	0.45	0.04	0.08	-
Fe2O3	1.09	57.5	64.2	6.48	48.8	66.9	8.08	8.34
FeO	44.3	34.5	32.4	39.5	33.4	32.5	33.6	31.4
MnO	1.83	1.03	1.19	3.49	1.20	0.06	9.07	10.7
MgO	0.04	0.05	0.03	0.03	-	-	0.03	0.07
CaO	0.41	0.12	0.03	0.01	4.18	0.04	-	0.01
Total	99.6	99.0	100.9	97.3	97.4	100.8	98.5	97.6
Si	0.003	0.001	0.009	0.002	0.058	0.006	0.002	0.001
Ti	0.986	0.155	0.058	0.934	0.227	0.034	0.919	0.918
Al	0.001	0.016	0.034	-	0.020	0.002	0.002	-
Fe3	0.021	1.67	1.83	0.127	1.41	1.92	0.156	0.163
Fe2	0.937	1.12	1.03	0.859	1.07	1.04	0.722	0.681
Mn	0.039	0.034	0.038	0.077	0.039	0.002	0.197	0.235
Mg	0.002	0.002	0.002	-	-	-	0.001	0.003
Ca	0.011	0.002	0.001	-	0.172	0.002	-	-

APPENDIX VIII

Microprobe analyses- Fe-Ti oxides from ferro-edenite syenite

	C333/4	C2226/1	C2226/3	C2226/4	C1397/1	C1397/2	C1397/3	C2235/3
SiO2	0.78	0.08	0.88	0.16	0.06	0.14	0.08	0.61
TiO2	45.9	45.0	0.44	0.58	6.86	0.25	0.06	13.5
Al2O3	0.19	-	0.08	0.07	-	-	0.04	0.07
Fe2O3	3.76	10.2	65.9	68.3	53.8	66.6	66.4	35.5
FeO	38.7	38.1	32.5	32.0	31.9	30.6	30.0	40.5
MnO	2.96	2.33	0.06	0.10	4.58	0.16	0.05	1.08
MgO	0.02	0.05	0.01	0.05	0.02	0.02	0.04	0.03
CaO	0.33	0.02	0.03	0.01	0.09	-	0.03	0.05
Total	92.7	95.8	99.85	101.3	97.3	97.8	96.7	91.2
Si	0.021	0.090	0.034	0.006	0.002	0.006	0.003	0.025
Ti	0.937	0.003	0.013	0.017	0.203	0.007	0.002	0.419
Al	0.006	0.003	0.004	0.003	-	-	0.002	0.003
Fe3	0.077	1.81	1.90	1.95	1.59	1.97	1.99	1.11
Fe2	0.880	1.09	1.04	1.02	1.05	1.01	1.00	1.40
Mn	0.068	0.003	0.002	0.003	0.152	0.005	0.002	0.038
Mg	0.001	0.001	0.001	0.003	0.001	0.001	0.002	0.002
Ca	0.010	0.003	0.001	-	0.004	-	0.001	0.002

APPENDIX VIII

Microprobe analyses- Fe-Ti oxides from ferro-edenite syenite

	C2190/2	C2190/3	C2004/1	C2004/3	C2006/1	C2006/3
SiO2	0.14	0.14	0.12	0.11	0.13	0.24
TiO2	46.0	0.40	43.8	49.7	47.8	46.8
Al2O3	0.04	0.17	0.02	0.08	0.01	-
Fe2O3	6.62	66.8	10.2	2.20	3.63	5.11
FeO	39.5	31.1	36.3	39.1	40.3	39.4
MnO	1.90	0.11	3.13	5.63	2.46	2.68
MgO	0.04	-	0.03	0.04	0.06	0.01
CaO	-	0.02	0.01	-	0.19	0.18
Total	94.2	98.7	93.6	96.9	94.5	94.5
Si	0.004	0.006	0.003	0.003	0.004	0.006
Ti	0.929	0.012	0.892	0.974	0.960	0.942
Al	0.001	0.008	0.001	0.003	-	-
Fe3	0.134	1.96	0.209	0.043	0.073	0.103
Fe2	0.888	1.01	0.822	0.851	0.900	0.882
Mn	0.043	0.004	0.072	0.124	0.056	0.061
Mg	0.002	-	0.001	0.002	0.002	-
Ca	-	0.001	-	-	0.005	0.005

APPENDIX VIII

Microprobe analyses - Fe-Ti oxides from quartz syenite

	C2071/2	C2071/3	C369/2	C369/3	C2060/2	C2060/3	C173/2	C173/3
SiO2	1.97	0.19	0.07	0.25	0.12	0.13	0.14	0.15
TiO2	0.13	7.17	46.2	3.89	1.86	2.12	48.5	49.2
Al2O3	0.03	0.67	0.03	0.03	0.61	0.79	0.04	-
Fe2O3	51.6	52.3	7.10	59.3	64.3	64.0	6.30	4.90
FeO	26.7	36.4	39.3	34.0	32.8	33.2	41.9	42.1
MnO	0.13	0.86	2.29	0.23	0.15	0.22	1.66	2.17
MgO	0.54	-	0.01	0.01	-	0.01	0.06	-
CaO	0.31	0.04	-	0.06	0.03	0.04	0.10	0.05
Total	81.4	97.7	95.1	97.8	99.9	100.6	98.7	98.6
Si	0.092	0.007	0.002	0.010	0.005	0.005	0.004	0.004
Ti	0.005	0.210	0.926	0.115	0.054	0.061	0.935	0.949
Al	0.002	0.031	0.001	0.001	0.028	0.035	0.001	-
Fe3	1.81	1.53	0.142	1.75	1.86	1.83	0.122	0.095
Fe2	1.04	1.19	0.876	1.11	1.05	1.06	0.898	0.904
Mn	0.005	0.028	0.052	0.008	0.005	0.007	0.036	0.047
Mg	0.037	-	-	0.001	-	0.001	0.002	-
Ca	0.016	0.002	-	0.003	0.001	0.002	0.003	0.001

APPENDIX VIII

Microprobe analyses - Fe-Ti oxides from quartz syenite

	C173/4	C2098/1	C2098/2	C2136/1	C2081/1	C2081/2	C2136/4	C330/1
SiO2	0.09	0.09	0.13	0.08	0.12	0.10	0.26	0.09
TiO2	46.9	47.8	47.9	46.7	50.1	0.79	45.7	49.8
Al2O3	0.08	0.09	0.06	0.01	0.06	0.31	0.05	0.03
Fe2O3	8.38	6.02	6.35	7.90	2.23	66.9	8.14	3.74
FeO	40.9	39.9	38.9	40.3	41.9	31.8	38.2	40.1
MnO	1.33	3.02	4.12	1.78	3.25	0.02	3.04	4.59
MgO	0.02	0.02	-	0.02	-	0.02	-	-
CaO	0.03	0.10	0.09	-	-	0.06	0.12	0.11
Total	97.7	97.0	97.5	96.7	97.6	100.0	95.5	98.4
Si	0.002	0.002	0.003	0.002	0.003	0.004	0.007	0.002
Ti	0.915	0.937	0.934	0.920	0.974	0.023	0.911	0.961
Al	0.002	0.003	0.002	-	0.002	0.014	0.002	0.001
Fe3	0.164	0.118	0.124	0.156	0.043	1.93	0.162	0.072
Fe2	0.886	0.869	0.844	0.882	0.906	1.02	0.846	0.861
Mn	0.029	0.067	0.091	0.040	0.071	0.001	0.068	0.100
Mg	0.001	0.001	-	0.001	-	0.001	-	-
Ca	0.001	0.003	0.003	-	-	0.003	0.003	0.003

APPENDIX VIII

Microprobe analyses - Fe-Ti oxides from quartz syenite

	C330/3	C2154/2	C2154/3
SiO2	0.05	0.26	0.05
TiO2	46.8	37.7	49.7
Al2O3	0.04	0.05	-
Fe2O3	5.79	27.9	3.81
FeO	40.6	30.9	42.1
MnO	1.39	3.20	2.60
MgO	0.03	0.04	-
CaO	0.09	-	-
Total	94.8	100.0	98.3
Si	0.001	0.007	0.001
Ti	0.940	0.725	0.962
Al	0.001	0.002	-
Fe3	0.116	0.536	0.074
Fe2	0.906	0.661	0.906
Mn	0.031	0.069	0.057
Mg	0.001	0.001	-
Ca	0.003	-	-